Network-Assisted Full-Duplex in Cell-Free Massive MIMO Systems for User-Centric Communications

Shuto Fukue

Department of Computer and Network Engineering
The University of Electro-Communications

This dissertation is submitted in partial fulfillment of the requirements for the degree of *Doctor of Philosophy*

March 2023

Document Description

Title:
Network-Assisted Full-Duplex in Cell-Free Massive MIMO Systems for User-Centric Communications

和訳:
ユーザセントリックな通信を実現するネットワーク全二重セルフリー大規模MIMOシステム

Author:
Shuto Fukue

Supervisory Committee:

Chairperson: Professor Koji Ishibashi

1. Member: Professor Takeo Fujii

2. Member: Professor Abreu Giuseppe

3. Member: Associate Professor Koichi Adachi

4. Member: Assistant Professor Katsuya Suto

Day of the Predefense: November 9th and 14th, 2022.

Day of the Defense: February 13th, 2023.

Copyright Notice

Acknowledgements

First of all, I am sincerely grateful to my supervisor, Professor Koji Ishibashi, for his kind and ardent support. His dedicated guidance, attitude toward research, and thoughtful discussions have motivated mainly me to focus on our research. Thanks to his strong support, I could have a lot of exciting and irreplaceable experiences in the last three years in our laboratory, making my life more colorful. I also express my deepest gratitude to Professor Giuseppe Thadeu Freitas de Abreu, who first accepted me at his laboratory and was recommendable to go to the Ph.D. course.

I would also like to thank the dissertation committee members, Professor Takeo Fujii, Professor Giuseppe Thadeu Freitas de Abreu, Associate Professor Koichi Adachi, and Assistant Professor Katsuya Suto, for spending considerable time reading my dissertation and providing their insightful comments.

I would like to gratitude Ph.D. Hiroki Iimori, Ph.D. Takanori Hara, and Mr. Kazuya Ohira for their many advice and help. I also want to thank the Advanced Wireless and Communication Research Center (AWCC) members and Abreu Lab. students for supporting each other in their student lives.

Last but not least, my special thanks go to my family for their continuous help and support throughout my life. This dissertation would not have been possible without their continued patience and endless support.

Shuto Fukue
Tokyo, Japan
February 1, 2023

Abstract

In this dissertation, we consider a cell-free (CF) massive multiple-input multiple-output (mMIMO) system with network-assisted full-duplex (NAFD), aiming for user-centric communication that reaches combinatorial requirements for high data rate, massive connectivity, and low-latency. The realization of NAFD CF-mMIMO requires proper resource allocation and effective suppression of new interference by inter-access point (AP) and inter-user equipment (UE). To this end, we propose several approaches to solve the NAFD CF-mMIMO challenges.

Firstly, we address the trade-off between system throughput and UE fairness in NAFD CF-mMIMO systems using the microwave, developing a joint AP access configuration, power allocation, and beamforming design scheme. The proposed design approach maximizes the geometric mean of the UEs' throughput performance under a transmit power constraint, yielding an excellent compromise between system throughput and UE fairness. However, the direct reformulation of the resulting optimization problem is hard to solve due to the non-convexity of the objective function and the binary constraint induced by the AP access configuration. We thus present an efficient (i.e., polynomial time complexity) solution for the problem via a combination of fractional programming (FP) and convex-concave procedure (CCP), assisted by a negative entropy regularizer that promotes a binary solution. Numerical simulations are offered to evaluate the proposed algorithm's throughput performance and fairness index, which confirm the proposed approach's effectiveness over existing methodologies both in throughput and fairness.

Next, we propose NAFD CF-mMIMO systems using millimeter-wave (mmWave) to expand bandwidth, which realizes high-throughput and large-capacity communication for adapting to future requirements. In addition, to mitigate the inter-UE interference, we propose a joint resource allocation and beamforming design with location-aided channel estimation. The key idea is to replace the estimates of the inter-UE channels with their approximates that can be obtained from knowledge of UE locations since mmWave channels are dominated by line-of-sight (LoS) paths due to their high propagation loss nature. Furthermore, a penalty method is proposed to guarantee the estimated channel error and prevent outages. This rough channel state information (CSI) with penalty enables the system to choose APs judiciously and design beamformers to enhance the performance of the NAFD CF-mMIMO system

significantly. Simulation results confirm that the total throughput of the proposed methods is close to that with the perfect channel knowledge of inter-UE channels.

These proposals address the user-centric communication system realized by NAFD CF-mMIMO systems.

Abstract

第6 世代移動体通信システムでは，指数関数的なトラフィックの増大に対応し，高度化する通信速度への要求を確実に満たすことが求められる．この要求を満足するには，ベストエフォート的な通信設計を脱却し，各ユーザの要求を確実に満たすユーザセントリックな設計を行う必要がある．これに対応し得る技術として，信号伝送を担うアクセスポイント（ AP: Access Point）を分散配置し，フロントホールを介して接続された中央制御装置（ CPU: Central Processor Unit）において統合的に信号処理を行うセルフリー大規模MIMO(CF-mMIMO: Cell-Free Massive Multiple-Input Multiple-Output)が活発に議論されている．一般にCF-mMIMOでは，複信方式として時分割多重（ TDD: Time Division Duplex）を用いるが，いずれの伝送方向においてもネットワーク内に待機ユーザが生じ，これがシステムの周波数利用効率を低下させてしまう．そこで，各APに上りまたは下りの伝送方向を割り当て，全二重通信を実現するネットワーク全二重（ NAFD: Network-Assisted Full-Duplex）を用いたCF-mMIMOが提案されている．NAFD CF-mMIMOは，優れた周波数利用効率を達成するが，システム全体の周波数利用効率を最大化するよう最適化を行うと，一部のユーザに通信資源が全く割り当てられなくなってしまい，CF-mMIMOの特徴であった通信品質の均質性、ユーザ間の公平性が失われてしまう．一方で、ユーザ間の公平性のみを考えて最適化すると，システム全体の周波数利用効率が大幅に低下してしまい，さらなるトラフィックの増大に対処できない．以上の背景を踏まえ，本論文ではシステム全体の周波数利用効率の最大化とユーザ公平性のトレードオフにおいて優れる新たなNAFD CF-mMIMOの設計法を提案した．本論文の構成は以下の通りである．

まず第2 章では，本論文の中心となるNAFDおよびCF-mMIMOについて包括的なサーベイを行っている．CF-mMIMOの歴史的な発展や関連研究について述べ，CF-mMIMOがユーザセントリック通信を実現しうる通信方式であることを示すと共に，これまでのCF-mMIMOで議論されてきた様々な無線資源割当・ビームフォーミング設計方式と複信方式を比較し，NAFD通信と容量の幾何平均最大化によるAP割当・ビームフォーミング設計がユーザセントリック通信を実現するための設計方式として適当であることについて、明らかにしている．

第3 章では、広域での通信を想定し，マイクロ波帯でのNAFD CF-mMIMOの設計を行った．具体的には，ユーザの公平性を担保しつつ，システム和容量を最大化する手法として，幾何平均最大化を導入し，これに基づくAPの上り・下りリンク割当と，干渉抑制のための資源割当・ビームフォーミング同時設計方式を提案した．幾何平均最大化に基づく最適化は，非凸最適化問題であるため，効率的に解を求めることが難しい．そこで，エントロピー正則化や分数計画法，CCP(Convex-Concave Procedure)といった凸緩和手法を用いて，問題を凸最適化問題へと再定式化することで，無線資源割当・ビームフォーミングの同時設計アルゴリズムを提案した．計算機シミュレーションによって，提案手法がTDD通信や従来方式で設計されたNAFD CF-mMIMOに対して，高い公平性を保ちながらシステム全体の周波数利用効率で優位な性能を発揮することを確認した．

続いて第4 章において，さらなる広帯域通信への要求に応えるべく，NAFD CF-mMIMOをミリ波帯へと拡張した．第3 章において提案したNAFD CF-mMIMOでは，ユーザ間干渉を含む全ての通信路状態情報が必要であったが，ユーザ間の通信路を推定することはオーバーヘッドが大きく，現実的ではない．一方ミリ波では，狭いエリアに多数のユーザが稠密に存在する環境が想定され，ユーザ間干渉の影響が顕著となる．そこで，ミリ波の通信路が主に見通し通信路の成分で構成される点に着目し，ユーザの位置情報に基づき得られる角度や距離の情報から，見通し通信路を再構成するユーザ間通信路推定手法を提案した．さらに提案推定法が，シャドウィング成分を過小評価してしまうことを防ぐため，推定誤差を補償するためのペナルティを付加した新たなAP割当・ビームフォーミング設計方式を提案した．提案最適化は，非凸最適化問題であることから，凸緩和によって効率的に最適解を求めることのできるアルゴリズムを提案した．計算機シミュレーションより，提案手法の性能が通信路状態情報既知の理想性能に漸近すると共に，広帯域化によって高いスループット特性が得られることを確認した．ゆえに，提案ユーザ間通信路推定とAP割当・ビームフォーミング設計によって，ミリ波におけるNAFD CF-mMIMOが，ユーザ間の公平性と高スループットを両立可能であることを示した．

以上より，本論文では，ユーザ間の公平性とシステム全体の周波数利用効率を両立したNAFD CF-mMIMOが実現可能であり，提案NAFD CF-mMIMOによってユーザセントリックな通信を実現可能であることを明らかにした．

Table of Contents

List of Figures **xv**

List of Tables **xix**

List of Algorithms **xxi**

List of Acronyms **xxvi**

Notation **xxvii**

1 Introduction **1**

1.1 Motivation 1

1.1.1 Cellular Network Evolutions 1

1.1.2 Future Requirements 6

1.1.3 User-Centric Communication 9

1.2 Related Works 13

1.2.1 Cell-Free Massive MIMO 13

1.2.2 Network-Assisted Full-Duplex 15

1.3 Thesis Contributions and Outline 18

1.3.1 Contributions 18

1.3.2 Outline 19

2 Overview of the Cell-Free Massive MIMO Systems **21**

2.1 Concept of Original Cell-Free Massive MIMO Systems 21

2.1.1 Channel Models 23

2.1.2 Comparison of the Signal Model between the Cellular and Cell-Free Massive MIMO 26

2.2 Resource Allocation and Beamforming Design 29

2.2.1 Sum-Rate Maximization 29

2.2.2 Max-Min Worst-Case Maximization 30
2.2.3 Geometric-Mean Maximization 30
2.3 Duplex Modes 31
2.3.1 Static TDD 31
2.3.2 Dynamic TDD 32
2.3.3 Full-Duplex 33
2.4 Chapter Summary 35

3 Joint Access Configuration and Beamforming for Network-Assisted Full-Duplex Cell-Free Massive MIMO 37
3.1 Background and Contributions 37
3.2 Channel and System Model 38
3.2.1 Single Antenna Case 38
3.2.2 Multiple-Antenna Case 42
3.3 Proposed Methods 43
3.3.1 Problem Formulation: Geometric Mean Maximization 44
3.3.2 Initialization: Pre-Selection of APs 51
3.4 Complexity Analysis 52
3.5 Numerical Results 55
3.5.1 State-of-the-Art Benchmark Solutions 55
3.5.2 Improved Benchmark Solutions 56
3.5.3 Computer simulations 58
3.5.4 Impact of Inter-UE Interference 75
3.6 Chapter Summary 78

4 Network-Assisted Full-Duplex with Localization-Aided Inter-Users Channel Estimation for Millimeter-Wave Cell-Free Massive MIMO systems 79
4.1 Background and Contributions 79
4.2 Channel and System Model 80
4.2.1 Channel Model 80
4.2.2 System Model 81
4.2.3 Problem Formulation 82
4.3 Model-Driven Channel Estimation 83
4.4 Joint Resource Allocation and Beamforming Design 85
4.4.1 Penalized Objective Function for Robust Design 85
4.4.2 Convex Reformulation of Problem (4.4.1) 86
4.5 Numerical Results 90

4.5.1 Comparison of Design Accuracy 91
4.5.2 Outage and Throughput 94
4.6 Chapter Summary 107

5 Conclusion and Future Work 109
5.1 Conclusion 109
5.2 Future Work 110
5.2.1 Scalable Network Design for user-centric communication with NAFD CF-mMIMO 111
5.2.2 Hybrid Beamforming Design for mmWave NAFD CF-mMIMO . . 113
5.2.3 Energy-Efficient NAFD CF-mMIMO 113
5.2.4 Robustness Against Traffic and Channel Fluctuation 114
5.2.5 Further Practical NAFD CF-mMIMO 115

Appendix A Introduction of Fractional Programming 117

Appendix B Convexification via Fractional Programming and Negative Entropy 119
B.1 Single-Antenna UEs Case 119
B.2 Multi-Antenna UEs Case 120

Appendix C Canonical form of QCP Formulation 123

References 127

Publications 142

List of Figures

1.1 Evolution of the Cellular Network Generations. 2
1.2 Illustration of the summary of the 5G use cases. 3
1.3 Frequency allocations in the US [12]. 4
1.4 Illustration of massive MIMO and beamforming technologies. 5
1.5 Forecast of data traffic per month by Ericcson [23]. 7
1.6 Comparison of the 5G and 6G requirements [24]. 8
1.7 Illustration of the inter-cell interference in the cellular networks. 9
1.8 Illustration of the distributed antenna systems. 10
1.9 Illustration of the cell-free massive MIMO systems. 11
1.10 Illustration of the network-assisted full-duplex cell-free massive MIMO systems. 12
1.11 The Overview of This Dissertation. 20

2.1 Illustration of inter-cell interference in UL communication. 22
2.2 Illustration of cell-free massive MIMO systems. 23
2.3 Illustration of the cross-interference of operating dynamic TDD mode in cellular networks. 31
2.4 Illustration of the full-duplex communication with self-interference. 34

3.1 Illustration of CF-mMIMO system based NAFD. 39
3.2 CDF of the sum SE for the sum-rate maximization and the max-min worst-case SotA benchmark solutions. 58
3.3 Comparison of the CDF of the total SE for different approaches under the predominantly DL ($q = 0.25$). 61
3.4 Comparison of the CDF of the total SE for different approaches under the balanced UL/DL ($q = 0.5$). 61
3.5 Comparison of the CDF of the total SE for different approaches under the predominantly UL ($q = 0.75$). 62
3.6 Convergence of η_ℓ over iterations. 64

3.7 Convergence of SEs over iterations. 64
3.8 Comparison of the CDF of the minimum SE for different approaches under the predominantly DL ($q = 0.25$). 66
3.9 Comparison of the CDF of the minimum SE for different approaches under the balanced UL/DL ($q = 0.5$). 66
3.10 Comparison of the CDF of the minimum SE for different approaches under the predominantly UL ($q = 0.75$). 67
3.11 Comparison of the CDF of the SE for different approaches under the predominantly DL ($q = 0.25$). 68
3.12 Comparison of the CDF of the SE for different approaches under the balanced UL/DL ($q = 0.5$). 68
3.13 Comparison of the CDF of the SE for different approaches under the predominantly UL ($q = 0.75$). 69
3.14 Comparison of the CDF of Jain's fairness index for UE using Algorithm 1 under the predominantly DL ($q = 0.25$). 71
3.15 Comparison of the CDF of Jain's fairness index for UE using Algorithm 1 under the balanced UL/DL ($q = 0.5$). 71
3.16 Comparison of the CDF of Jain's fairness index for UE using Algorithm 1 under the predominantly UL ($q = 0.75$). 72
3.17 Comparison of the CDF of Jain's fairness index for UE using Algorithm 1. . 72
3.18 Comparison of the CDF of Sum SE for UE using Algorithm 2. 74
3.19 Comparison of the CDF of Minimum SE for UE using Algorithm 2. 74
3.20 Comparison of the CDF of SE per UE using Algorithm 2. 75
3.21 Comparison of the CDF of "Sum SE" for UE with/without inter-UE CSI knowledge. 76
3.22 Comparison of the CDF of "Minimum SE" for UE with/without inter-UE CSI knowledge. 76
3.23 Comparison of the CDF of SE per UE with/without inter-UE CSI knowledge. 77

4.1 Comparison of the geometric mean of throughput versus the number of UEs ($N = 4$). 92
4.2 Comparison of the geometric mean of throughput versus the number of UEs ($N = 8$). 92
4.3 Comparison of the geometric mean of throughput versus the number of UEs ($N = 16$). 93
4.4 Comparison of the outage probability. 93
4.5 Comparison of the throughput versus penalty level ($K = 16, N = 4$). 95

4.6 Comparison of the throughput versus penalty level ($K = 16, N = 8$). 95
4.7 Comparison of the throughput versus penalty level ($K = 16, N = 16$). 96
4.8 Comparison of the CDF of the total throughput for $\rho_{k,k'}$ ($K = 16, N = 4$). . 97
4.9 Comparison of the CDF of the total throughput for $\rho_{k,k'}$ ($K = 16, N = 8$). . 97
4.10 Comparison of the CDF of the total throughput for $\rho_{k,k'}$ ($K = 16, N = 16$). . 98
4.11 Comparison of the average total throughput versus the number of UEs ($N = 4$). 100
4.12 Comparison of the average total throughput versus the number of UEs ($N = 8$). 100
4.13 Comparison of the average total throughput versus the number of UEs ($N = 16$). 101
4.14 Comparison of the CDF of Jain's fairness index for UE ($N = 4$). 102
4.15 Comparison of the CDF of Jain's fairness index for UE ($N = 8$). 102
4.16 Comparison of the CDF of Jain's fairness index for UE ($N = 16$). 103
4.17 Comparison of the average total throughput versus the number of paths ($K = 16, N = 8$). 106
4.18 Comparison of the average total throughput versus variance of the inter-UEs position error ($K = 16, N = 8$). 106

5.1 Illustration of scalable CF-mMIMO systems with user-centric crustering. . 111
5.2 Illustration of multi-CPU CF-mMIMO systems. 112

List of Tables

3.1 Simulation Parameters. 59

4.1 Simulation Parameters. 90

List of Algorithms

1 Joint CF-mMIMO Beamforming and UL/DL AP Allocation via Geometric Mean Maximization for Single-Antenna UEs. 47
2 Joint CF-mMIMO Beamforming and UL/DL AP Allocation via Geometric Mean Maximization for Multiple-Antenna UE 50
3 Solver for Fraction Programming 89
4 Joint NAFD CF-mMIMO Beamforming and Resource Allocation 89

List of Acronyms

1G first generation.

2G second generation.

3G third generation.

4G fourth generation.

5G fifth generation.

6G sixth generation.

AMPS advanced mobile phone system.

AoA angle of arrival.

AoD angle of departure.

AP access point.

AR augmented reality.

ASD azimuth spread of departure.

AWGN additive white Gaussian noise.

BS base station.

C-RAN cloud radio access network.

CCP convex–concave procedure.

CDF cumulative distribution function.

CDMA code division multiple access.

CF cell-free.

CoMP coordinated multi-point.

CPU central processing unit.

CSI channel state information.

DAS distributed antenna system.

DC difference of concave.

DL downlink.

DNN deep neural network.

DoF degrees of freedom.

EE energy efficiency.

eMBB enhanced mobile broadband.

FD full duplex.

FDD frequency division duplex.

FDMA frequency division multiple access.

FP fractional programming.

GPS global positioning system.

HARQ hybrid automatic repeat request.

HD half duplex.

IMT international mobile telecommunications.

IoE Internet-of-everything.

IoT Internet-of-things.

IP internet protocol.

ITU international telecommunication union.

LDT lagrangian dual transform.

LoS line-of-sight.

LSF large-scale fading.

LTE long-term evolution.

M2M machine-to-machine.

MBRLLC mobile broadband reliable low latency communication.

MIMO multiple-input-multiple-output.

mMIMO massive MIMO.

MMSE minimum mean-squared error.

mMTC massive machine-type communications.

mmWave millimeter wave.

MR mixed reality.

MSE mean-squared error.

mURLLC massive URLLC.

NAFD network-assisted full duplex.

NLoS non-line-of-sight.

NMT nordic mobile telephone.

OFDM orthogonal frequency division multiplexing.

PSTN public switched telephone networks.

QCP quadratically constrained program.

QoS quality of service.

QT quadratic transform.

QZSS quasi-zenith satellite system.

RRSSI relative received signal strength indicator.

RSSI received signal strength indicator.

SC-FDMA single carrier-frequency division multiple access.

SCA succesive convex approximation.

SDR software defined radio.

SE spectral efficiency.

SI self-interference.

SINR signal-to-interference-and-noise ratio.

SNR signal-to-noise ratio.

SNS social networking service.

SotA state-of-the-art.

TACS total access communications system.

TD-SCDMA time-division synchronous code division multiple access.

TDD time division duplex.

TDMA time division multiple access.

UE user equipment.

UL uplink.

ULA uniform linear array.

URLLC ultra reliable low latency communications.

USRP universal software radio peripheral.

VoLTE voice over LTE.

VR virtual reality.

WCDMA wideband code division multiple access.

WLAN wireless local area network.

ZF zero-forcing.

Notation

$\mathbb{C}$	the field of complex numbers
$\mathbb{R}$	the field of real numbers
$\mathbb{E}_a[\cdot]$	the expectation operation over a
$(\cdot)^*$	the conjugate of a complex value
$(\cdot)^{\mathrm{H}}$	the conjugate transpose of a vector/matrix
$(\cdot)^{\mathrm{T}}$	the transpose of a vector/matrix
$\boldsymbol{I}_N$	the N-order identity matrix
$\boldsymbol{O}_{N,M}$	the $N \times M$ zero matrix
$\boldsymbol{X}^{-1}$	the inverse of square matrix $\boldsymbol{X}$ (if it exists)
$\| \boldsymbol{x} \|_p$	the ℓ_p-norm of vector $\boldsymbol{x}$
$\mathrm{Tr}(\boldsymbol{X})$	the trace of square matrix $\boldsymbol{X}$
$\mathrm{diag}(\boldsymbol{x})$	the diagonal matrix with the elements of vector $\boldsymbol{x}$
$\mathcal{A} \setminus \mathcal{B}$	the set whose elements are in set $\mathcal{A}$ but not in set $\mathcal{B}$
$\mathcal{CN}(\mu, \sigma^2)$	the circularly-symmetric complex-valued Gaussian distribution with the mean μ and the variance σ^2
$\mathcal{CN}(\boldsymbol{\mu}, \boldsymbol{\Sigma})$	the multi-dimensional complex-valued Gaussian distribution with the mean $\boldsymbol{\mu}$ and the covariance matrix $\boldsymbol{\Sigma}$
$\lceil \cdot \rceil$	the ceiling function
$\log_a(x)$	the logarithm of x to base b

Chapter 1

Introduction

1.1 Motivation

1.1.1 Cellular Network Evolutions

Wireless communication is currently the core technology in an advanced information society that connects people via a network infrastructure. The first mobile phone service commenced operations in Saint Louis in 1946, which was for in-vehicle voice calls via public switched telephone networks (PSTN). This system, which only prepared six voice channels in the city, had limited communication capacity [1]. Hence, the use of finite frequency resources suitable for maximizing the number of users accommodated in the network was investigated. Accordingly, the cellular network, which divides a service area into a number of cells and repeated use of several frequencies in different cells, was proposed by AT&T Bell's Laboratory [1]. The technical innovation of a cellular network facilitated an explosive evolution in wireless communication systems carried through to today. The remainder of this section describes the history behind the standardization of mobile wireless communication systems and modern requirements. Fig. 1.1 shows a brief evolution from first generation (1G) to fifth generation (5G), which is currently in commercial use.

The 1G cellular network systems were analog systems and developed to provide voice calls for vehicles in 1980. These systems were operated by frequency division multiple access (FDMA) using analog modulation with circuit-switched controls, such as an advanced mobile phone system (AMPS) for the US, total access communications system (TACS) for the UK, and nordic mobile telephone (NMT) for North Europe [1].

At the end of the 1G period, mobile phones were widely used by businesspeople because the devices became portable, although they remained heavy. In the second generation (2G), generally called the global wireless communications system, a significant capacity increase

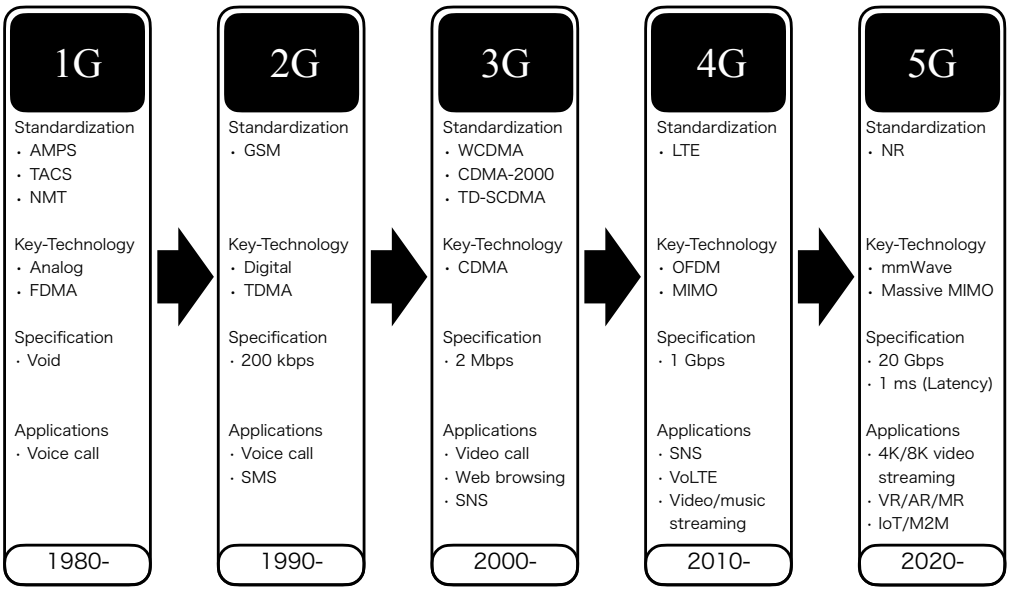

Fig. 1.1 Evolution of the Cellular Network Generations.

was introduced via digitalized communication using time division multiple access (TDMA) [2, 3]. Cost reduction of equipment owing to digitalization facilitated the explosive spread of cell phones. Simultaneously, simple text messaging and data communications of up to 200 kbps were realized by achieving large capacity. The third generation (3G) was standardized based on the international mobile telecommunications (IMT)-2000 recommendations from the international telecommunication union (ITU). IMT-2000 requires a data rate higher than 2 Mbps while fixed [4]. To achieve this requirement, each country deployed code domain multiplexing using code division multiple access (CDMA), such as wideband code division multiple access (WCDMA), CDMA-2000, and time-division synchronous code division multiple access (TD-SCDMA) [5].

With the advent of social networking service (SNS) and smartphones, academic and industrial communities conducted studies on increasing wireless communication capability to meet the skyrocketing demand for high throughput, corresponding to the growing information society. Hence, the fourth generation (4G), also called long-term evolution (LTE), was launched in 2012 using a combination of orthogonal frequency division multiplexing (OFDM), single carrier-frequency division multiple access (SC-FDMA), and multiple-input-multiple-output (MIMO) technologies [6]. The most notable technological evolution in 4G was the opening up of the spatial domain using MIMO and frequency domain signal processing. This spatial domain expansion exponentially increases the capacity of the network. Consequently, these technologies can reach data rate of up to 1 Gbps, including stable and low-latency communication for 4G. However, with the advent of smartphones,

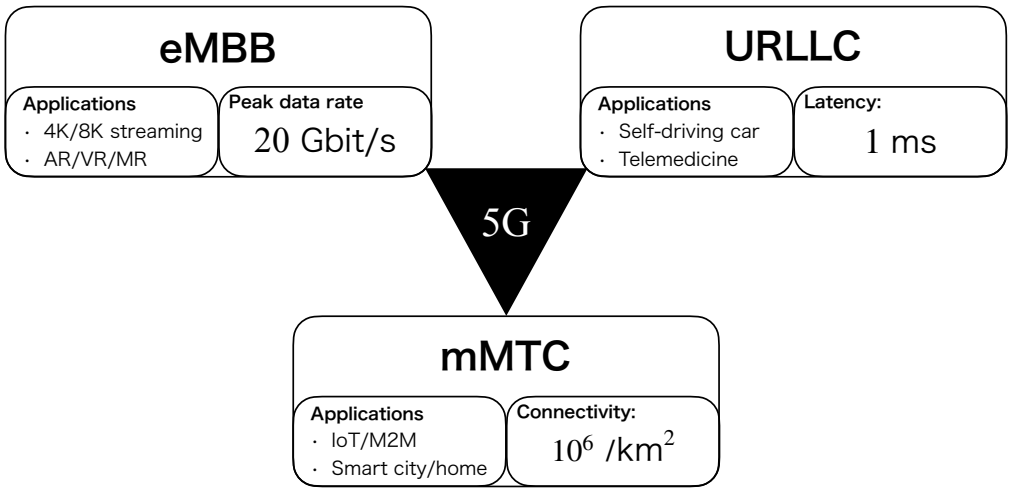

Fig. 1.2 Illustration of the summary of the 5G use cases.

internet content diversification has exploded and these technologies can no longer support demand on their own. From a traffic perspective, for example, communication methods, such as voice and video calling and instant messaging, have changed to voice over internet protocol (IP), also called voice over LTE (VoLTE), and modern messaging applications via SNS [7]. In addition, media streaming services have been developed with approximately 50% of the monthly mobile traffic in mid-2017 [8]. The increase in traffic caused by these factors is evidenced by reports published by Ericsson [8] and Cisco [9]. Other new applications, such as telemedicine, Internet-of-things (IoT), augmented reality (AR), virtual reality (VR), mixed reality (MR), smart cities, and connected cars, are expected to increase the number of wireless terminals and the demand for low-latency communications further. Novel concepts of 4G will enable the adoption of wireless communication systems in broader fields.

Therefore, unlike the evolution that primarily focused on increasing data rate until 4G, The 5G wireless communication systems are required to support a more diverse quality of service (QoS) requirements. Consequently, three important requirements and use cases of 5G systems, which are summarized in Fig. 1.2, were advocated by the IMT-2020 recommendations of ITU, which are as follows [10, 11]:

- Enhanced mobile broadband (eMBB) considers human-centric applications with super-high data rates and large-capacity requirements for media services, such as 4K/8K video streaming, AR, VR, and MR.

- Ultra reliable low latency communications (URLLC) attempts to achieve a stable connection with the stringent requirements of low-latency applications such as self-driving cars, industrial automation, and sensor networks.

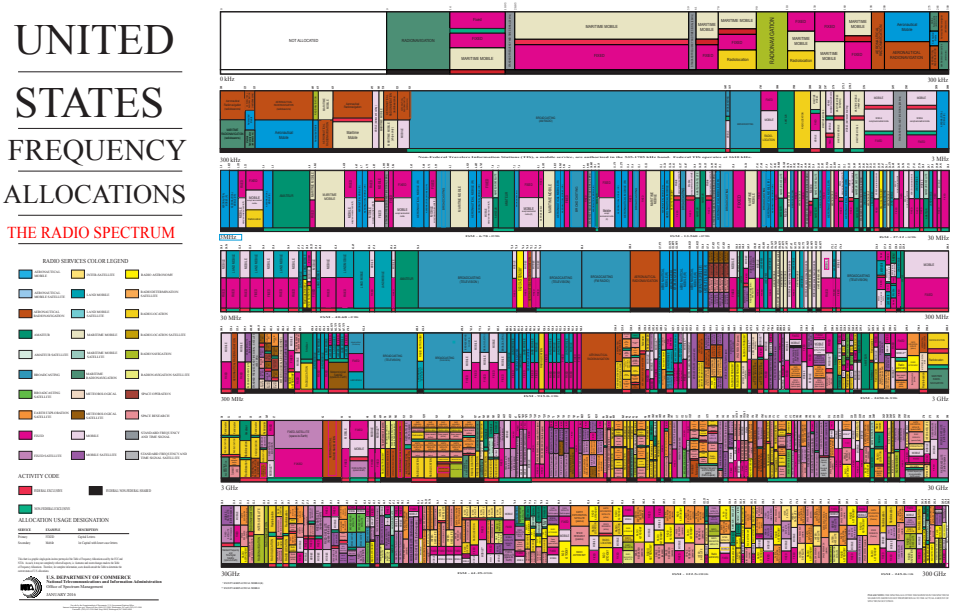

Fig. 1.3 Frequency allocations in the US [12].

- Massive machine-type communications (mMTC) supports device connections such as smart city/home, IoT networks, and machine-to-machine (M2M) communications.

Active use of time, frequency, and spatial domains is required to achieve these objectives. For the frequency dimension, OFDM is applied by following 4G and optimizing the use of in providing more bandwidth. However, the microwave bands used in 1G to 4G have been filling up with distributed bands dedicated to cellular communications, satellite, aerial communications, and wireless local area network (WLAN), and so on; hence, they are no longer available [12, 13]. Fig. 1.3 shows the summary of frequency allocations in the USA [12]. This figure shows that almost microwave bands are already allocated, and no further broadening of the bandwidth is possible. Consequently, in the 5G system, sub-6 GHz for long-distance communication and millimeter wave (mmWave) bands for ultra-high throughput are obtained to reserve a wider frequency band for communication. In particular, the mmWave band has achieved a broad bandwidth range, thereby contributing to the realization of extraordinarily high-speed and high-capacity communications. However, the mmWave band is significantly influenced by atmospheric attenuation [14–16]. More specifically, cellular systems have an inter-cell interference, where the transmitted signal of base station (BS) or user equipment (UE) at the edge of a cell is affected by neighboring cells. This interference is a critical limitation of cellular systems as it causes a trade-off between transmission power and interference in the design. To compensate for these effects, mitigating

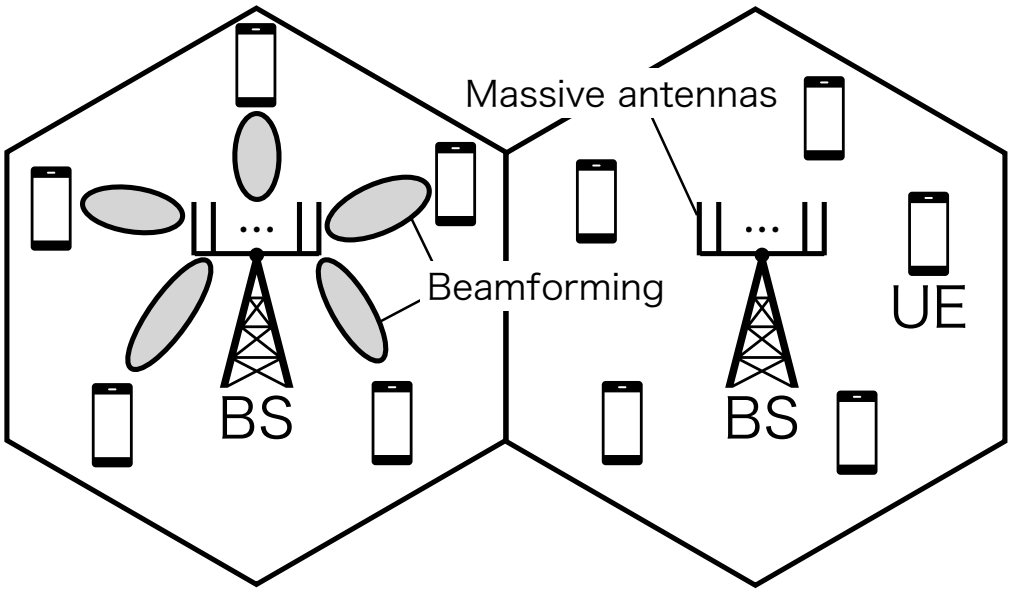

Fig. 1.4 Illustration of massive MIMO and beamforming technologies.

interference and ensuring propagation distance is ensured using beamforming. The massive MIMO (mMIMO) [17] technologies in Fig. 1.4 are used in 5G, where a large number of antennas are equipped at the BS to exploit spatial domain resources. This technology is made possible by the miniaturization of the antenna element due to shorter wavelengths. The mMIMO ensures the propagation distance and spatial partitioning of users by forming a sharp beam via high spatial degrees of freedom (DoF). In other words, in uplink (UL), all users transmit data to the BS over the same time-frequency resource, and the BS applies linear receive synthesis using a large number of channel observations to identify the desired signal from interfering signals. downlink (DL) users enjoy high-data rates separated in the spatial domain by receiving highly directional signals. With this highly spatially divided transmission support, mMIMO provides higher spectral efficiency (SE) than existing mobile systems [18, 19].

With mMIMO, we can efficiently utilize the DoFs of the frequency and spatial domains, but that of the time domain is not fully utilized. As the number of antenna elements and users increases, the temporal overhead for estimating the channels becomes very large. Therefore, UL training is used to take advantage of the channel duality in UL/DL using the same band, where users send pilot sequences simultaneously, and the BS collectively estimates the channel. Consequently, a time division duplex (TDD) is generally used for MIMO-based communication standards; this is true even for 5G. However, because the TDD orthogonally divides UL and DL users by time slots, there is always a standby user, thereby resulting in a bottleneck [20]. Furthermore, as the number of users increases, UL/DL traffic imbalances

are more likely to occur, thereby complicating the allocation of time resources. To mitigate this effect, a flexible/dynamic TDD is utilized to improve efficiency in the time domain. This technology monitors traffic conditions, and BS flexibly changes frame structure from 256 combinations of UL, DL, and Flexible symbols [21].

As mentioned above, 5G efficiently uses frequency, space, and time resources with dynamic TDD and mMIMO to meet increasingly sophisticated QoS requirements. However, data traffic continues to grow exponentially, and 5G technologies are expected not to be able to cope with future requirements. Consequently, we must consider the use cases and QoS requirements for sixth generation (6G) and beyond and develop technologies to satisfy them. The following section discusses the requirements for future wireless communications and the limitations of existing technologies.

1.1.2 Future Requirements

For 5G, three types of use cases must be addressed as explained above. However, momentum continues to accelerate as services diversify and expand. For example, the realization of extremely rich applications such as the Internet-of-everything (IoE), a further extension of IoT, metaverse, and real-time game streaming, has begun. Ericsson [22] reported that mobile traffic and the number of connections continue to increase exponentially and are accelerating. Based on [22], the company provides past and forecast data via Ericsson Mobile Visualizer [23]. For example, Fig. 1.5 shows the forecast of smartphone traffic which values generated by [23]. From this figure, we will be necessary to handle huge data traffic in the future. Therefore, the academic community is actively researching the QoS requirements and key technologies for the 6G. This suggests the need to further improve key technical requirements in 5G systems, at least in terms of peak data rates, connection density, latency, and energy efficiency (EE).

To identify the qualities required for 6G, as mentioned above, recent survey articles such as those in the literature [24–28] provide a quantitative analysis of QoS requirements.

For example, regarding 5G use cases, the performance requirements are as follows: [24]

- Data rate: 100 - 1000 times higher than 5G to support metaverse, 3D content, real-time game streaming, etc, by utilizing a high-frequency spectrum
- Latency: Undetectable (< 1 ms) or nonexistent latency times to support enhancing applications such as autonomous vehicles, metaverse, and medical imaging.

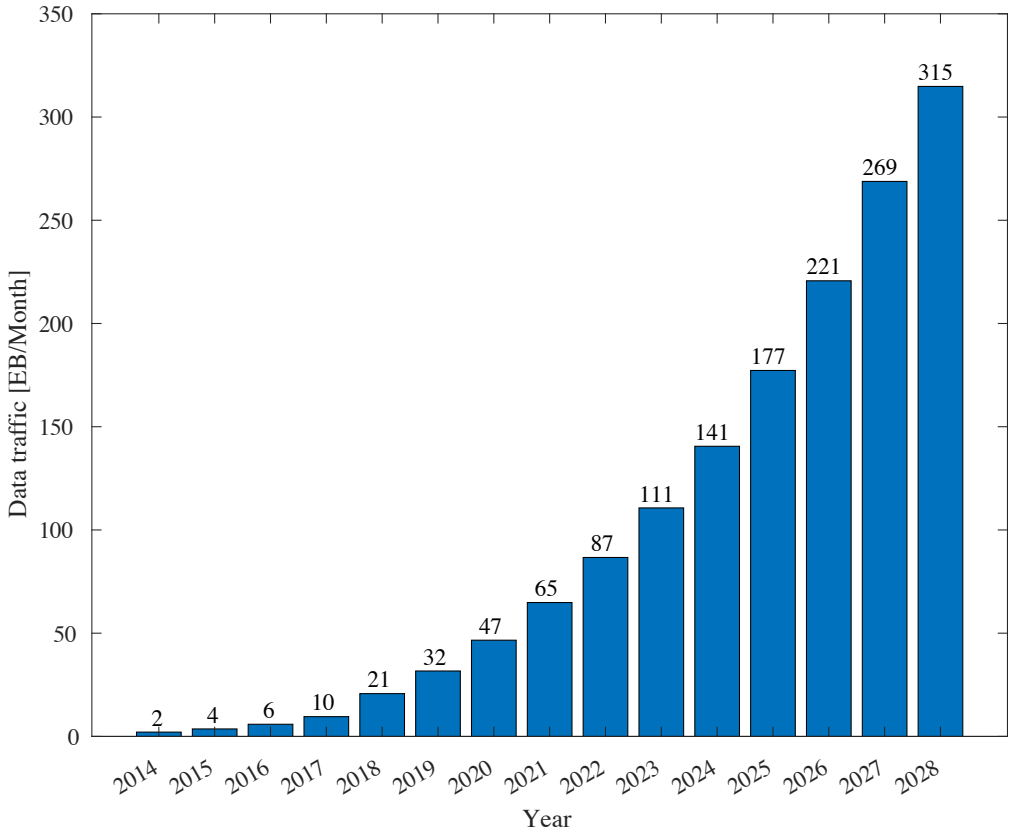

Fig. 1.5 Forecast of data traffic per month by Ericcson [23].

- Connective capacity: 10–1000 times greater than that of 5G system networks to support the IoE, which will enable flexible and efficient connectivity of more than 1 trillion levels of things rather than the current 1 billion levels of UE.

In addition, the applications supported by 6G include metaverse, autonomous vehicular/drone/robotics, IoE, and others that cannot be handled simply by satisfying the individual QoS described above. Therefore, as shown in Fig. 1.6, 6G use cases such as mobile broadband reliable low latency communication (MBRLLC) and massive URLLC (mURLLC), are said to not only satisfy the requirements of eMBB, URLLC, and mMTC individually but also impose a combination of them. In addition, many other requirements are being considered, all of which require the ultimate utilization of time, frequency, and spatial resources, far beyond 5G, to achieve their goals. Hence, similar to 5G, the expansion of each resource domain is necessary.

For the frequency and space domains, there is an extension to terahertz waves [29] and ultra-mMIMO [29]. The use of higher frequency bands triggers the attenuation of the propagation distance, leading to the densification of the network owing to the reduced cell size

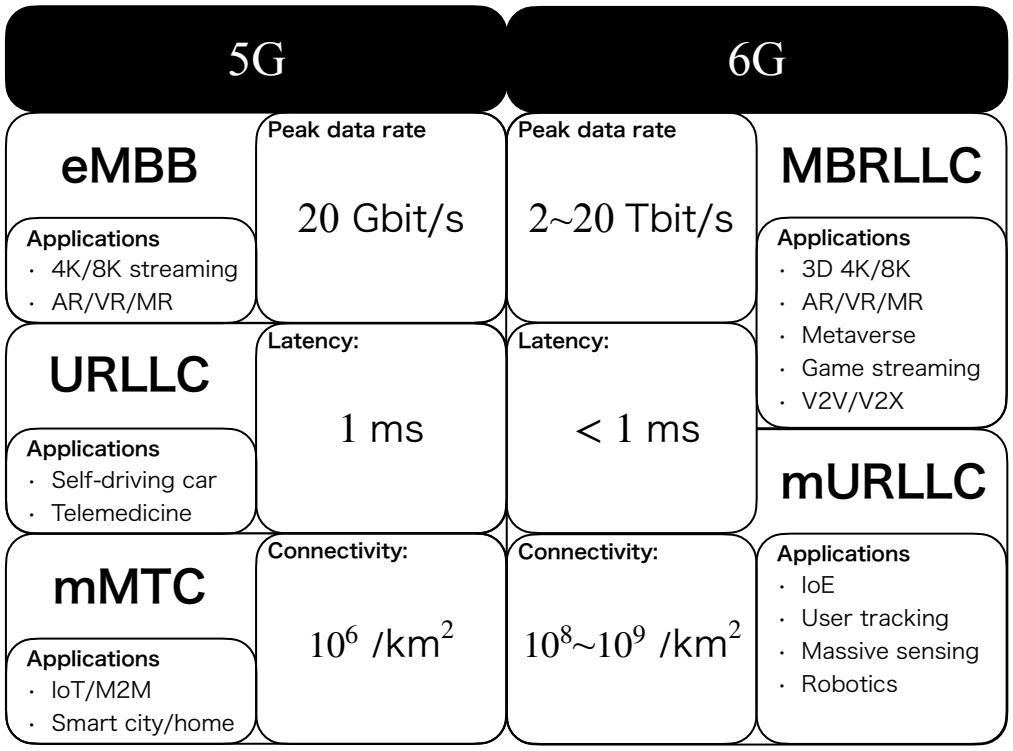

Fig. 1.6 Comparison of the 5G and 6G requirements [24].

[30]. An excessive network density creates several critical challenges. First, excessive network densification leads to uncontrollable inter-cell interference, which limits the overall network throughput [31–34]. Second, the most considerable current limitation of ultra-mMIMO and mMIMO is the correlation between the antennas. Theoretical and experimental studies have demonstrated that this spatial correlation limits the performance of mMIMO, which impossible to take advantage of spatial DoF using a large number of independent channels [35, 36].

In the time domain, TDD with the conventional frame structure in 5G can no longer be used for fatal overhead because the number of standby times for users exponentially increases in future systems. Therefore, full duplex (FD) communications are garnering attention to accommodate users more flexibly and efficiently. In FD communications, BS antennas are allocated into UL and DL and transmit and receive the signals simultaneously [37, 38]. However, FD communication is not realistic from the perspectives of hardware limitations and interference elimination owing to a large amount of interference within the BS, called self-interference (SI) [39, 40]. Moreover, inter-UL-DL interference makes the inter-cell interference larger and more complex than dynamic TDD systems This inter-UL-DL

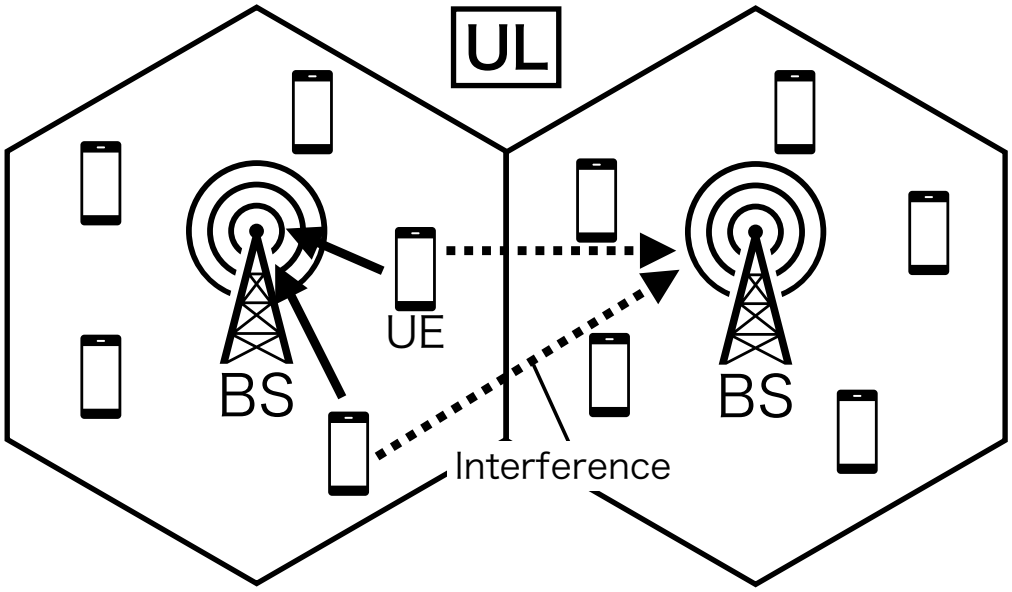

Fig. 1.7 Illustration of the inter-cell interference in the cellular networks.

interference cannot be dealt with unless the transmission signals of BSs or UEs in other cells are somehow known.

Thus, the spatial and temporal tightness of the network leads to an increase in interference, which inevitably limits the performance in terms of signal-to-interference-and-noise ratio (SINR) [41]. These problems emerge because conventional cellular networks have an inflexible network-centric structure, in which functions are densely concentrated in a single BS, and cells are formed based on BS. Therefore, meeting future demands will require fundamentally rethinking the current wireless system, including the concentration of functions in cellular networks and BS. This implies that a user-centric design that flexibly optimizes the entire network design in response to user requirements is essential for next-generation communication systems.

1.1.3 User-Centric Communication

In conventional cellular networks, each UE is connected to only one BS out of many cells. Fig. 1.7 shows a cellular network focusing on two cells. Looking at the cell on the left, the signal transmitted by the UE to the BS reaches the BS in the neighboring cell across the cell. The BS in the right cell cannot know the information needed to eliminate interference, resulting in inter-cell interference. In addition, as already mentioned, spatial network densification due to cell shrinkage and an increase in the number of active UEs simultaneously due to dynamic TDD cause additional interference. However, attempts have already been made

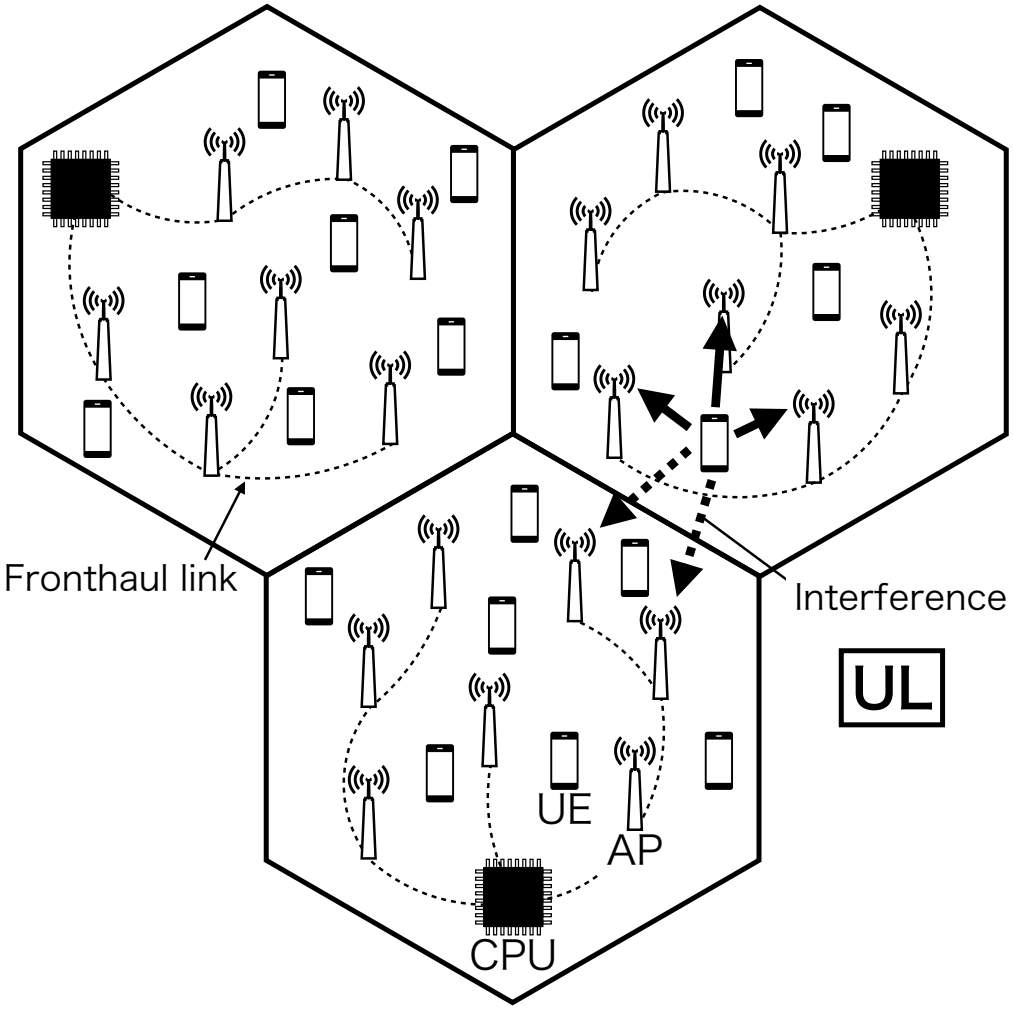

Fig. 1.8 Illustration of the distributed antenna systems.

to form clusters of BSs under certain rules with the user at the center and to communicate by considering the interference generated by all BSs involved. Such transmission designs have been considered in cooperative network MIMO, coordinated multi-point (CoMP) [42], cooperative small cells, and cloud radio access network (C-RAN) [43]. In addition to these approaches, distributed systems have been studied to suppress the effects of spatial correlations in mMIMO. Because spatial correlation can be eliminated by increasing the distance between antennas sufficiently, distributed systems such as distributed antenna system (DAS) [44, 45] have been studied, as illustrated in Fig. 1.8. These architectures split the BS function into two parts; an access point (AP) and a central processing unit (CPU), which are connected via fronthaul. The AP is responsible for signal transmission and reception, while the CPU is responsible for signal processing. The APs are distributed within a cell to

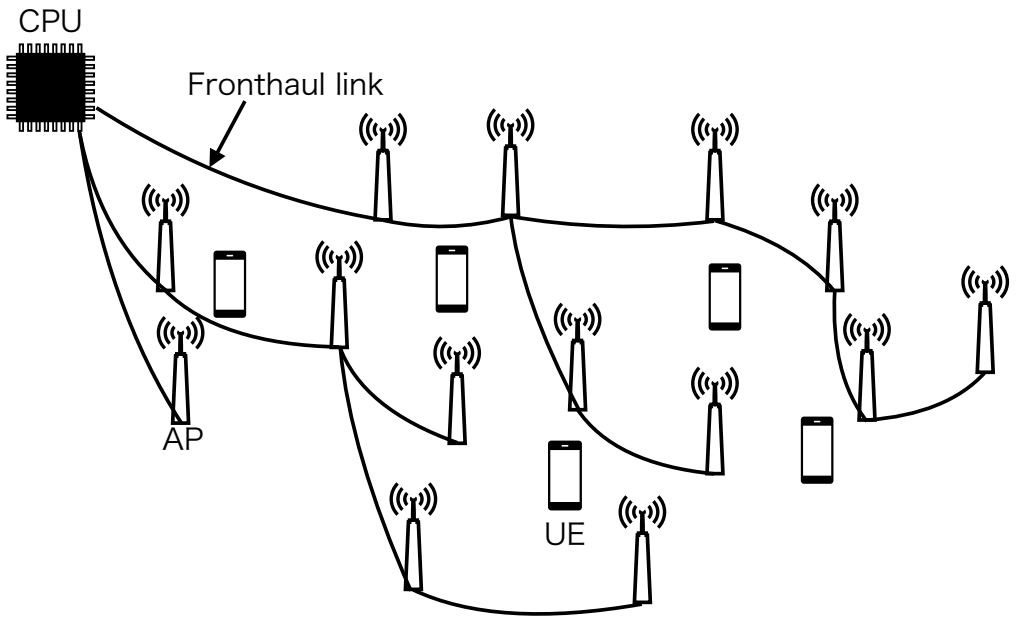

Fig. 1.9 Illustration of the cell-free massive MIMO systems.

increase the distance between the antennas and suppress spatial correlation. We consider combining these ideas to form a massive network. Namely, all cooperating BSs are replaced by APs and distributed, and interference is controlled via the CPU. As a result, this system can eliminate interference between cells by functioning as if the cell boundaries have disappeared. The combination of mMIMO operation and the cooperated/distributed network topologies brings high flexibility to wireless networks. This flexibility enables network optimization for each user, resulting in the new concept of user-centric communication by a cell-free (CF)-mMIMO as illustrated in Fig. 1.9 [46–48]. Owing to the antenna distribution strategy of CF-mMIMO systems, the spatial DoF due to the spatial correlation can be significantly reduced. Thus, enabling the ideal performance of the original mMIMO concept without the cell-edge effect to be reached. In fact, [49] compares the throughput characteristics of small cells and CF-mMIMO, and demonstrates that the latter performs better.

The introduction of the CF concept hints at the possibility of resolving the problems of inter-cell interference and spatial correlation. However, users have several actual traffic demands. Therefore, it can be inferred that a truly user-centric design cannot be achieved, provided the operation is confined to TDD. In particular, in CF-mMIMO, all the UEs belong to the same network in a service coverage area larger than the cell. Therefore, flexible and dynamic TDD designed for cellular applications cannot be utilized. Techniques that were previously adapted on a per-cell basis cannot be used in CF-mMIMO systems. This implies that the technical assets developed up to 5G for TDD, to handle traffic changes, imbalances

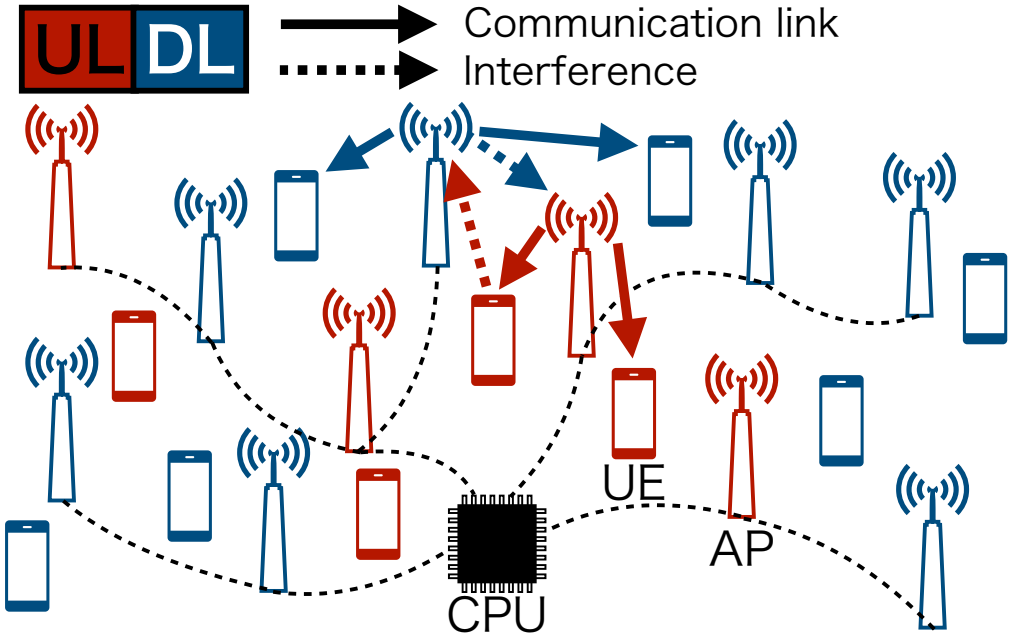

Fig. 1.10 Illustration of the network-assisted full-duplex cell-free massive MIMO systems.

cannot be adopted, and the problem of overhead due to standby users recurs, thus resulting in fatal data-rate limits and delays. Consequently, CF-mMIMO in TDD is not user-centric because it imposes significant constraints on the user at the convenience of the network. To fundamentally address this problem, it is necessary to consider FD communication. FD communication is a user-centric system because it completely eliminates the problem of standby users and allocates antenna resources based on the communication traffic demand with the user at the center. However, the strong SI makes its realization quite difficult. In distributed systems, such as CF-mMIMO and DAS, the AP can be considered single or several antennas. Because the number of AP antennas cannot be increased due to cost and the amount of data transmitted in the fronthaul. Therefore, assigning UL/DL to each AP can achieve network-assisted full duplex (NAFD), which makes the entire network appear as FD communication. In other words, in the NAFD approach as shown in Fig. 1.10, APs operate in the conventional half duplex (HD) mode, and each AP is allocated to either UL or DL transmissions. Accordingly, the network can be regarded as FD [50] due to UL/DL communication simultaneously whole service coverage area. In other words, NAFD is not occurred the SI owing to APs only communicating by UL/DL in contrast to FD. However, inter-UE and inter-AP interference occur instead of dynamic TDD and FD inter-UL-DL interference. We note that the aforementioned works should be distinguished from FD CF-mMIMO systems, which each AP is capable of FD transmission. In this context, we

focused on NAFD CF-mMIMO, to satisfy the system requirements for 6G and beyond. The realization of user-centric communication based on this new architecture maximizes spatial frequency utilization efficiency through extreme multiplexing in the temporal and spatial axes. This becomes one of the upper bounds of throughput that the physical layer can provide to the upper layers. As such, NAFD CF-mMIMO is expected to be a core technology to meet next-generation communications' complex and high-performance requirements. However, a truly user-centric system must provide fair services to all UEs, regardless of their environments. To achieve this, SE and throughput must be maximized while maintaining fairness as far as possible. Therefore, the ultimate objective of this research is to achieve truly user-centric communication through fair, high-SE and high throughput design using NAFD CF-mMIMO.

1.2 Related Works

In this section, with the above background, we introduce several conventional approaches addressing fundamental challenges facing user-centric approaches.

1.2.1 Cell-Free Massive MIMO

We first present related work on HD CF-mMIMO operating with TDD. Because our system is naturally based on CF-mMIMO, knowledge of related studies will be beneficial in several areas. In particular, the topics in the following sections are closely related to NAFD CF-mMIMO issues such as interference cancellation and AP mode selection.

Beamforming Design

Beamforming suppresses interference by spatially multiplexing the users. Various design schemes have been proposed for beamforming design depending on its purpose. This section introduces common objectives and solutions. First, an optimized precoding strategy with power allocation for DL CF-mMIMO systems was proposed in [51], which attempted to maximize the minimum throughput among UEs based on a three-derived lower bound of the achievable throughput of the system. A theoretical performance analysis of UL CF-mMIMO systems with either zero-forcing or conjugate beamformers were presented in [52] where power allocation strategies based on a tight approximation of the capacity were proposed. Recently, a joint design of analog beam selection and precoding was proposed in [53] to reduce power consumption while enhancing performance. Moreover, the overall energy efficiency in DL CF-mMIMO systems was considered in [54], in which an energy-efficient

joint power allocation and precoding scheme was designed using optimization and game theories. In the literature [55], a beamforming design using a tensor decomposition algorithm is proposed assuming a heterogeneous network where each user has a different number of antennas.

Resource Allocation

Another challenge of CF-mMIMO systems is the optimization of the allocation of UE to APs. Related to the former problem, a joint power allocation and a user-AP connection design scheme were proposed in [56] to maximize the system throughput in the TDD mode. A similar attempt to optimize AP UL/DL selection was investigated in [57] for energy-efficient green CF-mMIMO systems, which proposed a dynamic AP ON/OFF strategy depending on traffic demand. A joint power allocation and user-grouping method under QoS constraints for the DL of TDD CF-mMIMO systems was designed in [58] via generalized Benders decomposition to minimize total power consumption. In addition, an AP selection method using channel quality indicator based on SINR without instantaneous channel state information (CSI) was considered in [59].

MmWave

Extending CF-mMIMO to mmWave is a must challenge to ensure wide bandwidth. However, only several studies of mmWave CF-mMIMO are available in the literature.

The first study extending CF-mMIMO to mmWave is in the literature [60]. In literature [60], the AP uses zero-forcing (ZF)-based hybrid beamforming, and the UE uses 0-1 beamforming, which is the summation of the transmitted/received signals. The results show high throughput under light loads. Comparing the original CF-mMIMO and the user-centric clustering confirms the latter's superiority. Literature [61] extends from literature [60] and proposes DL power allocation by power efficiency optimization using sequential and alternating optimization.

Literature [62] proposed a pilot allocation scheme considering fronthaul capacity limitation, a max-min power allocation combined with block coordinate descent and sequential linear optimization, and a fronthaul quantization optimization algorithm. The pilot allocation scheme is superior to the classical random one while reducing computational complexity. Furthermore, the trade-off between achievable maximum-minimum user rate, fronthaul requirements, and optimal hardware complexity was confirmed. In addition, literature [63] proposed a downlink hybrid beamformer and max-min resource allocation dependent on instantaneous CSI and showed to achieve excellent max-min throughput.

In literature [64], a power-saving design was proposed by dynamically switching the APs on and off, assuming low traffic loads, and showed that the achievable power efficiency could be significantly improved.

Scalability

Scalability is usually a limitation of CF-mMIMO systems, where there are no clear system boundaries between cells. This is because actual systems do not have unlimited computational and communication resources hence, it is necessary to establish a demarcation somewhere. Because this study focuses on user-centric communication using NAFD and CF-mMIMO, scalability is out of scope; however, it is an important issue for CF systems and is therefore presented here. The early paper [65] declares that a scalable system must guarantee the complexity and resource requirements of signal processing to each AP must be finite when the number of users to infinity. The authors also show that this could be achieved through CSI estimation and minimum mean-squared error (MMSE) beamforming design based on user-centric clustering. For example, some papers [66, 67] consider multi-CPU CF-mMIMO, which distributes the computational load of signal processing by connecting multiple CPUs with backhaul and cooperative operation. In addition, a novel fronthaul topology enabling APs to share a serial fronthaul link with a per-user limited fronthaul bandwidth was considered in [68]. Similarly, a user-centric clustering and AP selection problem for UL TDD CF-mMIMO systems were addressed in [69].

1.2.2 Network-Assisted Full-Duplex

In this subsection, we present NAFD and similar studies. Because the idea of NAFD is core to this research, a comprehensive introduction is provided, from early investigations to the present study with CF-mMIMO.

Early Studies

In the first study of NAFD, the asymmetric and rapidly varying UL and DL traffic utilized the dynamic TDD with C-RAN systems. In [70], the authors proposed a simultaneous communication scheme for C-RANs in which UL/DL is allocated to radio remote heads, which be equivalent to APs of CF-mMIMO, operating in the HD mode connected to a centralized baseband unit poll, such that the network can operate in FD mode. The authors proposed a power allocation and beamforming design algorithm based on the EE maximization problem considering additional interference and verified the superiority of EE over conventional TDD C-RAN systems.

A similar proposal from the same period is an in-band FD communication in CoMP called CoMPflex [71]. This study analyzed the EE and sum rate for NAFD with inter-BS cooperation. In addition, the authors mentioned that this technology solves the hardware requirement of addressing self-interference, which is the most significant challenge in FD.

Dynamic TDD

Because UL/DL ratios are flexibly assigned to APs, which are regarded as BS, they are sometimes referred to as dynamic TDD. For CF-mMIMO systems, the study in [72] considered a dynamic TDD allocation scheme with different UL/DL ratios for some UE clusters to suppress packet delays, which is the delay of the queueing caused by packet arrivals. This scheme is similar to cellular dynamic TDD rather than NAFD, although there are parts of timeslots where simultaneous UL/DL communication occurs in the network. However, instead of deviating from the NAFD concept, it allows flexible changes in the trade-off between interference, delay, and computational complexity. However, the UE communication delay cannot be completely prevented because it operates in a TDD within each cluster. Note that this dissertation's discussion of the delay times is out-of-scope because these trade-offs do not occur in the perfect NAFD. Nevertheless, the study in [72] demonstrates that NAFD avoids standby UEs and contributes to high SE performance canceled the packet delay.

In [73], cellular FD and HD, TDD, and dynamic TDD (NAFD) cell-free systems were compared, and it was verified that NAFD CF-mMIMO achieved better SE performance than the others. Finally, in [74], the authors evaluated the actual equipment in terms of packet error rate for CF-MIMO communication in UL, DL, and dynamic TDD (NAFD) using universal software radio peripheral (USRP), which is a software defined radio (SDR) device. Although this study is a validation with a single UL/DL UE, verification experiments of distributed mMIMO have already been conducted in [75], thereby demonstrating the possibility of extending NAFD to CF-mMIMO.

Massive Antenna Systems

NAFD studies for massive antenna systems have assumed massive DAS or CF-mMIMO systems. The earliest study of NAFD in massive DAS is provided in the literature [76]. The literature [76] a simple AP allocation scheme that clusters by threshold and sorted signal-to-noise ratios (SNRs) for SE maximization in a CF-mMIMO network. The most significant point of this study is that it follows the strict definition of CF-mMIMO in terms of using the maximum ratio combiner.

Active studies in this area have been conducted by You et al. In the literature [77], the authors proposed deterministic SE analysis using the MMSE combiner and ZF precoder. In addition, literature [78, 79] proposed an AP mode selection and beamforming design scheme via semidefinite relaxation based on the total SE maximization problem.

Next, in [80–89], the authors studied various extensions and challenges of NAFD in CF-mMIMO. This method is shared with power transmission and energy harvesting in [80, 81] and extended the physical-layer security with artificial noise in [82, 83]. References [84, 85] replaced sum-rate maximization with mean-squared error (MSE) minimization and proposed AP allocation and beamforming design schemes based on succesive convex approximation (SCA) and Q-learning. Reference [86] solved the UL/DL mode allocation of APs by Q-learning using the total rate obtained from the allocation of user resource blocks based on traffic volume as the objective function. References [87–89] focused on interference and CSI estimation in the NAFD. Reference [87] focused on inter-UE interference and proposed an AP allocation scheme to minimize it. Reference [89] presents an ergodic analysis of data rates in the presence of pilot contamination and references [88] proposed a beam-training-based DL CSI estimation and pilot design inter-AP-UE and inter-AP for interference canceller design.

In most of the literature, with the exception of [89, 88], the CSI (inter-AP-UE, inter-AP, and inter-UE) is assumed to have a full or estimated noise-added CSI. In this study, we follow other references and assume that the CSI information is perfectly known to verify the upper-bound performance of methods proposed in our dissertation. However, in Chapter 4, we discuss the most significant problem in NAFD, which is inter-UE CSI estimation.

Finally, we introduce a study on URLLC, one of the latest QoS requirements. Literature [90] compared NAFD, TDD, and frequency division duplex (FDD) using two latency metrics models considering a URLLC scenario. As a result, the authors confirm that NAFD has superior latency performance to the latter two and showing the NAFD approach contributes to the requirements of URLLC.

As we have introduced, most of the literature on NAFD focuses on sum rate and energy efficiency. This is because NAFD provides network flexibility and high throughput via simultaneous UL/DL communication; however, the increased interference makes it difficult to apply fairness-oriented designs, such as max-min. However, maintaining the fairness for all UEs is essential to keep the fairness of all UEs from the perspective of user-centric communication. Therefore, this study proposes a design that can maintain fairness while benefiting from the flexibility of NAFD in handling dynamic traffic.

1.3 Thesis Contributions and Outline

In this section, we describe our contributions and this dissertation outline.

1.3.1 Contributions

As mentioned in the previous section, although a few promising studies exist, several challenges remain in achieving user-centric communication. These issues can be summarized as follows:

- Several NAFD studies have attempted to maximize the total SE. Our proposal in this dissertation is based on a best-effort philosophy that attempts to maximize the total performance of the entire network. Consequently, power is not allocated to users with significantly poor channel conditions. Hence, the network design was severely unfair among users. However, considering user-centric communication, it is not acceptable to discard such users for the convenience of the network; therefore, the network must be designed to save them whenever possible.

- Radio resource allocation, such as the AP mode, AP power, and beamforming design are fragmented; NAFD requires tight coordination of those from the perspective of interference suppression. However, designs achieved using separate algorithms are undesirable because there are cases in which one design determines the performance characteristics.

- The consideration of multi-antenna UEs has not been studied. In future wireless systems, the number of antennas on a device will naturally increase [91–93], as has already been achieved [94, 95]. However, to the best of our knowledge, no study in the literature has considered multi-antenna UE in NAFD CF-mMIMO. Therefore, it is necessary to develop a system design that considers multiple antennas.

- The sub-6 GHz band and the mmWave band are essential for 5G and, later 6G wireless communication systems. Therefore, the design methods are needed that can be used in both bands.

- The control of inter-UE interference is an area for further study. Several studies claim that all channels can be estimated. However, inter-UE channel estimation is impractical because of increased overhead. Nevertheless, the performance impact of inter-UE interference is significant, especially in dense networks, where the distance between UEs is small. Therefore, it is necessary to consider the degree of the impact of inter-UE interference and how to handle it.

Therefore, this dissertation addresses the aforementioned issues by proposing several ways to achieve user-centric communication.

1.3.2 Outline

The overview of this dissertation is shown in Fig. 1.11. This dissertation is organized as follows:

Chapter 2: Overview of the Cell-Free Massive MIMO Systems

An overview of CF-mMIMO, the resource allocation/beamforming design schemes, and the TDD/NAFD is given, and the motivation for using NAFD CF-mMIMO in this dissertation is clarified.

Chapter 3: Joint Access Configuration and Beamforming for Cell-Free Massive MIMO Systems With Network-Assisted Full-Duplex

In the previous section, we have introduced several studies of NAFD CF-mMIMO systems. Their proposals are aimed at improving overall system throughput and energy efficiency. However, as shown in the two previous sections, the requirements for 6G and beyond require not only overall performance and a user-centric network design to solve their demands, such as reliability, data rate, and capacity. This requires resource allocation and beamforming to relieve disadvantage-channel users while improving the total throughput. To this end, we propose a joint AP access configuration and beamforming design scheme to improve throughput while avoiding per-user performance bias. We also consider single-antenna and generalized multi-antenna users corresponding to current and future mobile terminals. Numerical results demonstrate that the proposed method outperforms performance in terms of SE and fairness to state-of-the-art (SotA) techniques.

Chapter 4: Network-Assisted Full-Duplex with Localization-Aided Inter-User Channel Estimation for Millimeter-Wave Cell-Free Massive MIMO

As indicated in Section 1.1.2, future wireless communications will have to cope with ultra-high throughput requirements, and it is essential to utilize mmWave to ensure high bandwidth. Therefore, the NAFD CF-mMIMO system in the microwave band considered in Chapter 3 is extended to study NAFD CF-mMIMO for the mmWave band. The impact of inter-UE interference is expected to increase in the densely populated environment of UEs envisaged for systems using the mmWave band. In practice, estimation of the inter-UE channel is

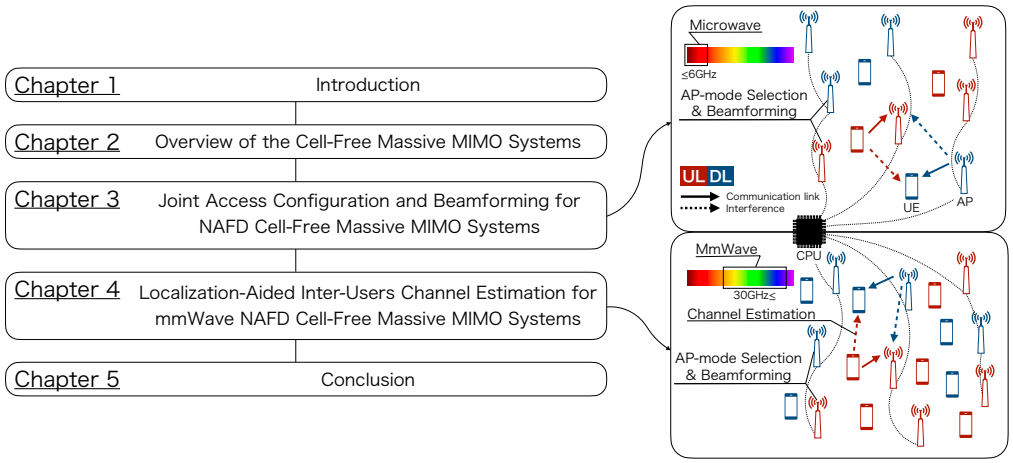

Fig. 1.11 The Overview of This Dissertation.

also difficult due to the estimation overhead. Therefore, we propose an inter-UE channel estimation scheme based on UE location information, utilizing the characteristics of mmWave channels. In addition, we propose a robust design that adds a penalty to the estimated inter-UE channel to prevent communication outages due to channel estimation errors

Therefore, joint resource allocation and beamforming design with location-aided channel estimation and inter-UE channel penalty is proposed to mitigate inter-UE interference and maximize performance. More specifically, we reconstruct the inter-UE channels based on a statistical channel model and knowledge of angle of arrival (AoA), angle of departure (AoD), and distance among UE's. Using these indirectly estimated inter-UE channels, adding the penalty, a beamforming design problem and AP mode selection aimed at interference suppression are formulated and solved efficiently via convex optimization. Computer simulations demonstrate the advantage of our proposed system quantitatively, confirming that the total throughput of the proposed method is the throughput performance close to the SotA with perfect inter-UE channel knowledge and made the throughput superior to the SotA without inter-UE channel knowledge and TDD. Despite these results, we also confirm that the proposed method has good fairness. In addition, these results also confirm sufficient robustness to user interference, the number of paths, and user location errors.

Chapter 5: Conclusion and Future Works

In this chapter, we conclude the dissertation and provide a perspective on future studies conducted in the PhD research.

Chapter 2

Overview of the Cell-Free Massive MIMO Systems

In this dissertation, we discussed the user-centric communication system based on NAFD CF-mMIMO. Therefore, in Chapter 3, a simultaneous design scheme for joint access configuration and beamforming is proposed to realize user-centricity with NAFD CF-mMIMO. This chapter presents the channel, received signal, beamforming, and multiplexing schemes of CF-mMIMO in order to help understand the advantages of NAFD CF-mMIMO. In addition, the challenges of conventional CF-mMIMO are summarized, and the advantages of NAFD CF-mMIMO are explained along with related studies.

2.1 Concept of Original Cell-Free Massive MIMO Systems

To discuss the concept of CF-mMIMO, we must first return to cellular mMIMO. Cellular mMIMO [17] achieves a higher SE by securing spatial DoF and UE multiplexing through beamforming by equipping the BS with massive antennas [18, 19]. However, the spatial correlation caused by the tight inter-antenna distance limits the SE performance because it does not ensure spatial DoF. In addition, cellular mMIMO is affected by inter-cell interference[1] caused by the transmitted signals of other cells, especially at the cell edge UEs, as shown in

[1]The impact of inter-cell interference is significant during channel estimation. This dissertation does not discuss it in detail because only the data communication phase is considered. In mMIMO, the channels of all UEs are estimated simultaneously by UL training using orthogonal pilot sequences. However, as the orthogonal pilot sequences are finite, they are shared between cells. Therefore, from inter-cell interference, the orthogonality of the series is lost as the same pilot sequence arrives at the BS. As a result, the estimated CSI is correlated with the UEs in other cells. The BS cannot separate the UEs in its own cell from those in other cells, which imposes a severe limit on throughput. This problem is called pilot contamination and is one of the key challenges in mMIMO.

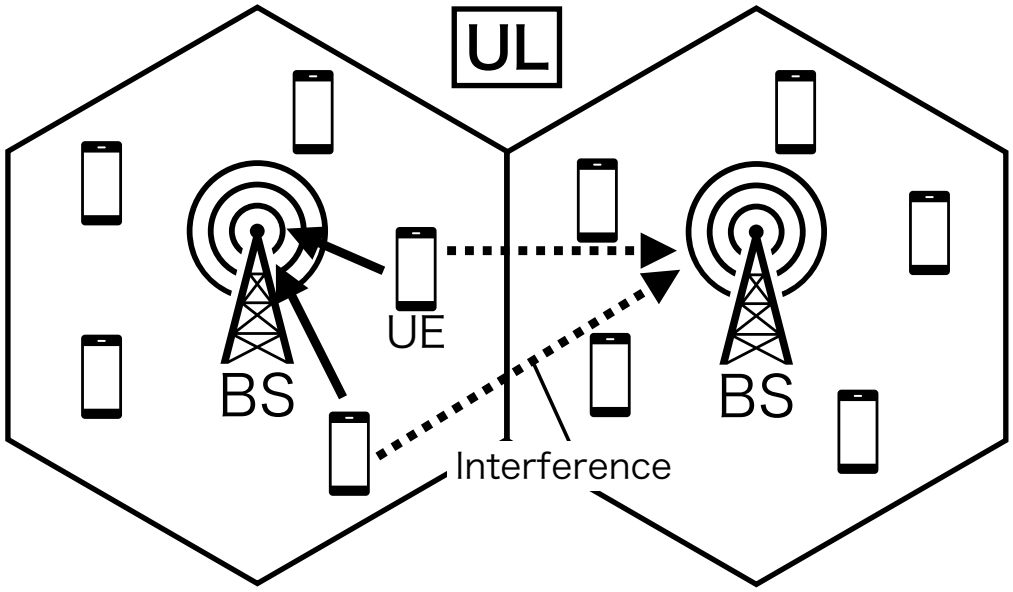

Fig. 2.1 Illustration of inter-cell interference in UL communication.

Fig. 2.1. The BS requires channel and transmission signal information for UEs in other cells to mitigate this interference. However, because each cell operates independently, there is no way to know them.

Distributed and inter-BS coordination systems have been studied as DAS and CoMP systems, respectively, to solve these issues. DAS distributes the APs for communication into a cell to reduce spatial correlation by securing inter-antenna distance. In literature [96, 97], cellular mMIMO was compared with distributed systems. The results show that the throughput of the distributed network is superior to that of cellular mMIMO owing to its high spatial DoF. CoMP enables the BS in each cell to cooperate in providing services to UEs by connecting them via fronthaul links, thus mitigating inter-cell interference. The original CF-mMIMO systems, shown in Fig. 2.2, are a more generalized and practical form of these systems.

This system divides the BS function into a CPU and distributed AP, with each corresponding fronthaul link via an optical fiber. By eliminating cell boundaries and distributing antennas, spatial correlation can be reduced, and spatial DoF is ensured. In addition, because all APs are managed by a single CPU, inter-cell interference can be canceled, as in a C-RAN. The performance of CF-mMIMO systems in terms of inter-cell interference has been compared with small-cell systems in terms of achievable DL/UL throughput [47, 46, 49]. The results show that the CF-mMIMO system provides a superior throughput over small cells. In addition, by applying max-min power control, a uniform service can be provided to all users in the coverage area. Owing to the aforementioned characteristics, CF-mMIMO

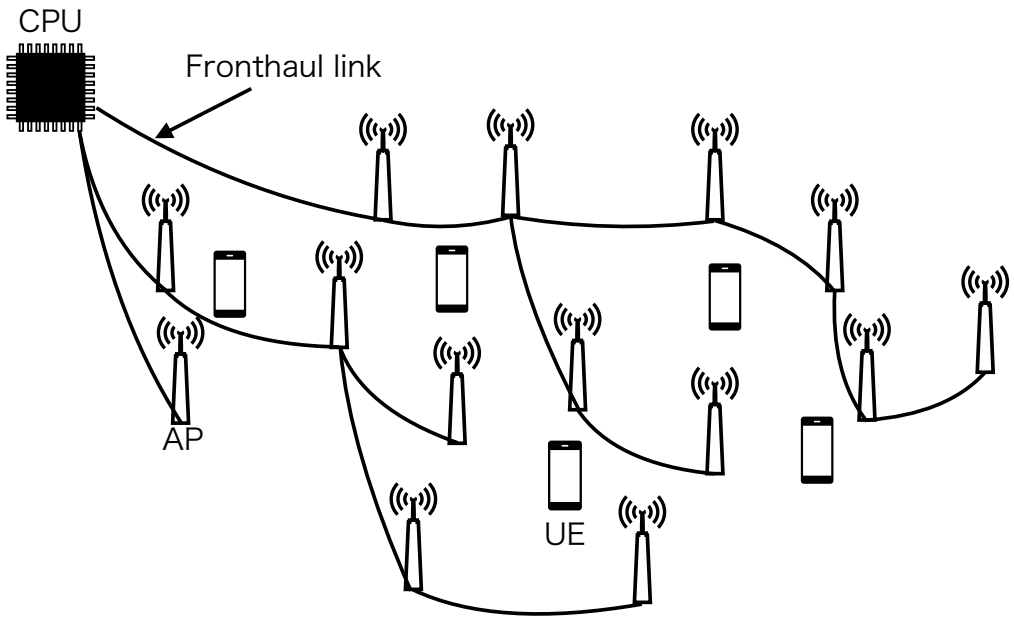

Fig. 2.2 Illustration of cell-free massive MIMO systems.

can be compared with mMIMO, especially by examining the channel model and received signal. Therefore, this section presents the received signal models used in many studies and introduces the differences with mMIMO. Most studies on CF-mMIMO use microwave models, as some studies have also considered models in the mmWave band, and each is described.

2.1.1 Channel Models

To clarify the advantage of CF-mMIMO, the signal models of cellular and CF- mMIMO need to be compared. Therefore, we first introduce the general MIMO channel models.

Microwave Band

The microwave band is very important for current and future wireless communication systems because its propagation and diffraction characteristics make it suitable for wireless systems. For this reason, many publications have considered the microwave band, and this dissertation is no exception. Therefore, an introduction to the channel models that are widely used in MIMO is presented. The correlated Rayleigh fading model is the most common model for mMIMO and CF-mMIMO, which considers inter-antenna correlation. A rice-fading model is also used by the line-of-sight (LoS) path when the inter-BS-UE and inter-AP-UE distances

are close. The comparison in this section assumes a correlated Rayleigh fading, which is the most widely used method.

First, we assume UEs are equipped with one antenna and the BS or AP with M antennas. Thus, the channel between the ℓ-th BS or AP and the k-th UE is given by

$$\boldsymbol{h}_{k,\ell} \sim \mathcal{CN}(\mathbf{0}, \boldsymbol{R}_{k,\ell}), \tag{2.1a}$$

where the small-scale fading matrices $\bar{\boldsymbol{H}}_{\ell,\ell'} \in \mathbb{C}^{M\times M}$ are modeled as $\text{vec}\left(\bar{\boldsymbol{H}}_{\ell,\ell'}\right) \sim \mathcal{CN}(\mathbf{0}, I_{M^2})$, and the matrices $\boldsymbol{R}_{k,\ell} \in \mathbb{C}^{M\times M}$ characterize the spatial correlation of the corresponding inter-UE-AP and inter-UE-AP communication channels.

It is important to note that in CF-mMIMO, the size of the spatial correlation matrix is determined by the number of antennas in the AP. This means that CF-mMIMO, where the AP has only one or several antennas, has no or negligible effect on the spatial correlation.

The spatial correlation model, corresponding to the MIMO channel model described above, has been considered in the past decades [98–100]. For example, a local scattering model based on a Gaussian angular distribution was considered in [101]. In contrast, a low-scattering angular-sparse model was studied in [102]. An azimuth spread of departure (ASD)-dependent flexible correlation model was investigated in [103], and a highly correlated scenario with a single scattered cluster was modeled by the one proposed in [104]. In particular, the local scattering model [105] is the most widely used for both mMIMO and CF-mMIMO [106, 107, 65].

MmWave band

To achieve the high throughput required for the next generation, the mmWave band is being intensively studied to ensure a wide bandwidth. Because mmWave waves have very high propagation attenuation, channel models comprising dominant LoS paths and several non-line-of-sight (NLoS) paths are widely used. In the literature [108], channel characteristics have been measured in the 28 GHz and 73 GHz bands, which are the most widely used in mmWave systems owing to their superior attenuation characteristics.

The mmWave channel between the $t \in \{k, \ell\}$-th transmitter and the $r \in \{k, \ell\}$-th receiver can be expressed as [108]

$$\boldsymbol{H}_{r,t} = \frac{1}{\sqrt{P}} \sum_{s=1}^{S} \sum_{p=1}^{P} \alpha_{r,t,p,s} \boldsymbol{a}(\boldsymbol{\psi}_{r,t,p,s}) \boldsymbol{a}(\boldsymbol{\psi}_{t,r,p,s})^{\mathrm{H}}, \tag{2.2}$$

where $\alpha_{r,t,p,s} \sim \mathcal{CN}(0, g_{r,t,p,s})$ denotes the small scale-fading with the channel gain $g_{r,t,p,s}$ for the p-th path between the t-th transmitter and the r-th receiver in the s-th scattering cluster,

$\boldsymbol{\psi}_{r,t,p,s} = [\phi_{r,t,p,s}, \theta_{r,t,p,s}]$ is a vector consisting of the p-th path AoAs or AoDs with azimuth angles $\psi_{r,t,p,s}$ and elevation angles $\theta_{r,t,p,s}$ in the s-th scattering cluster. In addition, $\boldsymbol{a}(\cdot)$ is the array response vector of the uniform linear array (ULA) in the APs or UEs given by

$$\boldsymbol{a}\left(\boldsymbol{\psi}_{r,t,p,s}\right) = \left[1, e^{-j\frac{2\pi}{\lambda}\nu(\boldsymbol{\psi}_{r,t,p,s})}, \ldots, e^{-j\frac{2\pi}{\lambda}(O-1)\nu(\boldsymbol{\psi}_{r,t,p,s})}\right]^{\mathrm{T}}, \tag{2.3}$$

where $O \in \{M, N\}$ is the number of antennas in the AP or UE; λ is the wavelength, and $\nu(\boldsymbol{\psi}_{r,t,p,s}) = \frac{\lambda}{2}\sin(\phi_{r,t,p,s})\sin(\theta_{r,t,p,s})$.

However, separating the paths of each scatterer cluster is in the practice of difficult. For this reason, many in the literature [24, 109–111] assume that the average of the paths arriving from a scatterer cluster is one path. Under such an assumption, one cluster can be approximated as one path. The mmWave channel between the $t \in \{k, \ell\}$-th transmitter and the $r \in \{k, \ell\}$-th receiver is given by [24, 109, 110]

$$\boldsymbol{H}_{r,t} = \sum_{p=1}^{P} \alpha_{r,t,p}\boldsymbol{a}(\boldsymbol{\psi}_{r,t,p})\boldsymbol{a}(\boldsymbol{\psi}_{t,r,p})^{\mathrm{H}}, \tag{2.4}$$

where $\alpha_{r,t,p} \sim \mathcal{CN}(0, g_{r,t,p})$ denotes the small-scale fading with the channel gain $g_{r,t,p}$ for the p-th path between the t-th transmitter and the r-th receiver, $\boldsymbol{\psi}_{r,t,p} = [\phi_{r,t,p}, \theta_{r,t,p}]$ is a vector consisting of the p-th path AoAs or AoDs with azimuth angles $\phi_{r,t,p}$ and elevation angle $\theta_{r,t,p}$.

The 28 GHz band is already in use for 5G, while the 73 GHz band is one of the candidates for 6G [112]. Furthermore, 73 GHz has been adopted in this dissertation because the channel characteristics have been verified by experiments in the literature [108]. Therefore, the 73 GHz large-scale fading (LSF) is given by [108]

$$\mathrm{LSF}^{73\mathrm{GHz}} = \begin{cases} 69.6 + 20\log_{10}(d_{t,r}) + z^{\mathrm{los}}_{t,r,1} & \text{LoS } (p = 1) \\ 86.6 + 24.5\log_{10}(d_{t,r}) + z^{\mathrm{nlos}}_{t,r,p} & \text{NLoS } (p \neq 1) \end{cases}, \tag{2.5}$$

where the $z^{\mathrm{los}}_{t,r,1} \sim \mathcal{N}(0, \sigma^2_{\mathrm{los}})$, $z^{\mathrm{nlos}}_{t,r,p} \sim \mathcal{N}(0, \sigma^2_{\mathrm{nlos}})$ are the shadowing with $\sigma_{\mathrm{los}} = 5.8$ [dB], $\sigma_{\mathrm{nlos}} = 8.0$ [dB] are the standard derivations of the log-normal shadowing.

In the mmWave channel, as in the microwave channel, CF-mMIMO is also less affected by inter-antenna correlation owing to the array response because of the small number of antennas in the AP.

2.1.2 Comparison of the Signal Model between the Cellular and Cell-Free Massive MIMO

Given the channel model described above, we compared cellular mMIMO and CF-mMIMO networks using the UL/DL signal model.

MMIMO and CF-mMIMO are assumed to operate in TDD mode respectively. The respective network parameters were as follows:

For the cellular mMIMO, we assume that B cells is in the service-coverage area. Each cell has one BS located at the center, and K UEs are randomly distributed. All UEs are equipped with a single antenna and transmit data signals simultaneously to the BSs in the same cell.

For CF-mMIMO, $K^{\text{ap}} = BK$ UEs distributed over the entire coverage area simultaneously transmits signals to the AP. The L APs are distributed at arbitrary locations and connected to a single CPU via the fronthaul. The UE and AP were equipped with 1 and $M^{\text{ap}} = M/L$ antennas, respectively.

Uplink

Under such an assumption, for cellular mMIMO, the UL signal vector $\boldsymbol{y}_b^{\text{bs}} \in \mathbb{C}^{M\times 1}$ received at the b-th BS can be written as

$$\boldsymbol{y}_b^{\text{bs}} = \sum_{k=1}^{K^{\text{bs}}} \sqrt{p_{k,b}}\boldsymbol{h}_{k,b} d_{k,b}^{\text{bs}} + \underbrace{\sum_{b'=1,b'\neq b}^{B} \sum_{k'=1}^{K} \sqrt{p_{k',b'}}\boldsymbol{h}_{k',b'} d_{k',b'}^{\text{bs}}}_{\text{Inter-cell interference}} + \boldsymbol{n}_b, \tag{2.6}$$

where $p_{k,b}$ is the k-th UE transmit power in b-th cell, $d_{k,b}^{\text{bs}} \in \mathbb{C}$ represents the data signal from the k-th UL UE in the b-th cell, and $\boldsymbol{n}_b \sim \mathcal{CN}(0, \sigma^2 I_M)$ is an additive white Gaussian noise (AWGN) vector with per-element variance σ^2. Here, the b-th BS has no way of knowing the CSI of the other cells or the transmitted signals. Therefore, the transmitted signals of the UE in the b'-th cell are uncontrollable inter-cell interference.

Next, for CF-mMIMO, the UL signal vector $\boldsymbol{y}_\ell^{\text{ap}} \in \mathbb{C}^{M^{\text{ap}}\times 1}$ received at the ℓ-th AP can be written as

$$\boldsymbol{y}_\ell^{\text{ap}} = \sum_{k=1}^{K^{\text{ap}}} \sqrt{p_k}\boldsymbol{h}_{k,\ell} d_k^{\text{ap}} + \boldsymbol{n}_\ell, \tag{2.7}$$

where p_k is the k-th UE transmit power, $d_k^{\text{ap}} \in \mathbb{C}$ represents the data signal from the k-th UE, and $\boldsymbol{n}_\ell \sim \mathcal{CN}(0, \sigma^2 I_{M^{\text{ap}}})$ is the AWGN vector with per-element variance σ^2.

The received signals in equation (2.6), (2.7) are combined at BS and AP, respectively. CF-mMIMO requires that the APs aggregate the combined received signals to the CPU before

the data signal estimation. Thus, the estimated data symbol of the k-th UE at the b-th BS can be written as

$$\widehat{d}_{k,b}^{\text{bs}} = \boldsymbol{v}_{k,b}^{\text{bs}\ \text{H}} \boldsymbol{y}_b^{\text{bs}}, \tag{2.8}$$

where $\boldsymbol{v}_{k,b}^{\text{bs}} \in \mathbb{C}^M$ denotes the combining vector at the b-th BS to detect the intended data transmitted by the k-th UL UE in b-th cell. Similarly, for CF-mMIMO, the estimated data symbol of k-th UE can be expressed as

$$\widehat{d}_k^{\text{ap}} = \sum_{\ell=1}^{L} \boldsymbol{v}_{k,\ell}^{\text{ap}\ \text{H}} \boldsymbol{y}_\ell^{\text{ul}} = \boldsymbol{v}_k^{\text{apH}} \boldsymbol{y}_\ell^{\text{ul}}, \tag{2.9}$$

where $\boldsymbol{v}_{k,\ell}^{\text{ap}} \in \mathbb{C}^{M^{\text{ap}}}$ denotes the combining vector at the ℓ-th AP to detect the intended data transmitted by the k-th UL UE.

The power of each data symbol from the UL UEs is normalized, and the SINR at cellular and CF- mMIMO can be respectively, written as

$$\Gamma_{k,b}^{\text{bs}} \triangleq \frac{p_k |\boldsymbol{v}_{k,b}^{\text{bs}\ \text{H}} \boldsymbol{h}_{k,b}|^2}{\sum\limits_{k=1,k'\neq k}^{K^{\text{bs}}} p_{k'} |\boldsymbol{v}_{k',b}^{\text{bs}\ \text{H}} \boldsymbol{h}_{k',b}|^2 + \underbrace{\sum\limits_{k\in\mathcal{K}_b}^{K^{\text{bs}}} \sum\limits_{k'=1}^{K} p_{k'} |\boldsymbol{v}_{k,b}^{\text{bs}\ \text{H}} \boldsymbol{h}_{k,b'}|^2}_{\text{Inter-cell interference}} + \sigma_{\text{bs}}^2 \left\|\boldsymbol{v}_{k,b}^{\text{bs}}\right\|_2^2}, \tag{2.10}$$

$$\Gamma_k^{\text{ap}} \triangleq \frac{p_k |\boldsymbol{v}_k^{\text{apH}} \boldsymbol{h}_k|^2}{\sum\limits_{k'=1,k\neq k'}^{K^{\text{ap}}} \sum\limits_{k'=1,k\neq k'}^{L} p_{k'} |\boldsymbol{v}_{k,\ell}^{\text{ap}\ \text{H}} \boldsymbol{h}_{k,\ell}|^2 + \sum\limits_{k'=1}^{K^{\text{ap}}} \sigma_{\text{ap}}^2 \left\|\boldsymbol{v}_k^{\text{ap}}\right\|_2^2}. \tag{2.11}$$

As mentioned previously, in cellular mMIMO, each cell operates independently. It can then be seen that the combiner cannot be designed by directly considering the second term in the equation (2.11). Thus the SINR is degraded owing to the inter-cell interference.

Downlink

In DL, the BS and AP transmit data symbols to the UEs over precoding. In addition, it is assumed that cellular mMIMO and CF-mMIMO operating in the TDD mode have UL/DL channel duality. Hence, the DL signal vector $\boldsymbol{y}_b^{\text{bs}} \in \mathbb{C}^{M\times 1}$ received at the b-th BS can be

written as

$$y_{k,b}^{\text{bs}} = \sum_{k=1}^{K^{\text{bs}}} \sqrt{p_{k,b}} \boldsymbol{h}_{k,b}^{\text{H}} \boldsymbol{w}_{k,b}^{\text{bs}} d_{k,b}^{\text{bs}} + \underbrace{\sum_{b'=1,b'\neq b}^{B} \sum_{k'=1}^{K} \sqrt{p_{k',b'}} \boldsymbol{h}_{k',b'} \boldsymbol{w}_{k',b'}^{\text{bs}} d_{k',b'}^{\text{bs}}}_{\text{Inter-cell interference}} + n_k, \tag{2.12}$$

where $p_{k,b}$ is the k-th UE transmit power in b-th cell, $d_{k,b}^{\text{bs}} \in \mathbb{C}$ represents the data signal for the k-th DL UE in the b-th cell, and $n_k \sim \mathcal{CN}(0, \sigma^2)$ is an AWGN vector with per-element variance σ^2.

Next, the UL signal vector $\boldsymbol{y}_{\ell}^{\text{ap}} \in \mathbb{C}^{M^{\text{ap}} \times 1}$ received at the ℓ-th AP can be written as

$$y_{k}^{\text{ap}} = \sum_{\ell=1}^{L} \sum_{k=1}^{K^{\text{ap}}} \sqrt{p_k} \boldsymbol{h}_{k,\ell}^{\text{H}} \boldsymbol{w}_{k,\ell}^{\text{ap}} d_{k}^{\text{ap}} + n_{\ell}, \tag{2.13}$$

where p_k is the k-th UE transmit power, $d_k^{\text{ap}} \in \mathbb{C}$ represents the data signal from the k-th UE, and $\boldsymbol{n}_{\ell} \sim \mathcal{CN}(0, \sigma^2 I_{M^{\text{ap}}})$ is the AWGN vector with per-element variance σ^2.

The data signal was estimated for each UE from the preceded received signal. For cellular mMIMO, the estimated data symbol of the k-th UE at the b-th BS can be written as

$$\widehat{d}_{k,b}^{\text{bs}} = y_{k,b}^{\text{bs}}, \tag{2.14}$$

Similarly, for CF-mMIMO, the estimated data symbol of k-th UE can be expressed as

$$\widehat{d}_{k}^{\text{ap}} = y_{k}^{\text{ap}}, \tag{2.15}$$

where $\boldsymbol{v}_{k,\ell}^{\text{ap}} \in \mathbb{C}^{M^{\text{ap}}}$ denotes the combining vector at the ℓ-th AP to detect the intended data transmitted by the k-th UL UE.

The power of each data symbol from the DL UEs is normalized, and the SINR at cellular and CF- mMIMO can be, respectively, written as

$$\Gamma_{k,b}^{\text{bs}} \triangleq \frac{p_k |\boldsymbol{h}_{k,b}^{\text{H}} \boldsymbol{w}_{k,b}^{\text{bs}}|^2}{\sum_{k=1,k'\neq k}^{K^{\text{bs}}} p_{k'} |\boldsymbol{h}_{k',b}^{\text{H}} \boldsymbol{w}_{k',b}^{\text{bs}}|^2 + \underbrace{\sum_{b'=1,b'\neq b}^{B} \sum_{k'=1}^{K} p_{k'} |\boldsymbol{h}_{k',b'}^{\text{H}} \boldsymbol{w}_{k',b'}^{\text{bs}}|^2}_{\text{Inter-cell interference}} + \sigma_{\text{bs}}^2}, \tag{2.16}$$

$$\Gamma_k^{\mathrm{ap}} \triangleq \frac{p_k \sum_{\ell=1}^{L} |\boldsymbol{h}_{k,\ell}^{\mathrm{H}} \boldsymbol{w}_k^{\mathrm{ap}}|^2}{\sum_{k'=1,k\neq k'}^{K^{\mathrm{ap}}} \sum_{\ell=1}^{L} p_{k'} |\boldsymbol{h}_{k',\ell}^{\mathrm{H}} \boldsymbol{w}_{k'}^{\mathrm{ap}}|^2 + \sigma_{\mathrm{ap}}^2}. \tag{2.17}$$

The above equation shows that cellular mMIMO suffers from inter-cell interference even in DL. Equations (2.10), (2.11), (2.16), and (2.17) show that CF-mMIMO has no inter-cell effects and has an advantage over cellular mMIMO in terms of interference suppression. In the next section, the design techniques for the power allocation and beamforming used in cellular mMIMO and CF-mMIMO are described.

2.2 Resource Allocation and Beamforming Design

In mMIMO, the power allocation and beamforming design are very important for interference control. Therefore, this section describes the beamforming design techniques that are widely used in mMIMO.

Beamforming design methods often use classical methods, such as the MMSE and ZF, and optimization-based design. This dissertation considers optimizing a network for user-centric communication. In addition, the geometric mean is used as the objective function to achieve total throughput and user fairness. Therefore, this section introduces an optimization-based resource allocation and beamforming design scheme and demonstrates the validity of using the geometric mean as the objective function.

2.2.1 Sum-Rate Maximization

First, we introduce a design scheme aimed at maximizing the total throughput. This scheme is referred to as the "sum-rate" maximization in most of the literature, followed in this dissertation. Sum-rate maximization, as the name implies, aims to maximize the throughput of the entire network. As such, it is often used in the literature considering the eMBB use case to show the upper bounds of network performance. However, this design preferentially allocates power to users in a good channel state. This is because users with poor channel states naturally have a smaller maximum throughput. For example, in literature [113], hybrid beamforming by deep neural network (DNN) with received signal strength indicator (RSSI) feedback in CF-mMIMO was proposed with the total throughput as the objective function. The results showed more significance than ZF regarding the total throughput. However, the difference between the users with the maximum and minimum throughputs is significant.

Therefore, it is not widely used in the CF-mMIMO literature, because it does not contribute to a stable QoS.

2.2.2 Max-Min Worst-Case Maximization

The max-min worst-case maximization design maximizes only the user with minimum throughput. To focus on the minimum throughput only, the throughput overall UEs approach uniformly. Therefore, to exploit the user-fairness advantages in CF-mMIMO, max-min worst-case maximization is widely used in resource allocation and beamforming designs.

The CF-mMIMO proposal by Marzzeta et al. also employs max-min for power allocation [46, 47, 49]. The results confirm that they have superior fairness compared with small cells. Other studies have also proposed classical beamforming designs combined with max-min power allocation [51, 114–116, 91]. However, the max-min worst-case maximization considers only the UEs with the minimum throughput, resulting in significant degradation of the aggregate throughput. Therefore, it cannot cope with the exponential increase in wireless traffic.

2.2.3 Geometric-Mean Maximization

In this dissertation, we want to maximize the total throughput while guaranteeing as much user fairness as much as possible to achieve a user-centric design. Therefore, we must consider designs that rescue the worst-case users while maximizing the total throughput. Optimization using the geometric mean as the objective function has the property of total value maximization while balancing parameters that have a mutual influence. Therefore, cellular mMIMO [105, Sec. 7.1], [117, 118] and CF-mMIMO [119, 117] for fairness-aware design widely use geometric-mean maximization.

In literature [120], a power allocation problem is formulated for CF-mMIMO with the geometric mean of throughput and power efficiency as objective functions. A closed-form iterative power allocation algorithm was proposed based on the formulated optimization problem. The results confirm that the proposed algorithm can rescue users with poor channel conditions while maintaining a good aggregate throughput. In other words, the geometric mean of throughput maximization can be used to design the algorithm without ignoring UEs with a poor/good channel state, as in sum-rate/max-min maximization. Therefore, the studies in the literature [120] have motivated using a geometric optimization problem to realize user-centric communication.

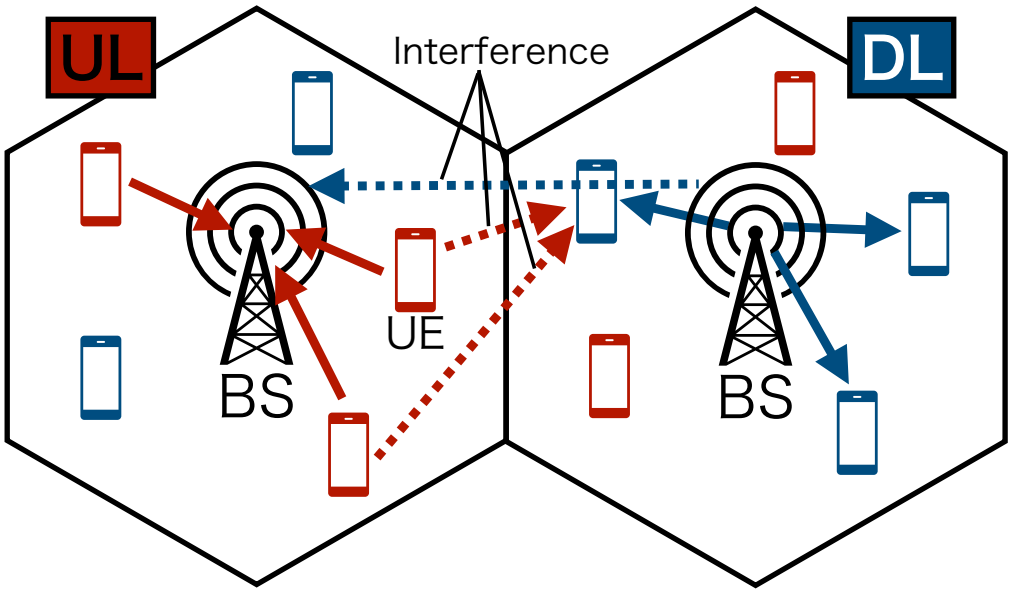

Fig. 2.3 Illustration of the cross-interference of operating dynamic TDD mode in cellular networks.

2.3 Duplex Modes

The duplex modes in wireless networks that continue to the present are mixtures of FDD and TDD. In CF-mMIMO, there is also literature on both multiplexing modes. In the FDD mode [121–124], two different frequency bands are allocated to the UL/DL, so that the network can transmit data simultaneously. Therefore, the UL and DL channels do not exhibit duality. The AP must perform CSI estimation for each UL/DL in the beamforming design. In particular, DL CSI estimation requires feedback on the estimated CSI from the UE, which is proportional to the number of APs; therefore, it is not practical to use FDD in CF-mMIMO with massive APs. For this reason, most CF-mMIMO studies assume operation in TDD mode.

2.3.1 Static TDD

Communication in TDD mode involves UL/DL data transmission in the same frequency band. Therefore, owing to channel duality, beamforming for the UL and DL can be designed using the CSI estimated during the UL pilot training. This property reduces the channel estimation overhead, which is why most studies on CF-mMIMO systems assume operation in the TDD mode. In the models assumed in most studies, the UL/DL configuration of the coverage area is statically allocated. It must be synchronized over the entire area and is called static TDD.

Static TDD has limited improvement in throughput and SE, as UEs are forced to stand by as long as both UL/DL users are present in the coverage area.

2.3.2 Dynamic TDD

However, 5G cellular networks support dynamic TDD to improve performance by gaining multiplexing flexibility. The 5G standardization defines a per-symbol UL/DL allocation, which includes flexible symbols from which each cell can arbitrarily choose its UL/DL. In other words, the dynamic TDD allows each cell to have a different UL/DL configuration depending on the traffic situation. This resulted in significantly increased SE and throughput owing to reduced standby times [125].

More specifically, current wireless communication use cases include asymmetric and sporadic traffic, such as video streaming and file uploads on social networking sites. The static TDD determines the UL/DL configuration of the entire coverage area based on the traffic statistics. This static configuration increases the probability of a deviation from the current traffic situation in a particular cell. In the worst case, a UL or DL is allocated even though there are only DL or UL users, resulting in no transmission or reception in that subframe. As a result, unsent packets accumulate, and massive queuing delays occur. This delay causes significant degradation of the respective UL/DL SE in a static TDD. The literature [126, 127] compares static TDD and dynamic TDD for asymmetric UL/DL traffic. The results show that static TDD, whose configuration ignores the UL/DL traffic ratio, degrades the throughput owing to an increased queueing delay. Conversely, a dynamic TDD can reduce the impact of this delay owing to its ability to cope with traffic fluctuations, showing a superior SE compared to a static TDD. Therefore, by negotiating the utilization of time resources, dynamic TDD systems can significantly improve the overall network SE and throughput [128].

In addition, they are effective for addressing hybrid automatic repeat request (HARQ) delays [129]. The HARQ feedback for the UL/DL in the static TDD of 4G standardization occurs in the UL/DL subframe [130]. As it is necessary to wait for the corresponding subframe for UL/DL, the UL/DL configuration defined in the 4G standardization provides a maximum delay of 5 ms. Conversely, 5G using dynamic TDD allows the UL/DL symbols to be configured within a slot. Thus, 5G standardization achieves a feedback delay requirement of <1 ms [131]. Consequently, the waiting time to retransmission is significantly reduced, contributing to a higher throughput. This method is particularly effective when handling small packets. As a result, SE can be improved, and latency is lowered owing to the reduced standby times.

Conversely, dynamic TDD largely affects the inter-BS-BS and inter-UE-UE interference (also called cross-link interference), as shown in Fig. 2.3. These interferences are caused

by neighboring cells using different UL/DL transmission directions. In particular, the throughput performance degradation of UL is exceptionally high in cellular networks because of the higher transmit power of BSs compared with UEs. This critical issue degrades the performance of dynamic TDD, and several countermeasures have been studied in the literature. In addition, as mentioned in Chapter 1, spatial multiplexing with CF-mMIMO is insufficient to achieve user-centric communications that can satisfy the QoS requirements of 6G and beyond. Therefore, it is necessary to achieve time-resource efficiency via the dynamic TDD of cellular networks or better technologies. Moreover, CF-mMIMO cannot use the dynamic TDD-like cellular mMIMO, because the network is not partitioned by cells. Therefore, multiplexing schemes that are flexible to changing user traffic conditions must also be considered for CF-mMIMO.

2.3.3 Full-Duplex

FD, as shown in Fig. 2.4, is a technology with time resource efficiency exceeding that of dynamic TDD. FD enables all users within the service coverage area to communicate simultaneously within the same frequency range by allocating UL/DL to each antenna. FD is the most user-centric multiplexing scheme that eliminates waiting users owing to UL/DL discrepancies. Therefore, this subsection considers the FD communication applied to CF-mMIMO.

A normal FD usually allocates UL/DL per antenna within a BS in centralized systems and per AP in distributed systems. Consequently, the literature [132] shows that if SI can be completely controlled, throughputs up to twice as high as dynamic TDD can be achieved. In addition, several studies have considered the FD in CF-mMIMO [133–136]. The literature [133] confirms that the theoretical analysis of FD CF-mMIMO shows that the total SE of the FD mode is 1.4 times higher than that of the HD mode. However, these results were achieved when the residual SI toward noise power due to interference cancellation was less than 90 dB [133].

The SI is a huge interference of more than 100 dB above the noise floor receiving on the UL antenna from the neighboring DL antenna [137]. Therefore, SI suppression is a significant concern in several FD studies. Consequently, the suppression of self-interference up to 110 dB has been demonstrated in the literature [138] using a 72-element antenna. However, cost issues remain in the implementation process. In particular, CF-mMIMO requires a distributed deployment of APs that must be cheap. In fact, most of the studies on CF-mMIMO report the requirement of one-four antennas for each AP, which are insufficient for SI suppression. Furthermore, the AP must be equipped with an RF-chain for both the UL and DL. Therefore, it is impractical to apply conventional FD to CF-mMIMO.

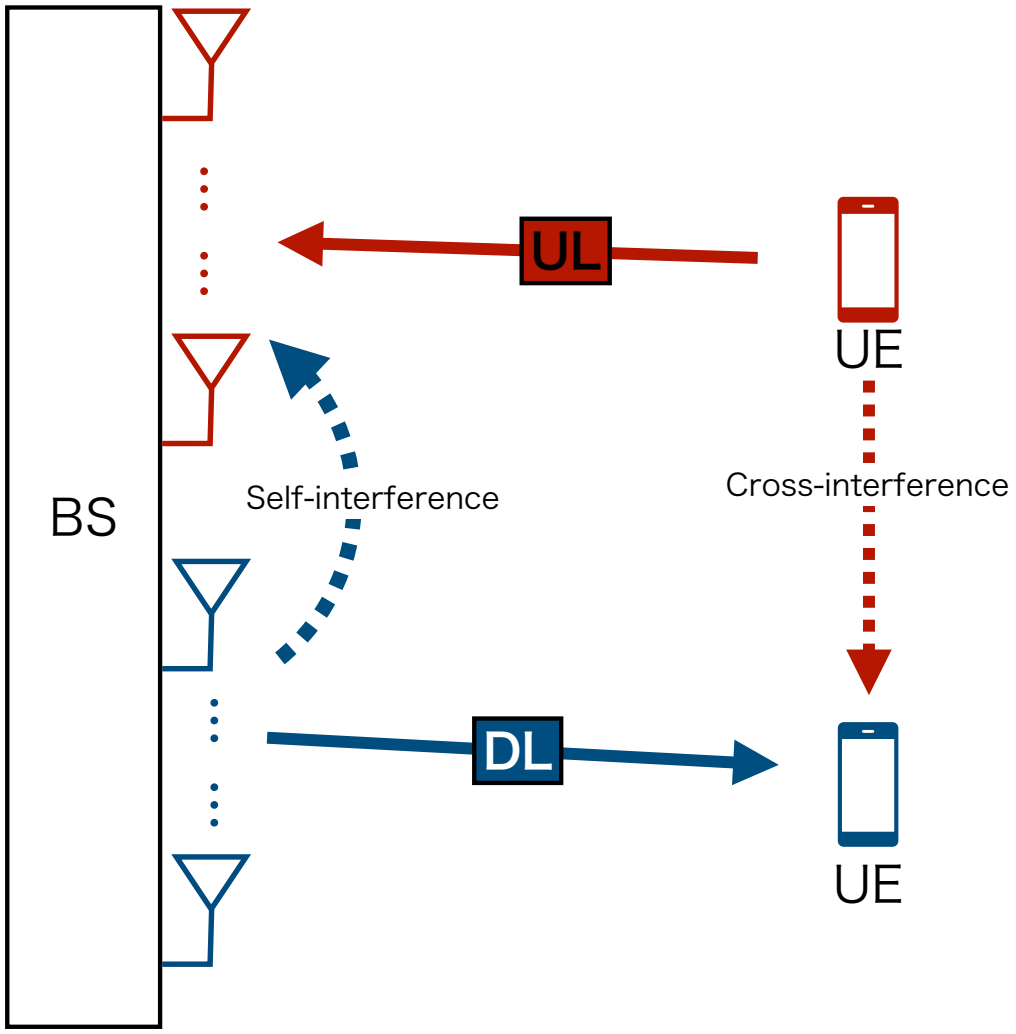

Fig. 2.4 Illustration of the full-duplex communication with self-interference.

In-Band Full-Duplex

A simple way to fundamentally solve the SI is to increase the distance between inter-DL-UL antennas. Such an attempt is called in-band FD and has existed since the continuous-wave radar in the 1940s [137]. A tutorial in the literature [137] introduced the concept of in-band FD to the wireless communication region. Based on this tutorial, this concept was first studied for cooperative networks, such as C-RAN [70] and CoMP [71]. In-band FD is based on the inter-cell coordination of BSs operating in the HD mode to provide FD communication across the entire network at the same frequency. This allows them to benefit from the increase in throughput owing to FD while eliminating SI. In addition, in-band FD in distributed networks was considered by assigning UL/DL to each AP in the DAS [139]. Focusing on

the UL UE, theoretical analysis has shown that in-band FD can achieve a good SINR for FD. Therefore, applying this concept to CF-mMIMO, a distributed cooperation network, is expected to improve the throughput with in-band FD.

Network-Assisted Full-Duplex

Motivated by the above discussions, NAFD CF-mMIMO, an extension of in-band FD has been proposed. NAFD CF-mMIMO, such as in-band FD, can benefit from simultaneous UL/DL communication, without the influence of SI. Conversely, inter-AP interference is higher than in-band FD because the number of neighboring APs increases owing to the distributed placement of the APs. In particular, inter-UE interference increases significantly compared to dynamic TDD mMIMO, where UEs only have links in the same direction within a cell. This contrasts with the dynamic TDD mMIMO, where the proportion of the influence of inter-BS interference is significant. Therefore, NAFD CF-mMIMO requires a higher interference-suppression performance than dynamic TDD. However, unlike cellular networks, CF-mMIMO can suppress inter-AP and inter-UE interference by optimizing the UL/DL configuration of APs. In literature [73], an AP configuration optimization by sum-rate maximization was proposed using an MMSE combiner and regularized ZF precoder for beamforming. A comparison of static/dynamic TDD cellular mMIMO and static TDD/NAFD for CF-mMIMO confirms the superiority of NAFD CF-mMIMO over all the other schemes in terms of SE. The literature presented in Section 1.2 also shows that NAFD CF-mMIMO can achieve higher throughput. In addition, it has been shown that beamforming design can further improve throughput.

The above discussion has shown the motivation for adopting NAFD CF-mMIMO to realize user-centric communication in this dissertation.

2.4 Chapter Summary

In this chapter, a comparison of existing technologies showed the advantages of NAFD CF-mMIMO and the motivation for considering it in this dissertation. The following is the summary and conclusion of this chapter and the proposals after that chapter.

The elimination of standby users achieves these results through simultaneous communication and a high degree of interference suppression by utilizing the spatial DoF of the CF-mMIMO. Therefore, NAFD CF-mMIMO is expected to meet future QoS requirements through a user-centric design with in-band FD and the CF-mMIMO. However, in past literature, optimization based on sum-rate maximization is used for the AP configuration and beamforming design. As described in Section 2.2.1, this design scheme sacrifices users for

the network-friendliness objective of maximizing total throughput. To achieve user-centric communication in future wireless systems, maximizing the total throughput at the physical layer while maintaining fairness as much as possible is essential. In other words, studying the AP configuration and beamforming design schemes using the geometric mean is worthwhile for achieving user-centric communication. In subsequent chapters, based on the discussions in this chapter, we propose a design scheme that provides a reasonable trade-off between fairness and total throughput in NAFD CF-mMIMO networks. First, as discussed in Section 3, we assume and discuss microwave bands that play an important role in current and future wireless systems. Subsequently, an extension to the mmWave band was provided to satisfy the throughput requirements for next-generation wireless systems. In addition, the impact of inter-UE interference, which has a more significant impact than conventional systems, was specifically considered.

Chapter 3

Joint Access Configuration and Beamforming for Network-Assisted Full-Duplex Cell-Free Massive MIMO

3.1 Background and Contributions

As introduced in Section 1.3.1, several techniques for access configuration and joint beamforming design for CF-mMIMO systems with NAFD communication scheme have been proposed in [72, 73, 87] and [76, 78, 79, 84–86], respectively. However, these proposals are not user-centric designs because they focus on total system throughput and energy efficiency. They also become particularly disadvantageous solutions for users who cannot obtain sufficient SINR due to path loss and/or interference.

To this end, we propose NAFD CF-mMIMO systems to realize user-centric communication. The system considers UEs equipped with single or multiple antennas, and provides a generalized design scheme for the evolution of UE terminals. In addition, we propose a novel joint AP access configuration, power allocation, and beamforming algorithm for this system, which attempts to achieve a locally optimized solution that balances system throughput and user fairness. Accordingly, motivated by recent studies such as [140, 118], we try to maximize the geometric mean of the UEs' throughput. Maximizing the geometric mean can maximize the total throughput utility while reducing the variance among the UE's achievable throughput. The formulated maximization problem involving the geometric mean objective function is highly intractable, not only because of the non-convexity of the SINR expression, but also because of the binary (discrete) feasibility set of the DL/UL AP access configuration. This challenge is addressed here via a combination of a negative-entropy-based regularizer,

fractional programming (FP), and convex–concave procedure (CCP). The resultant algorithm is based on an iteration of convex quadratically constrained program (QCP) subproblems. In addition, we consider both cases in which each UE is equipped with a single antenna or multiple antennas, tailoring the proposed algorithm for both scenarios. We confirm via computer simulation that the proposed method can flexibly respond to changes in traffic demand and exhibits excellent throughput characteristics while maintaining user fairness relative to the TDD.

3.2 Channel and System Model

Consider a CF-mMIMO system comprising of L multiple APs distributed over a certain coverage area, each equipped with M antennas. All APs assumed to be connected to a common CPU via a wired fronthaul link as illustrated in Fig. 3.1. Also, we employ a NAFD scheme to jointly serve K distinct randomly distributed UEs, each of which operates in either UL or DL mode during a given channel realization. In order to focus on the achievable performance of the system, it is assumed that perfect CSI is available at the CPU.

Hereafter, we shall denote the sets of all UEs by $\mathcal{K} = \{1, \ldots, K\}$, and the sets of UEs operating in DL and UL modes respectively by $\mathcal{K}^{\mathrm{dl}} \subset \mathcal{K}$ and $\mathcal{K}^{\mathrm{ul}} = \mathcal{K} \setminus \mathcal{K}^{\mathrm{dl}}$. Similarly, the sets of APs and of APs in DL and UL are respectively denoted by $\mathcal{L} = \{1, \ldots, L\}$, $\mathcal{L}^{\mathrm{dl}} \subset \mathcal{L}$, and $\mathcal{L}^{\mathrm{ul}} = \mathcal{L} \setminus \mathcal{L}^{\mathrm{dl}}$, respectively. Note that all devices are assumed to operate in HD mode, implying that there is no overlap between $\mathcal{K}^{\mathrm{dl}}$ and $\mathcal{K}^{\mathrm{ul}}$, and similarly between $\mathcal{L}^{\mathrm{dl}}$ and $\mathcal{L}^{\mathrm{ul}}$.

In what follows, two distinct system setups depending on the antenna configuration at UEs will be considered – namely, single-antenna or multiple-antenna UE scenarios – with the corresponding system and channel models introduced accordingly.

3.2.1 Single Antenna Case

In this subsection, we first consider the case of single-antenna UEs, describing the corresponding channel model as well as the associated received signal characterization in the considered NAFD CF-mMIMO system.

Channel Model

As mentioned in Chapter 1, widely used frequencies are sub-6 GHz in the systems until 5G to provide comprehensive network coverage. In addition, sub-6 GHz is also an important band after 6G to ensure coverage. Therefore, in this chapter, we consider models used in microwaves to ensure compatibility with systems until 5G.

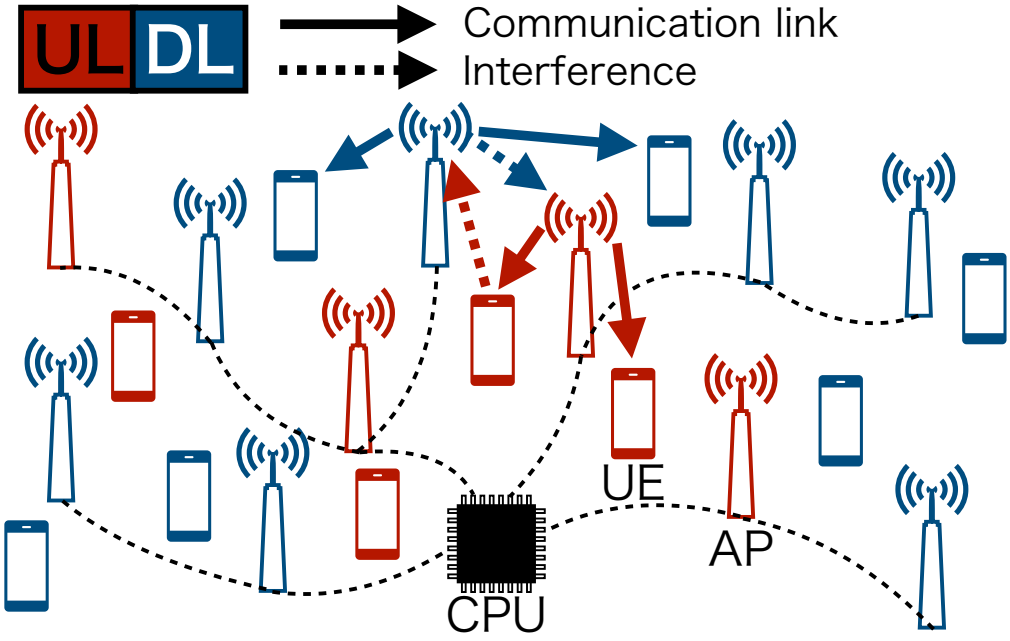

Fig. 3.1 Illustration of CF-mMIMO system based NAFD.

With $k \in \mathcal{K}$, $k' \in \mathcal{K} \setminus k$, $\ell \in \mathcal{L}$ and $\ell' \in \mathcal{L} \setminus \ell$, (*i.e.*, $k \neq k'$ and $\ell \neq \ell'$), it is assumed that the communication channel between the k-th UE and the ℓ-th AP, as well as the interference channel between the ℓ-th AP and the ℓ'-th AP are spatially correlated, whereas the channel between the k-th UE and k'-th UE is uncorrelated since UEs are independently and randomly distributed over the service area, and each has a single antenna.

Given the assumption mentioned above, the three distinct channels – *i.e.*, the communication channel $\boldsymbol{h}_{k,\ell}$ between the k-th UE and the ℓ-th AP, the inter-AP interference channel $\boldsymbol{H}_{\ell,\ell'}$ between the ℓ-th and the ℓ'-th APs, and the inter-UE interference channel $h_{k,k'}$ between the k-th and the k'-th UEs – can be respectively modeled as

$$\boldsymbol{h}_{k,\ell} \sim \mathcal{CN}(\boldsymbol{0}, \boldsymbol{R}_{k,\ell}), \tag{3.1a}$$

$$\boldsymbol{H}_{\ell,\ell'} = \boldsymbol{R}_{\ell,\ell'}^{\frac{1}{2}} \bar{\boldsymbol{H}}_{\ell,\ell'} \boldsymbol{R}_{\ell',\ell}^{\frac{1}{2}}, \tag{3.1b}$$

$$h_{k,k'} \sim \mathcal{CN}(0, g_{k,k'}), \tag{3.1c}$$

where the small-scale fading matrix $\bar{\boldsymbol{H}}_{\ell,\ell'} \in \mathbb{C}^{M \times M}$ are modeled as $\text{vec}\left(\bar{\boldsymbol{H}}_{\ell,\ell'}\right) \sim \mathcal{CN}(\boldsymbol{0}, I_{M^2})$.

In the latter equations, the matrices $\boldsymbol{R}_{k,\ell} \in \mathbb{C}^{M \times M}$ characterizes the spatial correlation of the corresponding UE-AP communication channel; while the matrices $\boldsymbol{R}_{\ell,\ell'} \in \mathbb{C}^{M \times M}$ and $\boldsymbol{R}_{\ell',\ell} \in \mathbb{C}^{M \times M}$ are the spatial correlation matrices between the ℓ'-th and ℓ-th APs. Also, $g_{k,k'}$ is a large-scale coefficient between the k-th and k'-th UEs given in [105, Sec. 4.1.3]. We adopt

in this article the approach most widely employed in CF-mMIMO systems [106, 107, 65], namely the local scattering model of [105], in which the spatial correlation matrices $\boldsymbol{R}_{k,\ell}$, $\boldsymbol{R}_{\ell,\ell'}$ and $\boldsymbol{R}_{\ell',\ell}$ are characterized by the equation [105, Eq. (2.23)]:

$$[\boldsymbol{R}]_{r,c} = g \cdot \int e^{2\pi j d_H (r-c)\sin(\bar{\varphi})} f(\bar{\varphi}) d\bar{\varphi}, \tag{3.2}$$

$$f(\bar{\varphi}) = \frac{1}{\sqrt{2\pi}\sigma_\varphi} e^{-\frac{\delta^2}{2\sigma_\varphi^2}}, \tag{3.3}$$

where $[\cdot]_{r,c}$ is an operator that extracts the element at the r-th row and c-th column of a given matrix, g denotes a large-scale fading coefficient by [105, Sec. 4.1.3], d_H is the antenna spacing normalized by wavelength, respectively, and the variable of integration $\bar{\varphi}$ is given by $\bar{\varphi} = \varphi + \delta$, with φ denoting a certain (deterministic) angle of arrival or departure and $\delta \sim \mathcal{N}(0, \sigma_\varphi^2)$ modeling a random fluctuation in angle spread with standard deviation σ_φ.

System Model

Given the channel model described above, in this subsection we turn our attention to the system model of the corresponding CF-mMIMO network operating in the NAFD mode. As one can easily infer, one of the main bottlenecks of such a system is the interference due to joint UL and DL transmission, which limits system performance if not properly handled.

In order to circumvent this issue, APs are assumed to be capable of performing coordinated beamforming, whereas single-antenna UEs can only control their transmit power. Under such assumption, the UL signal vector $\boldsymbol{y}_\ell^{\text{ul}} \in \mathbb{C}^{M\times 1}$ received at the ℓ-th AP with $\ell \in \mathcal{L}^{\text{ul}}$ can be written as

$$\boldsymbol{y}_\ell^{\text{ul}} = \sum_{k\in\mathcal{K}^{\text{ul}}} \sqrt{p_k^{\text{ul}}}\boldsymbol{h}_{k,\ell} d_k^{\text{ul}} + \overbrace{\sum_{\ell'\in\mathcal{L}^{\text{dl}}} \sum_{k'\in\mathcal{K}^{\text{dl}}} \boldsymbol{H}_{\ell,\ell'}^{\text{H}} \boldsymbol{w}_{k',\ell'}^{\text{ap}} d_{k'}^{\text{dl}}}^{\text{Inter-AP Interference}} + \boldsymbol{n}_\ell, \tag{3.4}$$

where $d_k^{\text{ul}} \in \mathbb{C}$ represents the data symbol from the k-th UL UE, $\boldsymbol{w}_{k',\ell'}^{\text{ap}}$ denotes the precoding vector employed by the ℓ'-th AP toward the k'-th DL UE, and $\boldsymbol{n}_\ell \sim \mathcal{CN}(0, \sigma_{\text{ul}}^2 I_M)$ is an AWGN vector with per-element variance σ_{ul}^2.

In light of equation (3.4), the aggregated estimate of the data symbol of the k-th UE at the ℓ-th AP can be written as

$$\widehat{d}_k^{\text{ul}} = \sum_{\ell\in\mathcal{L}^{\text{ul}}} \boldsymbol{v}_{k,\ell}^{\text{ap H}} \boldsymbol{y}_\ell^{\text{ul}}, \tag{3.5}$$

where $\boldsymbol{v}_{k,\ell}^{\text{ap}} \in \mathbb{C}^M$ denotes the combining vector at the ℓ-th AP to detect the intended data transmitted by the k-th UL UE.

Similarly, the DL signal $y_k^{\mathrm{dl}} \in \mathbb{C}$ received at the k-th UE with $k \in \mathcal{K}^{\mathrm{dl}}$ can be expressed as

$$y_k^{\mathrm{dl}} = \sum_{\ell \in \mathcal{L}^{\mathrm{dl}}} \boldsymbol{h}_{k,\ell}^{\mathrm{H}} \sum_{k' \in \mathcal{K}^{\mathrm{dl}}} \boldsymbol{w}_{k',\ell}^{\mathrm{ap}} d_{k'}^{\mathrm{dl}} + \overbrace{\sum_{k'' \in \mathcal{K}^{\mathrm{ul}}} \sqrt{p_{k''}^{\mathrm{ul}}} h_{k'',k} d_{k''}^{\mathrm{ul}}}^{\text{Inter-UE Interference}} + n_k, \tag{3.6}$$

where $d_k^{\mathrm{dl}} \in \mathbb{C}$, $\boldsymbol{w}_{k',\ell}^{\mathrm{ap}} \in \mathbb{C}^M$, and $n_k \sim \mathcal{CN}(0, \sigma_{\mathrm{dl}}^2)$ denotes the DL data symbol toward the k-th DL UE, the precoding vector employed by the ℓ-th AP, and the AWGN affecting the k-th UE, respectively.

Since each UE possesses a single antenna, an estimate of the intended signal can be simply written as[1]

$$\widehat{d}_k^{\mathrm{dl}} = y_k^{\mathrm{dl}}. \tag{3.7}$$

Assuming that the total transmit power at each DL AP is limited to $p^{\mathrm{dl,max}}$, *i.e.*, $\sum_{k \in \mathcal{K}^{\mathrm{dl}}} \|\boldsymbol{w}_{k,\ell}^{\mathrm{ap}}\|_2^2 \leq p^{\mathrm{dl,max}}$, and that the power of each data symbol from UL UEs is normalized, the SINR at UL and DL can be respectively written as

$$\Gamma_k^{\mathrm{ul}} \triangleq \frac{p_k^{\mathrm{ul}} |\boldsymbol{v}_k^{\mathrm{ap}\mathrm{H}} \boldsymbol{h}_k|^2}{\sum\limits_{\substack{k' \in \mathcal{K}^{\mathrm{ul}} \\ k \neq k'}} p_{k'}^{\mathrm{ul}} |\boldsymbol{v}_k^{\mathrm{ap}\mathrm{H}} \boldsymbol{h}_k|^2 + \sum\limits_{k' \in \mathcal{K}^{\mathrm{dl}}} |\boldsymbol{v}_k^{\mathrm{ap}\mathrm{H}} \boldsymbol{H}^{\mathrm{H}} \boldsymbol{w}_{k'}^{\mathrm{ap}}|^2 + \sigma_{\mathrm{ul}}^2 \left\|\boldsymbol{v}_k^{\mathrm{ap}}\right\|_2^2}, \tag{3.8}$$

$$\Gamma_k^{\mathrm{dl}} \triangleq \frac{\left|\boldsymbol{h}_k^{\mathrm{H}} \boldsymbol{w}_k^{\mathrm{ap}}\right|^2}{\sum\limits_{\substack{k' \in \mathcal{K}^{\mathrm{dl}} \\ k \neq k'}} |\boldsymbol{h}_k^{\mathrm{H}} \boldsymbol{w}_{k'}^{\mathrm{ap}}|^2 + \sum\limits_{k' \in \mathcal{K}^{\mathrm{ul}}} p_{k'}^{\mathrm{ul}} \left|h_{k',k}\right|^2 + \sigma_{\mathrm{dl}}^2}, \tag{3.9}$$

where $\boldsymbol{h}_k \triangleq [\boldsymbol{h}_{k,1}^{\mathrm{T}}, \ldots, \boldsymbol{h}_{k,L}^{\mathrm{T}}]^{\mathrm{T}}$, $\boldsymbol{v}_k^{\mathrm{ap}} \triangleq [\boldsymbol{v}_{k,1}^{\mathrm{ap\ T}}, \ldots, \boldsymbol{v}_{k,L}^{\mathrm{ap\ T}}]^{\mathrm{T}}$, $\boldsymbol{w}_k^{\mathrm{ap}} \triangleq [\boldsymbol{w}_{k,1}^{\mathrm{ap\ T}}, \ldots, \boldsymbol{w}_{k,L}^{\mathrm{ap\ T}}]^{\mathrm{T}}$, and

$$\boldsymbol{H} \triangleq \begin{bmatrix} \boldsymbol{H}_{1,1} & \cdots & \boldsymbol{H}_{L,1} \\ \vdots & \ddots & \vdots \\ \boldsymbol{H}_{1,L} & \cdots & \boldsymbol{H}_{L,L} \end{bmatrix}.$$

[1]One can consider the case where each UE is capable of multiplying a scalar quantity with the received signal y_k^{dl}. Although we omit such case here, the latter will be discussed in the subsequent section, where the more general case of UEs with multiple-antennas and beamforming capability at the receiver is addressed.

3.2.2 Multiple-Antenna Case

Next, we turn our attention to the scenario with multiple antenna UEs, generalizing the above system model accordingly. Throughout the section, the number of antennas equipped at each UE is assumed to be N.

Channel Model

Since the inter-APs channel model is independent of the number of antennas at UEs, suffice it to consider the channel models associated with UEs, namely, the communication channel $\boldsymbol{H}_{k,\ell}$ between the k-th UE and the l-th AP, and the inter-UE interference channel $\boldsymbol{H}_{k,k'}$ between the k-th and the k'-th UEs, which in the case of UEs with multiple antennas can be rewritten as

$$\boldsymbol{H}_{k,\ell} = \boldsymbol{R}_{k,\ell}^{\frac{1}{2}} \bar{\boldsymbol{H}}_{k,\ell} \boldsymbol{R}_{\ell,k}^{\frac{1}{2}}, \tag{3.10a}$$

$$\boldsymbol{H}_{k,k'} = \boldsymbol{R}_{k,k'}^{\frac{1}{2}} \bar{\boldsymbol{H}}_{k,k'} \boldsymbol{R}_{k',k}^{\frac{1}{2}}, \tag{3.10b}$$

where $\boldsymbol{R}_{k,\ell} \in \mathbb{C}^{M\times M}$, $\boldsymbol{R}_{\ell,k} \in \mathbb{C}^{N\times N}$ and $\boldsymbol{R}_{k,k'} \in \mathbb{C}^{N\times N}$ are spatial correlation matrices modeled by equation (3.2), while $\text{vec}\left(\bar{\boldsymbol{H}}_{k,\ell}\right) \sim \mathcal{CN}(\boldsymbol{0}, I_{MN})$ and $\text{vec}\left(\bar{\boldsymbol{H}}_{k,k'}\right) \sim \mathcal{CN}(\boldsymbol{0}, I_{N^2})$.

System Model

Straightforwardly, the UL and DL received signals can be respectively written as

$$\boldsymbol{y}_{\ell}^{\text{ul,m}} = \sum_{k\in\mathcal{K}^{\text{ul}}} \boldsymbol{H}_{k,\ell} \boldsymbol{w}_{k}^{\text{ue}} d_{k}^{\text{ul}} + \sum_{\ell'\in\mathcal{L}^{\text{dl}}} \sum_{k'\in\mathcal{K}^{\text{dl}}} \boldsymbol{H}_{\ell,\ell'}^{\text{H}} \boldsymbol{w}_{k',\ell'}^{\text{ap}} d_{k'}^{\text{dl}} + \boldsymbol{n}_{\ell}, \tag{3.11}$$

$$\boldsymbol{y}_{k}^{\text{dl,m}} = \sum_{\ell\in\mathcal{L}^{\text{dl}}} \boldsymbol{H}_{k,\ell}^{\text{H}} \sum_{k'\in\mathcal{K}^{\text{dl}}} \boldsymbol{w}_{k',\ell}^{\text{ap}} d_{k'}^{\text{dl}} + \sum_{k'\in\mathcal{K}^{\text{ul}}} \boldsymbol{H}_{k',k} \boldsymbol{w}_{k'}^{\text{ue}} d_{k'}^{\text{ul}} + \boldsymbol{n}_{k}, \tag{3.12}$$

where $\boldsymbol{w}_{k}^{\text{ue}} \in \mathbb{C}^{N}$ is the precoding vector employed by the k-th UE, and $\boldsymbol{n}_{k} \in \mathbb{C}^{N}$ and $\boldsymbol{n}_{\ell} \in \mathbb{C}^{N}$ are the AWGN vectors at the k-th UE and the ℓ-th AP, respectively.

In turn, the estimates of the UL and DL data symbols at the k-th UE are respectively given by

$$\widehat{d}_{k}^{\text{ul,m}} = \sum_{\ell\in\mathcal{L}^{\text{ul}}} \boldsymbol{v}_{k,\ell}^{\text{ap H}} \boldsymbol{y}_{\ell}^{\text{ul}}, \tag{3.13a}$$

and

$$\widehat{d}_{k}^{\text{dl,m}} = \boldsymbol{v}_{k}^{\text{ue H}} \boldsymbol{y}_{k}^{\text{dl}}, \tag{3.13b}$$

where $\boldsymbol{v}_{k}^{\text{ue}} \in \mathbb{C}^{N}$ is the combining vector employed by the k-th UE at DL.

Consequently, the corresponding SINRs are given by

$$\Gamma_k^{\mathrm{ul,m}} \triangleq \frac{|\boldsymbol{v}_k^{\mathrm{apH}} \boldsymbol{H}_k \boldsymbol{w}_k^{\mathrm{ue}}|^2}{\sum\limits_{\substack{k' \in \mathcal{K}^{\mathrm{ul}} \\ k \neq k'}} |\boldsymbol{v}_k^{\mathrm{apH}} \boldsymbol{H}_{k'} \boldsymbol{w}_k^{\mathrm{ue}}|^2 + \sum\limits_{k' \in \mathcal{K}^{\mathrm{dl}}} |\boldsymbol{v}_k^{\mathrm{apH}} \boldsymbol{H}^{\mathrm{H}} \boldsymbol{w}_{k'}^{\mathrm{ap}}|^2 + \sigma_{\mathrm{ul}}^2 \left\|\boldsymbol{v}_k^{\mathrm{ap}}\right\|_2^2}, \tag{3.14}$$

$$\Gamma_k^{\mathrm{dl,m}} \triangleq \frac{|\boldsymbol{v}_k^{\mathrm{ueH}} \boldsymbol{H}_k^{\mathrm{H}} \boldsymbol{w}_k^{\mathrm{ap}}|^2}{\sum\limits_{\substack{k' \in \mathcal{K}^{\mathrm{dl}} \\ k \neq k'}} |\boldsymbol{v}_k^{\mathrm{ueH}} \boldsymbol{H}_k^{\mathrm{H}} \boldsymbol{w}_{k'}^{\mathrm{ap}}|^2 + \sum\limits_{k' \in \mathcal{K}^{\mathrm{ul}}} |\boldsymbol{v}_k^{\mathrm{ueH}} \boldsymbol{H}_{k',k}^{\mathrm{H}} \boldsymbol{w}_{k'}^{\mathrm{ue}}|^2 + \sigma_{\mathrm{dl}}^2 \left\|\boldsymbol{v}_k^{\mathrm{ue}}\right\|_2^2}, \tag{3.15}$$

where $\boldsymbol{H}_k = [\boldsymbol{H}_{k,1}^{\mathrm{T}}, \ldots, \boldsymbol{H}_{k,L}^{\mathrm{T}}]^{\mathrm{T}}$.

3.3 Proposed Methods

In this section, we propose a joint dynamic resource allocation and beamforming scheme for CF-mMIMO systems operating in the NAFD mode, aiming at improving the system's total throughput, while maintaining the QoS fairness among UEs. A key ingredient of the proposed scheme is the replacement of objective functions such as the total system throughput and throughput max-min, which are popular in related works [105, 141–146, 115, 147], by the geometric mean, which is widely utilized in other research fields such as portfolio optimization [148].

This approach is motivated by arguments that maximizing the total throughput often leads to an unfair condition with widely varying user experiences [105], and that the maximization of minimum rate limits total system throughput [105]. In turn, it has been recently shown that maximizing the geometric mean throughput is an efficient approach to achieve the aforementioned trade-offs between the total throughput and user fairness [140]. In view of the above, we propose an optimization-based method that maximizes the geometric mean of UL and DL data rates by jointly optimizing the beamforming weights and AP allocation.

As shall be soon clarified, the problem formulation that ensues can be tackled efficiently via FP techniques, which have been recently employed in wireless communication to deal with optimization problems involving fractional terms such as SINR and EE [149, 150]. Although techniques such as Dinkelbach's algorithm have been used in the past in association with FP methods, new frameworks that yield tractable quadratic formulations while preserving convergence guarantee with first-order optimality for sum-of-ratio problems were recently proposed [144, 149, 151], which shall be adopted here as well, due to their advantage in terms of computational efficiency. For the sake of readability without compromising completeness, an introductory description of the FP techniques used here are offered in Appendix A.

3.3.1 Problem Formulation: Geometric Mean Maximization

Let us now proceed to formulate our geometric mean maximization problem aimed at the joint optimization of beamforming weights and UL/DL AP allocation, which admits efficient solution via FP and CCP. FP and CCP are techniques for solving fractional programming and difference of concave (DC) problems iteratively as convex optimization problems.

Single-Antenna UE

Consider the following geometric mean maximization problem:

$$\underset{\boldsymbol{\eta},\boldsymbol{v}^{\mathrm{ap}},\boldsymbol{w}^{\mathrm{ap}},\boldsymbol{p}^{\mathrm{dl}}}{\text{maximize}} \ \left(\prod_{k=1}^{K}\log_2\left(1+\Gamma_k\right)\right)^{\frac{1}{K}} \tag{3.16a}$$

$$\text{subject to} \ \ \eta_\ell \in \{0,1\}, \tag{3.16b}$$

$$\|\boldsymbol{v}_{k,\ell}^{\mathrm{ap}}\|_2^2 \leq \eta_\ell, \forall k \in \mathcal{K}^{\mathrm{ul}}, \forall \ell, \tag{3.16c}$$

$$\|\boldsymbol{w}_{k,\ell}^{\mathrm{ap}}\|_2^2 \leq p_{k,\ell}^{\mathrm{dl}}\bar{\eta}_\ell, \forall k \in \mathcal{K}^{\mathrm{dl}}, \forall \ell, \tag{3.16d}$$

$$\sum_{k=1}^{K} p_{k,\ell}^{\mathrm{dl}} \leq p^{\mathrm{dl,max}}, \forall \ell, \tag{3.16e}$$

$$N^{\mathrm{ul}} \leq \sum_{\ell=1}^{L}\eta_\ell, \tag{3.16f}$$

$$N^{\mathrm{dl}} \leq \sum_{\ell=1}^{L}\bar{\eta}_\ell, \tag{3.16g}$$

where $p_{k,\ell}^{\mathrm{dl}}$ is the transmit power at the ℓ-th AP towards the k-th UE, collected into the vector $\boldsymbol{p}^{\mathrm{dl}} \triangleq [p_{1,1}^{\mathrm{dl}},\cdots,p_{K,1}^{\mathrm{dl}},\cdots,p_{1,L}^{\mathrm{dl}},\cdots,p_{K,L}^{\mathrm{dl}}]^{\mathrm{T}}$; constraints (3.16b), (3.16c) and (3.16d), with $\bar{\eta}_\ell = 1-\eta_\ell$, $\boldsymbol{v}^{\mathrm{ap}} \triangleq [\boldsymbol{v}_1^{\mathrm{ap}\mathrm{T}},\ldots,\boldsymbol{v}_K^{\mathrm{ap}\mathrm{T}}]^{\mathrm{T}}$ and $\boldsymbol{w}^{\mathrm{ap}} \triangleq [\boldsymbol{w}_1^{\mathrm{ap}\mathrm{T}},\ldots,\boldsymbol{w}_K^{\mathrm{ap}\mathrm{T}}]^{\mathrm{T}}$, jointly enforce the selection of APs to UL and DL modes and the corresponding power limitations; constraints (3.16f) and (3.16g) enforce fairness by guaranteeing minimum numbers N^{ul} and N^{dl} of APs operating in UL and DL, respectively; and Γ_k is the SINR corresponding to the data intended

for the k-th UE, which is compactly rewritten as

$$\Gamma_k = \begin{cases} p_k^{\mathrm{ul}} \boldsymbol{v}_k^{\mathrm{ap}\mathrm{H}} \boldsymbol{h}_k \Big(\sum\limits_{\substack{k' \in \mathcal{K}^{\mathrm{ul}} \\ k \neq k'}} p_{k'}^{\mathrm{ul}} \boldsymbol{v}_k^{\mathrm{ap}\mathrm{H}} \boldsymbol{h}_{k'} \boldsymbol{h}_{k'}^{\mathrm{H}} \boldsymbol{v}_k^{\mathrm{ap}} \\ \quad + \sum\limits_{k' \in \mathcal{K}^{\mathrm{dl}}} \boldsymbol{v}_k^{\mathrm{ap}\mathrm{H}} \boldsymbol{H}^{\mathrm{H}} \boldsymbol{w}_{k'}^{\mathrm{ap}} \boldsymbol{w}_{k'}^{\mathrm{ap}\mathrm{H}} \boldsymbol{H} \boldsymbol{v}_k^{\mathrm{ap}} + \sigma_{\mathrm{ul}}^2 \left\| \boldsymbol{v}_k^{\mathrm{ap}} \right\|_2^2 \Big)^{-1} \boldsymbol{h}_k^{\mathrm{H}} \boldsymbol{v}_k^{\mathrm{ap}}, & \text{for } k \in \mathcal{K}^{\mathrm{ul}} \\ \boldsymbol{h}_k^{\mathrm{H}} \boldsymbol{w}_k^{\mathrm{ap}} \Big(\sum\limits_{\substack{k' \in \mathcal{K}^{\mathrm{dl}} \\ k \neq k'}} \boldsymbol{h}_k^{\mathrm{H}} \boldsymbol{w}_{k'}^{\mathrm{ap}} \boldsymbol{w}_{k'}^{\mathrm{ap}\mathrm{H}} \boldsymbol{h}_k + \sum\limits_{k' \in \mathcal{K}^{\mathrm{ul}}} \left| \sqrt{p_{k'}^{\mathrm{ul}}} h_{k',k} \right|^2 + \sigma_{\mathrm{dl}}^2 \Big)^{-1} \boldsymbol{w}_k^{\mathrm{H}} \boldsymbol{h}_k, & \text{for } k \in \mathcal{K}^{\mathrm{dl}} \end{cases}. \tag{3.17}$$

As indicated by constraints (3.16b), (3.16c), and (3.16d), the ℓ-th AP is allocated for UL transmission if and only if (iff) $\eta_\ell = 1$, or else for DL transmission iff $\eta_\ell = 0$. For the sake of notation simplicity, these binary indicator variables are collected in the vector $\boldsymbol{\eta} \triangleq [\eta_1, \ldots, \eta_L]$ in the statement (3.16a) of equation (3.16).

The main difficulties of solving Problem (3.16) are the facts that the objective is non-convex and that the selection variable η_ℓ is binary. Fortunately, this can be relaxed by the combination of FP and negative entropy regularization. As shown in Appendix B.1, the resulting continuous and convexified problem can be obtained as

$$\underset{\boldsymbol{\eta}, \boldsymbol{v}^{\mathrm{ap}}, \boldsymbol{w}^{\mathrm{ap}}, \boldsymbol{p}^{\mathrm{dl}}, \boldsymbol{\gamma}, \boldsymbol{s}}{\text{maximize}} \quad \Big(\prod_{k=1}^{K} f_k^{\mathrm{qt}} \left(\boldsymbol{v}^{\mathrm{ap}}, \boldsymbol{w}^{\mathrm{ap}}, \boldsymbol{p}^{\mathrm{dl}}, \boldsymbol{\gamma}, \boldsymbol{s} \right) \Big)^{\frac{1}{K}} + \zeta \sum_{\ell=1}^{L} \mathbb{P}(\eta_\ell) \tag{3.18a}$$

$$\text{subject to} \quad 0 \leq \eta_\ell \leq 1, \forall \ell, \tag{3.18b}$$

$$\left\| \begin{array}{c} 2\boldsymbol{v}_{k,\ell}^{\mathrm{ap}} \\ 1 - \eta_\ell \end{array} \right\|_2 \leq 1 + \eta_\ell, \forall k \in \mathcal{K}^{\mathrm{ul}}, \forall \ell, \tag{3.18c}$$

$$\left\| \begin{array}{c} 2\boldsymbol{w}_{k,\ell}^{\mathrm{ap}} \\ p_{k,\ell}^{\mathrm{dl}} - \bar{\eta}_\ell \end{array} \right\|_2 \leq p_{k,\ell}^{\mathrm{dl}} + \bar{\eta}_\ell, \forall k \in \mathcal{K}^{\mathrm{dl}}, \forall \ell, \tag{3.18d}$$

(3.16e) to (3.16g).

where $\mathbb{P}(\eta_i) \triangleq \eta_i \log \eta_i + (1-\eta_i) \log(1-\eta_i)$ is the penalty function, $\zeta \geq 0$ is a hyper-parameter used to adjust the strength of the penalty, and

$$f_k^{\mathrm{qt}}(\boldsymbol{v}^{\mathrm{ap}}, \boldsymbol{w}^{\mathrm{ap}}, \boldsymbol{p}^{\mathrm{dl}}, \boldsymbol{\gamma}, \boldsymbol{s}) \triangleq \alpha_k + \beta_k \Re\left\{ s_k^* \Gamma_k^{\mathrm{qt},1} \right\} - \|s_k\|_2^2 \, \Gamma_k^{\mathrm{qt},2}. \tag{3.19}$$

In the following this section, $\alpha_k \triangleq \log_2(1+\gamma_k) - \gamma_k$, $\beta_k \triangleq 2\sqrt{(1+\gamma_k)}$, $\gamma_k = \Gamma_k$, $s_k = \sqrt{(1+\gamma_k)} \Gamma_k^{\mathrm{qt},1} / \Gamma_k^{\mathrm{qt},2}$, $\boldsymbol{\gamma} \triangleq [\gamma_1, \ldots, \gamma_K]$, $\boldsymbol{s} \triangleq [s_1, \ldots, s_K]$, and the SINR quantities $\Gamma_k^{\mathrm{qt},1}$

and $\Gamma_k^{\mathrm{qt},2}$ respectively defined as

$$\Gamma_k^{\mathrm{qt},1} \triangleq \begin{cases} \sqrt{p_k^{\mathrm{ul}}}\boldsymbol{v}_k^{\mathrm{apH}}\boldsymbol{h}_k, & \text{for } k \in \mathcal{K}^{\mathrm{ul}}, \\ \boldsymbol{h}_k^{\mathrm{H}}\boldsymbol{w}_k^{\mathrm{ap}}, & \text{for } k \in \mathcal{K}^{\mathrm{dl}}, \end{cases} \tag{3.20}$$

and

$$\Gamma_k^{\mathrm{qt},2} \triangleq \begin{cases} \displaystyle\sum_{k' \in \mathcal{K}^{\mathrm{ul}}} p_{k'}^{\mathrm{ul}}\boldsymbol{v}_k^{\mathrm{apH}}\boldsymbol{h}_{k'}\boldsymbol{h}_{k'}^{\mathrm{H}}\boldsymbol{v}_k^{\mathrm{ap}} + \boldsymbol{v}_k^{\mathrm{apH}}\boldsymbol{H}^{\mathrm{H}}\boldsymbol{w}_{k'}^{\mathrm{ap}}\boldsymbol{w}_{k'}^{\mathrm{apH}}\boldsymbol{H}\boldsymbol{v}_k^{\mathrm{ap}} + \sigma_{\mathrm{ul}}^2\left\|\boldsymbol{v}_k^{\mathrm{ap}}\right\|_2^2, & \text{for } k \in \mathcal{K}^{\mathrm{ul}} \\ \displaystyle\sum_{k' \in \mathcal{K}^{\mathrm{dl}}} \boldsymbol{h}_k^{\mathrm{H}}\boldsymbol{w}_{k'}^{\mathrm{ap}}\boldsymbol{w}_{k'}^{\mathrm{apH}}\boldsymbol{h}_k + \left|\sqrt{p_{k'}^{\mathrm{ul}}}h_{k',k}\right|^2 + \sigma_{\mathrm{dl}}^2, & \text{for } k \in \mathcal{K}^{\mathrm{dl}} \end{cases}. \tag{3.21}$$

At this point, it is worth noticing that the objective function in (3.18a) is the difference between two concave functions, which motivates us to leverage the DC programming technique. In particular, we adopt CCP to find a solution of the problem, whereby equation (3.18a) is further modified into [152]

$$\begin{aligned} \underset{\boldsymbol{\eta},\boldsymbol{v}^{\mathrm{ap}},\boldsymbol{w}^{\mathrm{ap}},\boldsymbol{p}^{\mathrm{dl}},\boldsymbol{\gamma},\boldsymbol{s}}{\text{maximize}} \quad & \left(\prod_{k=1}^{K} f_k^{\mathrm{fin}}\left(\boldsymbol{v}^{\mathrm{ap}},\boldsymbol{w}^{\mathrm{ap}},\boldsymbol{p}^{\mathrm{dl}},\boldsymbol{\gamma},\boldsymbol{s}\right)\right)^{\frac{1}{K}} + \zeta\sum_{\ell=1}^{L}\eta_\ell\nabla\mathbb{P}(\eta_{\ell,t'}) \\ \text{subject to} \quad & \text{(3.16e) to (3.16g) and (3.18b) to (3.18d)} \end{aligned} \tag{3.22}$$

where index t' denotes the solution obtained at the $t-1$ iteration, and the first term of the objective is given by

$$f_k^{\mathrm{fin}}(\boldsymbol{v}^{\mathrm{ap}},\boldsymbol{w}^{\mathrm{ap}},\boldsymbol{p}^{\mathrm{dl}},\boldsymbol{\gamma},\boldsymbol{s}) \triangleq \alpha_k + \beta_k\Re\{s_k^*\Gamma_k^{\mathrm{qt},1}\} - \|s_k\|_2^2\,\tilde{\Gamma}_k^{\mathrm{qt},2}, \tag{3.23}$$

with $\tilde{\Gamma}_k^{\mathrm{qt},2}$ given as

$$\tilde{\Gamma}_k^{\mathrm{qt},2} \triangleq \begin{cases} \displaystyle\sum_{k' \in \mathcal{K}^{\mathrm{ul}}} p_{k'}^{\mathrm{ul}}\boldsymbol{v}_k^{\mathrm{apH}}\boldsymbol{h}_{k'}\boldsymbol{h}_{k'}^{\mathrm{H}}\boldsymbol{v}_k^{\mathrm{ap}} \\ \quad + \displaystyle\sum_{k' \in \mathcal{K}^{\mathrm{dl}}} \boldsymbol{v}_k^{\mathrm{apH}}\boldsymbol{H}^{\mathrm{H}}\boldsymbol{w}_{k',t'}^{\mathrm{ap}}\boldsymbol{w}_{k',t'}^{\mathrm{ap}\ \mathrm{H}}\boldsymbol{H}\boldsymbol{v}_k^{\mathrm{ap}} + \sigma_{\mathrm{ul}}^2\boldsymbol{v}_k^{\mathrm{apH}}\boldsymbol{v}_k^{\mathrm{ap}}, & \text{for } k \in \mathcal{K}^{\mathrm{ul}} \\ \displaystyle\sum_{k' \in \mathcal{K}^{\mathrm{dl}}} \boldsymbol{h}_k^{\mathrm{H}}\boldsymbol{w}_{k'}^{\mathrm{ap}}\boldsymbol{w}_{k'}^{\mathrm{apH}}\boldsymbol{h}_k + \sum_{k' \in \mathcal{K}^{\mathrm{ul}}}\left|\sqrt{p_{k'}^{\mathrm{ul}}}h_{k',k}\right|^2 + \sigma_{\mathrm{dl}}^2, & \text{for } k \in \mathcal{K}^{\mathrm{dl}} \end{cases}. \tag{3.24}$$

Finally, equation (3.22) can be solved by numerical convex optimization solvers such as SeDuMi and SDPT3 [153]. For convenience, we summarize in Algorithm 1 the step-by-step

Algorithm 1 Joint CF-mMIMO Beamforming and UL/DL AP Allocation via Geometric Mean Maximization for Single-Antenna UEs.

Input: Combining vectors $\boldsymbol{v}^{\mathrm{ap}}$, precorders $\boldsymbol{w}^{\mathrm{ap}}$, weights ζ and , $\forall k$, incrementation parameter ζ^{+}, and maximum number of iterations $t^{\max}$.

$\eta_{\ell}, \forall \ell \leftarrow$ Initialize as per equation (3.41)
$t \leftarrow 0$
repeat
  $\boldsymbol{\eta}_{t'} \leftarrow \boldsymbol{\eta}$
  $\boldsymbol{w}^{\mathrm{ap}}_{t'} \leftarrow \boldsymbol{w}$
  $\gamma_k \leftarrow \Gamma_k, \ \forall k$
  $s_k, \forall k \leftarrow \sqrt{(1+\gamma_k)}\Gamma^{\mathrm{qt},1}_k / \Gamma^{\mathrm{qt},2}_k, \ \forall k$
  Update $\boldsymbol{\eta}, \boldsymbol{v}^{\mathrm{ap}}, \boldsymbol{w}^{\mathrm{ap}}, \boldsymbol{p}^{\mathrm{dl}}, \boldsymbol{\gamma}$ and $\boldsymbol{s}$ by solving (3.22)
  $\zeta \leftarrow \zeta + \zeta^{+}$
  $t \leftarrow t + 1$
until convergence or $t = t^{\max}$

Output: $\boldsymbol{\eta}_{t'}, \boldsymbol{v}^{\mathrm{ap}}_{t'}, \boldsymbol{w}^{\mathrm{ap}}_{t'}$

recipe of the proposed joint beamforming design and UL/DL AP allocation scheme in the form of a pseudocode. Initialization procedures will be described in Subsection 3.3.2.

Multiple-Antenna UE

Let us next consider the extension of the work of the previous subsection to the general scenario where UEs are equipped with multiple antennas and thus have beamforming capabilities, requiring a reformulation of the optimization problem previously inrtoduced. To that end, and for the sake of notation convenience, let us first define the following quantities

$$\boldsymbol{v} = [\boldsymbol{v}^{\mathrm{apT}}_1, \ldots, \boldsymbol{v}^{\mathrm{apT}}_k, \boldsymbol{v}^{\mathrm{ueT}}_1, \ldots, \boldsymbol{v}^{\mathrm{ueT}}_K]^{\mathrm{T}}, \tag{3.25a}$$

$$\boldsymbol{w} = [\boldsymbol{w}^{\mathrm{ueT}}_1, \ldots, \boldsymbol{w}^{\mathrm{ueT}}_K, \boldsymbol{w}^{\mathrm{apT}}_1, \ldots, \boldsymbol{w}^{\mathrm{apT}}_K]^{\mathrm{T}}, \tag{3.25b}$$

$$\mathrm{UL}_{k,k'} \triangleq \boldsymbol{w}^{\mathrm{ueH}}_{k'} \boldsymbol{H}^{\mathrm{H}}_{k'} \boldsymbol{v}^{\mathrm{ap}}_k, \tag{3.25c}$$

$$\mathrm{DCLI}_{k,k'} \triangleq \boldsymbol{w}^{\mathrm{apH}}_{k'} \boldsymbol{H} \boldsymbol{v}^{\mathrm{ap}}_k, \tag{3.25d}$$

$$\mathrm{DL}_{k,k'} \triangleq \boldsymbol{w}^{\mathrm{apH}}_{k'} \boldsymbol{H}_{k'} \boldsymbol{v}^{\mathrm{ue}}_k, \tag{3.25e}$$

$$\mathrm{UCLI}_{k,k'} \triangleq \boldsymbol{w}^{\mathrm{ueH}}_{k'} \boldsymbol{H}^{\mathrm{H}}_{k',k} \boldsymbol{v}^{\mathrm{ue}}_k. \tag{3.25f}$$

Then, the geometric mean maximization problem posed in equation (B.1), extended to multiple-antenna UEs, yields

$$\begin{aligned}
\underset{\boldsymbol{\eta},\boldsymbol{v},\boldsymbol{w},\boldsymbol{p}^{\mathrm{dl}}}{\text{maximize}} \quad & \left(\prod_{k=1}^{K}\log_2\left(1+\Gamma_k^{\mathrm{m}}\right)\right)^{\frac{1}{K}}+\zeta\sum_{\ell=1}^{L}\mathbb{P}(\eta_\ell) && \text{(3.26a)}\\
\text{subject to} \quad & \left\|\boldsymbol{v}_k^{\mathrm{ue}}\right\|_2^2\leq 1,\forall k\in\mathcal{K}^{\mathrm{dl}}, && \text{(3.26b)}\\
& \left\|\boldsymbol{w}_k^{\mathrm{ue}}\right\|_2^2\leq p_k^{\mathrm{ul}},\forall k\in\mathcal{K}^{\mathrm{ul}}, && \text{(3.26c)}\\
& \text{(3.16b) to (3.16g),}
\end{aligned}$$

where Γ_k^{m} is given by

$$\Gamma_k^{\mathrm{m}}\triangleq\begin{cases}\mathrm{UL}_{k,k}^{\mathrm{H}}\Big(\sum\limits_{\substack{k'\in\mathcal{K}^{\mathrm{ul}}\\k\neq k'}}\mathrm{UL}_{k,k'}^{\mathrm{H}}\mathrm{UL}_{k,k'}\\ \qquad+\sum\limits_{k'\in\mathcal{K}^{\mathrm{dl}}}\mathrm{DCLI}_{k,k'}^{\mathrm{H}}\mathrm{DCLI}_{k,k'}+\sigma_{\mathrm{ul}}^2\left\|\boldsymbol{v}_k^{\mathrm{ap}}\right\|_2^2\Big)^{-1}\mathrm{UL}_{k,k}, & \text{for } k\in\mathcal{K}^{\mathrm{ul}}\\ \mathrm{DL}_{k,k}^{\mathrm{H}}\Big(\sum\limits_{k'\in\mathcal{K}^{\mathrm{dl}}}\mathrm{DL}_{k,k'}^{\mathrm{H}}\mathrm{DL}_{k,k'}\\ \qquad+\sum\limits_{k'\in\mathcal{K}^{\mathrm{ul}}}\mathrm{UCLI}_{k,k'}^{\mathrm{H}}\mathrm{UCLI}_{k,k'}+\sigma_{\mathrm{dl}}^2\left\|\boldsymbol{v}_k^{\mathrm{ue}}\right\|_2^2\Big)^{-1}\mathrm{DL}_{k,k}, & \text{for } k\in\mathcal{K}^{\mathrm{dl}}\end{cases}. \quad (3.27)$$

The bottleneck of Problem (3.26) is the non-convexity of equation (3.26a), which can be addressed by following the same approach employed in Subsection 3.3.1, namely, by transforming the problem using FP.For the sake of brevity, we summarize detailed derivations in Appendex B.2 and offer the resulting formulation, which yields

$$\begin{aligned}
\underset{\boldsymbol{v},\boldsymbol{w},\boldsymbol{p}^{\mathrm{dl}},\boldsymbol{\gamma},\boldsymbol{s}}{\text{maximize}} \quad & \left(\prod_{k=1}^{K}f_k^{\mathrm{qt,m}}\left(\boldsymbol{v},\boldsymbol{w},\boldsymbol{\gamma}\right)\right)^{\frac{1}{K}}+\zeta\sum_{\ell=1}^{L}\mathbb{P}(\eta_\ell) && \text{(3.28)}\\
\text{subject to} \quad & \text{(3.16e) to (3.16g), (3.18b) to (3.18d), (3.26b) and (3.26c)}
\end{aligned}$$

where

$$f_k^{\mathrm{qt,m}}\left(\boldsymbol{v},\boldsymbol{w},\boldsymbol{\gamma},\boldsymbol{s}\right)\triangleq\alpha_k+\beta_k\Re\{s_k^*\Gamma_k^{\mathrm{qt,m},1}\}-\|s_k\|_2^2\,\Gamma_k^{\mathrm{qt,m},2}, \quad (3.29)$$

with

$$\Gamma_k^{\mathrm{qt,m},1}\triangleq\begin{cases}\boldsymbol{v}_k^{\mathrm{apH}}\boldsymbol{H}_{k'}\boldsymbol{w}_{k'}^{\mathrm{ue}}, & \text{for } k\in\mathcal{K}^{\mathrm{ul}}\\ \boldsymbol{v}_k^{\mathrm{ueH}}\boldsymbol{H}_{k'}^{\mathrm{H}}\boldsymbol{w}_{k'}^{\mathrm{ap}}, & \text{for } k\in\mathcal{K}^{\mathrm{dl}}\end{cases}. \quad (3.30)$$

and $\Gamma_k^{\mathrm{qt,m,2}}$ is given by

$$\Gamma_k^{\mathrm{qt,m,2}} \triangleq \begin{cases} \sum\limits_{k' \in \mathcal{K}^{\mathrm{ul}}} \mathrm{UL}_{k,k'}^{\mathrm{H}} \mathrm{UL}_{k,k'} + \sum\limits_{k' \in \mathcal{K}^{\mathrm{dl}}} \mathrm{DCLI}_{k,k'}^{\mathrm{H}} \mathrm{DCLI}_{k,k'} + \sigma_{\mathrm{ul}}^2 \left\| \boldsymbol{v}_k^{\mathrm{ap}} \right\|_2^2, & \text{for } k \in \mathcal{K}^{\mathrm{ul}} \\ \sum\limits_{k' \in \mathcal{K}^{\mathrm{dl}}} \mathrm{DL}_{k,k'}^{\mathrm{H}} \mathrm{DL}_{k,k'} + \sum\limits_{k' \in \mathcal{K}^{\mathrm{ul}}} \mathrm{UCLI}_{k,k'}^{\mathrm{H}} \mathrm{UCLI}_{k,k'} + \sigma_{\mathrm{dl}}^2 \left\| \boldsymbol{v}_k^{\mathrm{ue}} \right\|_2^2, & \text{for } k \in \mathcal{K}^{\mathrm{dl}} \end{cases}. \tag{3.31}$$

Equation (3.28) is equivalent to equation (3.22), extended to the case of multiple-antenna UEs. Similar to equation (3.22), however, the problem described by equation (3.28) is still non-convex due to the fact that the term in equation (3.31) are products of different variables, which introduces variable coupling.

To circumvent this difficulty, we decouple equation (3.28) into two sub-problems, corresponding to the AP and UE sides, respectively. In particular, fixing UE beamforming vectors and focusing on the AP side, the joint resource allocation and beamforming design algorithm after the application of CCP to equation (3.28) yields

$$\begin{aligned} \underset{\substack{\boldsymbol{\eta}, \boldsymbol{v}^{\mathrm{ap}}, \boldsymbol{w}^{\mathrm{ap}} \\ \boldsymbol{p}^{\mathrm{dl}}, \boldsymbol{\gamma}, \boldsymbol{s}}}{\text{maximize}} \quad & \left(\prod_{k=1}^{K} f_{k,\mathrm{AP}}^{\mathrm{fin,m}} \left(\boldsymbol{v}^{\mathrm{ap}}, \boldsymbol{w}^{\mathrm{ap}} \boldsymbol{\gamma}, \boldsymbol{s} \right) \right)^{\frac{1}{K}} + \zeta \sum_{\ell=1}^{L} \eta_\ell \nabla \mathbb{P}(\eta_{\ell,t'}) \\ \text{subject to} \quad & \text{(3.16e) to (3.16g), (3.18b) to (3.18d),} \end{aligned} \tag{3.32}$$

with

$$f_{k,\mathrm{AP}}^{\mathrm{fin,m}}(\boldsymbol{v}^{\mathrm{ap}}, \boldsymbol{w}^{\mathrm{ap}}, \boldsymbol{\gamma}, \boldsymbol{s}) \triangleq \alpha_k + \beta_k \Re\{ s_k^* \tilde{\Gamma}_{k,\mathrm{AP}}^{\mathrm{qt,m,1}} \} - \| s_k \|_2^2 \tilde{\Gamma}_{k,\mathrm{AP}}^{\mathrm{qt,m,2}}, \tag{3.33}$$

where

$$\tilde{\Gamma}_{k,\mathrm{AP}}^{\mathrm{qt,m,1}} \triangleq \begin{cases} \boldsymbol{v}_k^{\mathrm{apH}} \boldsymbol{H}_k \boldsymbol{w}_{k,t'}^{\mathrm{ue}}, & \text{for } k \in \mathcal{K}^{\mathrm{ul}} \\ \boldsymbol{v}_{k,t'}^{\mathrm{ue\ H}} \boldsymbol{H}_k^{\mathrm{H}} \boldsymbol{w}_k^{\mathrm{ap}}, & \text{for } k \in \mathcal{K}^{\mathrm{dl}} \end{cases}, \tag{3.34}$$

Algorithm 2 Joint CF-mMIMO Beamforming and UL/DL AP Allocation via Geometric Mean Maximization for Multiple-Antenna UE

Input: Combining vectors $\boldsymbol{v}$, precorders $\boldsymbol{w}$, weights ζ and , $\forall k$, incrementation parameter ζ^{+}, and maximum number of iterations $t^{\max}$

$\eta_\ell, \forall \ell \leftarrow$ Initialize as per equation (3.41)
$t \leftarrow 1$
$\boldsymbol{\eta}_0 \leftarrow \boldsymbol{\eta}$
$\boldsymbol{w}_0^{\mathrm{ap}} \leftarrow \boldsymbol{w}^{\mathrm{ap}}$
repeat
  $\gamma_k \leftarrow \Gamma_k, \ \forall k$
  $s_k, \forall k \leftarrow \sqrt{(1+\gamma_k)}\Gamma_k^{\mathrm{qt},1}/\Gamma_k^{\mathrm{qt},2}, \forall k$
  Update $\boldsymbol{\eta}, \boldsymbol{v}^{\mathrm{ap}}$ and $\boldsymbol{w}^{\mathrm{ap}}$ by solving (3.32)
  $\boldsymbol{\eta}_{t'} \leftarrow \boldsymbol{\eta}$
  $\boldsymbol{w}_{t'}^{\mathrm{ap}} \leftarrow \boldsymbol{w}^{\mathrm{ap}}$
  $\gamma_k \leftarrow \Gamma_k, \ \forall k$
  $s_k, \forall k \leftarrow \sqrt{(1+\gamma_k)}\Gamma_k^{\mathrm{qt},1}/\Gamma_k^{\mathrm{qt},2}, \forall k$
  Update $\boldsymbol{v}^{\mathrm{ue}}$ and $\boldsymbol{w}^{\mathrm{ue}}$ by solving (3.36)
  $\zeta \leftarrow \zeta + \zeta^{+}$
  $t \leftarrow t + 1$
until Convergence or reach $t = t^{\max}$

Output: $\boldsymbol{\eta}_{t'}, \boldsymbol{v}_{t'}^{\mathrm{ap}}, \boldsymbol{w}_{t'}^{\mathrm{ap}}, \boldsymbol{v}_{t'}^{\mathrm{ue}}, \boldsymbol{w}_{t'}^{\mathrm{ue}}$

and $\tilde{\Gamma}_{k,\mathrm{AP}}^{\mathrm{qt,m},2}$ is given by

$$\tilde{\Gamma}_{k,\mathrm{AP}}^{\mathrm{qt,m},2} \triangleq \begin{cases} \sum\limits_{k' \in \mathcal{K}^{\mathrm{ul}}} \boldsymbol{v}_k^{\mathrm{ap}\mathrm{H}} \boldsymbol{H}_{k'} \boldsymbol{w}_{k',t'}^{\mathrm{ue}} \boldsymbol{w}_{k',t'}^{\mathrm{ue}\ \mathrm{H}} \boldsymbol{H}_{k'}^{\mathrm{H}} \boldsymbol{v}_k^{\mathrm{ap}} \\ \quad + \sum\limits_{k' \in \mathcal{K}^{\mathrm{dl}}} \boldsymbol{v}_k^{\mathrm{ap}\mathrm{H}} \boldsymbol{H}^{\mathrm{H}} \boldsymbol{w}_{k',t'}^{\mathrm{ap}} \boldsymbol{w}_{k',t'}^{\mathrm{ap}\ \mathrm{H}} \boldsymbol{H} \boldsymbol{v}_k^{\mathrm{ap}} + \sigma_{\mathrm{ul}}^2 \left\| \boldsymbol{v}_k^{\mathrm{ap}} \right\|_2^2, & \text{for } k \in \mathcal{K}^{\mathrm{ul}} \\ \sum\limits_{k' \in \mathcal{K}^{\mathrm{dl}}} \boldsymbol{v}_{k,t'}^{\mathrm{ue}\ \mathrm{H}} \boldsymbol{H}_{k'}^{\mathrm{H}} \boldsymbol{w}_{k'}^{\mathrm{ap}} \boldsymbol{w}_{k'}^{\mathrm{ap}\mathrm{H}} \boldsymbol{H}_{k'} \boldsymbol{v}_{k,t'}^{\mathrm{ue}} \\ \quad + \sum\limits_{k' \in \mathcal{K}^{\mathrm{ul}}} \boldsymbol{v}_{k,t'}^{\mathrm{ue}\ \mathrm{H}} \boldsymbol{H}_{k',k} \boldsymbol{w}_{k',t'}^{\mathrm{ue}} \boldsymbol{w}_{k',t'}^{\mathrm{ue}\ \mathrm{H}} \boldsymbol{H}_{k',k}^{\mathrm{H}} \boldsymbol{v}_{k,t'}^{\mathrm{ue}} + \sigma_{\mathrm{dl}}^2 \left\| \boldsymbol{v}_{k,t'}^{\mathrm{ue}} \right\|_2^2, & \text{for } k \in \mathcal{K}^{\mathrm{dl}} \end{cases}. \tag{3.35}$$

Finally, for fixed AP beamformers and the optimization problem to update UE beamforming counterparts is given by

$$\begin{aligned} \underset{\boldsymbol{v}^{\mathrm{ue}}, \boldsymbol{w}^{\mathrm{ue}}, \boldsymbol{\gamma}, \boldsymbol{s}}{\text{maximize}} \quad & \left(\prod_{k=1}^{K} f_{k,\mathrm{UE}}^{\mathrm{fin,m}} \left(\boldsymbol{v}^{\mathrm{ue}}, \boldsymbol{w}^{\mathrm{ue}}, \boldsymbol{\gamma}, \boldsymbol{s} \right) \right)^{\frac{1}{K}} \\ \text{subject to} \quad & \text{(3.26b) and (3.26c)}, \end{aligned} \tag{3.36}$$

where $\boldsymbol{v}^{\mathrm{ue}} = [\boldsymbol{v}_1^{\mathrm{ue}}, \ldots, \boldsymbol{v}_K^{\mathrm{ue}}]$, $\boldsymbol{w}^{\mathrm{ue}} = [\boldsymbol{w}_1^{\mathrm{ue}}, \ldots, \boldsymbol{w}_K^{\mathrm{ue}}]$,

$$f_{k,\mathrm{UE}}^{\mathrm{fin,m}}(\boldsymbol{v}^{\mathrm{ue}}, \boldsymbol{w}^{\mathrm{ue}}, \boldsymbol{\gamma}, \boldsymbol{s}) \triangleq \alpha_k + \beta_k \Re\{s_k^* \tilde{\Gamma}_{k,\mathrm{UE}}^{\mathrm{qt},m,1}\} - \|s_k\|_2^2 \, \Gamma_{k,\mathrm{UE}}^{\mathrm{qt},m,2}, \tag{3.37}$$

with

$$\tilde{\Gamma}_{k,\mathrm{UE}}^{\mathrm{qt,m,1}} = \begin{cases} \boldsymbol{v}_{k,t'}^{\mathrm{ap}\ \mathrm{H}} \boldsymbol{H}_k \boldsymbol{w}_k^{\mathrm{ue}}, & \text{for } k \in \mathcal{K}^{\mathrm{ul}} \\ \boldsymbol{v}_k^{\mathrm{ue H}} \boldsymbol{H}_k^{\mathrm{H}}, \boldsymbol{w}_{k,t'}^{\mathrm{ap}}, & \text{for } k \in \mathcal{K}^{\mathrm{dl}}. \end{cases} \tag{3.38}$$

and $\Gamma_{k,\mathrm{UE}}^{\mathrm{qt,m,2}}$ given by

$$\Gamma_{k,\mathrm{UE}}^{\mathrm{qt,m,2}} \triangleq \begin{cases} \displaystyle\sum_{k' \in \mathcal{K}^{\mathrm{ul}}} \boldsymbol{v}_{k,t'}^{\mathrm{ap}\ \mathrm{H}} \boldsymbol{H}_{k'} \boldsymbol{w}_{k'}^{\mathrm{ue}} \boldsymbol{w}_{k'}^{\mathrm{ue H}} \boldsymbol{H}_{k'}^{\mathrm{H}} \boldsymbol{v}_{k,t'}^{\mathrm{ap}} \\ \quad + \displaystyle\sum_{k' \in \mathcal{K}^{\mathrm{dl}}} \boldsymbol{v}_{k,t'}^{\mathrm{ap}\ \mathrm{H}} \boldsymbol{H}^{\mathrm{H}} \boldsymbol{w}_{k'}^{\mathrm{ap}} \boldsymbol{w}_{k'}^{\mathrm{ap H}} \boldsymbol{H} \boldsymbol{v}_{k,t'}^{\mathrm{ap}} + \sigma_{\mathrm{ul}}^2 \left\| \boldsymbol{v}_{k,t'}^{\mathrm{ap}} \right\|_2^2, & \text{for } k \in \mathcal{K}^{\mathrm{ul}} \\ \displaystyle\sum_{k' \in \mathcal{K}^{\mathrm{dl}}} \boldsymbol{v}_k^{\mathrm{ue H}} \boldsymbol{H}_{k'}^{\mathrm{H}} \boldsymbol{w}_{k',t'}^{\mathrm{ap}} \boldsymbol{w}_{k',t'}^{\mathrm{ap}\ \mathrm{H}} \boldsymbol{H}_{k'} \boldsymbol{v}_k^{\mathrm{ue}} \\ \quad + \displaystyle\sum_{k' \in \mathcal{K}^{\mathrm{ul}}} \boldsymbol{v}_k^{\mathrm{ue H}} \boldsymbol{H}_{k',k} \boldsymbol{w}_{k',t'}^{\mathrm{ue}} \boldsymbol{w}_{k',t'}^{\mathrm{ue}\ \mathrm{H}} \boldsymbol{H}_{k',k}^{\mathrm{H}} \boldsymbol{v}_k^{\mathrm{ue}} + \sigma_{\mathrm{dl}}^2 \left\| \boldsymbol{v}_k^{\mathrm{ue}} \right\|_2^2, & \text{for } k \in \mathcal{K}^{\mathrm{dl}} \end{cases} . \tag{3.39}$$

The optimization problems given in equations (3.32) and (3.36) can be solved using convex optimization solvers, leading to an alternating procedure for the joint resource allocation and beamforming design in CF-mMIMO with multiple-antenna UEs, which we summarize as a pseudo code in Algorithm 2.

3.3.2 Initialization: Pre-Selection of APs

Despite all the measures taken to convexify the problems whose solutions led to Algorithms 1 and 2, the fact that the underlying original problem given in equation (3.16) is non-convex, and in particular the combinatorial nature of the AP allocation vector $\boldsymbol{\eta}$, makes the performance of the methods described above dependent on reasonably good initializers.

We therefore introduce in this subsection a novel UL/DL pre-allocation method which can be used to initialize the AP selection vector $\boldsymbol{\eta}$ by taking advantage of the available CSI knowledge. To that end, consider the k-th UE for any given ℓ-th AP such that $k = \underset{k \in \mathcal{K}}{\mathrm{argmax}}(\mathbb{E}[\left\| \boldsymbol{h}_{k,\ell} \right\|_2^2])$, and define the corresponding relative received signal strength indicator (RRSSI)

$$\zeta_{k,\ell} \triangleq \frac{\left\| \boldsymbol{h}_{k,\ell} \right\|_2^2}{\max(\left\| \boldsymbol{h}_{1,\ell} \right\|_2^2, \ldots, \left\| \boldsymbol{h}_{K,\ell} \right\|_2^2)}. \tag{3.40}$$

Finally, let us consider a threshold ρ that characterizes the greediness to pre-allocate an AP, and initialize $\boldsymbol{\eta}$ by

$$\eta_\ell = \begin{cases} 1 & \text{if } k \in \mathcal{K}^{\text{ul}} \text{ and } \max\limits_{\substack{k' \in \mathcal{K}^{\text{dl}} \\ k' \neq k}} (\zeta_{k',\ell}) < \rho, \\ 0 & \text{if } k \in \mathcal{K}^{\text{dl}} \text{ and } \max\limits_{\substack{k' \in \mathcal{K}^{\text{ul}} \\ k' \neq k}} (\zeta_{k',\ell}) < \rho, \\ \text{uniform random} \in [0,1] & \text{otherwise.} \end{cases} \tag{3.41}$$

In plain words, what equation (3.41) implies is that: a) if a given ℓ-th AP is surrounded by an UL UE with a ρ-dominant RRSSI, then that AP is pre-allocated to UL; or else b) if conversely the AP is surrounded by a DL UE with a ρ-dominant RRSSI it is pre-allocated to DL; or else c) the AP is pre-allocated to UL or DL randomly.

We emphasize that this procedure is heuristic and obviously not optimal, but again, the procedure is intuitively better than a purely random pre-allocation, and only employed to initialize the vector $\boldsymbol{\eta}$ before the execution of Algorithm 1 or 2, from which optimized AP allocations are obtained, as shall be demonstrated in the sequel.

3.4 Complexity Analysis

Before moving on to the numerical performance evaluation of the proposed geometric-mean maximization-based method in comparison to the aforementioned benchmarks, it is of interest to analyze their computational complexities.

For starters, let us recall that the proposed method for the scenario with single-antenna UEs is fundamentally described by equation (3.22), while that for the case of multiple-antenna UEs is described by the pair of equations (3.32) and (3.36), which correspond to the optimization of APs and UEs, respectively. In turn, the improved sum-rate maximization and max-min rate SotA methods employed as benchmark are respectively described fundamentally by equations (3.53) and (3.54).

Next, notice that the most expensive operation associated with all these optimization problems is the computation of the corresponding QCPs ε-solution, whose canonical arithmetic complexity C can be upper-bounded by [154, 155]

$$C \leq \tilde{N}\left(\tilde{N}^2 + \tilde{M} + \sum_{m=1}^{\tilde{M}} Q_m^2\right)\sqrt{1+\tilde{M}}\,\text{digit}(\varepsilon), \tag{3.42}$$

where $\tilde{M}$, $\tilde{N}$, and Q_m respectively denote the number of constraints in the problem, the size (*i.e.*, vector dimension) of the real-valued multidimensional variable, and the size of the m-th constraint space; while the constant quantity $\text{digit}(\varepsilon)$ is the order of precision of the ε-solution in terms of its distance to the optimum [155].

Leaving details to Appendix C, after transforming equation (3.22) into the QCP canonical form described by equation (C.10), we obtain

$$\tilde{M}^{\text{ap}} = \overbrace{4}^{\text{from (3.16f), (3.16g), (C.2b), and (C.10b)}} + \underbrace{\bar{K}}_{\text{from (C.10c)}} + \overbrace{K}^{\text{from (C.8c) and (C.8d)}} + \underbrace{2L}_{\text{from (3.18b) and (3.16e)}} + \overbrace{LK}^{\text{from (3.18c) and (3.18d)}}, \tag{3.43a}$$

$$\tilde{N}^{\text{ap}} = \underbrace{1 + L - \bar{L} + (2M+1)LK}_{\text{from the variables } n, \boldsymbol{\eta}, \boldsymbol{v}^{\text{ap}}, \boldsymbol{w}^{\text{ap}} \text{ and } \boldsymbol{p}^{\text{dl}} \text{ stacked in } \boldsymbol{x} \text{ as in (C.10e)}} + \overbrace{\bar{K}}^{\text{from the auxiliary variable vector } \boldsymbol{o} \text{ as in (C.10g), stacked in } \boldsymbol{x}}, \tag{3.43b}$$

$$\begin{aligned}\sum_{m=1}^{\tilde{M}^{\text{ap}}} (Q_m^{\text{ap}})^2 = {} & \overbrace{4}^{\text{from (C.10b)}} + \underbrace{9\bar{K}}_{\text{from (C.10c)}} + \overbrace{2(L-\bar{L})^2}^{\text{from (3.16f) and (3.16g)}} + \overbrace{(L-\bar{L})}^{\text{from (3.18b)}} \\ & + \Big(\underbrace{(2M+1)^2 K^{\text{ul}}}_{\text{from (3.18c)}} + \overbrace{(2M+2)^2 K^{\text{dl}}}^{\text{from (3.18d)}} + \overbrace{K^2}^{\text{from (3.16e)}} \Big) L \\ & + \underbrace{4\big(K^{\text{ul}} + (K^{\text{dl}})^3\big) L^2 M^2}_{\text{dominant terms from (C.8c) and (C.8d)}},\end{aligned} \tag{3.43c}$$

where K^{ul} and K^{dl} are the number of UL UEs and that of DL UEs, respectively; $\bar{L}$ denotes the number of initialized APs according to equation (3.41); and $\bar{K} = \sum_{j=1}^{\lceil \log_2(K) \rceil} 2^{\lceil \log_2(K) \rceil - j}$ is the number of variables (including original and auxiliary) required to reformulate the geometric mean product described in equation (3.22) into its QCP canonical form as in equation (C.10).

From equations (3.42) through (3.43c), it follows that the total complexity of Algorithm 1 can be estimated at

$$\begin{aligned} C_1 &\leq \tilde{N}^{\text{ap}} \Big((\tilde{N}^{\text{ap}})^2 + \tilde{M}^{\text{ap}} + \sum_{m=1}^{\tilde{M}^{\text{ap}}} (Q_m^{\text{ap}})^2 \Big) \sqrt{1 + \tilde{M}^{\text{ap}}} \, \text{digit}(\varepsilon^{\text{ap}}) \\ &= O\big(L^3 M^3 K \sqrt{LK} \max(K^2, (K^{\text{dl}})^3) \big), \end{aligned} \tag{3.44}$$

where in the last line only the term of higher order is kept.

Next, we turn our attention to Algorithm 2, which differs from Algorithm 1 in the assumption that UEs are equipped with multiple antennas, implicating on the one hand that the optimization of the APs is updated from equation (3.22) to equation (3.32), and on the other hand that UEs are capable of beamforming as described by equation (3.36).

Looking at the AP side first, it is evident from the comparison of equations (3.22) and (3.32) that these differ only in the objective function, which are based on equations (3.23) and (3.33), respectively. In turn, these objective functions are dependent on the quantities $\Gamma_k^{\mathrm{qt},1}$ and $\tilde{\Gamma}_k^{\mathrm{qt},2}$ described in equations (3.19) and (3.24) in the single-antenna UE case; and on $\tilde{\Gamma}_{k,\mathrm{AP}}^{\mathrm{qt,m},1}$ and $\tilde{\Gamma}_{k,\mathrm{AP}}^{\mathrm{qt,m},2}$) as per equations (3.34) and (3.35) in the multiple-antenna UE case, respectively. Comparing therefore equations (3.34) and (3.35) to equations (3.19) and (3.24) directly, it can be seen that the only increase in complexity in solving problem (3.32) as opposed to (3.22) is the slight increase in the number of complex multiplications corresponding to the upgrade of channel vectors $\boldsymbol{h}_k$ to channel matrices $\boldsymbol{H}_k$, which is negligible compared to the costs accounted for in equation (3.44).

In other words, and in summary, we conclude that the computational complexity of the first part of Algorithm 2 corresponding to the optimization of APs as per equation (3.32) is of the same order of that of Algorithm 1, already estimated in equation (3.44).

In turn, the computational cost of the Problem (3.36), which is the UE beamforming part in Algorithm 2, can be evaluated following a similar previous procedure. Namely, transforming Problem (3.36) into the QCP canonical form following details to Appendix C, the number of constraints, the real-valued multivariable dimension, and the size of constraint space, respectively given by

$$\tilde{M}^{\mathrm{ue}} = 2K + \bar{K} + 2, \tag{3.45a}$$

$$\tilde{N}^{\mathrm{ue}} = 2NK + \bar{K} + 1, \tag{3.45b}$$

and

$$\sum_{m=1}^{\tilde{M}} (Q_m^{\mathrm{ue}})^2 = 4\left((K^{\mathrm{ul}})^3 + K^{\mathrm{dl}}\right) N^2 + 9\bar{K} + 4, \tag{3.45c}$$

the total complexity of Algorithm 2 can be estimated at

$$\begin{aligned} C_2 &\leq C_1 + \tilde{N}^{\mathrm{ue}}\left((\tilde{N}^{\mathrm{ue}})^2 + \tilde{M}^{\mathrm{ue}} + \sum_{m=1}^{\tilde{M}^{\mathrm{ue}}} (Q_m^{\mathrm{ue}})^2\right)\sqrt{1+\tilde{M}^{\mathrm{ue}}}\,\mathrm{digit}(\varepsilon) \\ &= C_1 + O(N^3 K\sqrt{K}\max(K^2, (K^{\mathrm{ul}})^3)). \end{aligned} \tag{3.46}$$

Finally, we consider the complexities of the total throughput maximization and max-min worst-case approaches, which are summarized fundamentally by equations (3.53) and (3.54), respectively.

To that end, first recognize that Problem (3.53) differs from Problem (3.32) only in the evaluation of a sum (as opposed to the geometric mean) in the objective function. Since this distinction has negligible impact in computational cost, it is concluded that the throughput maximization and the proposed method described in Algorithm 2 have the same complexity.

Similarly, moving the rate functions f_k^{fin} to a set of constraints, as done in the max-min worst-case approach under equation (3.54b), only slightly decreases the number of constraints of the QCP canonical form corresponding to equation (3.54), such that the max-min worst-case approach has actually a slightly lower computational complexity than the proposed summarized in Algorithm 2, which however results in a negligible overall change in the total cost.

Consequently, we will consider hereafter that the SotA benchmark methods are on par with the proposed method in terms of computational complexity.

3.5 Numerical Results

Before moving to a direct performance assessment of the proposed algorithms, it is useful to establish SotA benchmarks for comparison, and to analyze the complexity of the corresponding solutions, which will be pursued in the next subsections.

3.5.1 State-of-the-Art Benchmark Solutions

Two distinct approaches that form the basis of SotA benchmark solutions are the sum-rate maximization approach of [141–145], and the max-min worst-case strategy pursued in [146, 115, 147], both of which are briefly reviewed below for the convenience of the reader.

Since in the aforementioned articles only the case of single-antenna UEs is addressed, and since (as shall be latter shown) the proposed method already outperforms the latter in such a scenario, suffice it to consider here only benchmark approaches for the single-antenna UEs case. Under such conditions, the sum throughput maximization and max-min worst-case approaches are respectively described by the optimization problems

$$\begin{aligned} \underset{\boldsymbol{\eta},\boldsymbol{v}^{\text{ap}},\boldsymbol{w}^{\text{ap}},\boldsymbol{p}^{\text{dl}}}{\text{maximize}} \quad & \sum_{k\in\mathcal{K}} \log_2\left(1+\Gamma_k\right) \\ \text{subject to} \quad & \text{(3.16e) to (3.16g) and (3.18b), to (3.18d),} \end{aligned} \tag{3.47}$$

and

$$\underset{b,\boldsymbol{\eta},\boldsymbol{v}^{\mathrm{ap}},\boldsymbol{w}^{\mathrm{ap}},\boldsymbol{p}^{\mathrm{dl}}}{\text{maximize}} \quad b \tag{3.48a}$$

$$\text{subject to} \quad \log_2\left(1+\Gamma_k\right) \geq b, \forall k \tag{3.48b}$$

$$\text{(3.16e) to (3.16g) and (3.18b) to (3.18d)}$$

where b is the lower bound of the throughput of all UEs.

Obviously, the latter problems are not convex, due to the objective function in (3.47) and the constraint (3.48b), respectively. In existing works relying on these approaches [105, 141–146, 115, 147], the first-order Taylor approximation is typically employed to convexify and solve the problem.

Here, however, for the sake of consistency and in order to maintain an equal footing for the subsequent comparison with our own proposed method, we instead employ the lagrangian dual transform (LDT) and quadratic transform (QT) techniques of Lemmas 1 and 2 shown in Appendix A, respectively, without compromising the performance of the SotA methods [144, 149, 151].

In other words, here the problems (3.47) and (3.48) are respectively transformed via the same convexification techniques described in Section 3.3.1 into

$$\underset{\boldsymbol{\eta},\boldsymbol{v}^{\mathrm{ap}},\boldsymbol{w}^{\mathrm{ap}},\boldsymbol{p}^{\mathrm{dl}},\boldsymbol{\gamma},\boldsymbol{s}}{\text{maximize}} \quad \sum_{k\in\mathcal{K}} f_k^{\mathrm{fin}}\left(\boldsymbol{v}^{\mathrm{ap}},\boldsymbol{w}^{\mathrm{ap}},\boldsymbol{p}^{\mathrm{dl}},\boldsymbol{\gamma},\boldsymbol{s}\right) \tag{3.49}$$

$$\text{subject to} \quad \text{(3.16e) to (3.16g) and (3.18b) to (3.18d),}$$

and

$$\underset{b,\boldsymbol{\eta},\boldsymbol{v}^{\mathrm{ap}},\boldsymbol{w}^{\mathrm{ap}},\boldsymbol{p}^{\mathrm{dl}},\boldsymbol{\gamma},\boldsymbol{s}}{\text{maximize}} \quad b \tag{3.50a}$$

$$\text{subject to} \quad f_k^{\mathrm{fin}}\left(\boldsymbol{v}^{\mathrm{ap}},\boldsymbol{w}^{\mathrm{ap}},\boldsymbol{p}^{\mathrm{dl}},\boldsymbol{\gamma},\boldsymbol{s}\right) \geq b \tag{3.50b}$$

$$\text{(3.16e) to (3.16g) and (3.18b) to (3.18d),}$$

with f_k^{fin} as already defined in equation (3.23).

3.5.2 Improved Benchmark Solutions

As described in Subsection 3.3.1, the solutions of the problems described by equations (3.49) and (3.54) still suffer from the effect of relaxing the UL/DL allocation variable η_ℓ from its

discrete domain $\eta_\ell \in \{0, 1\}$ to its convex hull $\eta_\ell \in [0, 1]$, which can be alleviated by the introduction of the weighted negative entropy discretizer $\zeta\mathbb{P}(\eta_\ell)$ into the problem.

Concisely, under such modification, the η-discretized sum throughput maximization problem of equation (3.47) and the max-minimum throughput problem of equation (3.48) become, respectively

$$\begin{aligned} \underset{\boldsymbol{\eta},\boldsymbol{v}^{\mathrm{ap}},\boldsymbol{w}^{\mathrm{ap}},\boldsymbol{p}^{\mathrm{dl}}}{\text{maximize}} \quad & \sum_{k\in\mathcal{K}} \log_2\left(1+\Gamma_k\right) + \zeta \sum_{\ell=1}^{L} \mathbb{P}(\eta_\ell) \\ \text{subject to} \quad & \text{(3.16e) to (3.16g) and (3.18b), to (3.18d),} \end{aligned} \tag{3.51}$$

and

$$\underset{b,\boldsymbol{\eta},\boldsymbol{v}^{\mathrm{ap}},\boldsymbol{w}^{\mathrm{ap}},\boldsymbol{p}^{\mathrm{dl}}}{\text{maximize}} \quad b + \zeta \sum_{\ell=1}^{L} \mathbb{P}(\eta_\ell) \tag{3.52a}$$

$$\text{subject to} \quad \log_2\left(1+\Gamma_k\right) \geq b, \forall k \tag{3.52b}$$

$$\text{(3.16e) to (3.16g) and (3.18b) to (3.18d),}$$

which after the convexification techniques described in Subsection 3.3.1, *i.e.*, LDT, QT and CCP, respectively turn into

$$\begin{aligned} \underset{\substack{\boldsymbol{\eta},\boldsymbol{v}^{\mathrm{ap}},\boldsymbol{w}^{\mathrm{ap}},\\ \boldsymbol{p}^{\mathrm{dl}},\boldsymbol{\gamma},\boldsymbol{s}}}{\text{maximize}} \quad & \sum_{k\in\mathcal{K}} f_k^{\mathrm{fin}}\left(\boldsymbol{v}^{\mathrm{ap}}, \boldsymbol{w}^{\mathrm{ap}}, \boldsymbol{p}^{\mathrm{dl}}, \boldsymbol{\gamma}, \boldsymbol{s}\right) + \zeta \sum_{\ell=1}^{L} \eta_\ell \nabla\mathbb{P}(\eta_\ell^{t-1}) \\ \text{subject to} \quad & \text{(3.16e) to (3.16g) and (3.18b) to (3.18d),} \end{aligned} \tag{3.53}$$

and

$$\underset{\substack{b,\boldsymbol{\eta},\boldsymbol{v}^{\mathrm{ap}},\boldsymbol{w}^{\mathrm{ap}},\\ \boldsymbol{p}^{\mathrm{dl}},\boldsymbol{\gamma},\boldsymbol{s}}}{\text{maximize}} \quad b + \zeta \sum_{\ell=1}^{L} \eta_\ell \nabla\mathbb{P}(\eta_\ell^{t-1}) \tag{3.54a}$$

$$\text{subject to} \quad f_k^{\mathrm{fin}}\left(\boldsymbol{v}^{\mathrm{ap}}, \boldsymbol{w}^{\mathrm{ap}}, \boldsymbol{p}^{\mathrm{dl}}, \boldsymbol{\gamma}, \boldsymbol{s}\right) \geq b, \forall\, k \tag{3.54b}$$

$$\text{(3.16e) to (3.16g) and (3.18b) to (3.18d),}$$

again, with f_k^{fin} as defined in equation (3.23).

To offer a quick glimpse on the performances of these benchmark approaches relative to one another, Fig. 3.2 shows the cumulative distribution functions (CDFs) of the sum SEs achieved by both methods, with simulation parameters as specified in Section 3.5.3. In this and all subsequent figures, the labels "Min-rate" and "Sum-rate" refer respectively to

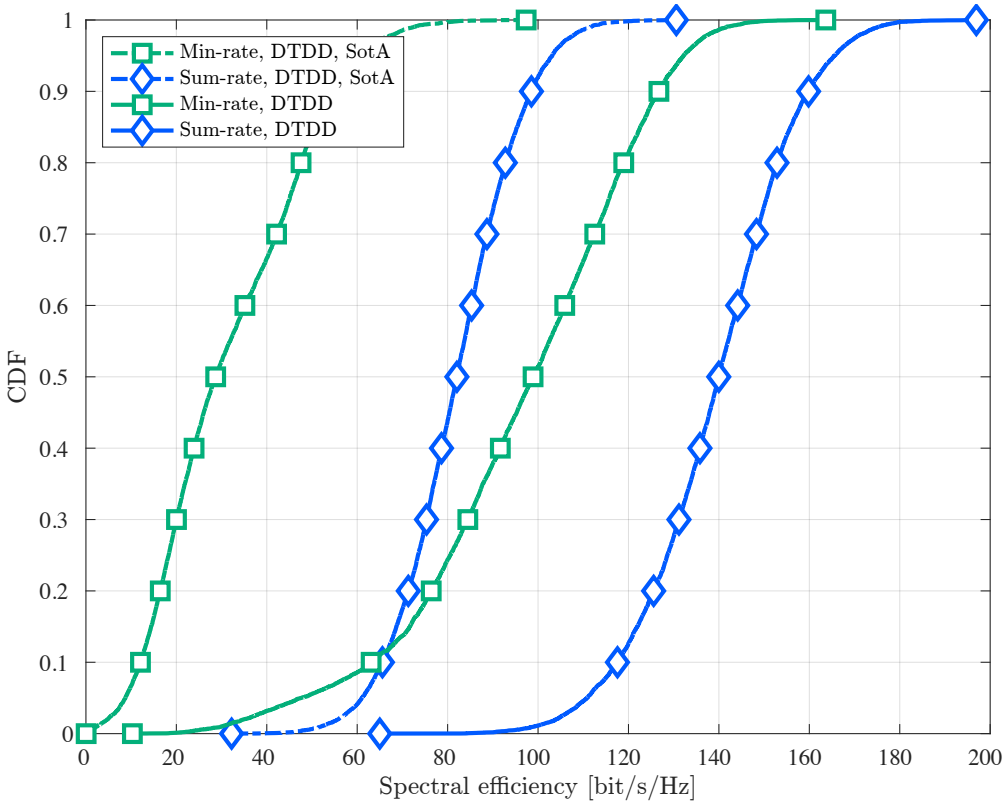

Fig. 3.2 CDF of the sum SE for the sum-rate maximization and the max-min worst-case SotA benchmark solutions.

the max-min worst-case and the sum-rate maximization methods, with the additional word "SotA" and dash-dot lines used to distinguish the methods revised in Subsection 3.5.1 from the improved benchmark versions of this subsection.

The figure shows that indeed the SotA schemes are significantly outperformed by the improved benchmark variations, due to rounding errors in the indicator variable η_ℓ. In view of these results, we will hereafter consider the improved benchmark alternatives when assessing the performance of our own proposed solution, emphasizing, however, that these benchmark schemes already incorporate contributions here introduced.

3.5.3 Computer simulations

Simulation Set-Up

Having established the complexity analysis of the proposed geometric-mean-based scheme for joint AP access configuration and beamforming, we proceed to numerically evaluate the performance of the proposed method under various conditions, comparing it with the SotA benchmarks.

In what follows it is assumed that APs are distributed in a regular grid formation within the effective service area, while UEs are randomly and uniformly distributed over the area. The remaining simulation parameters are summarized in Table 3.1, with the quantity d used in the modeling of large-scale fading denoting the distance between the transmitter and receiver, and the quantity z representing shadowing with a standard deviation of 10 [dB], as considered in related CF-mMIMO literature such as [65, 105]. Also following [65, 105], it is assumed that APs have a height of 10 m above the ground surface.

Table 3.1 Simulation Parameters.

Number of APs (L)	64
Number of antennas APs (M)	1
Number of UEs (K)	16
Number of antennas each UEs (N)	[1, 8]
Coverage area	500×500 [m^2]
Large-scale fading (g, $g_{k,k'}$)	$-35.3 - 37.6\log_{10}(d) + z$
Bandwidth	20 [MHz]
Noise figure	7 [dB]
Transmit power of each UE	100 [mW]
Maximum transmit power of each AP	1 [W]

In order to focus on the assessment on the improvement provided by the proposed method itself, perfect CSI knowledge is assumed at transmitters and receivers. This assumption have been widely used in other CF mMIMO literatures [156–159]. The convex optimization problems (3.22), (3.32), and (3.36) in Algorithms 1 and 2 are solved via CVX [153], using the SDPT3 backend and with the maximum number of iterations set to $t^{\max} = 30$.

In each realization of simulations performed, the weight applied to the negative entropy function is initialized to $\zeta = 0$ and, after the fifth iteration, increased at each iteration by the increment ζ^+, which is numerically optimized so as to maximize the system throughput of each tested method, including the improved benchmark SotA approaches described in Subsection 3.5.2.

Finally, in order to avoid numerical instability, the solution obtained at the previous iteration is utilized as the final output of the algorithm if the solver outputs an invalid solution in the middle of the loop.

Single-Antenna UE Case

Let us start by evaluating the performance of the proposed and SotA methods in the scenario where each UE has a single antenna. Fig. 3.5 shows the CDFs of the sum SEs for the different approaches compared, and different ratios of UEs operating in UL mode, as indicated by the quantity q.

The performance of the "MMSE" method in the conventional TDD mode is also included as a reference, with UL and DL MMSE beamformers respectively obtained from

$$\boldsymbol{v}_k^{\mathrm{ap}} \triangleq \sqrt{p_k^{\mathrm{ul}}} \left(\sum_{k \in \mathcal{K}^{\mathrm{ul}}} p_k^{\mathrm{ul}} \boldsymbol{h}_k \boldsymbol{h}_k^{\mathrm{H}} + \sigma_{ul}^2 I_{ML} \right)^{-1} \boldsymbol{h}_k, \tag{3.55a}$$

$$\boldsymbol{w}_k^{\mathrm{ap}} \triangleq \sqrt{p_k^{\mathrm{dl}}} \frac{\sqrt{p_k^{\mathrm{dl}}} \left(\sum_{k \in \mathcal{K}^{\mathrm{dl}}} p_k^{\mathrm{dl}} \boldsymbol{h}_k \boldsymbol{h}_k^{\mathrm{H}} + \sigma_{dl}^2 I_{ML} \right)^{-1} \boldsymbol{h}_k}{\left\| \sqrt{p_k^{\mathrm{dl}}} \left(\sum_{k \in \mathcal{K}^{\mathrm{dl}}} p_k^{\mathrm{dl}} \boldsymbol{h}_k \boldsymbol{h}_k^{\mathrm{H}} + \sigma_{dl}^2 I_{ML} \right)^{-1} \boldsymbol{h}_k \right\|_2}, \tag{3.55b}$$

where DL MMSE beamformer [160–162] is allocated by same power for all UEs as $p_k^{\mathrm{dl}} = p^{\mathrm{dl,max}}/(qK)$.

In all figures, the legend "Geo-Mean" refers to the performance of Algorithm 1, while "Sum-Rate" and "Min-Rate" refer to improved sum-rate maximization and max-min worst case benchmark approaches via equations (3.53) and (3.54), respectively. The legend "DTDD" corresponds to a system that operates in NAFD regardless of the AP access configuration, but with beamforming design employed, whereas "TDD" corresponds to a TDD-based system with time resource partition relative to the access request ratio q. The additional token "w/o Init" added to some of the legends, refer to systems in which the initialized pre-allocation of APs according to equation (3.41) is not performed. The curves corresponding to such alternatives are plotted with dash lines for further visibility. Finally, in all methods compared, the beamforming quantities are initialized by the maximum ratio (conjugate) beamforming method [65].

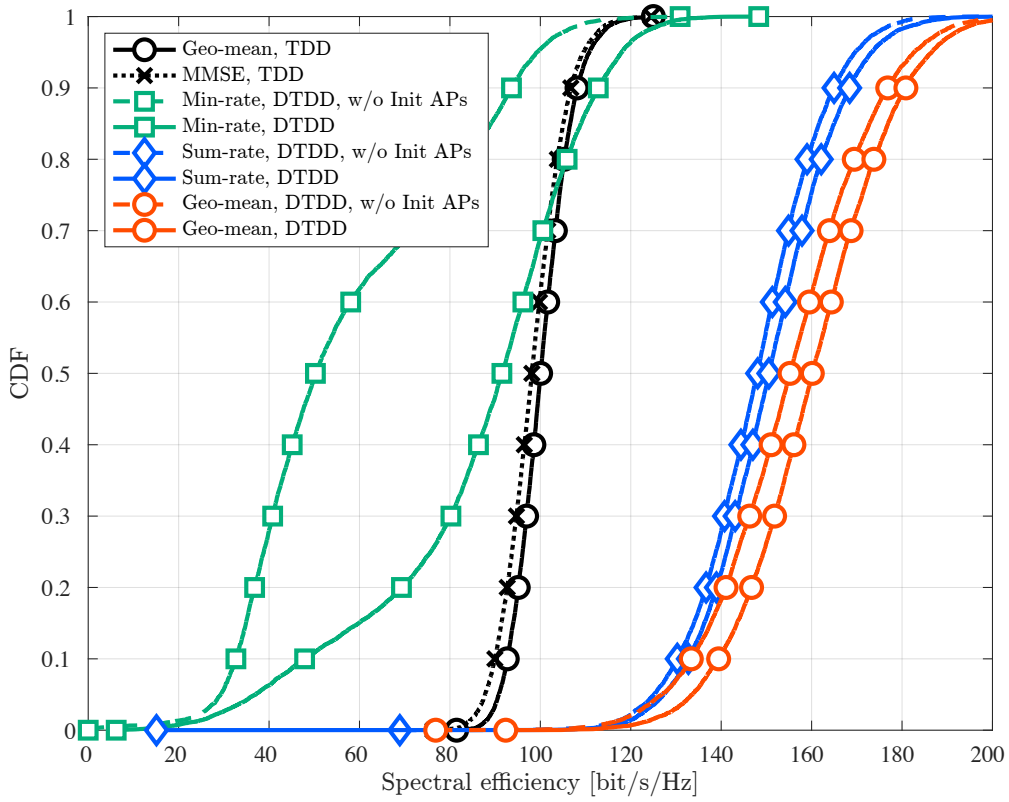

Fig. 3.3 Comparison of the CDF of the total SE for different approaches under the predominantly DL ($q = 0.25$).

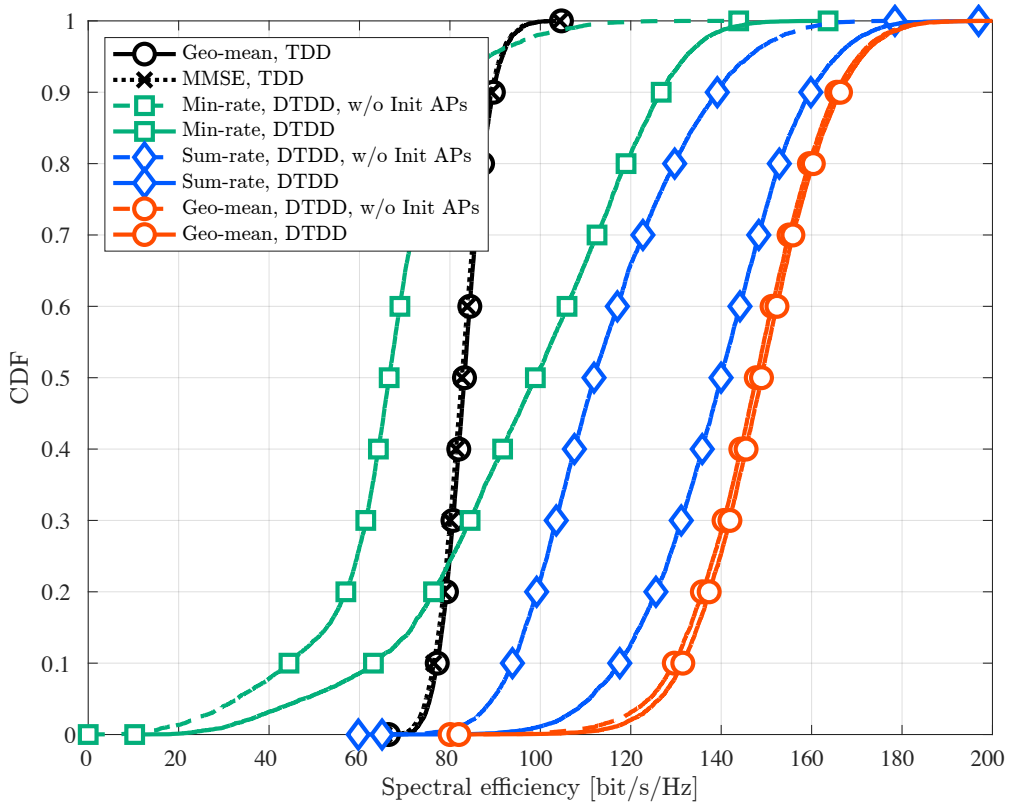

Fig. 3.4 Comparison of the CDF of the total SE for different approaches under the balanced UL/DL ($q = 0.5$).

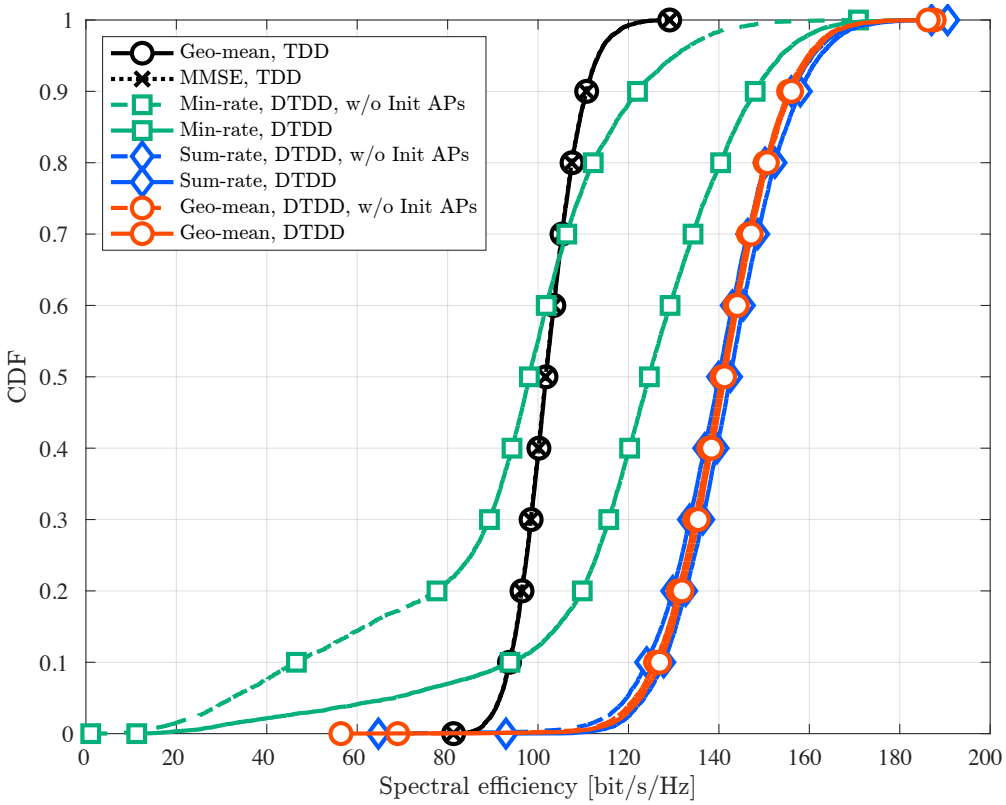

Fig. 3.5 Comparison of the CDF of the total SE for different approaches under the predominantly UL ($q = 0.75$).

From Fig. 3.5 – which covers a predominantly DL scenario ($q = 0.25$), a predominantly UL scenario ($q = 0.75$), and a balanced UL/DL scenario ($q = 0.5$) – it is found that dynamic TDD yields significantly higher SEs compared TDD mode, both with the proposed and SotA methods. This indicates that thanks to joint AP allocation and beamforming optimization, NAFD takes better advantage of time resources to serve users, and of spatial resources to control harmful interference, ultimately resulting in higher rates.

It is also observed that among all methods compared, the max-min worst-case approach is the most sensitive to initialization, with large performance gains resulting from the pre-allocation of Subsection 3.3.2 observed under that particular method. The max-min worst-case scheme is also found to be the most sensitive to the UL and DL demands, with large differences in overall SE observed between predominantly DL, balanced, and predominantly UL scenarios.

In turn, it is found that both the sum-rate maximization and the proposed geometric mean maximization approaches are most reliable and best-performing methods, with the latter slightly outperforming the former especially under predominantly DL conditions. At this point we might once again emphasize, however, that the sum-rate maximization method

benchmark whose results are shown in Fig. 3.5 already include the improvements described in Subsection 3.5.2, such that the gains of the proposed method against SotA as-is, *e.g.* [141–145], is actually larger, as can be seen from Fig. 3.2.

We also remark that both the max-min worst-case and sum-rate maximization methods impose a trade-off between performance and QoS fairness, sacrificing either of the two important communication requirements. In contrast, as shall be shown latter, the proposed algorithm is designed to tackle this issue avoiding the sacrifice of fairness while improving upon the SE performance of SotA alternatives.

Convergence

Before evaluating the fairness of the methods compared, let us briefly study the average convergence behavior of the three distinct approaches in terms of the number of APs allocated to UL, under the same balanced conditions of Fig. 3.4.

To this end, we plot in Fig. 3.6 the values of η_ℓ obtained with the improved benchmark SotA and proposed methods, as a function of the number of iterations. The results indicate that the AP access configuration reached by the proposed method differs significantly from those of the improved SotA methods. It is also noticeable, in fact, that the proposed approach is the only one that arrives at a configuration in which the same number of APs are allocated to UL and DL, as intuitively expected for the balanced UL/DL case considered. Given that fundamentally only the objective function of the proposed method differs from those of the improved SotA alternatives, and since the same negative entropy based discretizer is utilized in all methods compared, this finding confirms the efficacy of the geometric mean rate, as opposed to the other more traditional figures of merit, as the objective of joint allocation and beamforming optimization techniques for CF-mMIMO systems.

Finally, we compare in Fig. 3.7 the convergence behavior of the proposed and improved benchmark SotA algorithms in terms of the achieved average SE computed with the continuously-relaxed η_ℓ at each iteration. Notice that the SE performance shown in Fig. 3.7 is not the actual SE with discretized $\eta_\ell \in \{0, 1\}$. At the last iteration ($t = 30$), however, we fix η_ℓ's to either 0 or 1, which results in slight decrement in performance due to rounding at $t = 30$.

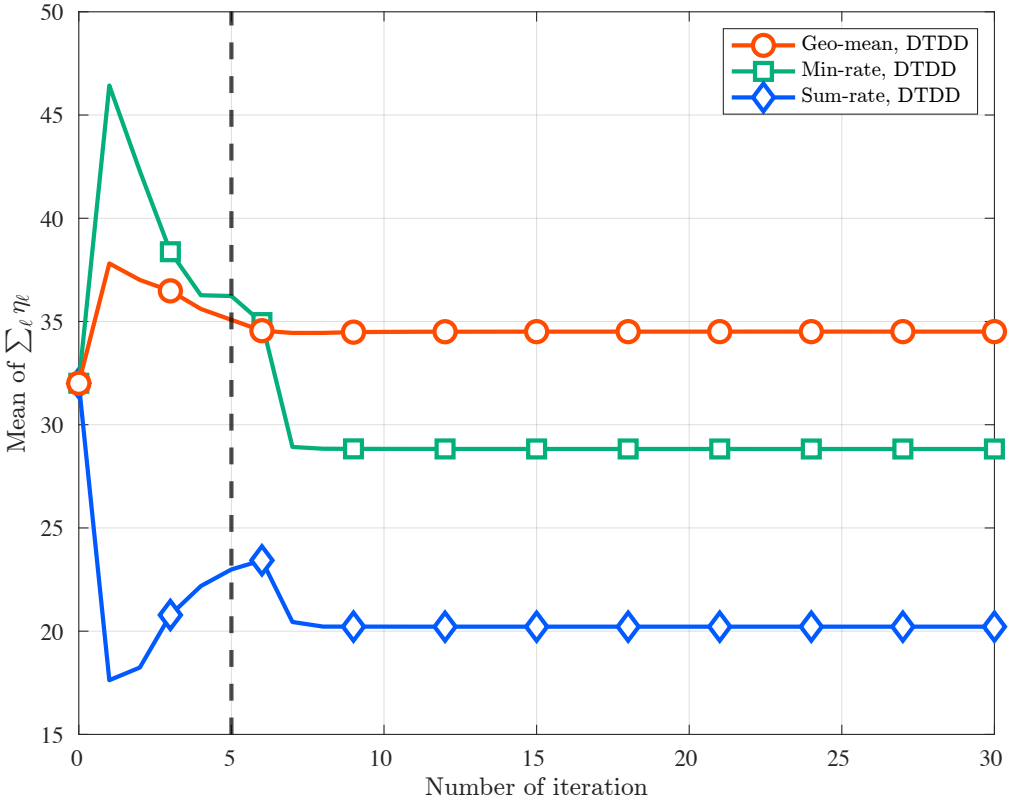

Fig. 3.6 Convergence of η_ℓ over iterations.

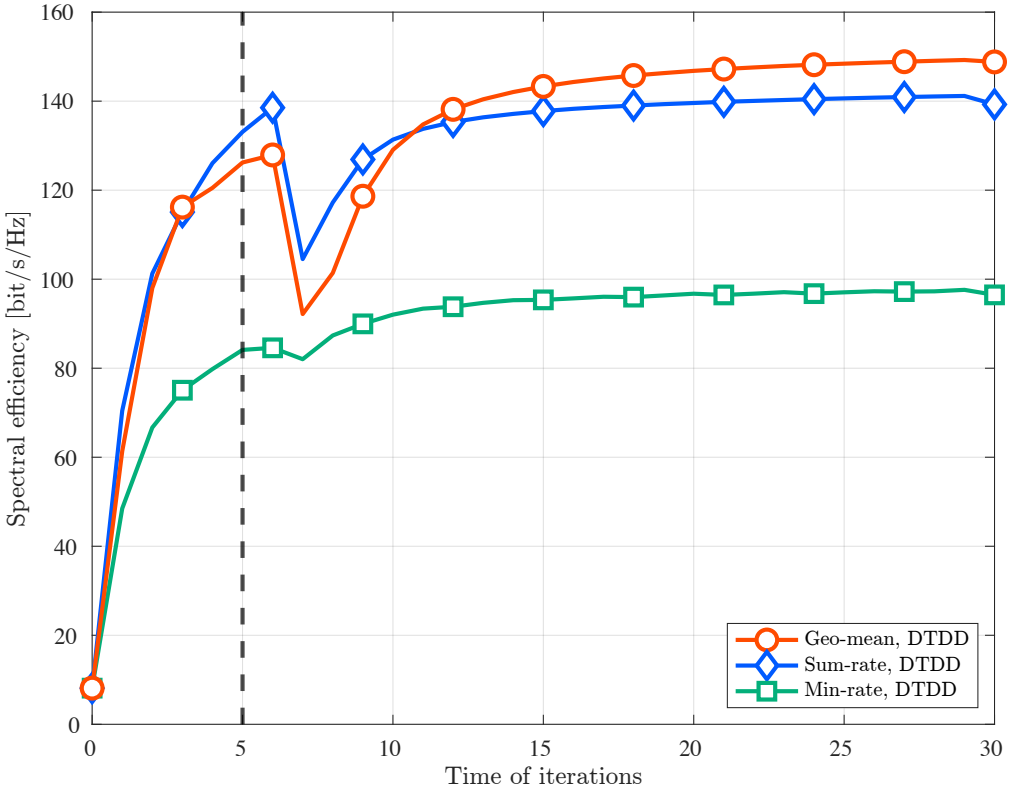

Fig. 3.7 Convergence of SEs over iterations.

It can be observed from the figure that the SE continuously increases as the number of iterations grows, except for the point $t = 5$ when the penalty parameter starts to add up.

Fairness

Next, we study the fairness among UEs achieved by the proposed and benchmarking joint AP allocation and beamforming schemes considered. To that end, plots of the CDFs of the minimum SE among UEs achieved with each system are shown in Fig. 3.10. The results show that among the NAFD techniques compared, the sum-rate maximization method is the one that exhibits the poorest minimum SE performance, both of the "Predominantly DL" and "Balanced UL/DL", which is as expected since this approach tends to allocate spatial DoF to the UEs with higher SINRs, in detriment of UEs with lower SINRs, leading to a maximization of total throughput at the expense of unfair conditions for UEs.

Interestingly, the proposed geometric mean approach is found to be the best among all those compared in terms of the minimum SE performance, outperforming even the max-min worst case scheme, despite the fact that the latter is designed precisely to maximize the rate of the weakest user. Although this result can seem counter-intuitive at first, it can be justified as follows.

Firstly, in an average sense, the max-min worst case method is significantly more sensitive to the initial state of the AP allocation variable vector $\boldsymbol{\eta}$ than its counterparts, as previously observed in Fig. 3.5 and now further evidenced by the results of Fig. 3.10. Secondly, in a per-realization sense, the max-min worst case approach is also found to be, among the methods compared, the one that exhibits the largest drop at 5th iteration, in which the incremental penalty ζ^+ is added so as to promote a binary selection for the AP access configuration as seen in Fig. 3.6. These results together indicate that the max-min worst case is the method that proves least capable of handling the binary nature of the AP allocation variable. In contrast, the proposed geometric mean approach is effective in addressing the non-convexity and the binary constraint on the AP access configuration, resulting in fairer solutions than the max-min worst case method.

Moreover, the result of max-min worst-case approach is inferior to the sum-rate maximization method for "Predominantly UL". Because the latter method allows the AP can allocate more power to UEs. As a result, the minimum SE is significantly higher because the UL UE, which constrains power by only AP allocation, becomes a worst-case UE more often. The sum-rate maximization approach results in the "Balanced UL/DL" results also suggest this causes correctness.

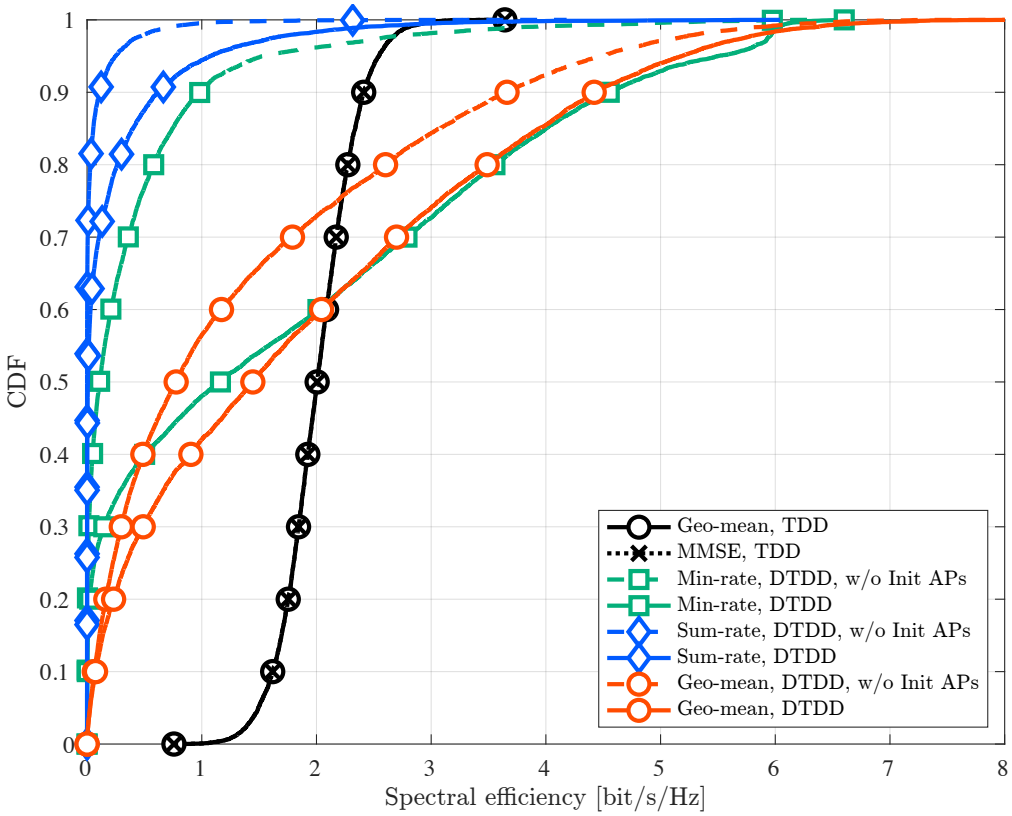

Fig. 3.8 Comparison of the CDF of the minimum SE for different approaches under the predominantly DL ($q = 0.25$).

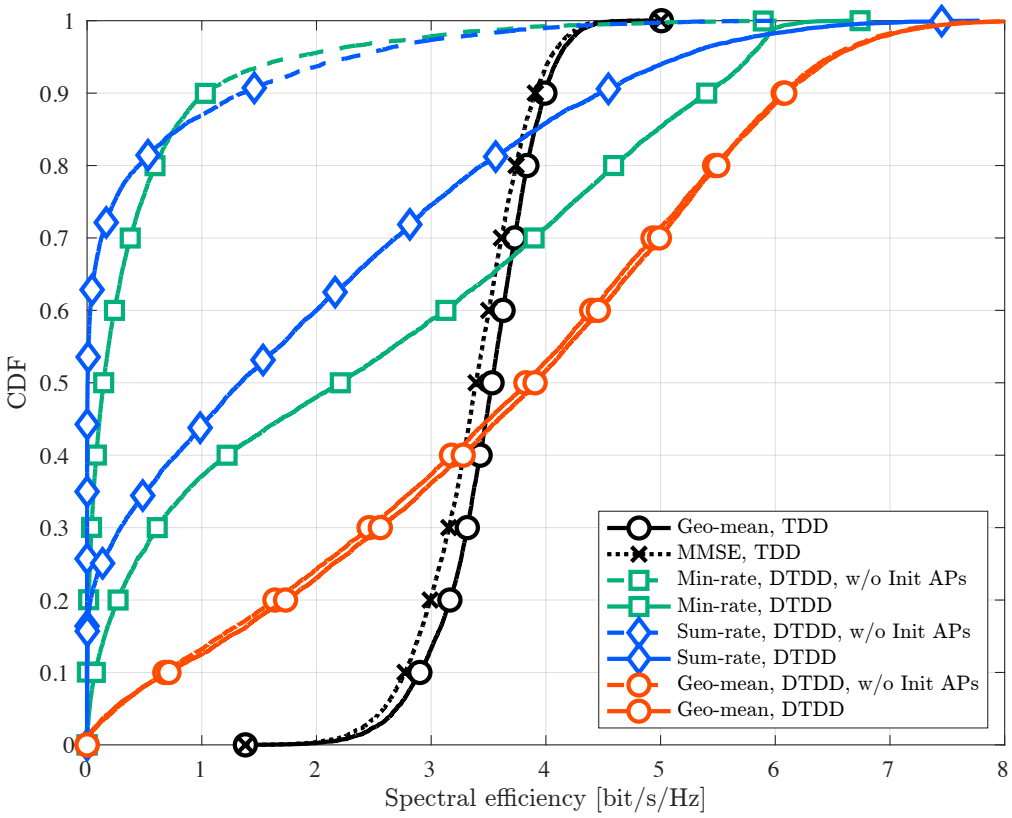

Fig. 3.9 Comparison of the CDF of the minimum SE for different approaches under the balanced UL/DL ($q = 0.5$).

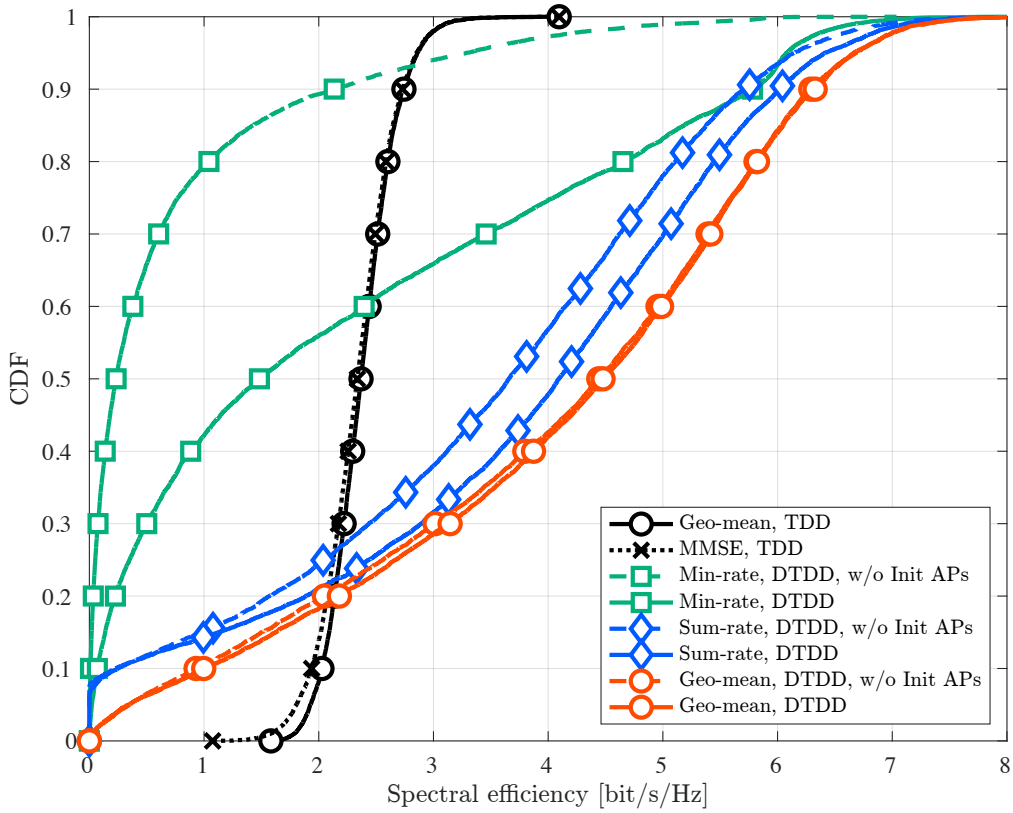

Fig. 3.10 Comparison of the CDF of the minimum SE for different approaches under the predominantly UL ($q = 0.75$).

The SEs of each user are shown in Fig. 3.13. The geometric mean approach has a steeper CDF curve than the other methods in all cases. In particular, we note the significant improvement concerning the poor performance UE, as mentioned in the comparison in Fig. 3.10. Nevertheless, the performance of the top UEs also approaches that of the sum-rate maximization method, indicating that the trade-off between fairness and performance can be resolved while maintaining the total performance. In the sum-rate maximization approach and the max-min worst case, the SE is higher on average using the pre-selection of APs. These results show that fixing the high-gain channel by preallocation effectively leads the solution to a better local optimum.

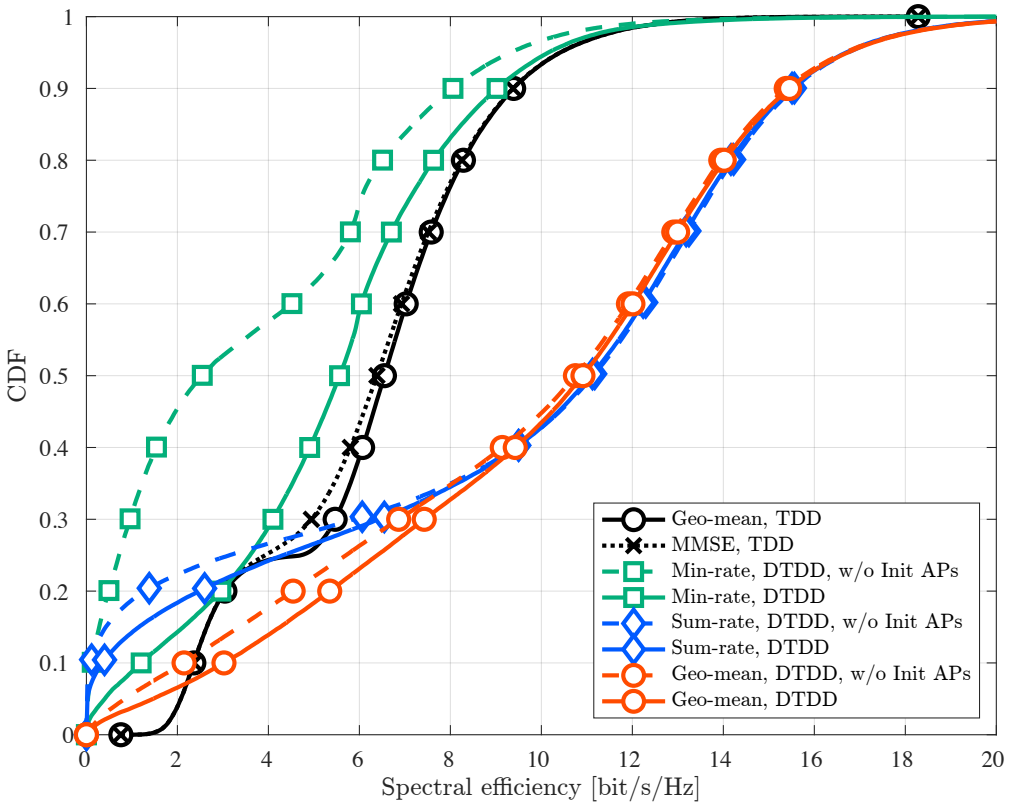

Fig. 3.11 Comparison of the CDF of the SE for different approaches under the predominantly DL ($q = 0.25$).

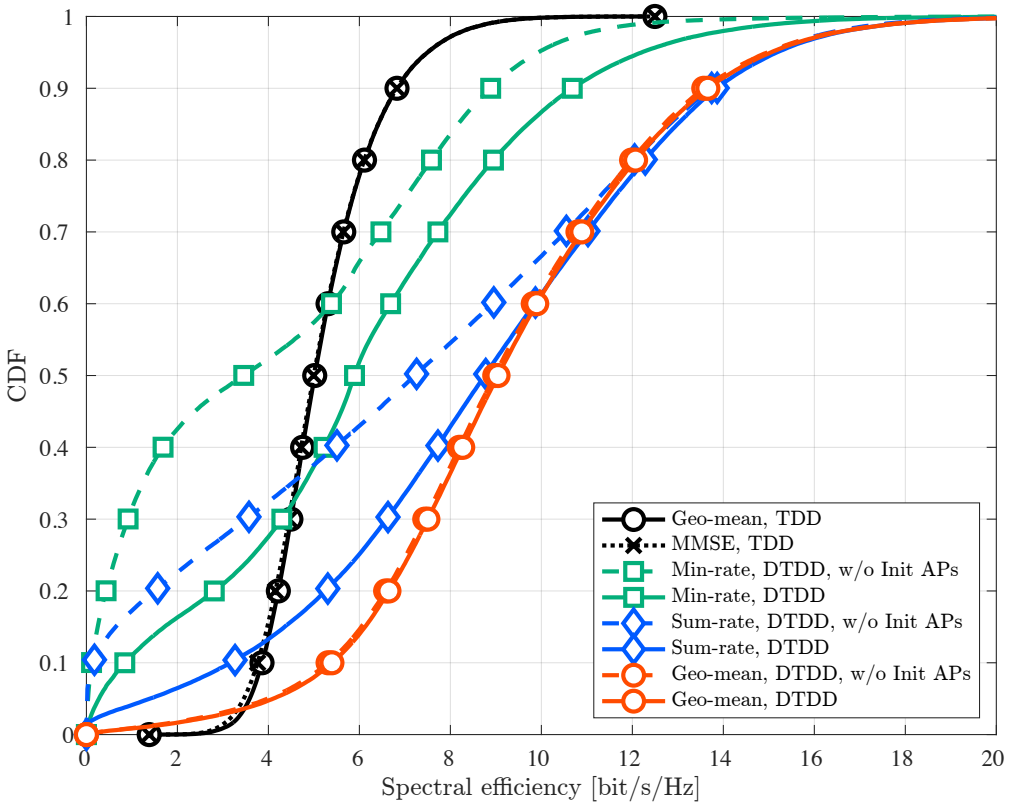

Fig. 3.12 Comparison of the CDF of the SE for different approaches under the balanced UL/DL ($q = 0.5$).

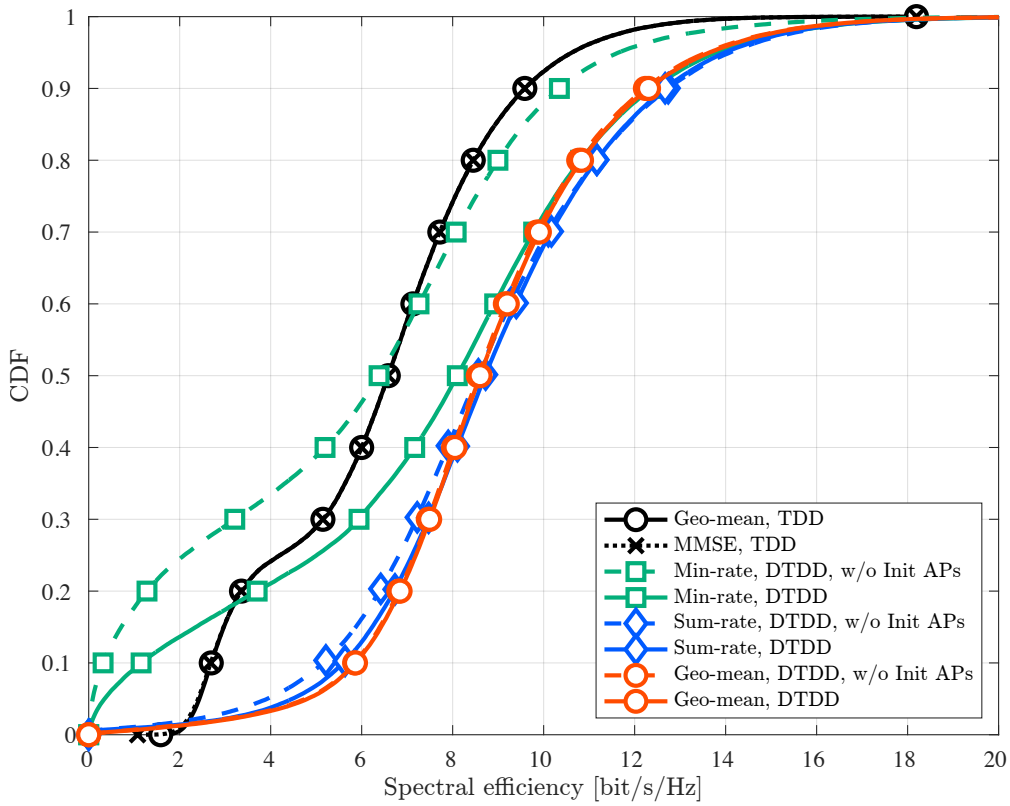

Fig. 3.13 Comparison of the CDF of the SE for different approaches under the predominantly UL ($q = 0.75$).

The comparison of the CDFs of the SEs above confirms that they have uniform SE performance while achieving a high total SE. In addition to those results, a comparison is made by the fairness index to assess the fairness of the three technologies further. We use it to compare Jain's fairness indices [163], defined by

$$\text{Jain's Fairness} \triangleq \frac{\left(\sum_{k\in\mathcal{K}} \log_2\left(1+\Gamma_k\right)\right)^2}{K\sum_{k\in\mathcal{K}}\left(\log_2\left(1+\Gamma_k\right)\right)^2}. \tag{3.56}$$

This index lies between $1/K$ to 1. Thus, when the index becomes 1, the fairest communication among users is realized.

Fig. 3.17 shows the CDF of Jain's fairness indices. Non-surprisingly, the max-min worst case algorithm in "Predominantly DL" is shown to deliver the most fair results among the NAFD schemes compared, which however comes at the expense significantly lower rates, as shown previously. This is also why the TDD mode results are the ones with the highest Jain's

fairness indices, since under such method there is no inter-AP/UE interference, although the throughput itself is inferior.

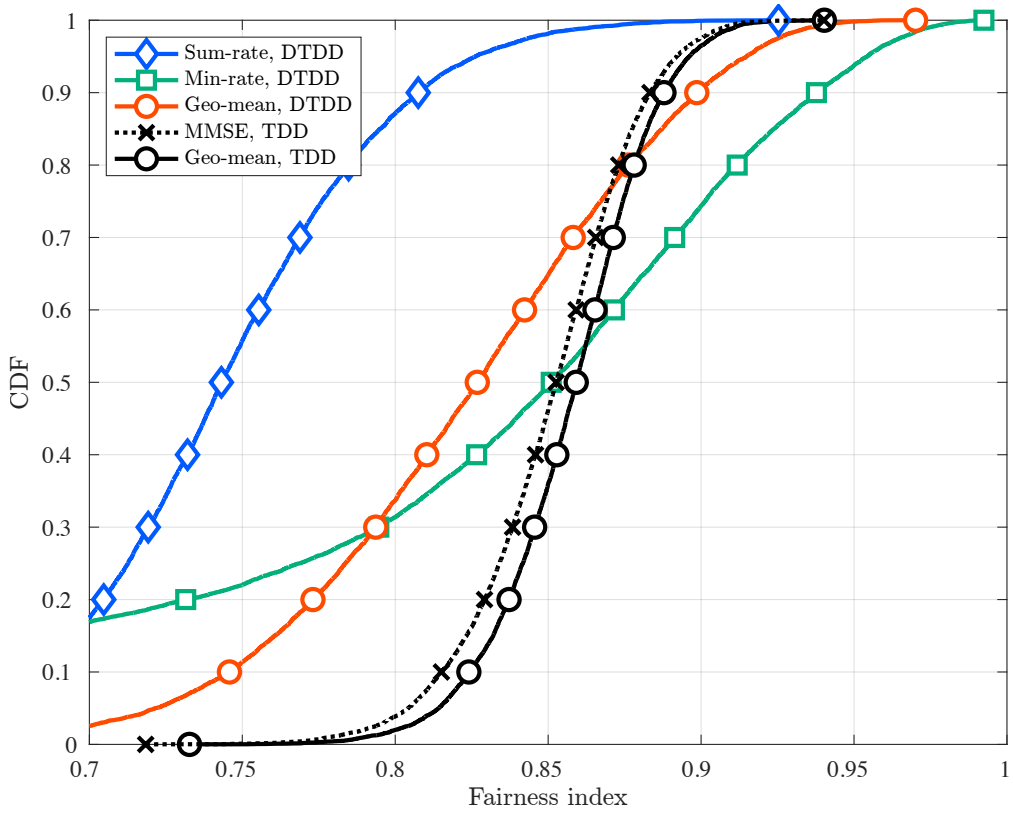

Fig. 3.14 Comparison of the CDF of Jain's fairness index for UE using Algorithm 1 under the predominantly DL ($q = 0.25$).

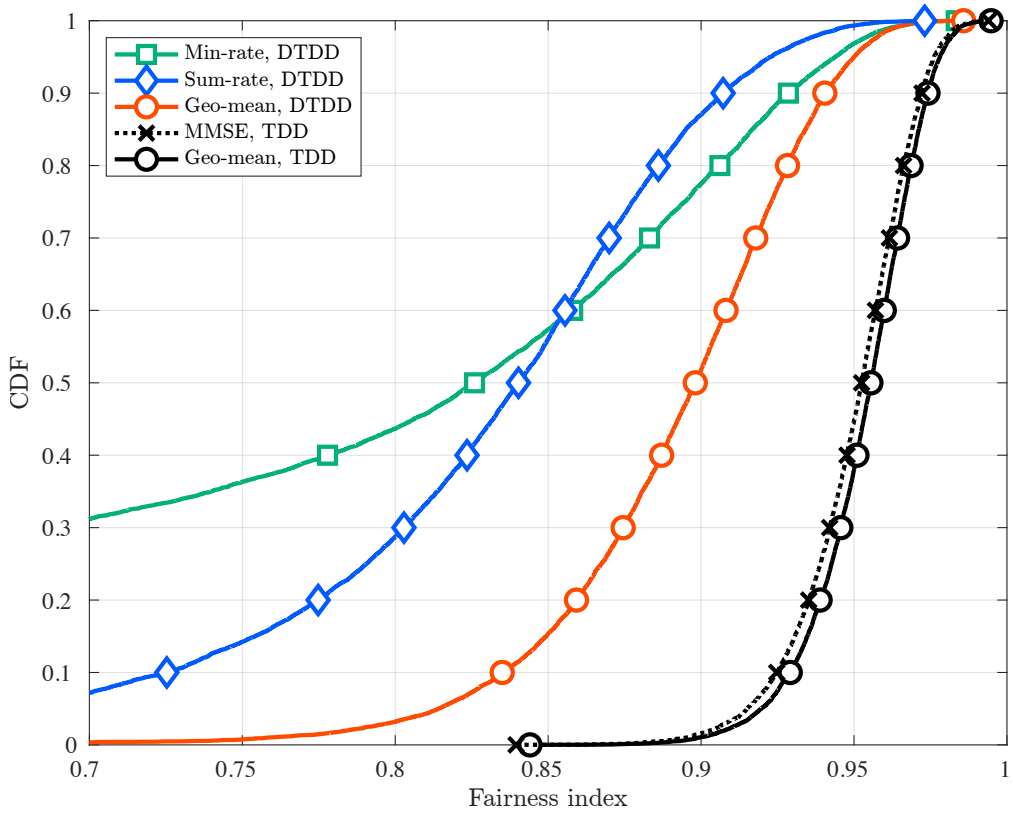

Fig. 3.15 Comparison of the CDF of Jain's fairness index for UE using Algorithm 1 under the balanced UL/DL ($q = 0.5$).

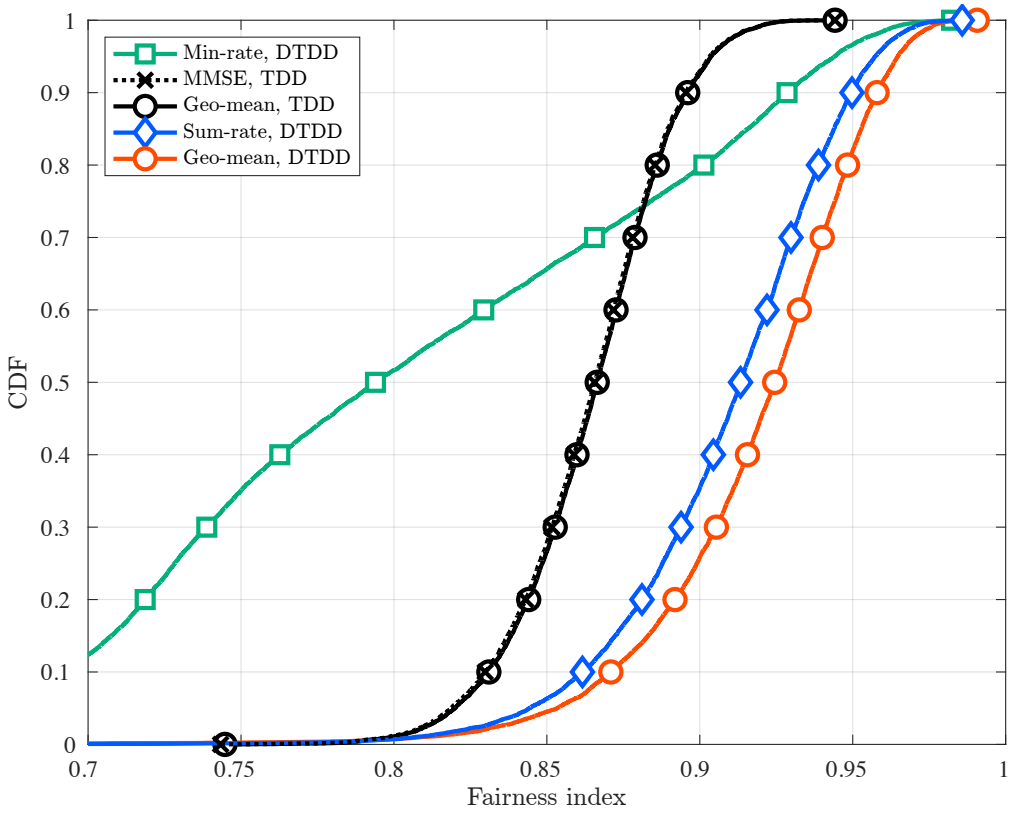

Fig. 3.16 Comparison of the CDF of Jain's fairness index for UE using Algorithm 1 under the predominantly UL ($q = 0.75$).

Fig. 3.17 Comparison of the CDF of Jain's fairness index for UE using Algorithm 1.

On the other hand, the max-min approach has the worst fairness for "Predominantly DL" and "Predominantly UL". This is due to the incompatibility of this approach with binary constraints, as described in Fig. 3.10 to 3.13. The geometric mean approach also shows fairness higher than TDD for part of the "Predominantly DL" and most of the "Predominantly UL". Since the overall SE of the DL varies with the power allocation in equation (3.55b), the TDD results in a significant difference when the UL/DL ratio is unbalanced. Therefore, TDD has lower fairness at "Predominantly DL" and most of the "Predominantly UL".

All in all, it is concluded from Fig. 3.5 to 3.17 that the proposed geometric mean method yields the best compromise of SE and fairness among those compared. To elaborate, the proposed geometric mean method outperforms the greedy sum-rate maximization scheme in achieving the largest total rate, as shown in Fig. 3.5, while exhibiting Jain's fairness indices not far from the latter, as seen in Fig. 3.17; outperforms the fairness-oriented max-min worst case method in ensuring a higher rate to poorest UE, as seen in Fig. 3.10; and achieves the best balance in the allocation of APs to UL/DL, as seen in Fig. 3.6.

Multiple-Antenna UEs Case

Having demonstrated the effectiveness of the proposed geometric mean approach compared to SotA benchmarks, we now turn our attention to the gains obtained by increasing the number of antennas at UEs, under the correlated channel model of [105], described by equation (3.2), with the angular standard deviation is $\sigma_\varphi = 20$ [deg] and the antenna spacing is $d_H = 1/2$.

To that end, we compare in Fig. 3.20 the SE performance of Algorithm 2 against that of the sum-rate maximization approach, for various cases with different number N of antennas at each UE. For $N = 1$, the performance of Algorithm 1 is also shown as a further reference. In addition, we clarify that since the maximum ratio transmission can not be directly utilized as a beamforming vector in multiple-antenna scenarios, a Gaussian initialization is adopted to initialize the beamforming vectors in this figure.

It can be observed from the figure that the SE performances of both the proposed geometric-mean and sum-rate maximization approaches increase with N, with a significant advantage of the proposed method over the SotA, both in terms of total and minimum SE. Here, it is worth emphasizing that due to the geographical nature of the local scattering model [105], in which the spatial distribution of UEs and APs directly determine the parameters d_H and φ, strongly influencing the correlation matrices $\boldsymbol{R}_{k,\ell}$, the MIMO channels to which Algorithm 2 is subjected to tend to be highly correlated. This, in turn, indicate that a large portion of the gains obtained by Algorithm 2 is due not to the added channel diversity, but rather to the effective exploitation of the added degrees of freedom, by the proposed joint AP allocation and beamforming scheme, to aligning harmful interference while increasing the intended signal power.

It is also worth-noting that for $N = 1$, the performance of Algorithm 2 is essentially identical to that of Algorithm 1, as expected, with only a slight difference in terms of sum SE observed, which is attributed to the scalar weight "precoding" included in Algorithm 2, but not in Algorithm 1.

Finally, it is also noticeable that the performance of sum-rate maximization approach degrades greatly compared to Algorithm 2, especially when N is small. Given that in such scenarios ($N \to 1$) UEs are more limited, this indicates that Algorithm 2 is indeed capable of finding a better solution to the allocation of APs than the sum-rate maximization approach.

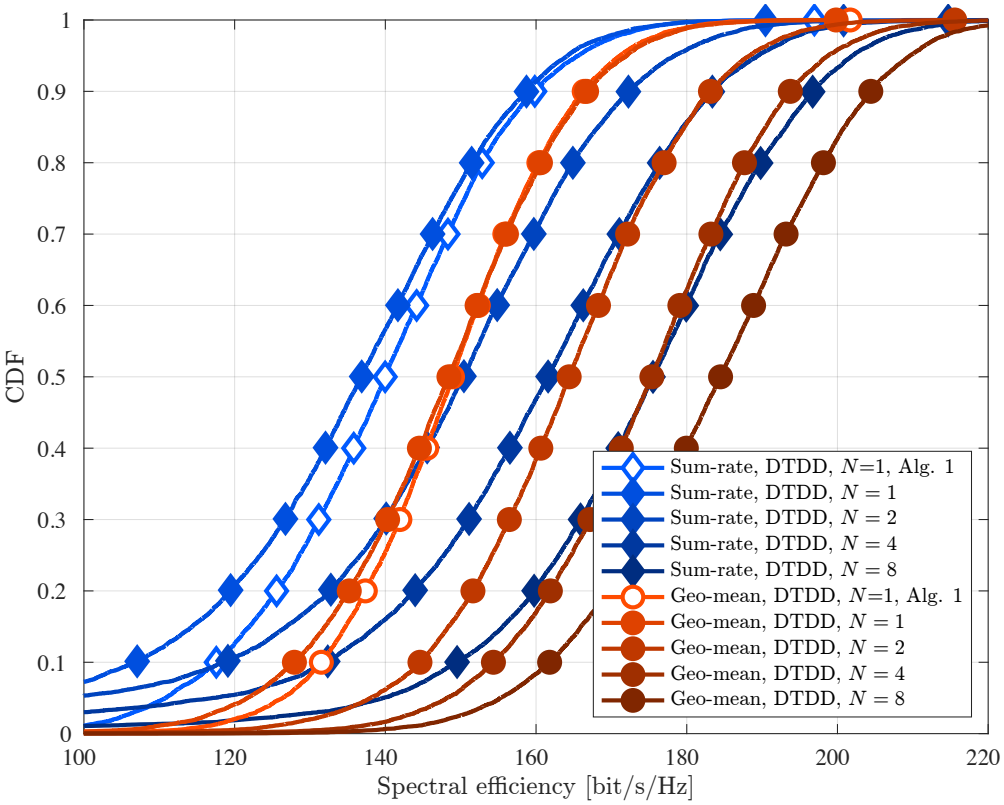

Fig. 3.18 Comparison of the CDF of Sum SE for UE using Algorithm 2.

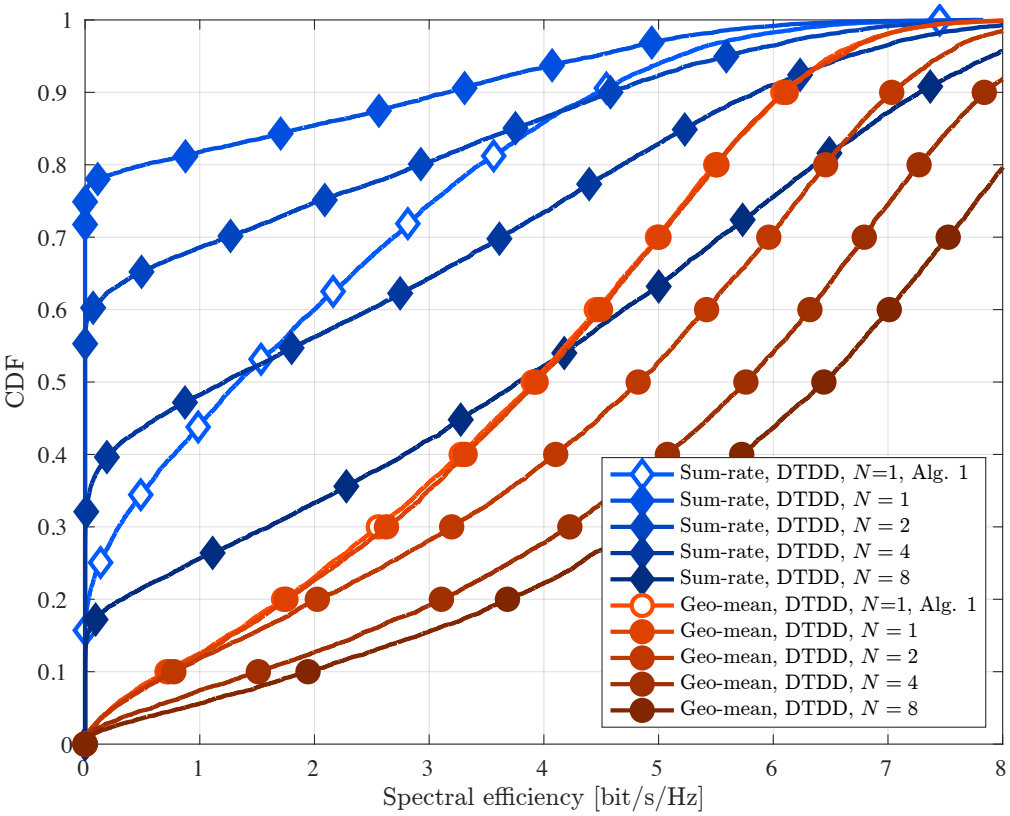

Fig. 3.19 Comparison of the CDF of Minimum SE for UE using Algorithm 2.

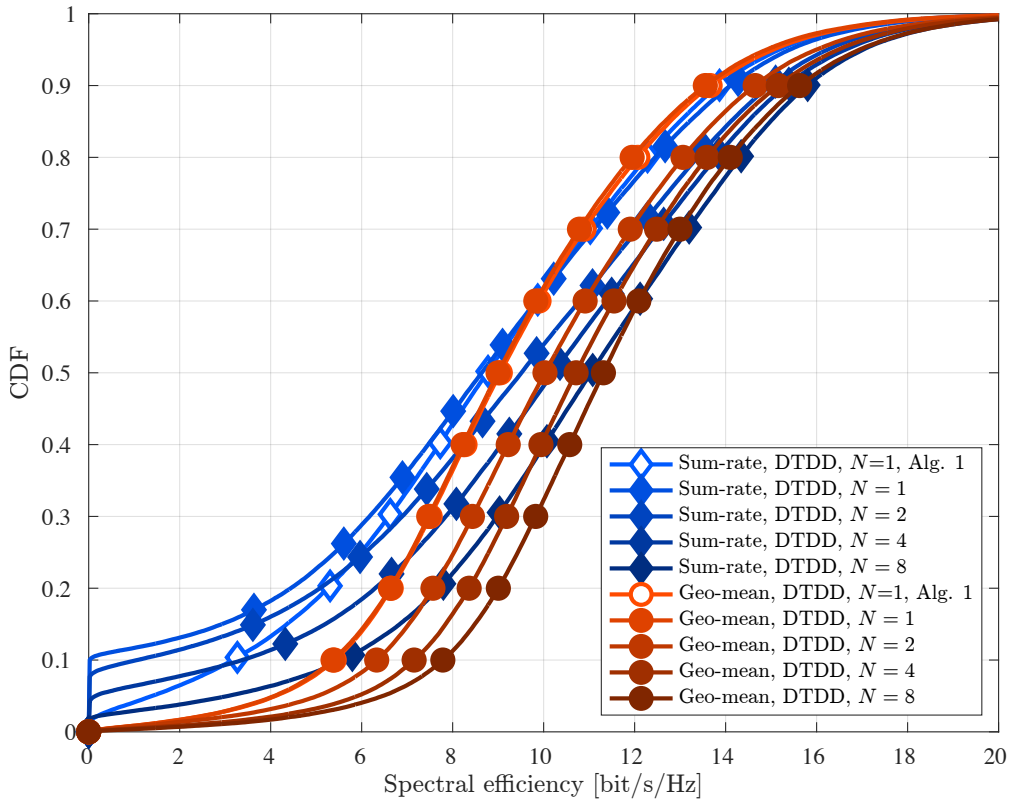

Fig. 3.20 Comparison of the CDF of SE per UE using Algorithm 2.

3.5.4 Impact of Inter-UE Interference

Finally, we confirm the effect of inter-UE interference. In mention above, we have shown that the proposed method can adequately suppress interference if only perfect CSI is available. However, inter-UE CSI estimation is not realistic of the significant overhead in channel estimation. In particular, the expected exponential increase in the number of UEs in the future wireless system will make the impact more effective. To this end, we clarify the performance impact of inter-UE interference.

We consider a more densely populated situation to see the impact of interference clearly than in the previous simulations. Thus, the service area size is 250×250 [m^2] with $L = 36$ APs and $K = 32$ UEs. Also, the UEs are equipped with $N = 8$ antennas. The parameters of the algorithm are $N^{\mathrm{ul}} = 1$, $N^{\mathrm{dl}} = 1$, and $t^{\max} = 10$. The hyper parameter ζ increase is assumed to be done after waiting for first loop. Also, the AP mode is fixed at $t = 5$, and the subsequent loops are designed only for beamforming.

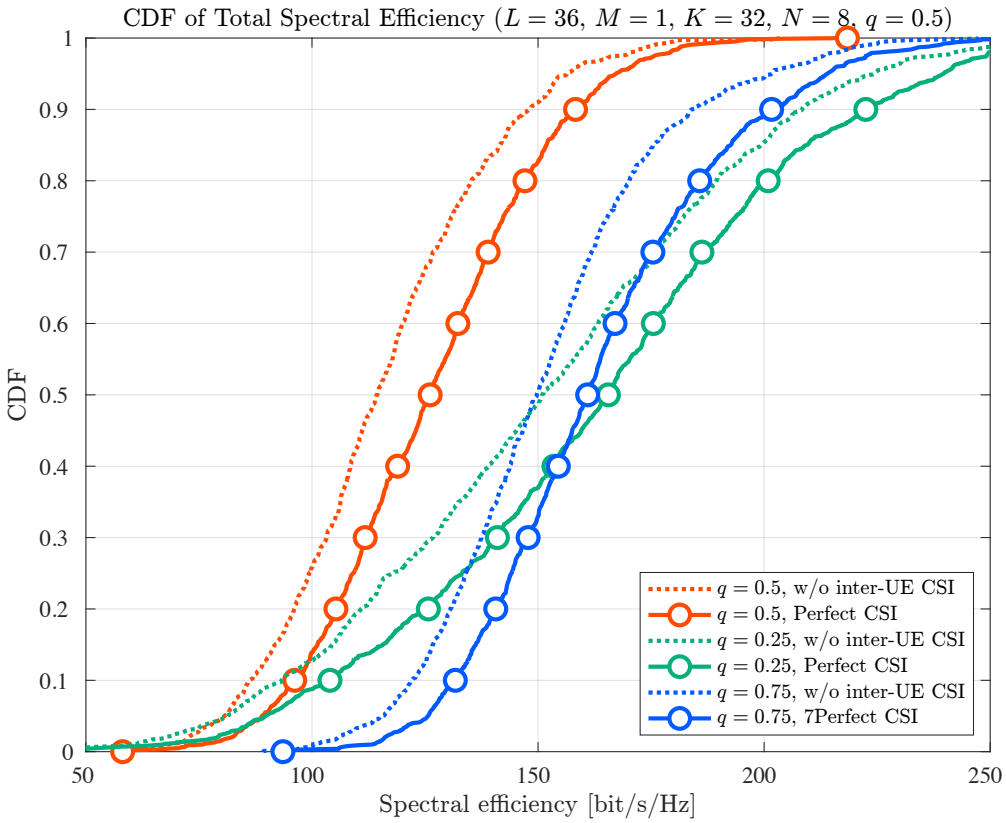

Fig. 3.21 Comparison of the CDF of "Sum SE" for UE with/without inter-UE CSI knowledge.

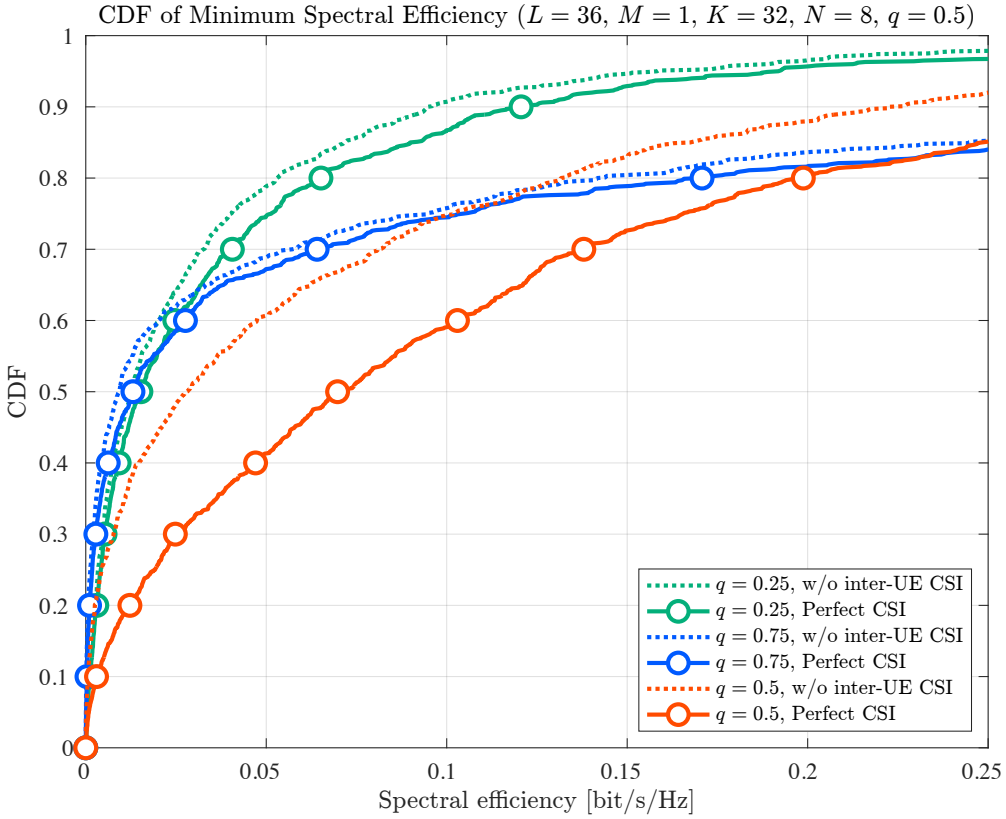

Fig. 3.22 Comparison of the CDF of "Minimum SE" for UE with/without inter-UE CSI knowledge.

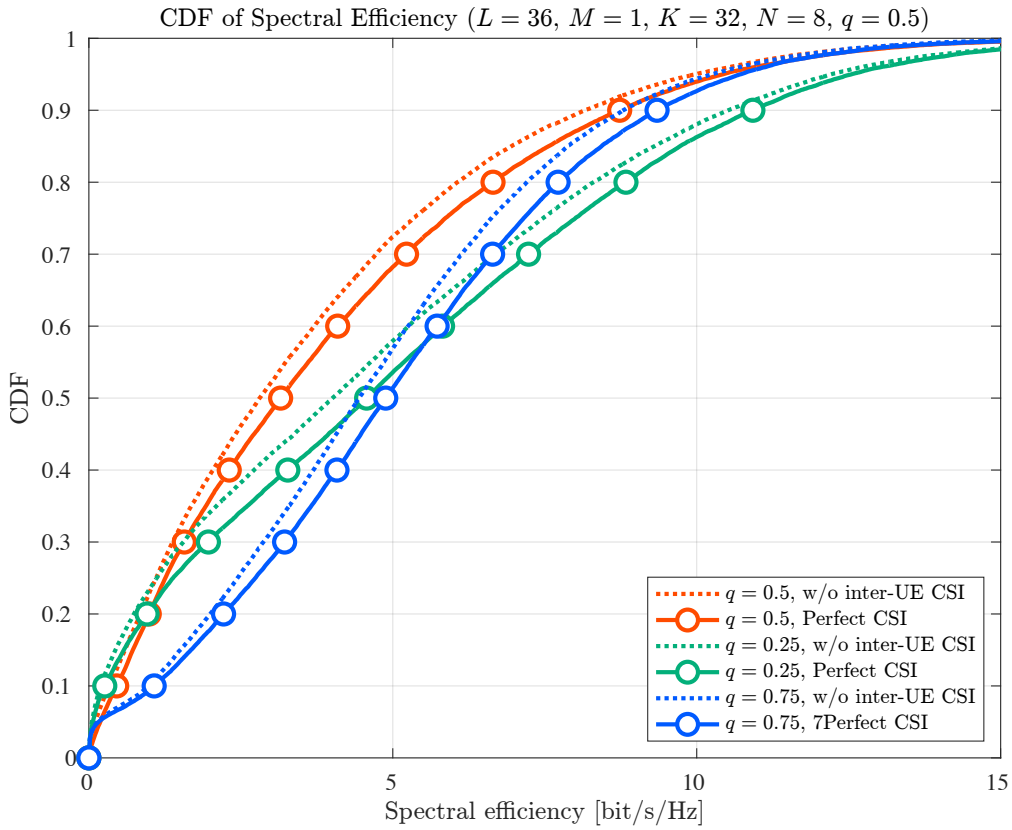

Fig. 3.23 Comparison of the CDF of SE per UE with/without inter-UE CSI knowledge.

Fig. 3.23 shows the CDFs of the SEs for the cases with perfect channel knowledge and without inter-UE channel knowledge considered. Here, legends $q = 0.25/0.5/0.75$ in the figure indicate the ratio of UL UEs per K. Also, "w/o inter-UE CSI" is the result of the CPU without inter-UE channel knowledge, i.e., $\boldsymbol{H}_{k,k'} = \boldsymbol{O}_{N\times N}$, and The "Perfect CSI" is the results of the CPU with perfect channel knowledge, same to considering up to Fig. 3.20. This degradation is because the algorithm ignored the inter-UE interference term, resulting in a degradation of the accuracy of the AP configuration and beamforming design. About the same SE degradation of $q = 0.25$, $q = 0.5$ in Fig. 3.22 as in Fig. 3.21 and 3.23. Interestingly, only the "Minimum SE" of $q = 0.5$ case showed 50% SE degradation. For $q = 0.5$, the SE of "Perfect CSI" is higher than the others, *i.e.*, the AP allocation and beamforming design can get a better local optimal solution, which may have a more significant impact on the SE in the unknown of inter-UE channel. Therefore, highly accurate inter-UE channel estimation is required for NAFD CF-mMIMO systems.

To this end, we propose a new inter-UE channel estimation method in the next chapter to solve the dilemma of performance degradation and channel estimation overhead.

3.6 Chapter Summary

In this chapter, we studied a NAFD aided CF-mMIMO system in which UL and DL UEs are simultaneously served by the system over shared wireless resources, proposing a novel joint AP access configuration and beamforming scheme to optimize both the system throughput and user fairness of such a system, both for the case of UEs with single and multiple antennas. The proposed method is based on geometric-mean figure of metric, incorporating also a novel mechanism to enforce the discreteness of the AP allocation variables η_ℓ via the introduction of a regularized negative entropy function in the objective. In order to relax the non-convexity of the newly formulated problem, FPs techniques were employed; and a simple heuristic to initialize η_ℓ is also introduced. It is shown via software simulations that the proposed method is not only capable of balancing rate performance and fairness, but in fact outperforms the conventional sum-rate maximization and max-min worst case methods.

Having verified the effectiveness of the proposed approach in NAFD-aided CF-mMIMO systems, open problem as inter-UE interference and channel estimation, which confirm in 3.5.3. In addition, requirements of future wireless systems need to secure more bandwidth using mmWave or more. In the next chapter, we consider the mmWave model and propose an inter-UE channel estimation scheme using its characteristics and a resource allocation and beamforming design scheme using the estimated channel.

Chapter 4

Network-Assisted Full-Duplex with Localization-Aided Inter-Users Channel Estimation for Millimeter-Wave Cell-Free Massive MIMO systems

4.1 Background and Contributions

In the previous chapter, the AP mode assignment and beamforming design for NAFD were done assuming microwave bands. However, as discussed in Section 1.1.2, 6G should achieve a throughput of 100 to 1000 times higher than 5G. In order to meet the strong demand for 6G, the use of mmWave channels is essential to ensure wider bandwidth. Moreover, as discussed in the previous chapter, the analysis showed that the impact of inter-UE interference is significant in NAFD systems. For this purpose, it is necessary to estimate the inter-UE channel with high accuracy.

MmWave channels are characterized by a small number of dominant paths, strong directivity, and some dominance of LoS components [15, 164]. Due to its nature, mmWave channels can therefore be well characterized by AoA, AoD, and the distance between the communication pair. Therefore, beamforming design methods without channel estimation have been studied in [165, 110, 166] for mmWave communications. Therefore, if UEs' locations are available in CF-mMIMO systems, the information can be used to estimate the inter-UE channels, leading to the best performance of NAFD.

The estimation of UE's location has been actively discussed not only in academia but also in standardization bodies such as 3GPP. Estimation techniques such as channel charting [167]

and multidimensional scaling [168] are actively investigated, which can precisely estimate UEs' locations using received signal power obtained by large antennas and/or distributed nodes, which is obviously suitable for CF-mMIMO systems.

This chapter studies NAFD CF-mMIMO systems over mmWave channels. Joint resource allocation and beamforming design with location-aided channel estimation is proposed to mitigate inter-UE interference and maximize the performance. More specifically, we reconstruct the inter-UE channels based on a statistical channel model and knowledge of AoA, AoD, and distance among UE's. In addition, penalizing the estimated inter-UE channels is proposed for a robust design. Using these indirectly estimated inter-UE channels, a beamforming design problem and AP mode selection aimed at interference suppression is formulated and solved efficiently via convex optimization. Computer simulations demonstrate the advantage of our proposed system quantitatively, confirming that the total throughput of the proposed method is close to that of a system with perfect knowledge of inter-UE channels.

4.2 Channel and System Model

This section introduces a system and channel model for CF-mMIMO with NAFD. The system model has remained the nearly as that of the previous chapter. However, the channel model is changed to a narrow-band mmWave model. In addition, the mmWave system is suitable for a UE with multiple antennas because interference mitigation is performed using beamforming, which takes advantage of small antenna elements [164, 15]. Therefore, we only consider the UEs with multiple antennas.

Consider a CF-mMIMO system, in which L multiple APs equipped with M antennas are distributed over an effective coverage area. It is assumed that all APs are connected to common CPU via a wired fronthaul. Each UE equipped with N antennas communicates to all AP via the NAFD scheme, either UL or DL. In order to analyze the impact of inter-UE interference, we assume that the CPU has perfect knowledge of the inter-AP-UE and inter-AP CSIs

Let $\mathcal{K} = \{1, \ldots, K\}$ and $\mathcal{L} = \{1, \ldots, L\}$ denote the set of UE and AP, respectively. Also, the set $\mathcal{K}^{\text{dl}} \subset \mathcal{K}$, $\mathcal{K}^{\text{ul}} = \mathcal{K} \setminus \mathcal{K}^{\text{dl}}$, $\mathcal{L}^{\text{dl}} \subset \mathcal{L}$, and $\mathcal{L}^{\text{ul}}$ denote the subset of the UEs and APs assigned to DL or UL mode, respectively.

4.2.1 Channel Model

The NAFD CF-mMIMO system has three channels: inter-AP-UE, inter-AP, and inter-UE, due to the APs and UEs transmit signals simultaneously. For the sake of generalization, let us

assume that a signal is transmitted from the t-th transmitter (DL AP or UL UE) to the r-th receiver (UL AP or DL UE). The mmWave channel between the t-th transmitter and the r-th receiver can be expressed as [24, 110, 109, 108]

$$\boldsymbol{H}_{r,t} = \sum_{p=1}^{P} \alpha_{r,t,p} \boldsymbol{a}(\boldsymbol{\psi}_{r,t,p}) \boldsymbol{a}(\boldsymbol{\psi}_{t,r,p})^{\mathrm{H}}, \tag{4.1}$$

where $\alpha_{r,t,p} \sim \mathcal{CN}(0, g_{r,t,p})$ denotes the small scale fading with the channel gain $g_{r,t,p}$ for the p-th path between the t-th transmitter and the r-th receiver, $\boldsymbol{\psi}_{r,t,p} = [\phi_{r,t,p}, \theta_{r,t,p}]$ is a vector consists of the p-th path AoAs or AoDs with azimuth angle $\phi_{r,t,p}$ and elevation angle $\theta_{r,t,p}$.

Also, $\boldsymbol{a}(\cdot)$ is the array response vector of ULA in the APs or UEs given by

$$\boldsymbol{a}\left(\boldsymbol{\psi}_{r,t,p}\right) = \left[1, e^{-j\frac{2\pi}{\lambda}\nu(\boldsymbol{\psi}_{r,t,p})}, \ldots, e^{-j\frac{2\pi}{\lambda}(O-1)\nu(\boldsymbol{\psi}_{r,t,p})}\right]^{\mathrm{T}}, \tag{4.2}$$

where $O \in \{M, N\}$ is the number of antennas in the AP or UE, λ is the wavelength, and $\nu(\boldsymbol{\psi}_{r,t,p}) = \frac{\lambda}{2}\sin(\phi_{r,t,p})\sin(\theta_{r,t,p})$.

4.2.2 System Model

The received signals of the ℓ-th UL AP and the k-th DL UE can be respectively written as

$$\boldsymbol{y}_{\ell}^{\mathrm{ul}} = \sum_{k \in \mathcal{K}^{\mathrm{ul}}} \boldsymbol{H}_{k,\ell} \boldsymbol{w}_{k}^{\mathrm{ue}} d_{k}^{\mathrm{ul}} + \sum_{\ell' \in \mathcal{L}^{\mathrm{dl}}} \sum_{k' \in \mathcal{K}^{\mathrm{dl}}} \boldsymbol{H}_{\ell,\ell'}^{\mathrm{H}} \boldsymbol{w}_{k',\ell'}^{\mathrm{ap}} d_{k'}^{\mathrm{dl}} + \boldsymbol{n}_{\ell}, \tag{4.3a}$$

$$\boldsymbol{y}_{k}^{\mathrm{dl}} = \sum_{\ell \in \mathcal{L}^{\mathrm{dl}}} \boldsymbol{H}_{k,\ell}^{\mathrm{H}} \sum_{k' \in \mathcal{K}^{\mathrm{dl}}} \boldsymbol{w}_{k',\ell}^{\mathrm{ap}} d_{k'}^{\mathrm{dl}} + \sum_{k' \in \mathcal{K}^{\mathrm{ul}}} \boldsymbol{H}_{k',k} \boldsymbol{w}_{k'}^{\mathrm{ue}} d_{k'}^{\mathrm{ul}} + \boldsymbol{n}_{k}, \tag{4.3b}$$

where d_{k}^{ul} and d_{k}^{dl} are the UL and DL data symbols for the k-th UE, $\boldsymbol{w}_{k}^{\mathrm{ue}} \in \mathbb{C}^{N}$ and $\boldsymbol{w}_{k,\ell}^{\mathrm{ap}} \in \mathbb{C}^{M}$ are the precoding vector employed by the k-th UE and ℓ-th AP, and $\boldsymbol{n}_{k} \sim \mathcal{CN}(0, \boldsymbol{I}_{N})$ and $\boldsymbol{n}_{\ell} \sim \mathcal{CN}(0, \boldsymbol{I}_{M})$ are the AWGN vectors at the k-th UE and the ℓ-th AP, respectively.

In the UL, the received signals are combined at each AP and sent to the CPU. Therefore, the detected data symbol for the k-th UE $\hat{d}_{k}^{\mathrm{ul}}$ is represented by

$$\widehat{d}_{k}^{\mathrm{ul}} = \sum_{\ell \in \mathcal{L}^{\mathrm{ul}}} \boldsymbol{v}_{k,\ell}^{\mathrm{ap}\ \mathrm{H}} \boldsymbol{y}_{\ell}^{\mathrm{ul}} = \boldsymbol{v}_{k}^{\mathrm{apH}} \boldsymbol{y}^{\mathrm{ul}}, \tag{4.4a}$$

where $\boldsymbol{v}_{k,\ell}^{\mathrm{ap}} \in \mathbb{C}^{N}$ is the combining vector employed by the ℓ-th AP for the k-th UE in UL and $\boldsymbol{v}_{k}^{\mathrm{ap}} = [\boldsymbol{v}_{k,1}^{\mathrm{ap}\ \mathrm{H}}, \ldots, \boldsymbol{v}_{k,L}^{\mathrm{ap}\ \mathrm{H}}]^{\mathrm{H}}$. Similarly, in DL, the detected data symbols at the k-th UE $\hat{d}_{k}^{\mathrm{dl}}$ are given by

$$\widehat{d}_{k}^{\mathrm{dl}} = \boldsymbol{v}_{k}^{\mathrm{ueH}} \boldsymbol{y}_{k}^{\mathrm{dl}}, \tag{4.4b}$$

where $\boldsymbol{v}_k^{\mathrm{ue}} \in \mathbb{C}^N$ is the combining vector employed by the k-th UE in DL.

Finally, the SINRs of the k-th UE in UL and DL are given by

$$\Gamma_k^{\mathrm{ul}} \triangleq \frac{|\boldsymbol{v}_k^{\mathrm{ap}\mathrm{H}} \boldsymbol{H}_k \boldsymbol{w}_k^{\mathrm{ue}}|^2}{\sum\limits_{\substack{k' \in \mathcal{K}^{\mathrm{ul}} \\ k \neq k'}} |\boldsymbol{v}_k^{\mathrm{ap}\mathrm{H}} \boldsymbol{H}_{k'} \boldsymbol{w}_k^{\mathrm{ue}}|^2 + \sum\limits_{k' \in \mathcal{K}^{\mathrm{dl}}} |\boldsymbol{v}_k^{\mathrm{ap}\mathrm{H}} \boldsymbol{H}^{\mathrm{H}} \boldsymbol{w}_{k'}^{\mathrm{ap}}|^2 + \sigma_{\mathrm{ul}}^2 \left\|\boldsymbol{v}_k^{\mathrm{ap}}\right\|_2^2}, \tag{4.5a}$$

$$\Gamma_k^{\mathrm{dl}} \triangleq \frac{|\boldsymbol{v}_k^{\mathrm{ue}\mathrm{H}} \boldsymbol{H}_k^{\mathrm{H}} \boldsymbol{w}_k^{\mathrm{ap}}|^2}{\sum\limits_{\substack{k' \in \mathcal{K}^{\mathrm{dl}} \\ k \neq k'}} |\boldsymbol{v}_k^{\mathrm{ue}\mathrm{H}} \boldsymbol{H}_k^{\mathrm{H}} \boldsymbol{w}_{k'}^{\mathrm{ap}}|^2 + \sum\limits_{k' \in \mathcal{K}^{\mathrm{ul}}} |\boldsymbol{v}_k^{\mathrm{ue}\mathrm{H}} \boldsymbol{H}_{k',k}^{\mathrm{H}} \boldsymbol{w}_{k'}^{\mathrm{ue}}|^2 + \sigma_{\mathrm{dl}}^2 \left\|\boldsymbol{v}_k^{\mathrm{ue}}\right\|_2^2}, \tag{4.5b}$$

where $\boldsymbol{H}_k = [\boldsymbol{H}_{k,1}^{\mathrm{T}}, \ldots, \boldsymbol{H}_{k,L}^{\mathrm{T}}]^{\mathrm{T}}$, and $\boldsymbol{w}_k^{\mathrm{ap}} = [\boldsymbol{w}_{k,1}^{\mathrm{ap}\ \mathrm{T}}, \ldots, \boldsymbol{w}_{k,L}^{\mathrm{ap}\ \mathrm{T}}]^{\mathrm{T}}$.

4.2.3 Problem Formulation

This chapter aims at maximizing the total throughput through a geometric mean maximization problem. The reasons for using the geometric mean for the objective function are presented in the previous chapter.

Before introducing the problem, optimization variables are collected into the vector as

$$\boldsymbol{v} \triangleq [\boldsymbol{v}_1^{\mathrm{ap}\mathrm{T}}, \ldots, \boldsymbol{v}_k^{\mathrm{ap}\mathrm{T}}, \boldsymbol{v}_1^{\mathrm{ue}\mathrm{T}}, \ldots, \boldsymbol{v}_K^{\mathrm{ue}\mathrm{T}}]^{\mathrm{T}}, \tag{4.6a}$$

$$\boldsymbol{w} \triangleq [\boldsymbol{w}_1^{\mathrm{ue}\mathrm{T}}, \ldots, \boldsymbol{w}_K^{\mathrm{ue}\mathrm{T}}, \boldsymbol{w}_1^{\mathrm{ap}\mathrm{T}}, \ldots, \boldsymbol{w}_K^{\mathrm{ap}\mathrm{T}}]^{\mathrm{T}}, \tag{4.6b}$$

$$\boldsymbol{p}^{\mathrm{dl}} \triangleq [p_{1,1}^{\mathrm{dl}}, \cdots, p_{K,1}^{\mathrm{dl}}, \cdots, p_{1,L}^{\mathrm{dl}}, \cdots, p_{K,L}^{\mathrm{dl}}]^{\mathrm{T}}, \tag{4.6c}$$

and $\boldsymbol{\eta} \triangleq [\eta_1, \ldots, \eta_L]^{\mathrm{T}}$, where η_ℓ is an indicator variable for the AP UL or DL mode selection and $p_{k,\ell}^{\mathrm{dl}}$ is the transmit power at the ℓ-th AP towards the k-th UE.

Having the geometric mean of the UE's throughput as the objective function, the original optimization problem for the total throughput maximization is formulated as is given by

$$\underset{\boldsymbol{\eta}, \boldsymbol{v}, \boldsymbol{w}, \boldsymbol{p}^{\mathrm{dl}}}{\text{maximize}} \ \left(\prod_{k=1}^{K} \log_2 (1 + \Gamma_k) \right)^{\frac{1}{K}} \tag{4.7a}$$

$$\text{subject to } \eta_\ell \in \{0, 1\}, \forall \ell, \tag{4.7b}$$

$$\|\boldsymbol{v}_{k,\ell}^{\mathrm{ap}}\|_2^2 \leq \eta_\ell, \forall k \in \mathcal{K}^{\mathrm{ul}}, \forall \ell, \tag{4.7c}$$

$$\|\boldsymbol{w}_{k,\ell}^{\mathrm{ap}}\|_2^2 \leq p_{k,\ell}^{\mathrm{dl}} \bar{\eta}_\ell, \forall k \in \mathcal{K}^{\mathrm{dl}}, \forall \ell, \tag{4.7d}$$

$$\sum_{k \in \mathcal{K}} p_{k,\ell}^{\mathrm{dl}} \leq p^{\mathrm{dl,max}}, \forall \ell, \tag{4.7e}$$

$$N^{\mathrm{ul}} \leq \sum_{\ell=1}^{L} \eta_\ell, \tag{4.7f}$$

$$N^{\mathrm{dl}} \leq \sum_{\ell=1}^{L} \bar{\eta}_\ell, \tag{4.7g}$$

$$\left\|\boldsymbol{v}_k^{\mathrm{ue}}\right\|_2^2 \leq 1, \forall k \in \mathcal{K}^{\mathrm{dl}}, \tag{4.7h}$$

$$\left\|\boldsymbol{w}_k^{\mathrm{ue}}\right\|_2^2 \leq p_k^{\mathrm{ul}}, \forall k \in \mathcal{K}^{\mathrm{ul}}, \tag{4.7i}$$

with $\bar{\eta}_\ell = 1 - \eta_\ell$, where constraint (4.7b) jointly enforce the selection of APs to UL and DL modes with corresponding power limitations on constraints (4.7c), (4.7d), and (4.7e), constraints (4.7h) and (4.7h) similarly enforce the corresponding power limitations to combiner and precoder for UEsi, respectively.

Also, constraints (4.7f) and (4.7g) guarantee the minimum numbers of operating APs in UL or DL by N^{ul} and N^{dl}. Γ_k is the SINR corresponding to the k-th UE, which is compactly rewritten as

$$\Gamma_k \triangleq \begin{cases} \mathrm{UL}_{k,k}^{\mathrm{H}} \Big(\sum\limits_{k' \in \mathcal{K}^{\mathrm{ul}}, k \neq k'} \mathrm{UL}_{k,k'}^{\mathrm{H}} \mathrm{UL}_{k,k'} + \\ \quad \sum\limits_{k' \in \mathcal{K}^{\mathrm{dl}}} \mathrm{DCLI}_{k,k'}^{\mathrm{H}} \mathrm{DCLI}_{k,k'} + \sigma_{\mathrm{ul}}^2 \left\|\boldsymbol{v}_k^{\mathrm{ap}}\right\|_2^2 \Big)^{-1} \mathrm{UL}_{k,k}, & \text{for } k \in \mathcal{K}^{\mathrm{ul}} \\ \mathrm{DL}_{k,k}^{\mathrm{H}} \Big(\sum\limits_{k' \in \mathcal{K}^{\mathrm{dl}}, k \neq k'} \mathrm{DL}_{k,k'}^{\mathrm{H}} \mathrm{DL}_{k,k'} + \\ \quad \sum\limits_{k' \in \mathcal{K}^{\mathrm{ul}}} \mathrm{UCLI}_{k,k'}^{\mathrm{H}} \mathrm{UCLI}_{k,k'} + \sigma_{\mathrm{dl}}^2 \left\|\boldsymbol{v}_k^{\mathrm{ue}}\right\|_2^2 \Big)^{-1} \mathrm{DL}_{k,k}, & \text{for } k \in \mathcal{K}^{\mathrm{dl}} \end{cases}. \tag{4.8}$$

The received signal and interference terms for UL and DL are respectively defined as

$$\mathrm{UL}_{k,k'} \triangleq \boldsymbol{w}_{k'}^{\mathrm{ue}\mathrm{H}} \boldsymbol{H}_{k'}^{\mathrm{H}} \boldsymbol{v}_k^{\mathrm{ap}}, \mathrm{DCLI}_{k,k'} \triangleq \boldsymbol{w}_{k'}^{\mathrm{ap}\mathrm{H}} \boldsymbol{H} \boldsymbol{v}_k^{\mathrm{ap}}, \tag{4.9a}$$

$$\mathrm{DL}_{k,k'} \triangleq \boldsymbol{w}_{k'}^{\mathrm{ap}\mathrm{H}} \boldsymbol{H}_{k'} \boldsymbol{v}_k^{\mathrm{ue}}, \mathrm{UCLI}_{k,k'} \triangleq \boldsymbol{w}_{k'}^{\mathrm{ue}\mathrm{H}} \boldsymbol{H}_{k',k}^{\mathrm{H}} \boldsymbol{v}_k^{\mathrm{ue}}. \tag{4.9b}$$

4.3 Model-Driven Channel Estimation

This section introduces the channel estimation method via the reconstruction using the channel model. The only variables that can be inferred from the location information of the UE among the variables that compose equation (4.1) are AoA $\boldsymbol{\psi}_{k,k',1}$, AoD $\boldsymbol{\psi}_{k',k,1}$ of the LoS path and the distance $d_{k,k'}$ between the k-th UE and the k'-th UE. The estimated channels are obtained from the typical mmWave channel model in equation (4.1). The estimated channel

$\hat{\boldsymbol{H}}_{k,k'}$ can be written

$$\hat{\boldsymbol{H}}_{k,k'} \triangleq \hat{\alpha}_{k,k'}\sqrt{\hat{g}_{k,k'} + z_{k,k'}}\boldsymbol{a}(\boldsymbol{\psi}_{k,k',1})\boldsymbol{a}^{\mathrm{H}}(\boldsymbol{\psi}_{k',k,1}) + \Delta_{k,k'}, \tag{4.10}$$

where $\hat{g}_{k,k'}$ is the path-gain of the LoS path estimated by the path-loss model and $\hat{\alpha}_{k,k'} \sim \mathcal{CN}(0,1)$, $z_{k,k'}$, $\Delta_{k,k'}$ are unknown variables representing the small-scale fading of LoS path, shadowing component, and NLoS path channel, respectively.

The path-loss component $g_{k,k'}$ in equation (4.10) can be estimated from a distance between UEs by assuming the mmWave propagation model [108]. Therefore, the estimated path-loss $\hat{g}_{k,k'}$ is given by

$$\hat{g}_{k,k'} = 10^{\frac{\hat{g}^{\mathrm{dB}}_{k,k'}}{10}}, \tag{4.11}$$

$$\hat{g}^{\mathrm{dB}}_{k,k'} = \mathrm{CT} + \mathrm{PE} \times 10\log_{10}(d_{k,k'}), \tag{4.12}$$

where CT is a constant term, PE is a path loss exponent, and $d_{k,k'}$ is the distance between the k-th and k'-th UEs. On the other hand, the shadowing components $z_{k,k'}$ are stochastic, and it is difficult to estimate their instantaneous values from the UE location information only. Therefore, the shadowing effect is averaged out in the following, and hence $z_{k,k'} = 0$.

The gain of the LoS path is dominant in mmWave channels, and the effect of the NLoS path is limited. Therefore, assuming that $\Delta_{k,k'}$ is sufficiently small compared to $\sqrt{\hat{g}_{k,k'}}$, it can be approximated by

$$\begin{aligned}\hat{\boldsymbol{H}}_{k,k'} &\approx \hat{\alpha}_{k,k'}\sqrt{\hat{g}_{k,k',1}}\boldsymbol{a}(\boldsymbol{\psi}_{k,k',1})\boldsymbol{a}^{\mathrm{H}}(\boldsymbol{\psi}_{k',k,1}) \\ &= \hat{\alpha}_{k,k'}\hat{\boldsymbol{H}}_{k,k',1}.\end{aligned} \tag{4.13}$$

We consider using the estimated channel from equation (4.10) for the inter-UE channel in the objective function (4.7). Then, since the unknown variable $\alpha_{k,k'}$ is included in the interference power between UEs, it becomes difficult to solve equation (4.7) efficiently. To this end, we consider suppressing the inter-UE interference power on average and taking the expected value of $\alpha_{k,k'}$, which can be expressed as

$$\mathbb{E}_{\hat{\alpha}_{k,k'}}\left[|\hat{\alpha}_{k,k'}\boldsymbol{v}_k^{\mathrm{ueH}}\hat{\boldsymbol{H}}^{\mathrm{H}}_{k',k}\boldsymbol{w}^{\mathrm{ue}}_{k'}|^2\right] = \left|\boldsymbol{v}_k^{\mathrm{ueH}}\hat{\boldsymbol{H}}^{\mathrm{H}}_{k',k}\boldsymbol{w}^{\mathrm{ue}}_{k'}\right|^2. \tag{4.14}$$

As a result, the estimated channel $\hat{\boldsymbol{H}}_{k,k'}$ can be approximated by

$$\hat{\boldsymbol{H}}_{k,k'} \approx \hat{\boldsymbol{H}}_{k,k',1}. \tag{4.15}$$

In these above, eliminating the random variables, the estimated inter-UE channel $\hat{\boldsymbol{H}}_{k,k'}$ is given by equation (4.15). In the next section, we propose a convex relaxation scheme to efficiently solve the resource allocation and beamforming design problem in (4.7).

4.4 Joint Resource Allocation and Beamforming Design

In this section, we propose the robust AP mode selection and beamforming design scheme using the estimated channel $\hat{\boldsymbol{H}}_{k,k'}$, which is given by problem (4.7). However, such a design scheme is a discrete non-convex problem that is NP-hard. For efficient design, problem (4.7) is necessary to be reformulated so that it can be solved in polynomial time, such as a convex problem.

4.4.1 Penalized Objective Function for Robust Design

For considering more realistic systems, the CPU needs to know the throughput to decide the data rate of each communicating UE. Therefore, the estimated throughput by the CPU may differ from the actual throughput because the CPU calculates the throughput using the estimated channels. This is fine if the actual throughput is greater than the estimated throughput. However, when the estimated throughput exceeds the actual throughput, an outage occurs in the network [169]. This problem is a critical issue for establishing communication in NAFD CF-mMIMO.

The main reason for the outage in the proposed method is the neglect of the shadowing in the estimated large-scale fading $\hat{g}^{\mathrm{dB}}_{k,k'}$. Therefore, based on the estimated channel, the power gap of the estimated large-scale fading is guaranteed by adding a penalty to the inter-UE interference power in the objective function. First, the estimated channel with penalty between the k-th UE and k'-th UE is defined as

$$\begin{aligned}\bar{\boldsymbol{H}}_{k,k'} &= \sqrt{\hat{g}_{k,k',1} + \rho_{k,k'}}\,\boldsymbol{a}(\boldsymbol{\psi}_{k,k',1})\boldsymbol{a}^{\mathrm{H}}(\boldsymbol{\psi}_{k',k,1}) \\ &\triangleq \sqrt{\rho_{k,k'}}\hat{\boldsymbol{H}}_{k,k'},\end{aligned} \tag{4.16}$$

where $\rho_{k,k'} = 10^{\rho^{\mathrm{dB}}_{k,k'}/10}$ is the penalty.

From equation (4.16), the estimated SINR with the penalty for the reformulation of the objective function is given by

$$\bar{\Gamma}_k \triangleq \begin{cases} \mathrm{UL}_{k,k}^{\mathrm{H}} \Big(\sum\limits_{k' \in \mathcal{K}^{\mathrm{ul}}, k \neq k'} \mathrm{UL}_{k,k'}^{\mathrm{H}} \mathrm{UL}_{k,k'} + \\ \sum\limits_{k' \in \mathcal{K}^{\mathrm{dl}}} \mathrm{DCLI}_{k,k'}^{\mathrm{H}} \mathrm{DCLI}_{k,k'} + \sigma_{\mathrm{ul}}^2 \left\| \boldsymbol{v}_k^{\mathrm{ap}} \right\|_2^2 \Big)^{-1} \mathrm{UL}_{k,k}, \quad \text{for } k \in \mathcal{K}^{\mathrm{ul}} \\ \mathrm{DL}_{k,k}^{\mathrm{H}} \Big(\sum\limits_{k' \in \mathcal{K}^{\mathrm{dl}}, k \neq k'} \mathrm{DL}_{k,k'}^{\mathrm{H}} \mathrm{DL}_{k,k'} + \\ \sum\limits_{k' \in \mathcal{K}^{\mathrm{ul}}} \overline{\mathrm{UCLI}}_{k,k'}^{\mathrm{H}} \overline{\mathrm{UCLI}}_{k,k'} + \sigma_{\mathrm{dl}}^2 \left\| \boldsymbol{v}_k^{\mathrm{ue}} \right\|_2^2 \Big)^{-1} \mathrm{DL}_{k,k}, \quad \text{for } k \in \mathcal{K}^{\mathrm{dl}} \end{cases}, \tag{4.17}$$

where $\overline{\mathrm{UCLI}}_{k,k'}$ is the power of the inter-UEs interference, which is expressed as

$$\overline{\mathrm{UCLI}}_{k,k'} \triangleq \boldsymbol{w}_{k'}^{\mathrm{ue}\mathrm{H}} \bar{\boldsymbol{H}}_{k',k}^{\mathrm{H}} \boldsymbol{v}_k^{\mathrm{ue}}, \tag{4.18}$$

From the above, the joint robust resource allocation and beamforming design can be reformulated as

$$\begin{aligned} \underset{\boldsymbol{\eta}, \boldsymbol{v}, \boldsymbol{w}, \boldsymbol{p}^{\mathrm{dl}}}{\text{maximize}} \quad & \Big(\prod_{k=1}^{K} \log_2 \left(1 + \bar{\Gamma}_k \right) \Big)^{\frac{1}{K}} \\ \text{subject to} \quad & \text{(4.7b) to (4.7i)}, \end{aligned} \tag{4.19}$$

4.4.2 Convex Reformulation of Problem (4.4.1)

Problem (4.4.1) can be relaxed to a convex optimization problem using the same procedure as in the previous chapter. First, the discrete constraint (4.7b) is converted to the $\{0, 1\}$ using a negative entropy function, and problem (4.4.1) can be reformulated as

$$\begin{aligned} \underset{\boldsymbol{\eta}, \boldsymbol{v}, \boldsymbol{w}, \boldsymbol{p}^{\mathrm{dl}}}{\text{maximize}} \quad & \Big(\prod_{k=1}^{K} \log_2 \left(1 + \bar{\Gamma}_k \right) \Big)^{\frac{1}{K}} + \zeta \sum_{\ell=1}^{L} \mathbb{P}(\eta_\ell) && \text{(4.20a)} \\ \text{subject to} \quad & 0 \leq \eta_\ell \leq 1, \forall \ell && \text{(4.20b)} \\ & \left\| \begin{array}{c} 2\boldsymbol{v}_{k,\ell}^{\mathrm{ap}} \\ 1 - \eta_\ell \end{array} \right\|_2 \leq 1 + \eta_\ell, \forall k \in \mathcal{K}^{\mathrm{ul}}, \forall \ell, && \text{(4.20c)} \\ & \left\| \begin{array}{c} 2\boldsymbol{w}_{k,\ell}^{\mathrm{ap}} \\ p_{k,\ell}^{\mathrm{dl}} - \bar{\eta}_\ell \end{array} \right\|_2 \leq p_{k,\ell}^{\mathrm{dl}} + \bar{\eta}_\ell, \forall k \in \mathcal{K}^{\mathrm{dl}}, \forall \ell, && \text{(4.20d)} \\ & \text{(4.7e) to (4.7i)}, \end{aligned}$$

where $\mathbb{P}(\eta_\ell) = \eta_\ell \log(\eta_\ell) + (1-\eta_\ell)\log(1-\eta_\ell)$ is the penalty function based on the negative entropy.

Next, as with Multiple-Antenna UEs Case in Section 3.3.1, we omit the detail of reformulation and summarize it in Appendix B.2. Therefore, after applying LDT and QT, equation (4.20) is reformulated as

$$\underset{\boldsymbol{v},\boldsymbol{w},\boldsymbol{p}^{\mathrm{dl}},\boldsymbol{\gamma},\boldsymbol{s}}{\text{maximize}} \quad \left(\prod_{k=1}^{K} f_k^{\mathrm{qt,m}}\left(\boldsymbol{v},\boldsymbol{w},\boldsymbol{\gamma}\right)\right)^{\frac{1}{K}} + \zeta \sum_{\ell=1}^{L} \mathbb{P}(\eta_\ell) \tag{4.21}$$

$$\text{subject to} \quad \text{(4.7e) to (4.7i), (4.20b) to (4.20d),} \tag{4.22}$$

where

$$f_k^{\mathrm{qt,m}}\left(\boldsymbol{v},\boldsymbol{w},\boldsymbol{\gamma},\boldsymbol{s}\right) \triangleq \alpha_k + \beta_k \Re\{s_k^* \Gamma_k^{\mathrm{qt,m,1}}\} - \|s_k\|_2^2 \bar{\Gamma}_k^{\mathrm{qt,m,2}}, \tag{4.23}$$

with

$$\Gamma_k^{\mathrm{qt,m,1}} \triangleq \begin{cases} \boldsymbol{v}_k^{\mathrm{apH}} \boldsymbol{H}_{k'} \boldsymbol{w}_{k'}^{\mathrm{ue}}, & \text{for } k \in \mathcal{K}^{\mathrm{ul}} \\ \boldsymbol{v}_k^{\mathrm{ueH}} \boldsymbol{H}_{k'}^{\mathrm{H}} \boldsymbol{w}_{k'}^{\mathrm{ap}}, & \text{for } k \in \mathcal{K}^{\mathrm{dl}} \end{cases} \tag{4.24}$$

and $\bar{\Gamma}_k^{\mathrm{qt,m,2}}$ is given by

$$\bar{\Gamma}_k^{\mathrm{qt,m,2}} \triangleq \begin{cases} \sum\limits_{k' \in \mathcal{K}^{\mathrm{ul}}} \mathrm{UL}_{k,k'}^{\mathrm{H}} \mathrm{UL}_{k,k'} + \sum\limits_{k' \in \mathcal{K}^{\mathrm{dl}}} \mathrm{DCLI}_{k,k'}^{\mathrm{H}} \mathrm{DCLI}_{k,k'} + \sigma_{\mathrm{ul}}^2 \left\|\boldsymbol{v}_k^{\mathrm{ap}}\right\|_2^2, & \text{for } k \in \mathcal{K}^{\mathrm{ul}} \\ \sum\limits_{k' \in \mathcal{K}^{\mathrm{dl}}} \mathrm{DL}_{k,k'}^{\mathrm{H}} \mathrm{DL}_{k,k'} + \sum\limits_{k' \in \mathcal{K}^{\mathrm{ul}}} \overline{\mathrm{UCLI}}_{k,k'}^{\mathrm{H}} \overline{\mathrm{UCLI}}_{k,k'} + \sigma_{\mathrm{dl}}^2 \left\|\boldsymbol{v}_k^{\mathrm{ue}}\right\|_2^2, & \text{for } k \in \mathcal{K}^{\mathrm{dl}} \end{cases} \tag{4.25}$$

Here, we consider to split the problem into AP and UE sides and solving them alternately in order to resolve the non-convexity caused by the coupling of different variables. In particular, fixing UE beamforming vectors and focusing on the AP side, the joint resource allocation and beamforming design algorithm is reformulated by applying CCP to equation (4.21). From the above, the optimization problem in (4.7) can be relaxed to the convex optimization problem, which can be solved iteratively by alternately updating each variable in each iteration. Firstly, the optimization problem for the AP-side resource allocation and beamforming update with fixed UE-side variables is formulated as

$$\underset{\boldsymbol{\eta},\boldsymbol{v}^{\mathrm{ap}},\boldsymbol{w}^{\mathrm{ap}}\boldsymbol{p}^{\mathrm{dl}},}{\text{maximize}} \quad \left(\prod_{k=1}^{K} f_{k,\mathrm{AP}}^{\mathrm{fin}}\left(\boldsymbol{v}^{\mathrm{ap}},\boldsymbol{w}^{\mathrm{ap}}\right)\right)^{\frac{1}{K}} + \zeta \sum_{\ell=1}^{L} \eta_\ell \nabla \mathbb{P}(\eta_{\ell,t'}) \tag{4.26a}$$

$$\text{subject to} \quad \text{(4.7e) to (4.7g), (4.20b) to (4.20d),}$$

where index t' denotes the solution obtained at the $t-1$ iteration, $\boldsymbol{v}^{\mathrm{ap}} \triangleq [\boldsymbol{v}_1^{\mathrm{ap}\mathrm{T}}, \ldots, \boldsymbol{v}_K^{\mathrm{ap}\mathrm{T}}]^{\mathrm{T}}$, and $\boldsymbol{w}^{\mathrm{ap}} \triangleq [\boldsymbol{w}_1^{\mathrm{ap}\mathrm{T}}, \ldots, \boldsymbol{w}_K^{\mathrm{ap}\mathrm{T}}]^{\mathrm{T}}$, and the objective function is

$$f_{k,\mathrm{AP}}^{\mathrm{fin}}(\boldsymbol{v}^{\mathrm{ap}}, \boldsymbol{w}^{\mathrm{ap}}) \triangleq \alpha_k + \beta_k \Re\{s_k^* \Gamma_{k,\mathrm{AP}}^{\mathrm{qt},1}\} - \|s_k\|_2^2 \, \bar{\Gamma}_{k,\mathrm{AP}}^{\mathrm{qt},2}, \tag{4.27}$$

where $\alpha_k \triangleq \log_2(1+\gamma_k) - \gamma_k$ and $\beta_k \triangleq 2\sqrt{(1+\gamma_k)}$. The auxiliary variables $\boldsymbol{\gamma} \triangleq [\gamma_1, \ldots, \gamma_K]$ and $\boldsymbol{s} \triangleq [s_1, \ldots, s_K]$ are optimal at $\gamma_k^\star = \bar{\Gamma}_k$, $s_k^\star = \sqrt{(1+\gamma_k)}\Gamma_{k,\mathrm{AP}}^{\mathrm{qt},1}/\bar{\Gamma}_{k,\mathrm{AP}}^{\mathrm{qt},2}$, and the SINR quantities $\Gamma_{k,\mathrm{AP}}^{\mathrm{qt},1}$ and $\bar{\Gamma}_{k,\mathrm{AP}}^{\mathrm{qt},2}$ respectively defined as

$$\Gamma_{k,\mathrm{AP}}^{\mathrm{qt},1} \triangleq \begin{cases} \boldsymbol{v}_k^{\mathrm{ap}\mathrm{H}} \boldsymbol{H}_k \boldsymbol{w}_{k,t'}^{\mathrm{ue}}, & \text{for } k \in \mathcal{K}^{\mathrm{ul}} \\ \boldsymbol{v}_{k,t'}^{\mathrm{ue}\ \mathrm{H}} \boldsymbol{H}_k^{\mathrm{H}} \boldsymbol{w}_k^{\mathrm{ap}}, & \text{for } k \in \mathcal{K}^{\mathrm{dl}}, \end{cases} \tag{4.28}$$

$$\bar{\Gamma}_{k,\mathrm{AP}}^{\mathrm{qt},2} \triangleq \begin{cases} \sum\limits_{k' \in \mathcal{K}^{\mathrm{ul}}} \boldsymbol{v}_k^{\mathrm{ap}\mathrm{H}} \boldsymbol{H}_{k'} \boldsymbol{w}_{k',t'}^{\mathrm{ue}} \boldsymbol{w}_{k',t'}^{\mathrm{ue}\ \mathrm{H}} \boldsymbol{H}_{k'}^{\mathrm{H}} \boldsymbol{v}_k^{\mathrm{ap}} + \\ \quad \sum\limits_{k' \in \mathcal{K}^{\mathrm{dl}}} \boldsymbol{v}_k^{\mathrm{ap}\mathrm{H}} \boldsymbol{H}^{\mathrm{H}} \boldsymbol{w}_{k',t'}^{\mathrm{ap}} \boldsymbol{w}_{k',t'}^{\mathrm{ap}\ \mathrm{H}} \boldsymbol{H} \boldsymbol{v}_k^{\mathrm{ap}} + \sigma_{\mathrm{ul}}^2 \left\| \boldsymbol{v}_k^{\mathrm{ap}} \right\|_2^2, & \text{for } k \in \mathcal{K}^{\mathrm{ul}} \\ \sum\limits_{k' \in \mathcal{K}^{\mathrm{dl}}} \boldsymbol{v}_{k,t'}^{\mathrm{ue}\ \mathrm{H}} \boldsymbol{H}_{k'}^{\mathrm{H}} \boldsymbol{w}_{k'}^{\mathrm{ap}} \boldsymbol{w}_{k'}^{\mathrm{ap}\mathrm{H}} \boldsymbol{H}_{k'} \boldsymbol{v}_{k,t'}^{\mathrm{ue}} + \\ \quad \sum\limits_{k' \in \mathcal{K}^{\mathrm{ul}}} \boldsymbol{v}_{k,t'}^{\mathrm{ue}\ \mathrm{H}} \bar{\boldsymbol{H}}_{k',k} \boldsymbol{w}_{k',t'}^{\mathrm{ue}} \boldsymbol{w}_{k',t'}^{\mathrm{ue}\ \mathrm{H}} \bar{\boldsymbol{H}}_{k',k}^{\mathrm{H}} \boldsymbol{v}_{k,t'}^{\mathrm{ue}} + \sigma_{\mathrm{dl}}^2 \left\| \boldsymbol{v}_{k,t'}^{\mathrm{ue}} \right\|_2^2, & \text{for } k \in \mathcal{K}^{\mathrm{dl}} \end{cases} . \tag{4.29}$$

Finally, the optimization problem to update UE beamforming counterparts for the obtained AP beamformers is given by

$$\begin{aligned} \underset{\boldsymbol{v}^{\mathrm{ue}}, \boldsymbol{w}^{\mathrm{ue}}, \boldsymbol{\gamma}, \boldsymbol{s}}{\text{maximize}} \quad & \left(\prod_{k=1}^{K} f_{k,\mathrm{UE}}^{\mathrm{fin}} \left(\boldsymbol{v}^{\mathrm{ue}}, \boldsymbol{w}^{\mathrm{ue}}, \boldsymbol{\gamma}, \boldsymbol{s} \right) \right)^{\frac{1}{K}} \\ \text{subject to} \quad & \text{(4.7h) and (4.7i)}, \end{aligned} \tag{4.30}$$

where $\boldsymbol{v}^{\mathrm{ue}} = [\boldsymbol{v}_1^{\mathrm{ue}}, \ldots, \boldsymbol{v}_K^{\mathrm{ue}}]$, $\boldsymbol{w}^{\mathrm{ue}} = [\boldsymbol{w}_1^{\mathrm{ue}}, \ldots, \boldsymbol{w}_K^{\mathrm{ue}}]$, $\boldsymbol{s} \triangleq [s_1, \ldots, s_K]$ optimal at $s_k^\star = \sqrt{(1+\gamma_k)}\Gamma_{k,\mathrm{UE}}^{\mathrm{qt},1}/\bar{\Gamma}_{k,\mathrm{UE}}^{\mathrm{qt},2}$, and

$$f_{k,\mathrm{UE}}^{\mathrm{fin}}(\boldsymbol{v}^{\mathrm{ue}}, \boldsymbol{w}^{\mathrm{ue}}, \boldsymbol{\gamma}, \boldsymbol{s}) \triangleq \alpha_k + \beta_k \Re\{s_k^* \Gamma_{k,\mathrm{UE}}^{\mathrm{qt},m,1}\} - \|s_k\|_2^2 \, \Gamma_{k,\mathrm{UE}}^{\mathrm{qt},m,2}, \tag{4.31}$$

with the SINR quantities $\Gamma_{k,\mathrm{UE}}^{\mathrm{qt},1}$ and $\bar{\Gamma}_{k,\mathrm{UE}}^{\mathrm{qt},2}$ respectively defined as

$$\Gamma_{k,\mathrm{UE}}^{\mathrm{qt},1} = \begin{cases} \boldsymbol{v}_{k,t'}^{\mathrm{ap}\ \mathrm{H}} \boldsymbol{H}_k \boldsymbol{w}_k^{\mathrm{ue}}, & \text{for } k \in \mathcal{K}^{\mathrm{ul}} \\ \boldsymbol{v}_k^{\mathrm{ue}\mathrm{H}} \boldsymbol{H}_k^{\mathrm{H}}, \boldsymbol{w}_{k,t'}^{\mathrm{ap}}, & \text{for } k \in \mathcal{K}^{\mathrm{dl}}, \end{cases} \tag{4.32}$$

$$\bar{\Gamma}_{k,\mathrm{UE}}^{\mathrm{qt},2} \triangleq \begin{cases} \sum\limits_{k' \in \mathcal{K}^{\mathrm{ul}}} \boldsymbol{v}_{k,t'}^{\mathrm{ap}\ \mathrm{H}} \boldsymbol{H}_{k'} \boldsymbol{w}_{k'}^{\mathrm{ue}} \boldsymbol{w}_{k'}^{\mathrm{ue}\mathrm{H}} \boldsymbol{H}_{k'}^{\mathrm{H}} \boldsymbol{v}_{k,t'}^{\mathrm{ap}} + \\ \quad \sum\limits_{k' \in \mathcal{K}^{\mathrm{dl}}} \boldsymbol{v}_{k,t'}^{\mathrm{ap}\ \mathrm{H}} \boldsymbol{H}^{\mathrm{H}} \boldsymbol{w}_{k'}^{\mathrm{ap}} \boldsymbol{w}_{k'}^{\mathrm{ap}\mathrm{H}} \boldsymbol{H} \boldsymbol{v}_{k,t'}^{\mathrm{ap}} + \sigma_{\mathrm{ul}}^2 \left\| \boldsymbol{v}_{k,t'}^{\mathrm{ap}} \right\|_2^2, & \text{for } k \in \mathcal{K}^{\mathrm{ul}} \\ \sum\limits_{k' \in \mathcal{K}^{\mathrm{dl}}} \boldsymbol{v}_{k}^{\mathrm{ue}\mathrm{H}} \boldsymbol{H}_{k'}^{\mathrm{H}} \boldsymbol{w}_{k',t'}^{\mathrm{ap}} \boldsymbol{w}_{k',t'}^{\mathrm{ap}\ \mathrm{H}} \boldsymbol{H}_{k'} \boldsymbol{v}_{k}^{\mathrm{ue}} + \\ \quad \sum\limits_{k' \in \mathcal{K}^{\mathrm{ul}}} \boldsymbol{v}_{k}^{\mathrm{ue}\mathrm{H}} \bar{\boldsymbol{H}}_{k',k} \boldsymbol{w}_{k',t'}^{\mathrm{ue}} \boldsymbol{w}_{k',t'}^{\mathrm{ue}\ \mathrm{H}} \bar{\boldsymbol{H}}_{k',k}^{\mathrm{H}} \boldsymbol{v}_{k}^{\mathrm{ue}} + \sigma_{\mathrm{dl}}^2 \left\| \boldsymbol{v}_{k}^{\mathrm{ue}} \right\|_2^2, & \text{for } k \in \mathcal{K}^{\mathrm{dl}} \end{cases} . \tag{4.33}$$

Algorithm 3 Solver for Fraction Programming

Input: Combining vectors $\boldsymbol{v}$, precorders $\boldsymbol{w}$, weights ζ, and incrementation parameter ζ^+

if AP side design part **then**
  $[\gamma_k\ s_k], \leftarrow [\bar{\Gamma}_k, \sqrt{(1+\gamma_k)}\Gamma_{k,\mathrm{AP}}^{\mathrm{qt},1}/\bar{\Gamma}_{k,\mathrm{AP}}^{\mathrm{qt},2}], \forall k$
  Update $\boldsymbol{\eta}, \boldsymbol{v}^{\mathrm{ap}}$ and $\boldsymbol{w}^{\mathrm{ap}}$ by solving. (4.26)
  $\zeta \leftarrow \zeta + \zeta^+$
else
  $[\gamma_k\ s_k], \leftarrow [\Gamma_k, \sqrt{(1+\gamma_k)}\Gamma_{k,\mathrm{UE}}^{\mathrm{qt},1}/\bar{\Gamma}_{k,\mathrm{UE}}^{\mathrm{qt},2}], \forall k$
  Update $\boldsymbol{v}^{\mathrm{ue}}$ and $\boldsymbol{w}^{\mathrm{ue}}$ by solving (4.30).
end if

Output: $[\boldsymbol{\eta}, \boldsymbol{v}^{\mathrm{ap}}, \boldsymbol{w}^{\mathrm{ap}}]$ or $[\boldsymbol{v}^{\mathrm{ue}}, \boldsymbol{w}^{\mathrm{ue}}]$

Algorithm 4 Joint NAFD CF-mMIMO Beamforming and Resource Allocation

Input: Combining vectors $\boldsymbol{v}$, precorders $\boldsymbol{w}$, weights ζ, incrementation parameter ζ^+, and maximum number of iterations $t^{\max}$

$[t, t'] \leftarrow [0, -1]$
repeat
  $[t, t'] \leftarrow [t+1, t]$
  Run the algorithm 3 for AP side.
  $[\eta_{\ell,t'}, \boldsymbol{v}_{k,t'}^{\mathrm{ap}}, \boldsymbol{w}_{k,t'}^{\mathrm{ap}}] \leftarrow [\eta_\ell, \boldsymbol{v}_k^{\mathrm{ap}}, \boldsymbol{w}_k^{\mathrm{ap}}], \forall k$
  Run the algorithm 3 for UE side.
  $[\boldsymbol{v}_{k,t'}^{\mathrm{ue}}, \boldsymbol{w}_{k,t'}^{\mathrm{ue}}] \leftarrow [\boldsymbol{v}_k^{\mathrm{ue}}, \boldsymbol{w}_k^{\mathrm{ue}}], \forall k$
  if Reach $t = t^{\mathrm{fix}}$ **then**
    Fix $\boldsymbol{\eta}$ to $\{0, 1\}$.
  end if
until Convergence or reach $t = t^{\max}$.

Output: $\boldsymbol{\eta}$, $\boldsymbol{v}$, and $\boldsymbol{w}$

The updating of variables by equations (4.26) and (4.30) is summarized in Algorithm 3. Next, the entire flow of the iterative optimization algorithm is summarized in Algorithm 4. In addition, this chapter improves the accuracy of the beamforming design in the subsequent loops by fixing η_ℓ to 0 or 1 after the t^{fix}-th iteration.

4.5 Numerical Results

In this section, the effect of the inter-UEs interference and the performance of the proposed methods are analyzed via computational simulations. In the simulation, a dense scenario with many UEs in a small area served by an NAFD CF-mMIMO system is considered to confirm the effect of inter-UE interference.

The APs are distributed in a regular grid formation, while UEs are uniformly distributed within the effective service area, leading to a UL/DL ratio of $1:1$. The common simulation parameters are summarized in Table 4.1. In addition, the AoA and AoD for the NLoS component of the channel are modeled as uniformly distributed within the interval $[0, 2\pi)$.

Table 4.1 Simulation Parameters.

Number of APs (L)	36
Number of AP antennas (M)	1
Number of path (P)	3
Coverage area	100×100 [m^2]
Large-scale fading ($g_{r,t}$)	[108, Table I]
Carrier frequency	73 [GHz]
Bandwidth (W)	730 [MHz]
Noise figure	7 [dB]
Maximum transmit power of each UE	100 [mW]
Maximum transmit power of each AP	1 [W]
Minimum number of APs allocated (N^{ul}, N^{dl})	1

The APs and UEs are assumed to be placed 10 m and 1.5 m above the ground surface, respectively. To focus on the effects of inter-UE interference, we assume that the CPU has perfect knowledge of the inter-AP-UE and inter-AP channels. The convex optimization problems (4.26) and (4.30) in Algorithm 4 are solved via CVX [153], using the SDPT3 backend. The AP mode (UL or DL) is fixed after $t^{\text{fix}} = 5$ iterations, and the maximum number of iterations used in algorithm 4 is $t^{\max} = 10$. The weights applied to the negative entropy function are initialized to $\zeta = 0$ and incremented by $\zeta^+ = 1$ but not applied in the first loop. After the given number of iterations, we fix the AP allocations and use Algorithm 2 to finalize

the beamforming design. For comparison, Algorithm 2 is also used as SotA method in the following.

4.5.1 Comparison of Design Accuracy

Figs. 4.1, 4.2, 4.3 compare the proposed approach with the SotA with and without CSI of inter-UE channels in terms of an average geometric mean of throughput as a function of the number of UEs. Note that N indicates the number of UE antennas. When we compare the SotA without CSI with that with CSI, the degradation is about 5% when $N = 4, 8$ and about 10% when $N = 16$. This clearly shows the effectiveness of UE beamforming without the inter-UE channel penalty to mitigate inter-UE interference. When we focus on the performance of the proposed approach, despite the proposed approach does not have CSI of inter-UE channels, the performance approaches the SotA with perfect CSI and is superior to the SotA without CSI. This confirms that our optimization with the proposed CSI estimation using UE-locations is remarkably effective.

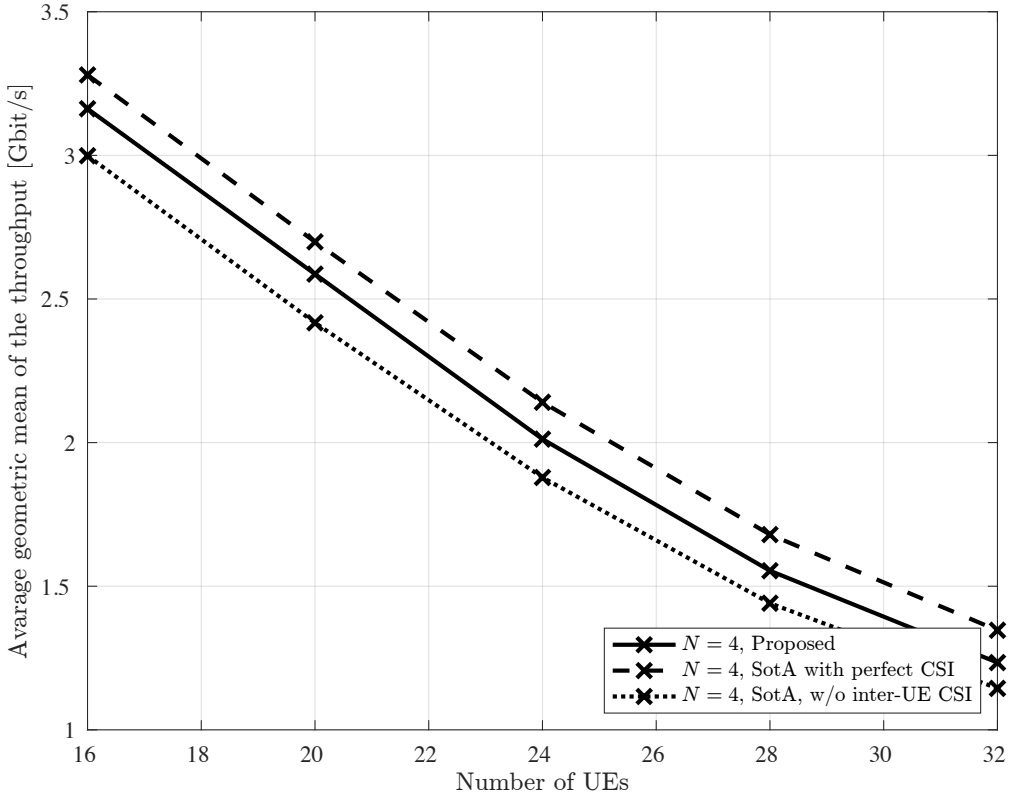

Fig. 4.1 Comparison of the geometric mean of throughput versus the number of UEs ($N = 4$).

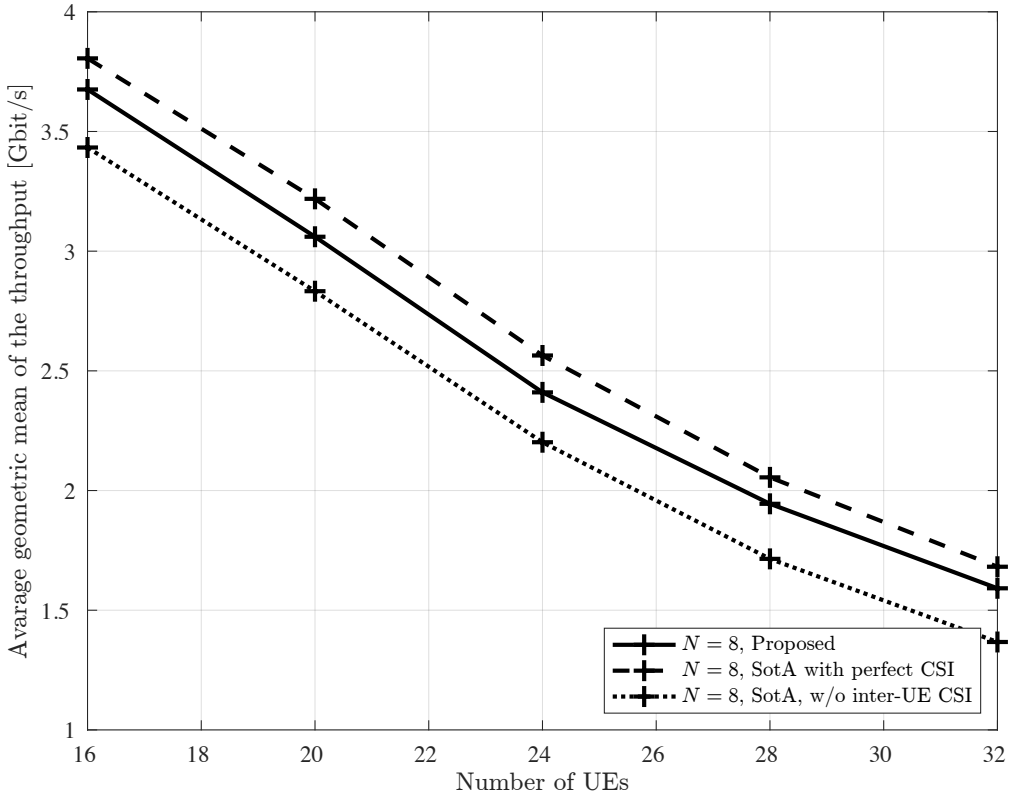

Fig. 4.2 Comparison of the geometric mean of throughput versus the number of UEs ($N = 8$).

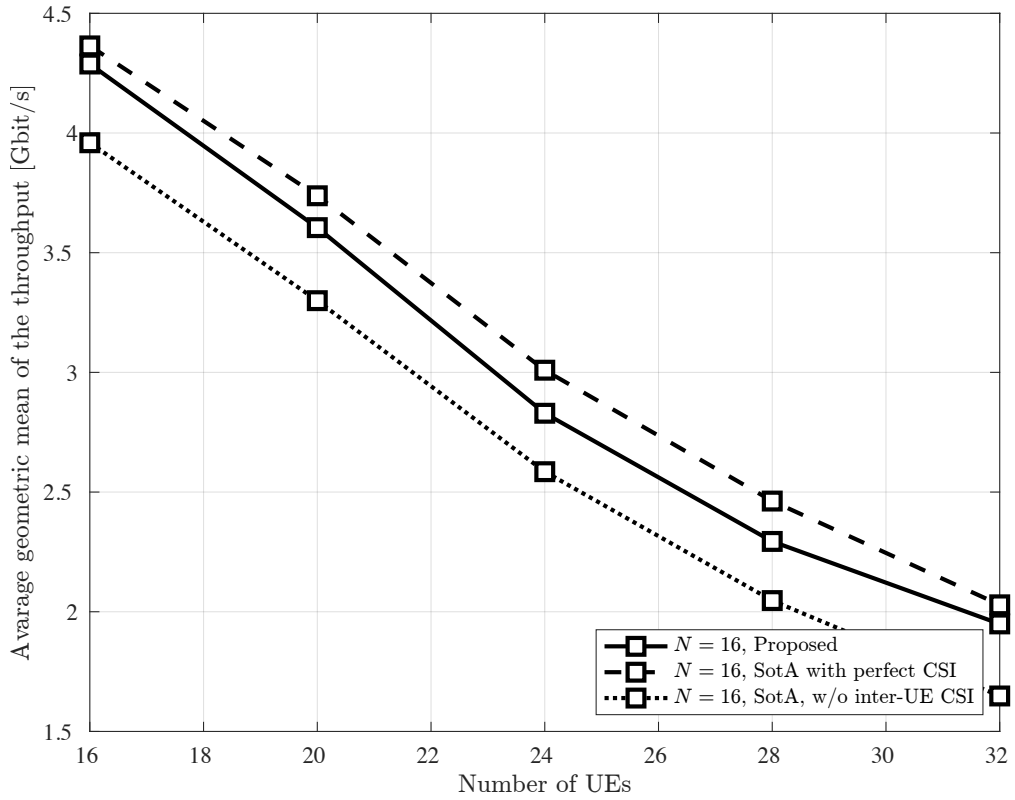

Fig. 4.3 Comparison of the geometric mean of throughput versus the number of UEs ($N = 16$).

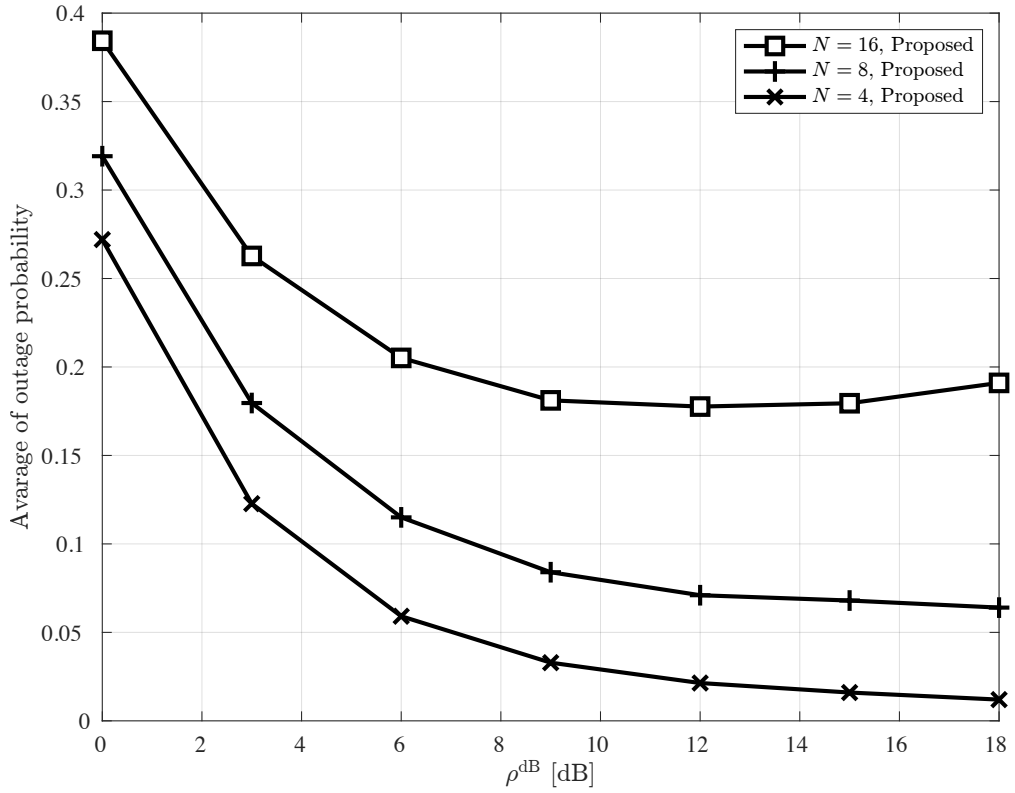

Fig. 4.4 Comparison of the outage probability.

4.5.2 Outage and Throughput

In the previous section, we confirmed the proposed method to close the perfect CSI case. On the other hand, the CPU must use the estimated CSI to determine the data rate to communicate the UE. Therefore, if the estimated throughput of the k-th UEs is greater than the true throughput, the communication becomes outage [169, Section 5.4.1].

In this section, we discuss the outage probability of the network and the throughput considering the outage. First, the estimated SINR of k-th DL UE is expressed as

$$\hat{\Gamma}_k^{\mathrm{dl}} \triangleq \frac{|\boldsymbol{v}_k^{\mathrm{ueH}} \boldsymbol{H}_k^{\mathrm{H}} \boldsymbol{w}_k^{\mathrm{ap}}|^2}{\sum\limits_{\substack{k' \in \mathcal{K}^{\mathrm{dl}} \\ k \neq k'}} |\boldsymbol{v}_k^{\mathrm{ueH}} \boldsymbol{H}_k^{\mathrm{H}} \boldsymbol{w}_{k'}^{\mathrm{ap}}|^2 + \sum\limits_{k' \in \mathcal{K}^{\mathrm{ul}}} |\boldsymbol{v}_k^{\mathrm{ueH}} \hat{\boldsymbol{H}}_{k',k}^{\mathrm{H}} \boldsymbol{w}_{k'}^{\mathrm{ue}}|^2 + \sigma_{\mathrm{dl}}^2 \left\|\boldsymbol{v}_k^{\mathrm{ue}}\right\|_2^2}. \tag{4.34}$$

The outage makes perfect error correction impossible because the data rate exceeds channel capacity. Moreover, the system can not confirm that data is correct even if the signal is received error-free. Therefore, to discuss the worst case, let the throughput at the occurrence of an outage be zero. Then, from equations (4.34) and (4.5b), the k-th UE outage decision is defined by

$$o_k \triangleq \begin{cases} 1 & \text{if } \hat{\boldsymbol{\Gamma}}_k^{\mathrm{dl}} - \boldsymbol{\Gamma}_k^{\mathrm{dl}} > 0 \\ 0 & \text{if } \hat{\boldsymbol{\Gamma}}_k^{\mathrm{dl}} - \boldsymbol{\Gamma}_k^{\mathrm{dl}} \leq 0 \end{cases}. \tag{4.35}$$

From equation (4.35), the outage probability of the DL UE and throughput considering the outage UEs are respectively given by

$$\mathrm{OutageProbability} \triangleq \sum_{k \in \mathcal{K}^{\mathrm{dl}}} \frac{o_k}{K^{\mathrm{dl}}}, \tag{4.36}$$

$$\mathrm{Throughput}_k = \begin{cases} W \log_2(1 - \Gamma_k^{\mathrm{ul}}) & \text{for } k \in \mathcal{K}^{\mathrm{ul}} \\ \bar{o}_k W \log_2(1 - \Gamma_k^{\mathrm{dl}}) & \text{for } k \in \mathcal{K}^{\mathrm{dl}} \end{cases}, \tag{4.37}$$

where $\bar{o}_k = 1 - o_k$ is the expression of the k-th outage DL UE, K^{dl} is the number of DL UEs, and W is the bandwidth. Note that UL UEs do not occur outages by not using the estimated channel in the beamforming design.

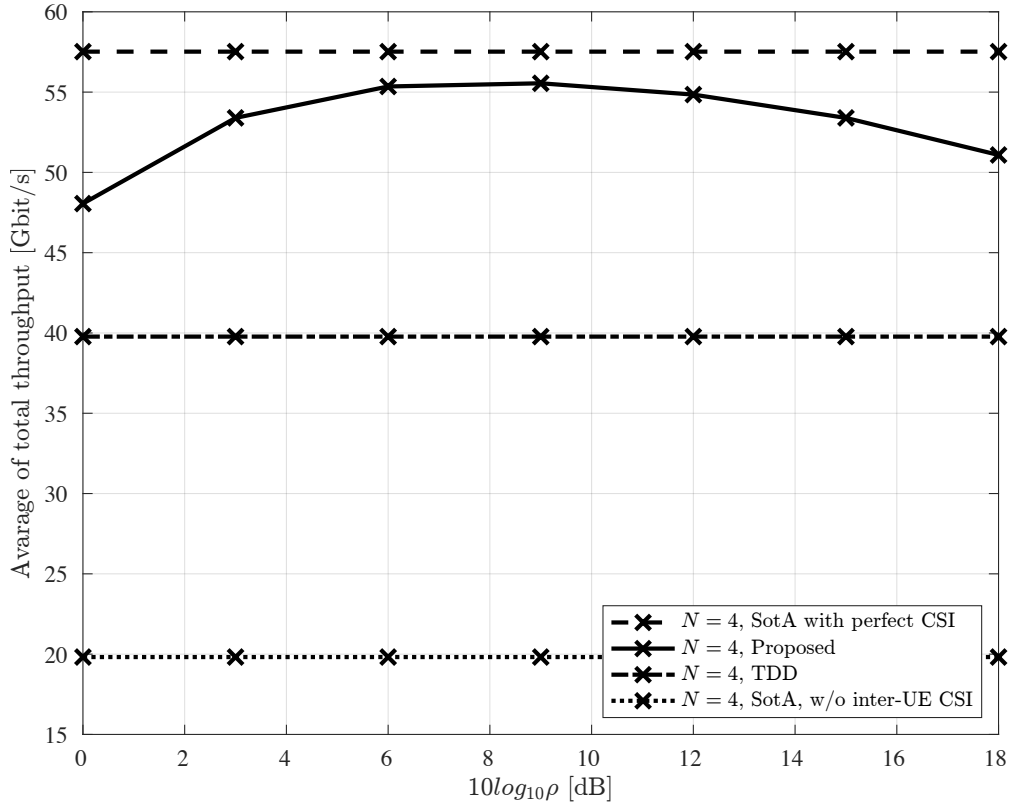

Fig. 4.5 Comparison of the throughput versus penalty level ($K = 16, N = 4$).

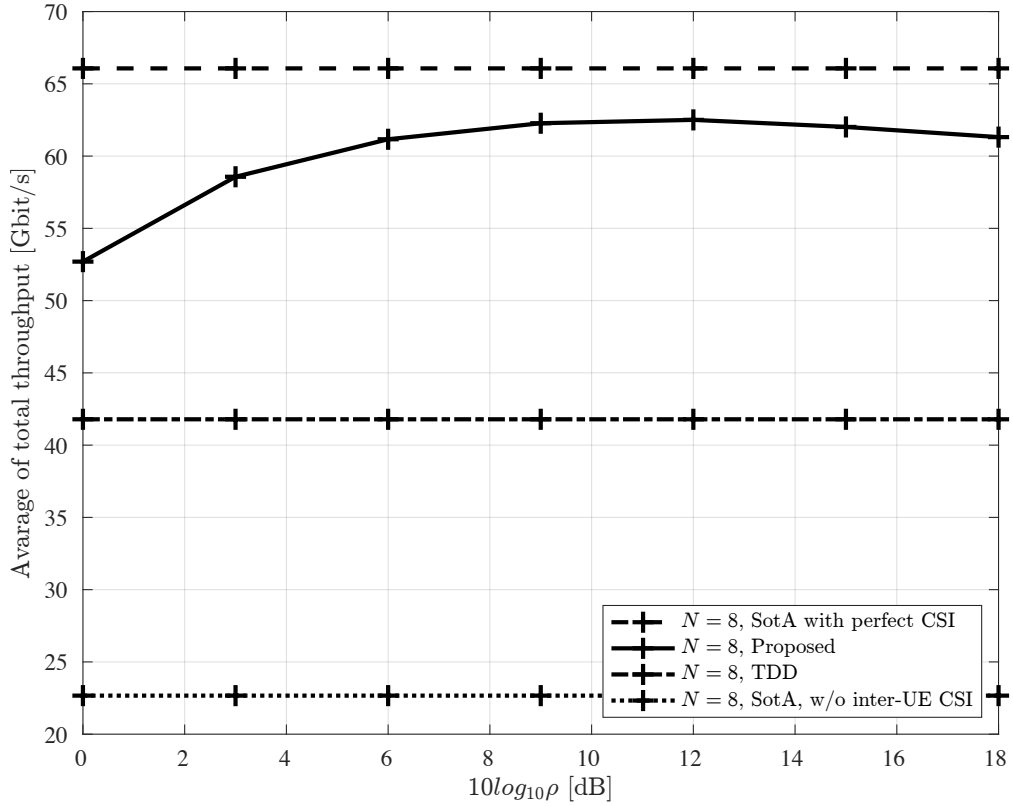

Fig. 4.6 Comparison of the throughput versus penalty level ($K = 16, N = 8$).

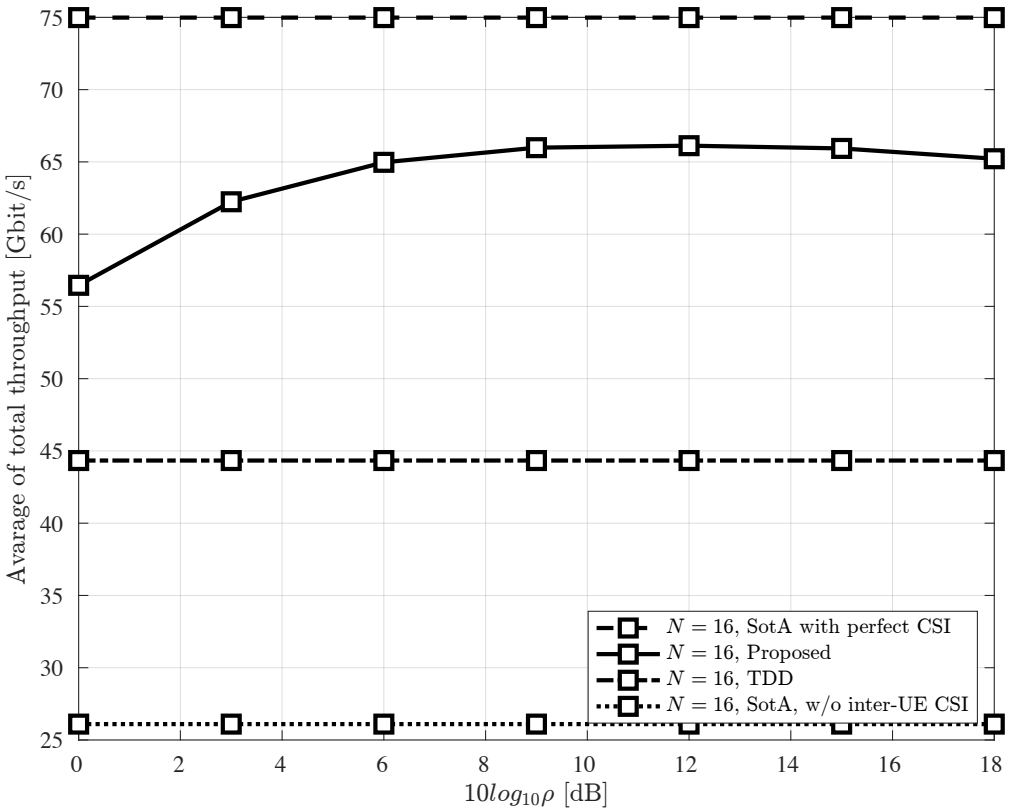

Fig. 4.7 Comparison of the throughput versus penalty level ($K = 16, N = 16$).

Fig. 4.4 compares the change in average outage probability with varying the size of the penalty coefficient. Unless otherwise specified below, the number of UEs here is $K = 16$, and the optimal penalty ρ^{dB} is selected for the results. The change in outage probability of $N = 4, 8$ shows decreases as the penalty increases. These clearly show the effectiveness of the inter-UE channel penalty in guaranteeing estimation error. Focusing on $N = 8$, the outage probability increases with $\rho^{\mathrm{dB}} = 12$. The impact of the penalty on the estimated channel power is proportional to the number of UE antennas. Therefore, increasing the penalty too much is thought to result in an overestimation of the interference power and an over-allocation of power to UEs with a better actual SINR than the estimated SINR. This confirms that the proposed optimization with penalty-based estimated interference power guarantee is highly effective. However, the optimal values of the penalty coefficients need to be investigated for each number of UE antennas.

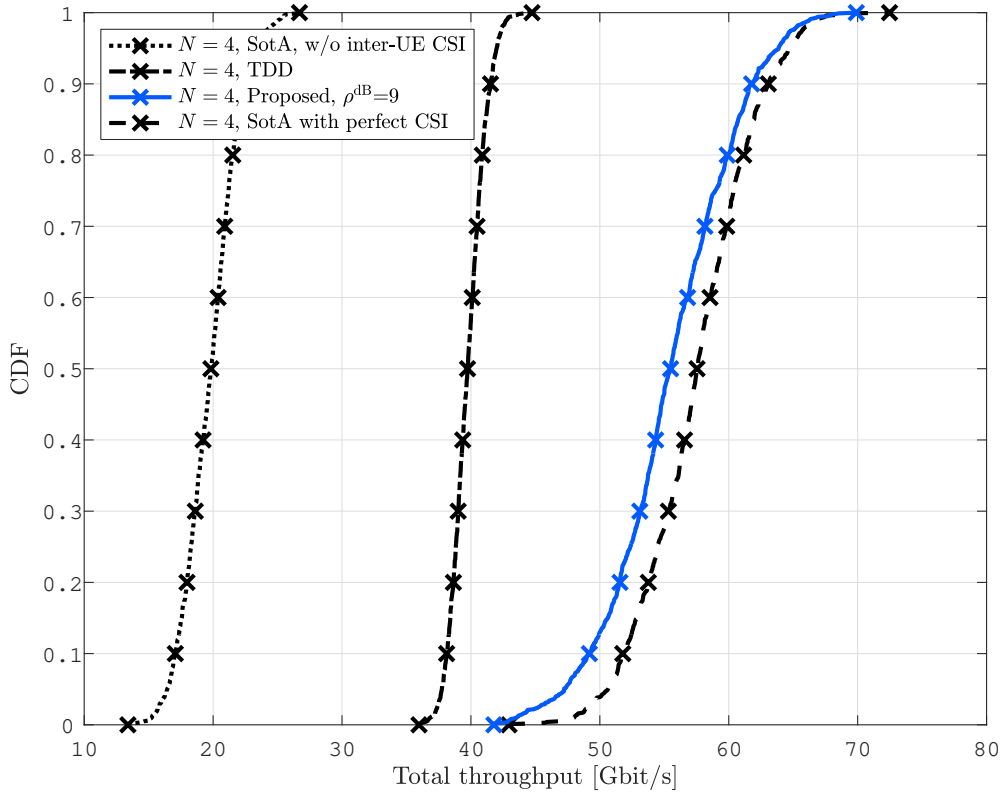

Fig. 4.8 Comparison of the CDF of the total throughput for $\rho_{k,k'}$ ($K = 16, N = 4$).

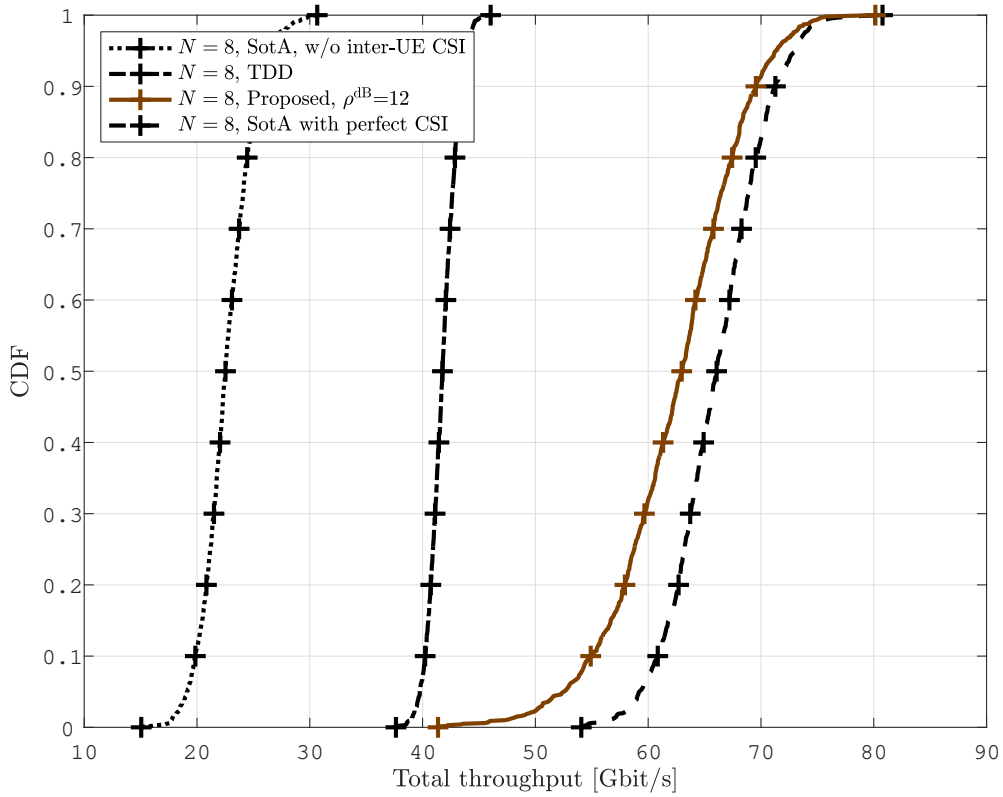

Fig. 4.9 Comparison of the CDF of the total throughput for $\rho_{k,k'}$ ($K = 16, N = 8$).

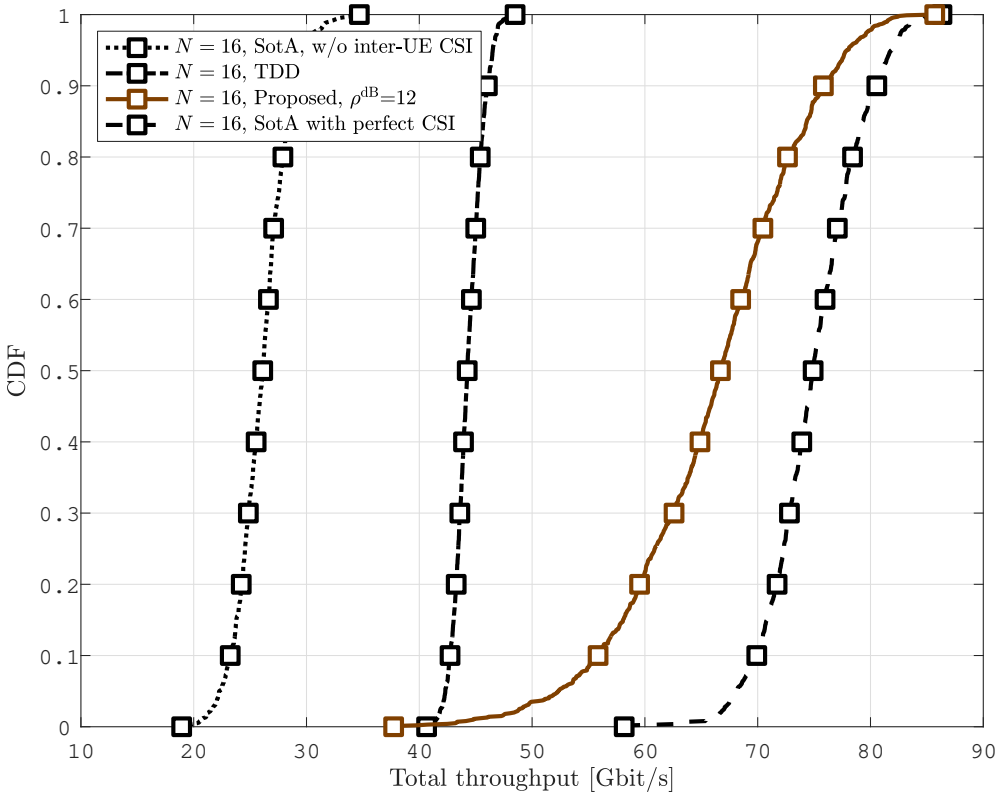

Fig. 4.10 Comparison of the CDF of the total throughput for $\rho_{k,k'}$ ($K = 16, N = 16$).

Now let's check the throughput characteristics taking into account the outage. When outages occur, the DL UE throughput is zero, so the impact on total throughput is enormous. Therefore, the advantages over TDD identified in Section 3.5.3 also be reconfirmed. The TDD beamforming design uses Algorithm 4 with the penalty hyperparameter $\zeta = 0$. Also, the ℓ-th AP allocation variable is set to $\eta_\ell = 1$ for UL and $\eta_\ell = 0$ for DL, respectively. The TDD timeslot is simply allocaiton from the UL/DL UEs ratio, *i.e.* $\mathrm{Throughput}_k^{\mathrm{tdd}} = 0.5\mathrm{Throughput}_k$. Fig. 4.8, 4.9, 4.10 compare SotA with and without CSI in the inter-UE channel, the proposed method, and TDD with CDF for the total throughput. Note that the rho in the legend indicates the magnitude of the penalty: comparing TDD with SotA without CSI, it can be seen that the degradation is about 50% for all SotA antenna numbers. This shows the enormous impact of inter-UE interference. Turning to the performance of the proposed method, despite not having CSI for the complete inter-UE channel, the proposed method approaches SotA with complete CSI and outperforms TDD. This confirms that the proposed CSI estimation using UE-location and optimization with error guarantee by penalty is highly effective. In addition, these results clearly show that even without inter-UE CSI, the throughput performance of NAFD CF-mMIMO with the proposed method is superior to that of TDD. However, the

outage ratio increases with the number of antennas, which increases the difference between SotA with perfect CSI and the proposed method.

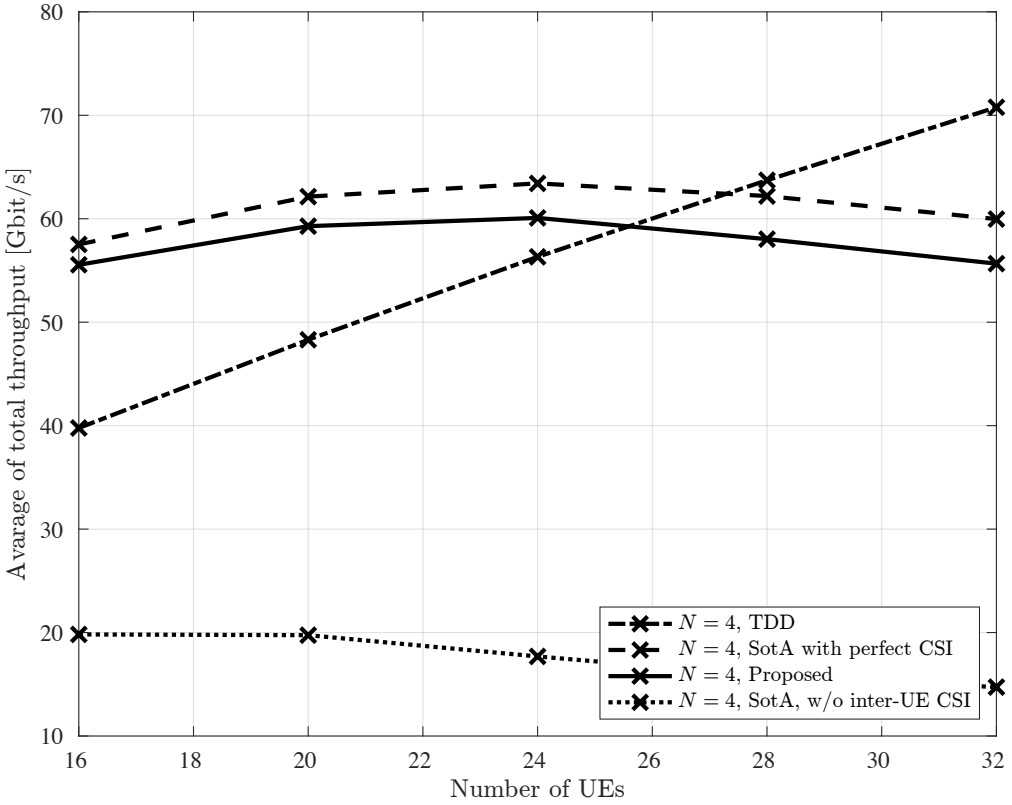

Fig. 4.11 Comparison of the average total throughput versus the number of UEs (N = 4).

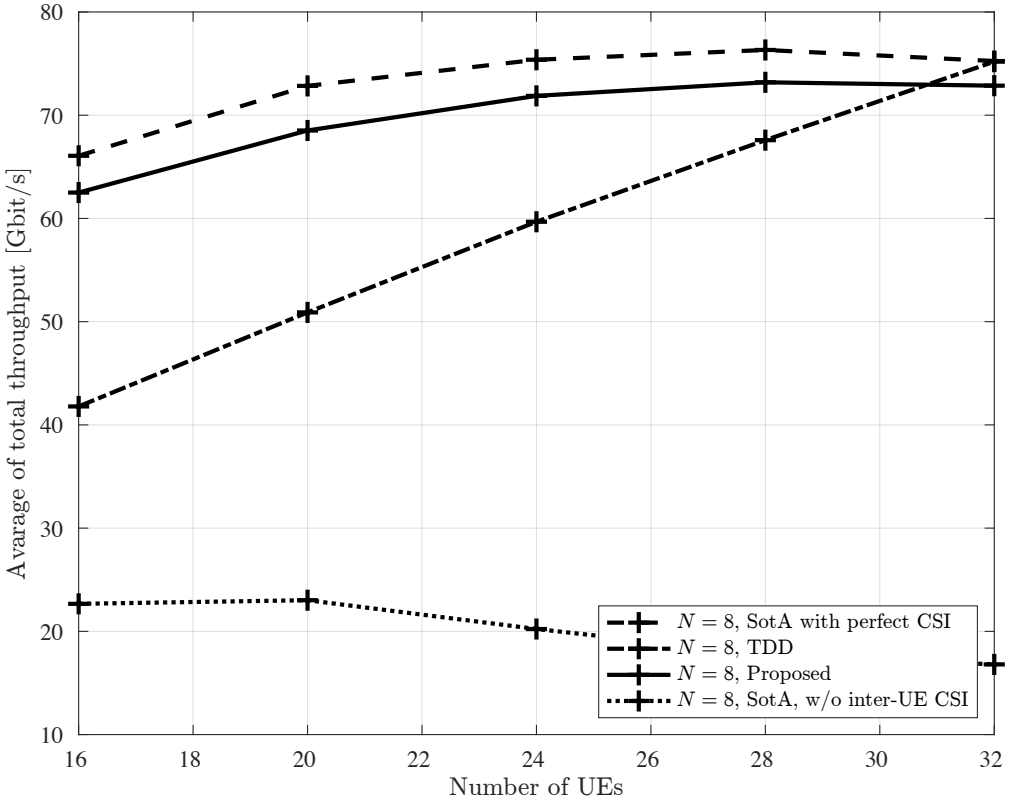

Fig. 4.12 Comparison of the average total throughput versus the number of UEs (N = 8).

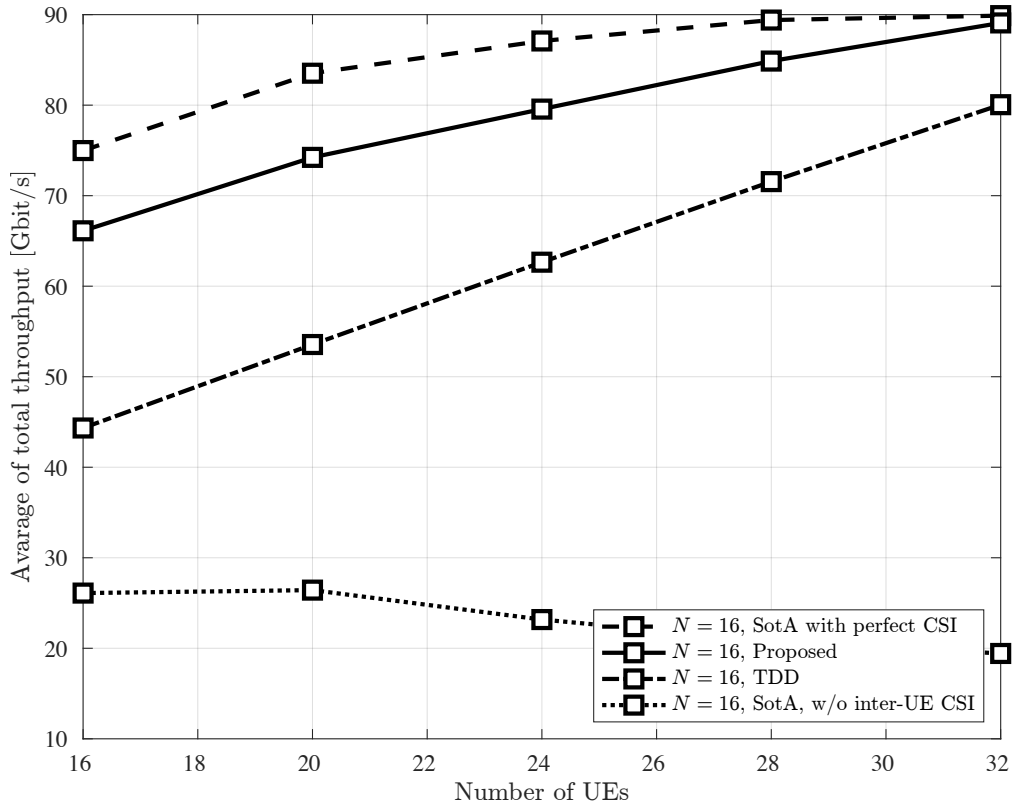

Fig. 4.13 Comparison of the average total throughput versus the number of UEs ($N = 16$).

The throughput is confirmed when inter-UE interference increases. Figs. 4.11, 4.12, 4.13 compares the change in the number of UEs and the average total throughput. It can be seen that the number of UEs and total throughput are proportional to the number of UEs, as TDD has no inter-UE interference. Comparing SotA with the proposed method and TDD, it can be seen that TDD and throughput are reversed, with the number of UEs $K = 28, 32$ for $N = 4, 8$. This indicates that the impact of inter-UE interference on throughput is enormous. However, the number of UEs $K = 28, 32$ compared to the number of APs $L = 36$ is exceptionally high. This situation is no longer "massive" MIMO. Therefore, mmWave NAFD CF-mMIMO outperforms TDD in the practical UE number range. In addition, focusing on $N = 16$, it outperforms TDD for any number of UEs. This indicates that increasing the number of UE antennas can effectively suppress inter-UE interference. When focusing on SotA with perfect CSI and the proposed method, the performance approaches that of SotA with perfect CSI at all numbers of UEs and shows superior performance. This confirms the superiority of CF-mMIMO over TDD and the effectiveness of the optimization using the proposed method.

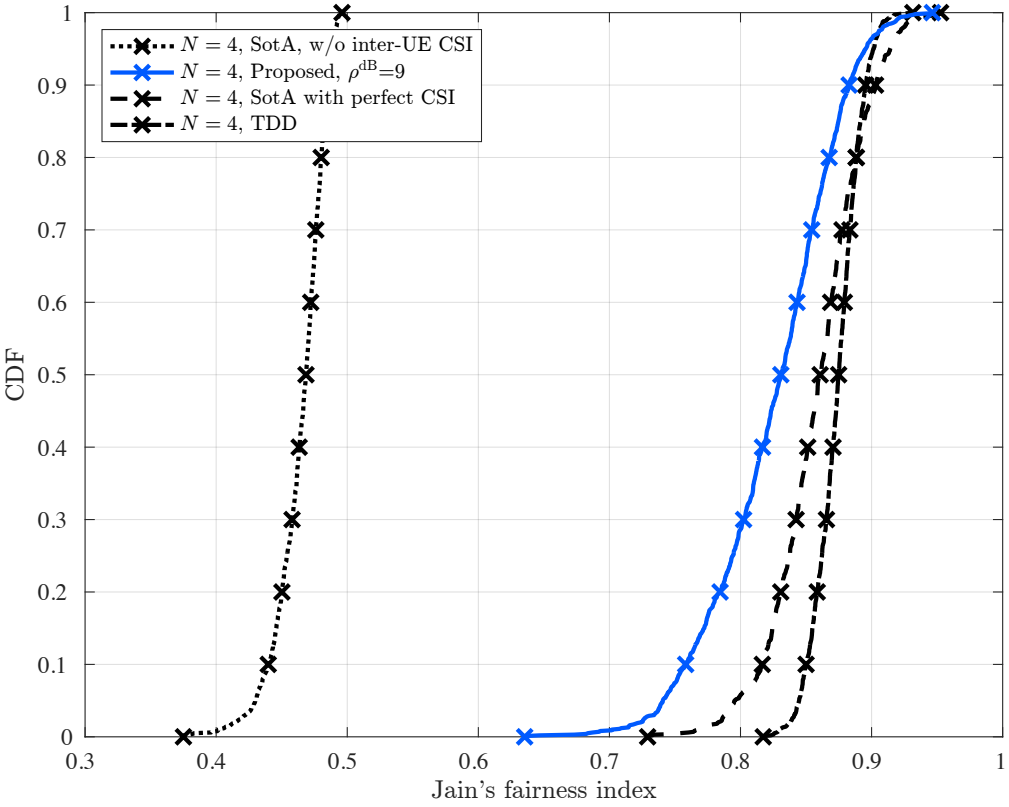

Fig. 4.14 Comparison of the CDF of Jain's fairness index for UE ($N = 4$).

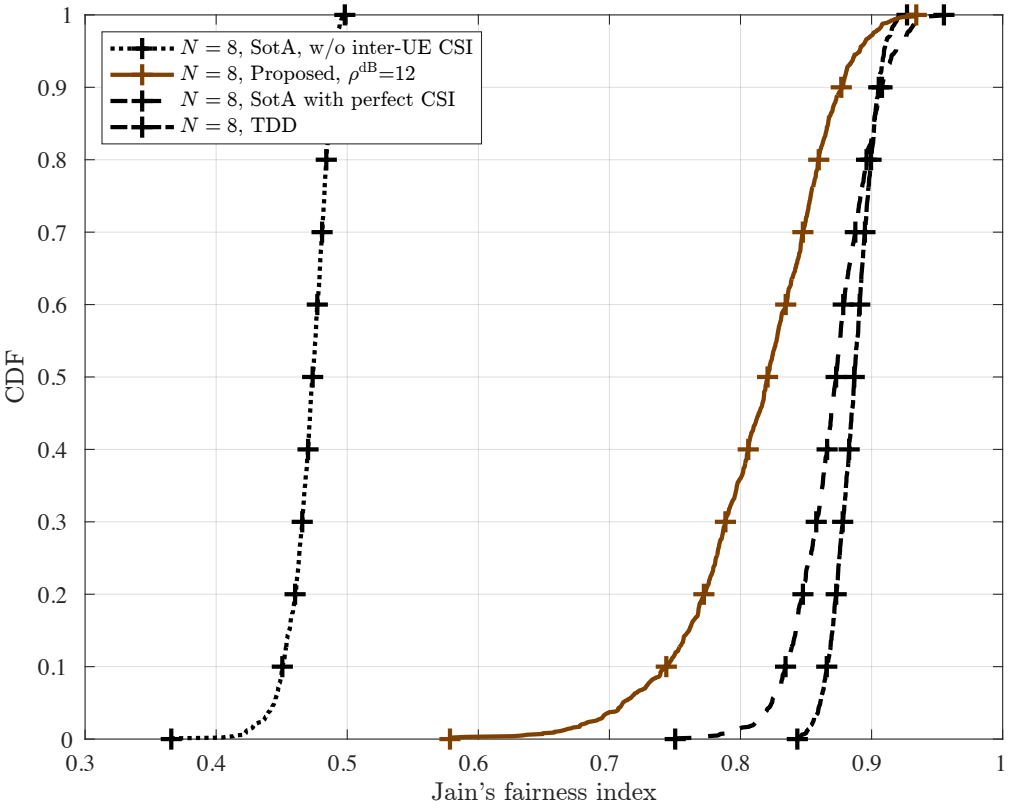

Fig. 4.15 Comparison of the CDF of Jain's fairness index for UE ($N = 8$).

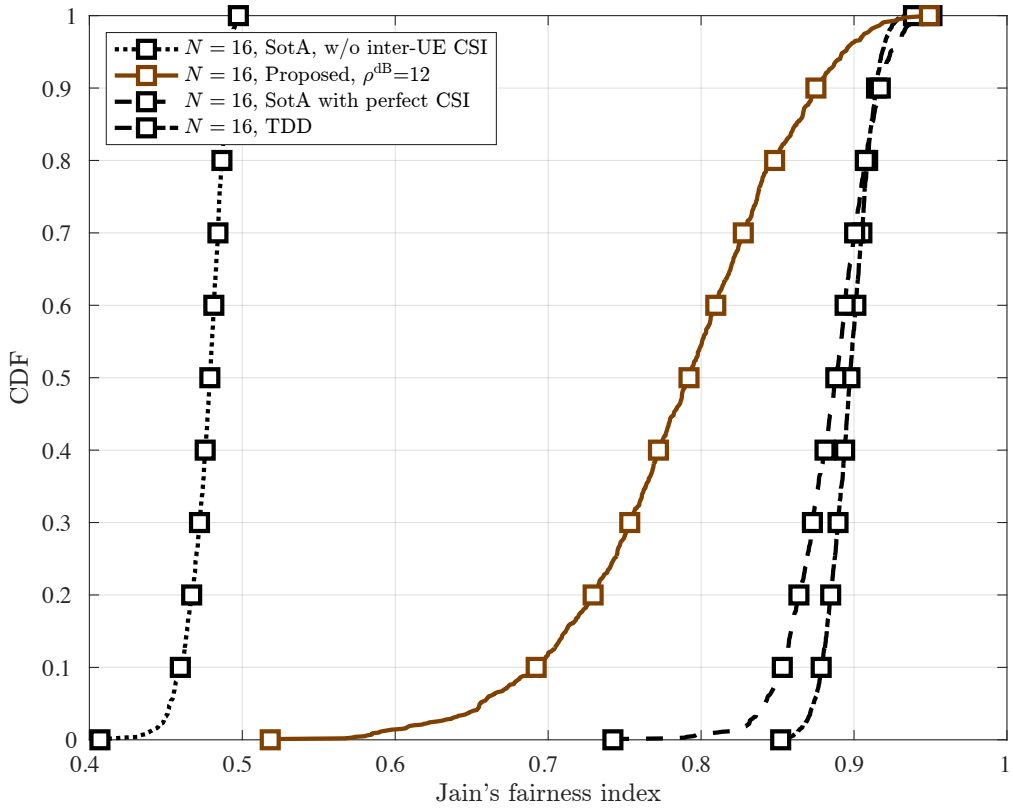

Fig. 4.16 Comparison of the CDF of Jain's fairness index for UE ($N = 16$).

Fairness

As mentioned in the previous subsection, the proposed method in this chapter is outage due to estimation errors in the inter-UE channel. Therefore, the fairness to TDD is expected to degrade compared to the proposal in Chapter 3. Hence, an evaluation similar to the comparison made in Section 3.5.3 is performed to check the fairness degradation. We use it to compare Jain's fairness indices [163], defined by

$$\text{Jain's Fairness} \triangleq \frac{\left(\sum_{k\in\mathcal{K}} \log_2\left(1+\Gamma_k\right)\right)^2}{K\sum_{k\in\mathcal{K}}\left(\log_2\left(1+\Gamma_k\right)\right)^2}. \tag{4.38}$$

This index lies between $1/K$ to 1. Thus, when the index becomes 1, the fairest communication among UEs is realized. Figs. 4.14, 4.15, 4.16 compare Jain's fairness indices for UE. Comparing TDD and SotA with perfect CSI, it can be seen that they have close fairness properties. This corresponds to the comparison in Section 3.5.3, which is more asymptotic to TDD. However, in Section 3.5.3, the UE has only one antenna. This confirms that the

interference control performance is enhanced, and high fairness can be achieved when the UE has multiple antennas. Suppose we focus on the proposed method and the SotA with perfect CSI. In that case, we can also see the degradation of fairness as the number of antennas increases. This is due to the increase in the outage probability due to the effect of channel estimation errors as the number of antennas increases. However, compared to the CDF for total throughput in the previous section, there is a significant advantage in throughput performance over TDD. In addition, a comparison of the proposed method with SotA without CSI shows a significant improvement in the fairness of the proposed method. This confirms that the proposed method has the best properties in the trade-off between fairness and throughput. These results show that mmWave NAFD CF-mMIMO achieves both the desired throughput and fairness while benefiting from the throughput improvement due to the use of mmWave bands.

Robustness Against Channel Model and UE Position Error

Finally, the robustness against different channel models and errors of UE position is discussed. The mmWave channel model [24, 109, 110] and parameters [170–172] used in this chapter is widely used in mMIMO, so that the comparisons made so far are reasonable. However, the number of paths may differ. Therefore, the robustness against changes in the number of paths in practical situations has to be checked. Fig. 4.17 compares the number of paths with the average total throughput. Focusing on all the results, it can be seen that the performance degrades as the number of paths increases. However, when comparing each performance, the performance order is the same as in the previous discussion. In particular, focusing on the proposed method, the range of performance degradation is higher compared to SotA and TDD. This is because the proposed method ignores the NLoS paths in the inter-UE channel. However, it still performs better than SotA and TDD without inter-UE CSI. As the number of paths in the mmWave channel model is from one to several, the proposed method is validated within a reasonable range.

Next, check the robustness of the user location information against errors. In this chapter, it is assumed that the complete UE location is known. However, in reality, there are errors because the location information of the UE needs to be estimated. In this section, we assume global positioning system (GPS)-based UE position estimation. Error models for GPS have been proposed in several studies [165, 173, 174]. In literature [173], an error model for GPS based on a commercially produced sensor is presented. Using this error model, the error in the UE position information is given by

$$\hat{r}_k = \sqrt{(x_k + n_k^{\mathrm{x}})^2 + (y_k + n_k^{\mathrm{y}})}, \tag{4.39}$$

where (x_k, y_k) are the true horizontal positions of the k-th UE, $n_k^{\mathrm{x}} \sim \mathcal{N}(0, \sigma_{\mathrm{p}}^2/2), n_k^{\mathrm{y}} \sim \mathcal{N}(0, \sigma_{\mathrm{p}}^2/2)$ are their estimation errors.

Fig. 4.18 compares the error variance and the average total throughput when the error in equation (4.39) is added to the UE location information. The results for all methods except the proposed method are constant as they are not affected by the errors. Focusing on the proposed method, it can be seen that the error variance degrades by approximately 10% at 5 m. However, CF-mMIMO can provide highly accurate position estimation using multidimensional scaling [168] and other methods, using the distributed APs as anchors. In addition, GPS is currently capable of highly accurate position estimation using quasi-zenith satellite system (QZSS) [175] such as "MICHIBIKI". Therefore, the proposed method has good throughput performance in the practical range.

The discussion so far confirms that the proposed optimization with CSI estimation using UE-location and inter-UE channel penalty is remarkably effective.

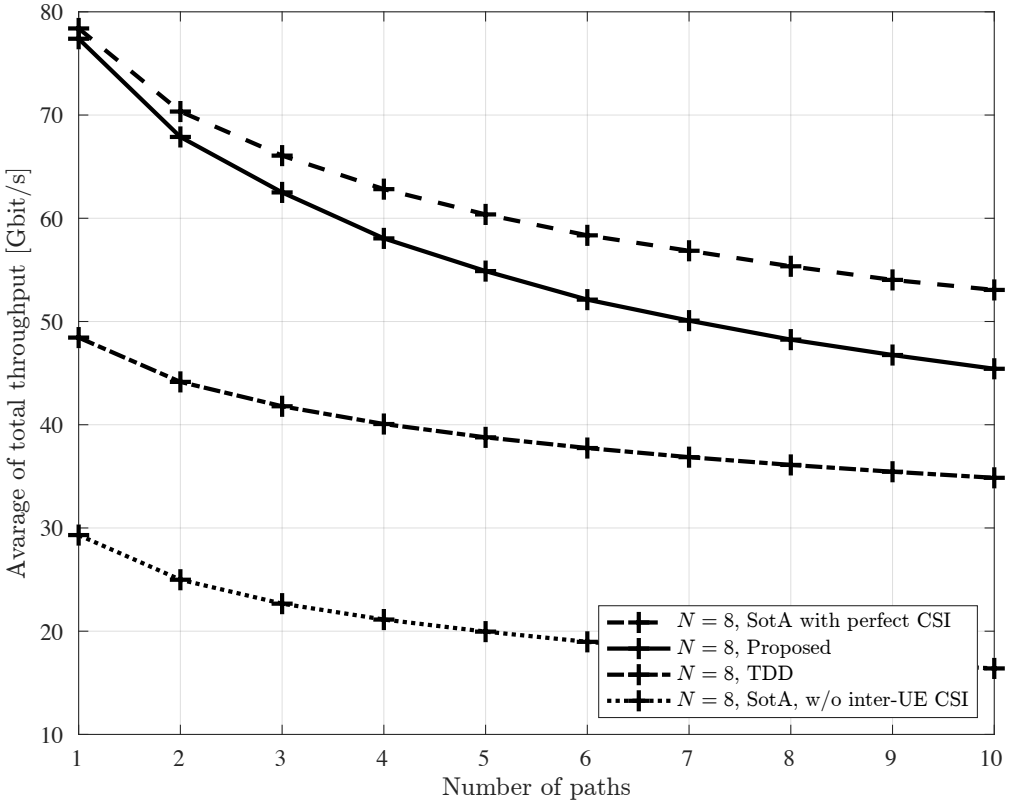

Fig. 4.17 Comparison of the average total throughput versus the number of paths ($K = 16, N = 8$).

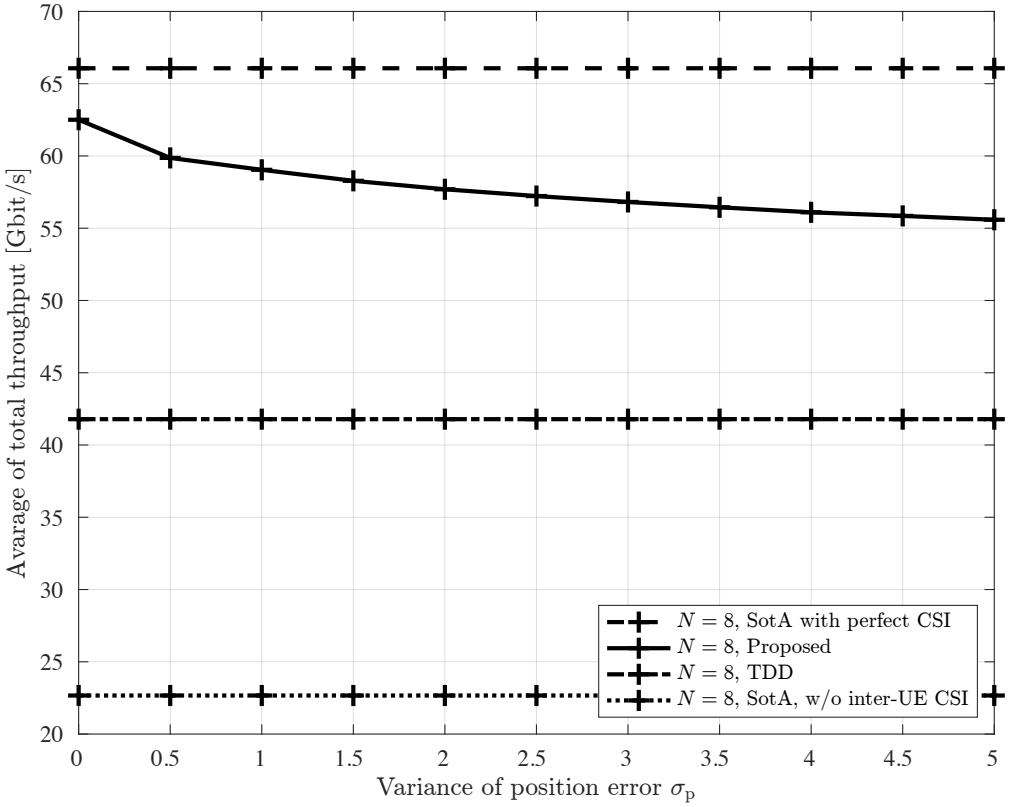

Fig. 4.18 Comparison of the average total throughput versus variance of the inter-UEs position error ($K = 16, N = 8$).

4.6 Chapter Summary

This chapter studied the NAFD CF-mMIMO systems using the mmWave band. It proposed the inter-UE channel estimation method, which reconstructs the channels among UEs using their locations, and the inter-UE channel penalty method for robustness. In addition, the joint AP mode selection and beamforming design method with this estimation and penalty technique are proposed. Numerical results confirmed that our proposed approach could achieve the throughput performance close to the SotA with perfect inter-UE channel knowledge and made the throughput superior to the SotA without inter-UE channel knowledge and TDD. Despite these results, we also confirmed that the proposed method has good fairness. Moreover, these results also confirm sufficient robustness to user interference, the number of paths, and user location errors.

From the above, we confirmed that NAFD CF-mMIMO proposed in Chapter 3 could be used in the mmWave and higher frequency bands. The analysis of the densely populated networks in this chapter shows that NAFD is an accommodating system even when the number of UEs increases.

Chapter 5

Conclusion and Future Work

Finally, this chapter concludes this dissertation and provides future work on the study.

5.1 Conclusion

In this dissertation, we have worked towards the realization of user-centric communication using NAFD CF-mMIMO, which is fair to the user and meets the future requirements of radio systems by achieving a significant improvement in SE through the excessive use of time and space resources and ultra-high throughput through bandwidth expansion. Systems that meet the requirements of the future. These contribute to some of the 5G and 6G use cases, eMBB and MBRLLC.

Chapter 1 first introduced the current cellular networks, future requirements, and user-centric communications. Then, we introduced the related works for CF-mMIMO and NAFD systems. Based on them, we described the several challenges of NAFD CF-mMIMO for user-centric communication. Finally, we summarized the contributions and outline of this dissertation. On top of that, the SE and throughput must be maximized while maintaining fairness as far as possible to ensure the challenges were fair services to all UEs, regardless of their environments. The challenges of CF-mMIMO for user-centric communication were also described.

Chapter 2 overviewed CF-mMIMO and described the beamforming design and multiplexing schemes such as TDD and dynamic TDD, FD, and NAFD. Continuing, we identified the advantages of NAFD CF-mMIMO and the motivation to realize user-centric communication.

In Chapter 3, we proposed the joint access configuration and beamforming design method, which solved the trade-off between total SE performance and fairness for NAFD CF-mMIMO systems. Moreover, we considered the single-antenna UEs case and generally the multiple-antenna UEs case.

The proposed initial problems were non-convex problems due to the combination constraint and fractional function. To this end, we relaxed them to the convex optimization problems using several techniques, *e.g.*, the negative entropy penalty method, LDT, QT, and CCP. We showed that our proposed design method has superior performance over the SotA method while maintaining high fairness. In addition, we analyzed the computational complexity of the proposed method and showed that it is comparable to the SotA method. We showed the proposed method for the multiple-antenna UEs, which could obtain additional gain through beamforming design by increasing the number of antennas. Finally, we analyzed the impact of inter-UE interference and showed the importance of the inter-UE channel estimation.

Finally, in Chapter 4, NAFD CF-mMIMO was extended to mmWave, ensuring the bandwidth for high-speed communication. As mmWave increases the impact of inter-UE interference by making the network more densely populated, we proposed an inter-UE channel estimation method that uses channel characteristics and UE location information. In addition, a penalized method was proposed to guarantee the channel estimation error by shadowing the estimated channel using the proposed method. A robust joint AP mode selection and beamforming design were represented using the above-penalized estimated inter-UE channels. Computer simulations confirmed that the beamforming design with the proposed penalized estimation inter-UE channel is adequate. Furthermore, a comparison of the outage-aware throughput confirmed that the proposed method significantly improved the throughput by ensuring high bandwidth without compromising fairness to TDD.

The design of the UEs is based on the following principles. The methods described in this thesis address asymmetric UL/DL traffic configurations and meet the throughput requirements described in Chapter 1 while being impartial. Flexible and impartial design using the methods described in Chapters 3 and 4 eliminates network-centric treatment of UEs and allows designing for the UE situation. As a result, user-centric communication using NAFD CF-mMIMO is enabled, and uniform and fast communication are achieved without affecting the environment, such as traffic composition and channel conditions. Thus, the user-centric communication with NAFD CF-mMIMO is the potential to meet the high-speed and high-capacity communication requirements of the 5G and 6G use cases of eMBB and MBRLLC.

5.2 Future Work

Although the proposals in this dissertation have contributed to the satisfying requirement of user-centric communication, there are several remaining topics for NAFD CF-mMIMO systems. In this section, we provide the future works on the study in this dissertation.

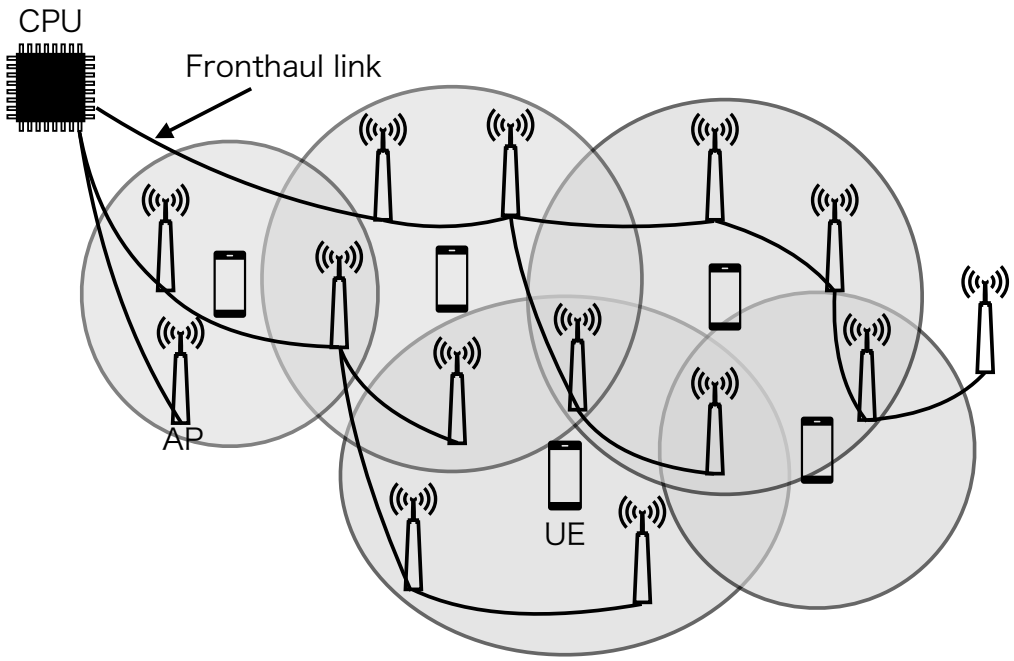

Fig. 5.1 Illustration of scalable CF-mMIMO systems with user-centric crustering.

5.2.1 Scalable Network Design for user-centric communication with NAFD CF-mMIMO

Although the proposed system in our dissertation has contributed to the design of user-centric NAFD CF-mMIMO systems, it has not considered the scalability of the network. Therefore, as it stands now, achieving a practical implementation architecture is challenging due to computational resources and back/fronthaul capacity limitations.

Scalability is one of the key challenges of the feasibility of CF-mMIMO [176, 65]. As CF-mMIMO does not have the cell, the load on the CPU increases in proportion to the network size. The network must be virtually split and signal processing distributed to reduce the computational complexity and data size.

For this reason, in many studies of scalable CF-mMIMO [65, 177, 178, 66, 179], the AP is responsible for some signal processing and limits of the achievable area to ensure scalability. However, network-centric designs, such as static allocation based on AP location, present CF-mMIMO with the same challenges as cellular networks. Therefore, a user-centric network design method is required that enables dynamic allocation based on the channel state of the UE instead of the conventional network-centric method. A scalable CF-mMIMO with user-centric clustering is one of the current hot topics to solve this issue, [65]. In addition, for more scalability, multi-CPU CF-mMIMO is also being studied.

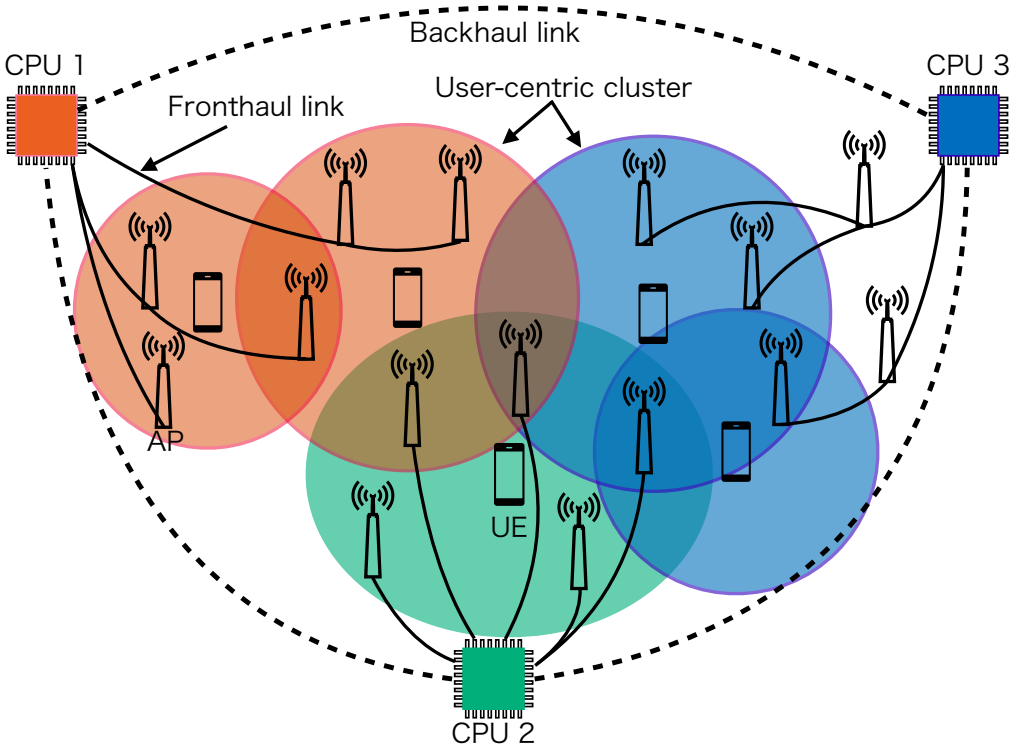

Fig. 5.2 Illustration of multi-CPU CF-mMIMO systems.

User-centric clustering forms clusters of APs around a UE, as shown in Fig. 5.1. In addition, the APs are also responsible for signal processing, such as linear synthesis, thereby reducing the computational load on the CPU. The CPU only needs to handle the linearly synthesized data. Moreover, the AP only needs to communicate with the UEs in its cluster, thus significantly reducing the load of CPU and APs. In user-centric clustering, each AP generally retains all CSI with UEs with high interference. In other words, inter-cluster interference is controllable compared to inter-cell interference in cellular networks. As a result, CF-mMIMO's characteristics, such as spatial multiplexing and uniform communication quality, can be maintained while reducing the signal processing load.

In addition, multi-CPU CF-mMIMO, as shown in Fig. 5.2, is also being studied for more scalability, [178, 66, 179]. The multi-CPU CF-mMIMO system is virtually divided, and each CPU processing to connected APs. Each CPU manages APs, which are directly connected to the CPU via wired fronthaul links. The inter-CPUs are connected by backhaul and share the information processed by each CPU. This makes the system more scalable, as the CPUs only need to manage the APs connected in the fronthaul. However, the backhaul has large capacity limitations, such as analog to digital converter, which add quantization noise to the information shared by the CPU. Therefore, clustering methods that take these limitations into account are being considered.

However, NAFD CF-mMIMO needs to consider the UL/DL mode assignment of APs for clustering. Besides, the inter-AP-UE CSI-based clustering, currently widely considered, may cause huge interference due to inter-UE and inter-AP interference.

Therefore, addressing scalability in NAFD CF-mMIMO is an important and challenging research direction.

5.2.2 Hybrid Beamforming Design for mmWave NAFD CF-mMIMO

Although fully digital beamforming was proposed in Chapter 4, hybrid analog-digital beamforming will be used in practice due to cost and other issues. Therefore, the hybrid beamforming design is challenging to realize the proposed system. This method can be applied to NAFD systems after AP mode assignment. However, due to the limited AP functionality, CF-mMIMO requires low-complexity beamforming design techniques.

On the other hand, 5G systems also attempt to select analog beamforming from a codebook, such as a beam sweeping, to ensure signal gain and reduce overhead during initial access for mMIMO [180]. Location-based beam selection is also being studied [165, 181, 182], as discussed in Chapter 4. In CF-mMIMO, such attempts have been studied due to the demand for AP functionality limitations. Literature [53] studied hybrid beamforming design based on analog beamforming selection assuming an AP with multiple antennas. Also, literature [183] studied analog beamforming alignment on the multiple-antenna UEs. These studies do not consider AP selection or clustering but NAFD essential DL/UL AP selection. Therefore, The design is more complex in NAFD due to the necessity of considering AP selection and inter-UE and inter-AP interference. In context, Low complexity hybrid-beamforming design for NAFD CF-mMIMO is a challenging and exciting research direction. Solving this problem will become scalable and low-latency CF-mMIMO systems.

5.2.3 Energy-Efficient NAFD CF-mMIMO

In this dissertation, the main objective was to cope with high throughput requirements by maximizing fairness and SE. However, the increasing power consumption due to the increasing number of terminals is one of the major problems in 6G and beyond. This paper contributed to fluctuations in the UL/DL asymmetry of the traffic by NAFD CF-mMIMO. On the other hand, the user traffic load also time vary when assuming a more realistic environment. Therefore, considering the energy efficiency, AP must operate with minimum power consumption when users have low throughput requirements. However, in much of the literature, including this dissertation, designs have been made to maximize SE without considering power consumption [54, 184]. As a result, the power consumption of APs is

very high regardless of the traffic. Consequently, several studies are energy efficiency is maximized through AP power allocation and beamforming designs. However, as long as all APs are in use, power consumption increases proportionately to the number of AP. This is also a scalability issue, as indicated in Subsection 5.2.1.

In CF-mMIMO, the power consumption of sleeping APs can be significantly reduced by dynamically switching APs ON/OFF [13, 57, 64, 185]. However, if switching AP ON/OFF is chosen by energy efficiency optimization, the SE may be significantly degraded.

Therefore, literature [185] proposes a power consumption minimization method with AP switching that considers both power consumption and SE requirement. This study showed that power consumption could be significantly reduced compared to minimizing only the transmission power of the AP. Literature [64] considered mmWave CF-mMIMO and proposed an AP switching method adaptable to the number of UEs and their statistical distribution in environments with spatially non-uniform traffic distribution in realistic wireless networks. The results show that the achievable energy efficiency can be significantly improved.

In CF-mMIMO, as in these studies, only the ON/OFF allocation of APs needs to be considered. However, NAFD CF-mMIMO must allocate the UL/DL and ON/OFF of the APs, which is a three-state combinatorial optimization problem. In addition, a joint algorithm has to be considered, as each variable has a trade-off between SE and energy efficiency. Therefore, the power minimization problem through ON/OFF switching in NAFD CF-mMIMO is an important and challenging research direction.

We have room for improvement in terms of practicality, as follows.

5.2.4 Robustness Against Traffic and Channel Fluctuation

In this dissertation study, a flexible network for asymmetric UL/DL traffic construction is achieved. However, there is an implicit assumption that the CSI and UL/DL traffic composition is constant over a long period. Therefore, when time variability is high, CSI estimation, AP mode assignment, and beamforming design are frequently required, leading to increased overhead. To address this issue, time-varying designs should be considered. For beamforming design, the CSI estimation overhead is reduced by beam tracking using user position information, as described in literature [186]. In addition, literature [187] uses statistical CSI for analog beams and instantaneous CSI for digital beamforming in multi-cell mMIMO to reduce the overhead of inter-cell interference estimation. These are combined with the aforementioned hybrid beamforming and scalable designs for inter-cluster interference. This would improve scalability as well as robustness to time variations. A statistical model is given for the time variability of the traffic. Therefore, it is considered possible to deal with this by optimizing the time-averaging using a model tailored to the use case.

5.2.5 Further Practical NAFD CF-mMIMO

In this dissertation, we proposed NAFD CF-mMIMO system for user-centric communication. These require to need a new approach, dealing with these issues is important and challenging

- Although this dissertation proposed a promising design for achieving user-centric communication with NAFD CF-mMIMO, the computational complexity depends on the number of APs and UEs, as shown in Section 3.4. Therefore, the computation load easily becomes to high as the network expands. Therefore, further complexity reduction is needed to alleviate the issue.
- Chapter 4 proposed inter-UE channel estimation for inter-UE interference suppression, but inter-AP-UE and inter-UE channels have not been proposed. On the other hand, these channel estimation methods have already been widely studied. However, optimal estimation schemes must be considered to improve channel estimation accuracy.
- In Chapter 4, NAFD CF-mMIMO was extended to mmWave. However, due to the physical characteristics of strong straightness in the mmWave band, outages occur by a pedestrian blockage. Therefore, it is necessary to investigate methods to guarantee path shielding, $e.g.$, by using image-based prediction.

Appendix A

Introduction of Fractional Programming

In this section, we introduce FP techniques that enable a convex approximation of a function involving fractions and logarithmic terms. With these remarks made, and for the sake of clarity of exposition, it will prove useful to compactly summarize the following approximation techniques, respectively referred to as the LDT and the QT and proposed in [151, 144].

Lemma 1 (LDT [144, Theor. 4]) *Consider the following weighted sum-of-logarithms problem:*

$$\underset{\boldsymbol{x}}{\text{maximize}} \quad \sum_{m=1}^{M} w_m \log_2 \left(1 + \boldsymbol{\alpha}_m^{\mathrm{H}}(\boldsymbol{x}) \boldsymbol{B}_m^{-1}(\boldsymbol{x}) \boldsymbol{\alpha}_m(\boldsymbol{x})\right) \tag{A.1a}$$

$$\text{subject to} \quad \boldsymbol{x} \in \mathcal{X} \tag{A.1b}$$

where w_m, $\boldsymbol{\alpha}_m(\boldsymbol{x})$, $\boldsymbol{B}_m(\boldsymbol{x})$, and $\mathcal{X}$ denotes a nonnegative weight, complex-valued vector, Hermitian positive definite matrix for all m, and nonempty constraint set, respectively.

Applying LDT to the above problem, we obtain

$$\underset{\boldsymbol{x}, \boldsymbol{\gamma}}{\text{maximize}} \quad f_r(\boldsymbol{x}, \boldsymbol{\gamma}) \tag{A.2a}$$

$$\text{subject to} \quad \boldsymbol{x} \in \mathcal{X} \tag{A.2b}$$

where

$$f_r(\boldsymbol{x}, \boldsymbol{\gamma}) = \sum_{m=1}^{M} w_m \log\left(1 + \gamma_m\right) - w_m \gamma_m$$
$$+ w_m (1 + \gamma_m) \boldsymbol{\alpha}_m^{\mathrm{H}}(\boldsymbol{x}) \left(\boldsymbol{\alpha}_m(\boldsymbol{x}) \boldsymbol{\alpha}_m^{\mathrm{H}}(\boldsymbol{x}) + \boldsymbol{B}_m(\boldsymbol{x})\right)^{-1} \boldsymbol{\alpha}_m(\boldsymbol{x}),$$

and $\gamma_m^\star \triangleq \boldsymbol{\alpha}_m^{\mathrm{H}}(\boldsymbol{x})\boldsymbol{B}_m^{-1}(\boldsymbol{x})\boldsymbol{\alpha}_m(\boldsymbol{x})$ *is introduced as an auxiliary variable to establish equivalence on the objective value.*

Lemma 2 (QT [151, Theor. 2]) *Consider the following sum-of-ratios maximization problem.*

$$\underset{\boldsymbol{x}}{\text{maximize}} \quad \sum_{m=1}^{M} \boldsymbol{\alpha}_m^{\mathrm{H}}(\boldsymbol{x})\, \boldsymbol{B}_m^{-1}(\boldsymbol{x})\, \boldsymbol{\alpha}_m(\boldsymbol{x}) \tag{A.3a}$$

$$\text{subject to} \quad \boldsymbol{x} \in \mathcal{X}. \tag{A.3b}$$

where $\boldsymbol{\alpha}_m(\boldsymbol{x})$ *and* $\boldsymbol{B}_m(\boldsymbol{x})$ *are given in Lemma 1.*

Applying QT to the above sum-of-ratio maximization problem, we obtain

$$\underset{\boldsymbol{x},\boldsymbol{S}}{\text{maximize}} \quad \sum_{m=1}^{M} 2\Re\left\{\boldsymbol{s}_m^{\mathrm{H}}\boldsymbol{\alpha}_m(\boldsymbol{x})\right\} - \boldsymbol{s}_m^{\mathrm{H}}\boldsymbol{B}_m(\boldsymbol{x})\,\boldsymbol{s}_m \tag{A.4a}$$

$$\text{subject to} \quad \boldsymbol{x} \in \mathcal{X}, \tag{A.4b}$$

where $\boldsymbol{S} = [\boldsymbol{s}_1, \ldots, \boldsymbol{s}_M]$ *denotes a newly introduced auxiliary variable that possesses an optimal solution given by* $\boldsymbol{s}_m^\star = \boldsymbol{B}_m^{-1}(\boldsymbol{x})\,\boldsymbol{\alpha}_m(\boldsymbol{x})$.

Together, Lemmas 1 and 2 yield an iterative procedure to solve sum-of-logarithms problems on the auxiliary variables $\boldsymbol{s}$ and $\boldsymbol{\gamma}$, whose convergence was studied in [151, 144].

Appendix B

Convexification via Fractional Programming and Negative Entropy

In this appendix, we discuss in detail what was omitted in Section 3.3.1, namely, the conversion of binary variable η_ℓ to continuous numbers and the convexification of the geometric mean objective function.

B.1 Single-Antenna UEs Case

First, notice that constraints (3.16c) and (3.16d) are discrete constraints, which leads to a combinatorial problem. In order to circumvent the combinatorial nature of the optimization over $\boldsymbol{\eta}$, equation (3.16) can be relaxed by replacing $\eta_\ell \in \{0, 1\}$ with its convex hull $\eta_\ell \in [0, 1]$ and by introducing a penalizing term into the objective based on a negative entropy function, as described in [142]. In particular, let $\mathbb{P}(\eta_\ell)$ be the negative entropy function and λ be a given weight. Then, equation (3.16) can be rewritten (*i.e.*, relaxed) as

$$\underset{\boldsymbol{\eta},\boldsymbol{v}^{\mathrm{ap}},\boldsymbol{w}^{\mathrm{ap}},\boldsymbol{p}^{\mathrm{dl}}}{\text{maximize}} \quad \left(\prod_{k=1}^{K} \mu_k \log_2\left(1+\Gamma_k\right)\right)^{\frac{1}{K}} + \zeta \sum_{\ell=1}^{L} \mathbb{P}(\eta_\ell) \tag{B.1a}$$

$$\text{subject to} \quad 0 \leq \eta_\ell \leq 1, \forall \ell, \tag{B.1b}$$

$$\left\| \begin{array}{c} 2\boldsymbol{v}_{k,\ell}^{\mathrm{ap}} \\ 1-\eta_\ell \end{array} \right\|_2 \leq 1+\eta_\ell, \forall k \in \mathcal{K}^{\mathrm{ul}}, \forall \ell, \tag{B.1c}$$

$$\left\| \begin{array}{c} 2\boldsymbol{w}_{k,\ell}^{\mathrm{ap}} \\ p_{k,\ell}^{\mathrm{dl}} - \bar{\eta}_\ell \end{array} \right\|_2 \leq p_{k,\ell}^{\mathrm{dl}} + \bar{\eta}_\ell, \forall k \in \mathcal{K}^{\mathrm{dl}}, \forall \ell, \tag{B.1d}$$

(3.16e) to (3.16g).

where $\mathbb{P}(\eta_i) \triangleq \eta_i \log \eta_i + (1-\eta_i)\log(1-\eta_i)$, $\lambda \geq 0$, and the AP selection constraints are represented as second-order cone constraints.

Despite this reformulation and the removal of the combinatorial issue on $\boldsymbol{\eta}$, equation (B.1) is still intractable because of the non-convexity of the objective function on the remaining variables. To resolve this challenge, Lemma 1 can be applied to equation (B.1) yielding

$$\begin{aligned} \underset{\boldsymbol{\eta},\boldsymbol{v}^{\mathrm{ap}},\boldsymbol{w}^{\mathrm{ap}},\boldsymbol{p}^{\mathrm{dl}},\boldsymbol{\gamma}}{\text{maximize}} \quad & \left(\prod_{k=1}^{K} f_k\left(\boldsymbol{v}^{\mathrm{ap}},\boldsymbol{w}^{\mathrm{ap}},\boldsymbol{p}^{\mathrm{dl}},\boldsymbol{\gamma}\right)\right)^{\frac{1}{K}} + \zeta \sum_{\ell=1}^{L} \mathbb{P}(\eta_\ell) \qquad \text{(B.2a)} \\ \text{subject to} \quad & \text{(3.16e) to (3.16g) and (B.1b) to (B.1d)}, \end{aligned}$$

with

$$f_k\left(\boldsymbol{v}^{\mathrm{ap}},\boldsymbol{w}^{\mathrm{ap}},\boldsymbol{p}^{\mathrm{dl}},\boldsymbol{\gamma}\right) \triangleq \mu_k \log_2(1+\gamma_k) - \mu_k\gamma_k + \mu_k\,(1+\gamma_k)\,\Gamma_k^{\mathrm{ldt}}, \qquad \text{(B.3)}$$

where in equation (B.4), $\gamma_k = \Gamma_k$, $\boldsymbol{\gamma} \triangleq [\gamma_1,\ldots,\gamma_K]$, and Γ_k^{ldt} is as given by

$$\Gamma_k^{\mathrm{ldt}} \triangleq \begin{cases} p_k^{\mathrm{ul}} \boldsymbol{v}_k^{\mathrm{ap}\mathrm{H}} \boldsymbol{h}_k \Big(\sum\limits_{k' \in \mathcal{K}^{\mathrm{ul}}} p_{k'}^{\mathrm{ul}} \boldsymbol{v}_k^{\mathrm{ap}\mathrm{H}} \boldsymbol{h}_{k'} \boldsymbol{h}_{k'}^{\mathrm{H}} \boldsymbol{v}_k^{\mathrm{ap}} \\ \quad + \sum\limits_{k' \in \mathcal{K}^{\mathrm{dl}}} \boldsymbol{v}_k^{\mathrm{ap}\mathrm{H}} \boldsymbol{H}^{\mathrm{H}} \boldsymbol{w}_{k'}^{\mathrm{ap}} \boldsymbol{w}_{k'}^{\mathrm{ap}\mathrm{H}} \boldsymbol{H} \boldsymbol{v}_k^{\mathrm{ap}} + \sigma_{\mathrm{ul}}^2 \left\|\boldsymbol{v}_k^{\mathrm{ap}}\right\|_2^2 \Big)^{-1} \boldsymbol{h}_k^{\mathrm{H}} \boldsymbol{v}_k^{\mathrm{ap}}, & \text{for } k \in \mathcal{K}^{\mathrm{ul}} \\ \boldsymbol{h}_k^{\mathrm{H}} \boldsymbol{w}_k^{\mathrm{ap}} \Big(\sum\limits_{k' \in \mathcal{K}^{\mathrm{dl}}} \boldsymbol{h}_k^{\mathrm{H}} \boldsymbol{w}_{k'}^{\mathrm{ap}} \boldsymbol{w}_{k'}^{\mathrm{ap}\mathrm{H}} \boldsymbol{h}_k \\ \quad + \sum\limits_{k' \in \mathcal{K}^{\mathrm{ul}}} \left|\sqrt{p_{k'}^{\mathrm{ul}}} h_{k',k}\right|^2 + \sigma_{\mathrm{dl}}^2 \Big)^{-1} \boldsymbol{w}_k^{\mathrm{H}} \boldsymbol{h}_k, & \text{for } k \in \mathcal{K}^{\mathrm{dl}} \end{cases} . \qquad \text{(B.4)}$$

Equation (B.2) can be seen as a weighted SINR maximization problem, wherein the binary AP selection is aided by the negative entropy penalty function. This problem is, however, still not straightforwardly solvable due to the convex-over-convex formulation of the SINR expression, which however can be easily convexified via the QT. Thus, it applies Lemma 2, the SINR expression in equation (B.2) can be reformulated to convex function as equation (3.18).

B.2 Multi-Antenna UEs Case

Following the previous section, the multi-antenna UEs case is also discussed. For the first sake of convenience, let the equation (3.25) be repeated to show the quantities

$$\mathrm{UL}_{k,k'} \triangleq \boldsymbol{w}_{k'}^{\mathrm{ue}\mathrm{H}} \boldsymbol{H}_{k'}^{\mathrm{H}} \boldsymbol{v}_k^{\mathrm{ap}}, \quad \mathrm{DCLI}_{k,k'} \triangleq \boldsymbol{w}_{k'}^{\mathrm{ap}\mathrm{H}} \boldsymbol{H} \boldsymbol{v}_k^{\mathrm{ap}},$$

$$\mathrm{DL}_{k,k'} \triangleq \boldsymbol{w}_{k'}^{\mathrm{ap}\mathrm{H}} \boldsymbol{H}_{k'} \boldsymbol{v}_k^{\mathrm{ue}}, \quad \mathrm{UCLI}_{k,k'} \triangleq \boldsymbol{w}_{k'}^{\mathrm{ue}\mathrm{H}} \boldsymbol{H}_{k',k}^{\mathrm{H}} \boldsymbol{v}_k^{\mathrm{ue}}.$$

In this case, the only change is adding the UE's beamforming, so the policy for applying FP will follow the same process. Therefore, in the same way as the transformation performed for (B.1), Lemma 1 can be applied to (3.26) yielding

$$\begin{aligned} \underset{b,\boldsymbol{\eta},\boldsymbol{v},\boldsymbol{w},\boldsymbol{p},\boldsymbol{\gamma}}{\text{maximize}} \quad & \left(\prod_{k=1}^{K} f_k^{\mathrm{ldt,m}} \left(\boldsymbol{v}, \boldsymbol{w}, \boldsymbol{\gamma} \right) \right)^{\frac{1}{K}} + \zeta \sum_{\ell=1}^{L} \mathbb{P}(\eta_\ell) \qquad \text{(B.5a)} \\ \text{subject to} \quad & \text{(3.16e) to (3.16g), (B.1b) to (B.1d), (3.26b), and (3.26c),} \end{aligned}$$

with

$$f_k^{\mathrm{ldt,m}} \left(\boldsymbol{v}, \boldsymbol{w}, \boldsymbol{\gamma} \right) = \mu_k \log_2(1 + \gamma_k) - \mu_k \gamma_k + \sum_{k=1}^{K} \mu_k \left(1 + \gamma_k \right) \Psi_k^{\mathrm{ldt,m}} i, \qquad \text{(B.6)}$$

where $\boldsymbol{v}^{\mathrm{ap}} = [\boldsymbol{v}_1^{\mathrm{ap}}, \ldots, \boldsymbol{v}_K^{\mathrm{ap}}]$, $\boldsymbol{v}^{\mathrm{ue}} = [\boldsymbol{v}_1^{\mathrm{ue}}, \ldots, \boldsymbol{v}_K^{\mathrm{ue}}]$, and $\Gamma_k^{\mathrm{ldt,m}}$ is given by

$$\Psi_k^{\mathrm{ldt,m}} = \begin{cases} \mathrm{UL}_{k,k} \left(\sum\limits_{k' \in \mathcal{K}^{\mathrm{ul}}} \mathrm{UL}_{k,k'} \mathrm{UL}_{k,k'}^{\mathrm{H}} \right. \\ \quad \left. + \sum\limits_{k' \in \mathcal{K}^{\mathrm{dl}}} \mathrm{DCLI}_{k,k'} \mathrm{DCLI}_{k,k'}^{\mathrm{H}} + \sigma_{\mathrm{ul}}^2 \left\| \boldsymbol{v}_k^{\mathrm{ap}} \right\|_2^2 \right)^{-1} \mathrm{UL}_{k,k}^{\mathrm{H}} & k \in \mathcal{K}^{\mathrm{ul}} \\ \mathrm{DL}_{k,k} \left(\sum\limits_{k' \in \mathcal{K}^{\mathrm{dl}}} \mathrm{DL}_{k,k'} \mathrm{DL}_{k,k'}^{\mathrm{H}} \right. \\ \quad \left. + \sum\limits_{k' \in \mathcal{K}^{\mathrm{ul}}} \mathrm{UCLI}_{k,k'} \mathrm{UCLI}_{k,k'}^{\mathrm{H}} + \sigma_{\mathrm{dl}}^2 \left\| \boldsymbol{v}_k^{\mathrm{ue}} \right\|_2^2 \right)^{-1} \mathrm{DL}_{k,k}^{\mathrm{H}} & k \in \mathcal{K}^{\mathrm{dl}} \end{cases}. \qquad \text{(B.7)}$$

As with equation (B.2), equation (B.5) can be seen as a weighted SINR maximization problem, wherein the negative entropy penalty function aids the binary AP selection. Therefore, this problem has the same issue: the convex-over-convex formulation of the SINR. In addition, because of the coupling variable in equation (B.7), it is necessary to split the problem into AP and UE sides after convex relaxation using QT.

Appendix C

Canonical form of QCP Formulation

In this section, we describe how problem (3.22) is put into the QCP canonical from, so as to enable the calculation of its computational complexity. To that end, first consider the canonical form of a real-valued conic QCP, which is expressed as [155]

$$\begin{aligned}
\underset{\boldsymbol{x}}{\text{minimize}} \quad & \boldsymbol{c}^T\boldsymbol{x} && \text{(C.1a)}\\
\text{subject to} \quad & \|\boldsymbol{c}\|_2 \leq d_0, && \text{(C.1b)}\\
& \|\boldsymbol{A}_{\mathrm{m}}\boldsymbol{x} + \boldsymbol{b}_{\mathrm{m}}\|_2 \leq \boldsymbol{c}_{\mathrm{m}}^T\boldsymbol{x} + d_{\mathrm{m}}, \forall m \in \{1, \ldots, \tilde{M}\}, && \text{(C.1c)}\\
& \boldsymbol{x} \in \mathbb{R}^{\tilde{N}}, \quad \boldsymbol{b}_{\mathrm{m}} \in \mathbb{R}^{Q_{\mathrm{m}}}. && \text{(C.1d)}
\end{aligned}$$

Next, consider the following minimization problem equivalent to the maximization problem of equation (3.22),

$$\begin{aligned}
\underset{\substack{n,\boldsymbol{\eta},\boldsymbol{v}^{\mathrm{ap}},\boldsymbol{w}^{\mathrm{ap}},\\ \boldsymbol{p}^{\mathrm{dl}},\boldsymbol{\gamma},\boldsymbol{s}}}{\text{minimize}} \quad & -n - \sum_{\ell=1}^{L} \lambda\eta_\ell \nabla\mathbb{P}(\eta_\ell^{t-1}) && \text{(C.2a)}\\
\text{subject to} \quad & 0 \leq n, && \text{(C.2b)}\\
& n \leq \left(\prod_{k=1}^{K} o_k\right)^{\frac{1}{K}}, && \text{(C.2c)}\\
& f_k^{\mathrm{fin},-}\left(\boldsymbol{v}^{\mathrm{ap}}, \boldsymbol{w}^{\mathrm{ap}}, \boldsymbol{p}^{\mathrm{dl}}, \boldsymbol{\gamma}, \boldsymbol{s}\right) \leq o_k, \forall k, && \text{(C.2d)}\\
& \text{(3.16e), to (3.16g), (3.18b), to (3.18d),}
\end{aligned}$$

where n and o_k are auxiliary variables and

$$f_k^{\mathrm{fin},-}\left(\boldsymbol{v}^{\mathrm{ap}}, \boldsymbol{w}^{\mathrm{ap}}, \boldsymbol{p}^{\mathrm{dl}}, \boldsymbol{\gamma}, \boldsymbol{s}\right) \triangleq \|s_k\|_2^2\, \tilde{\Gamma}_k^{\mathrm{qt},2} - \beta_k \Re\left\{s_k^* \Gamma_k^{\mathrm{qt},1}\right\} - \alpha_k. \qquad \text{(C.3)}$$

In order to put equation (C.2d) into the form of equation (C.1c), each term in equation (C.3) must be expressed in terms of real variables, with a distinction for the UEs operating in UL and DL, respectively.

In particular, for UEs in UL (*i.e.*, $k \in \mathcal{K}^{\mathrm{ul}}$), the quadratic term in equation (C.3) can be rewritten as

$$\tilde{\Gamma}_k^{\mathrm{qt},2} = \boldsymbol{v}_k^{\mathrm{ap,real}^{\mathrm{T}}} \boldsymbol{D}^{\mathrm{ul}^{\mathrm{T}}} \boldsymbol{D}^{\mathrm{ul}} \boldsymbol{v}_k^{\mathrm{ap,real}}, \tag{C.4}$$

where

$$\boldsymbol{v}_k^{\mathrm{ap,real}} \triangleq [\Re(\boldsymbol{v}_k)^{\mathrm{T}} \Im(\boldsymbol{v}_k)^{\mathrm{T}}]^{\mathrm{T}}, \tag{C.5a}$$

$$\boldsymbol{D}^{\mathrm{ul}} \triangleq \begin{bmatrix} \Re\{\mathrm{SIN}\} & -\Im\{\mathrm{SIN}\} \\ \Im\{\mathrm{SIN}\} & \Re\{\mathrm{SIN}\} \end{bmatrix}^{\frac{1}{2}}, \tag{C.5b}$$

$$\mathrm{SIN} \triangleq \sum_{k' \in \mathcal{K}^{\mathrm{ul}}} p_{k'}^{\mathrm{ul}} \boldsymbol{h}_{k'} \boldsymbol{h}_{k'}^{\mathrm{H}} + \sum_{k' \in \mathcal{K}^{\mathrm{dl}}} \boldsymbol{H}^{\mathrm{H}} \boldsymbol{w}_{k'}^{t-1} \boldsymbol{w}_{k'}^{t-1,\mathrm{H}} \boldsymbol{H} + \sigma_{\mathrm{ul}}^2 I_{ML}. \tag{C.5c}$$

Similarly, for UEs in DL (*i.e.*, $k \in \mathcal{K}^{\mathrm{dl}}$), the quadratic term in equation (C.3) becomes

$$\tilde{\Gamma}_k^{\mathrm{qt},2} = \boldsymbol{w}^{\mathrm{ap,real}^{\mathrm{T}}} (\boldsymbol{D}^{\mathrm{dl}})^{\mathrm{T}} \boldsymbol{D}^{\mathrm{dl}} \boldsymbol{w}^{\mathrm{ap,real}} + r_k^{\mathrm{const}}, \tag{C.6}$$

with

$$r_k^{\mathrm{const}} \triangleq \sum_{k' \in \mathcal{K}^{\mathrm{ul}}} \left| \sqrt{p_{k'}^{\mathrm{ul}}} h_{k',k} \right|^2 + \sigma_{\mathrm{dl}}^2, \tag{C.7a}$$

$$\boldsymbol{w}^{\mathrm{ap,real}} \triangleq [\boldsymbol{w}_1^{\mathrm{ap,real}^{\mathrm{T}}} \ldots \boldsymbol{w}_{K^{\mathrm{dl}}}^{\mathrm{ap,real}^{\mathrm{T}}}]^{\mathrm{T}}, \tag{C.7b}$$

$$\boldsymbol{w}_k^{\mathrm{ap,real}} \triangleq [\Re(\boldsymbol{w}_k)^{\mathrm{T}}, \Im(\boldsymbol{w}_k)^{\mathrm{T}}]^{\mathrm{T}}, \tag{C.7c}$$

$$\boldsymbol{D}^{\mathrm{dl}} \triangleq \mathrm{blkdiag}\left(\boldsymbol{D}_1^{\mathrm{dl}}, \ldots, \boldsymbol{D}_{K^{\mathrm{dl}}}^{\mathrm{dl}}\right)^{\frac{1}{2}}, \tag{C.7d}$$

$$\boldsymbol{D}_{k'}^{\mathrm{dl}} \triangleq \begin{bmatrix} \Re\left\{\boldsymbol{h}_{k'} \boldsymbol{h}_k^{\mathrm{H}}\right\} & -\Im\left\{\boldsymbol{h}_{k'} \boldsymbol{h}_k^{\mathrm{H}}\right\} \\ \Im\left\{\boldsymbol{h}_{k'} \boldsymbol{h}_k^{\mathrm{H}}\right\} & \Re\left\{\boldsymbol{h}_{k'} \boldsymbol{h}_k^{\mathrm{H}}\right\} \end{bmatrix}, \tag{C.7e}$$

where $\mathrm{blkdiag}(\cdot)$ is a block diagonal matrix.

In turn, the second term in equation (C.3) can be written as

$$\beta_k \Re\left\{s_k^* \Gamma_k^{\mathrm{qt},1}\right\} = \begin{cases} \sqrt{p_k^{\mathrm{ul}}} \boldsymbol{q}^{\mathrm{T}} \boldsymbol{v}_k^{\mathrm{ap,real}} & k \in \mathcal{K}^{\mathrm{ul}} \\ \boldsymbol{q}^{\mathrm{T}} \boldsymbol{w}_k^{\mathrm{ap,real}} & k \in \mathcal{K}^{\mathrm{dl}} \end{cases}$$

where

$$\boldsymbol{q}^{\mathrm{T}} \triangleq \beta_k \begin{bmatrix} \Re(\boldsymbol{s}_k) & \Im(\boldsymbol{s}_k) \end{bmatrix} \begin{bmatrix} \Re(\boldsymbol{h}_k) & -\Im(\boldsymbol{h}_k) \\ \Im(\boldsymbol{h}_k) & \Re(\boldsymbol{h}_k) \end{bmatrix}.$$

Using the above, equation (C.2) can be rewritten as

$$\underset{\substack{n,\boldsymbol{\eta},\boldsymbol{v}^{\mathrm{ap}},\boldsymbol{w}^{\mathrm{ap}},\\ \boldsymbol{p}^{\mathrm{dl}},\boldsymbol{\gamma},\boldsymbol{s}}}{\text{minimize}} \quad -n - \sum_{\ell=1}^{L} \lambda\eta_\ell \nabla\mathbb{P}(\eta_\ell^{t-1}) \tag{C.8a}$$

$$\text{subject to} \quad n \leq \left(\prod_{k=1}^{K} o_k\right)^{\frac{1}{K}}, \tag{C.8b}$$

$$\left\| \begin{matrix} \|\boldsymbol{s}\|_2 \boldsymbol{D}^{\mathrm{ul}} \boldsymbol{v}_k^{\mathrm{ap,real}} \\ \frac{o_k - \sqrt{p_k^{\mathrm{ul}}} \boldsymbol{q}^{\mathrm{T}} \boldsymbol{v}_k^{\mathrm{ap,real}} - \alpha_k}{2} \end{matrix} \right\|_2 \leq \frac{o_k + \sqrt{p_k^{\mathrm{ul}}} \boldsymbol{q}^{\mathrm{T}} \boldsymbol{v}_k^{\mathrm{ap,real}} + \alpha_k}{2}, \forall k \in \mathcal{K}^{\mathrm{ul}} \tag{C.8c}$$

$$\left\| \begin{matrix} \|\boldsymbol{s}\|_2 \boldsymbol{D}^{\mathrm{dl}} \boldsymbol{w}^{\mathrm{ap,real}} \\ \frac{o_k - \boldsymbol{q}^{\mathrm{T}} \boldsymbol{w}^{\mathrm{ap,real}} + r_k^{\mathrm{const}} - \alpha_k}{2} \end{matrix} \right\|_2 \leq \frac{o_k + \boldsymbol{q}^{\mathrm{T}} \boldsymbol{w}^{\mathrm{ap,real}} - r_k^{\mathrm{const}} + \alpha_k}{2}, \forall k \in \mathcal{K}^{\mathrm{dl}} \tag{C.8d}$$

(3.16e) to (3.16g), (3.18c), (3.18d), and (C.2b).

As an upper bound of the computational complexity is of interest, letting $2^{\lceil \log_2 K \rceil}$ be an upper bound on the order of the geometric mean constraint in (C.8b), it can be rewritten as shown in [155, Sec. 2.3.1] based on hierarchical structure, such that equation (C.8) reduces to

$$\underset{\substack{n,\boldsymbol{\eta},\boldsymbol{v}^{\mathrm{ap}},\boldsymbol{w}^{\mathrm{ap}},\\ \boldsymbol{p}^{\mathrm{dl}},\boldsymbol{\gamma},\boldsymbol{s}}}{\text{minimize}} \quad -n - \sum_{\ell=1}^{L} \lambda\eta_\ell \nabla\mathbb{P}(\eta_\ell^{t-1}) \tag{C.9a}$$

$$\text{subject to} \quad n \leq o_{\lceil \log_2 K \rceil, 1}, \tag{C.9b}$$

$$o_{j,i} \leq \sqrt{o_{j-1,2i-1} o_{j-1,2i}}, \quad \forall i \in [1, \ldots, 2^{\lceil \log_2 K - j \rceil}], \quad j \in [1, \ldots, \lceil \log_2 K \rceil], \tag{C.9c}$$

(3.16e) to (3.16g), (3.18b) to (3.16e), (C.2b), (C.8c), and (C.8d).

Finally, equation (C.9c) can be put in the following QCP canonical form

$$\underset{\boldsymbol{x}}{\text{minimize}} \quad \boldsymbol{c}^{\mathrm{T}} \boldsymbol{x} \tag{C.10a}$$

$$\text{subject to} \quad n \leq o_{\lceil \log_2 K \rceil, 1}, \tag{C.10b}$$

$$\left\| \begin{bmatrix} o_{j,i} \\ \frac{o_{j-1,2i-1}-o_{j-1,2i}}{2} \end{bmatrix} \right\|_2 \leq \frac{o_{j-1,2i-1}+o_{j-1,2i}}{2},$$

$$\forall i \in [1,\ldots,2^{\lceil \log_2 K \rceil - j}], j \in [1,\ldots,\lceil \log_2 K \rceil], \tag{C.10c}$$

(3.16e) to (3.16g), (3.18b) to (3.18d),

(C.2b), (C.8c) and (C.8d),

where $\boldsymbol{c}$, $\boldsymbol{x}$ and $\boldsymbol{o}$ are auxiliary vectors defined as

$$\boldsymbol{c} \triangleq \left[-1, -\lambda\nabla\mathbb{P}(\eta_1^{t-1}), \ldots, -\lambda\nabla\mathbb{P}(\eta_L^{t-1}), 0, \ldots, 0\right]^{\mathrm{T}}, \tag{C.10d}$$

$$\boldsymbol{x} \triangleq \left[n, \boldsymbol{\eta}^{\mathrm{T}}, \boldsymbol{v}^{\mathrm{ap,real}\,\mathrm{T}}, \boldsymbol{w}^{\mathrm{ap,real}\,\mathrm{T}}, \boldsymbol{p}^{\mathrm{dl}\,\mathrm{T}}, \boldsymbol{o}^{\mathrm{T}}\right]^{\mathrm{T}}, \tag{C.10e}$$

and

$$\boldsymbol{v}^{\mathrm{ap,real}} \triangleq [\boldsymbol{v}_1^{\mathrm{ap,real}\,\mathrm{T}}, \ldots, \boldsymbol{v}_{K^{\mathrm{ul}}}^{\mathrm{ap,real}\,\mathrm{T}}], \tag{C.10f}$$

$$\boldsymbol{o} \triangleq [o_{1,1}, \ldots, o_{\lceil \log_2 K \rceil, 2^{\lceil \log_2 K \rceil - 1}}]^{\mathrm{T}}. \tag{C.10g}$$

References

[1] A. F. Molisch, *Wireless Communications*, 2nd ed. Wiley Publishing, Jan. 2011.

[2] M. Mouly, M.-B. Pautet, and T. Haug, *The GSM System for Mobile Communications*. Telecom Publishing, Jan. 1992.

[3] M. Rahnema, "Overview of the GSM system and protocol architecture," *IEEE Commun. Mag.*, vol. 31, no. 4, pp. 92–100, Apr. 1993.

[4] I. TG, "M.1311 : Framework for modularity and radio commonality within IMT-2000," Oct. 1997.

[5] C. Huang, "An analysis of CDMA 3G wireless communications standards," in *Proc. 1999 IEEE 49th Veh. Technol. Conf. (Cat. No.99CH36363)*, vol. 1, May 1999, pp. 342–345 vol.1.

[6] H. Ekstrom, A. Furuskar, J. Karlsson, M. Meyer, S. Parkvall, J. Torsner, and M. Wahlqvist, "Technical solutions for the 3G long-term evolution," *IEEE Commun. Mag.*, vol. 44, no. 3, pp. 38–45, Mar. 2006.

[7] K. David and H. Berndt, "6G Vision and Requirements: Is There Any Need for Beyond 5G?" *IEEE Veh. Technol. Mag.*, vol. 13, no. 3, pp. 72–80, Jul. 2018.

[8] Ericsson, "Ericsson mobility report june 2017," Jun. 2017. [Online]. Available: https://www.ericsson.com/49de56/assets/local/reports-papers/mobility-report/documents/2017/ericsson-mobility-report-june-2017.pdf

[9] Cisco, "Cisco Annual Internet Report (2018-2023) White Paper," Mar. 2020. [Online]. Available: https://www.cisco.com/c/en/us/solutions/collateral/executive-perspectives/annual-internet-report/white-paper-c11-741490.html

[10] M. Series, "IMT vision–framework and overall objectives of the future development of IMT for 2020 and beyond," *Recommendation ITU*, vol. 2083, p. 0, 2015.

[11] J. Navarro-Ortiz, P. Romero-Diaz, S. Sendra, P. Ameigeiras, J. J. Ramos-Munoz, and J. M. Lopez-Soler, "A survey on 5G usage scenarios and traffic models," *IEEE Commun. Surv. Tut.*, vol. 22, no. 2, pp. 905–929, Feb. 2020.

[12] NITA, "US Frequency Allocation Chart," Jan. 2016. [Online]. Available: https://www.ntia.doc.gov/files/ntia/publications/january_2016_spectrum_wall_chart.pdf

[13] W. Hong, Z. H. Jiang, C. Yu, D. Hou, H. Wang, C. Guo, Y. Hu, L. Kuai, Y. Yu, Z. Jiang, Z. Chen, J. Chen, Z. Yu, J. Zhai, N. Zhang, L. Tian, F. Wu, G. Yang, Z.-C. Hao, and J. Y. Zhou, "The role of millimeter-wave technologies in 5G/6G wireless communications," *IEEE J. Microw.*, vol. 1, no. 1, pp. 101–122, Jan. 2021.

[14] A. N. Uwaechia and N. M. Mahyuddin, "A comprehensive survey on millimeter wave communications for fifth-generation wireless networks: Feasibility and challenges," *IEEE Access*, vol. 8, pp. 62 367–62 414, Mar. 2020.

[15] T. S. Rappaport, S. Sun, R. Mayzus, H. Zhao, Y. Azar, K. Wang, G. N. Wong, J. K. Schulz, M. Samimi, and F. Gutierrez, "Millimeter wave mobile communications for 5G cellular: It will work!" *IEEE Access*, vol. 1, pp. 335–349, May 2013.

[16] I. A. Hemadeh, K. Satyanarayana, M. El-Hajjar, and L. Hanzo, "Millimeter-wave communications: Physical channel models, design considerations, antenna constructions, and link-budget," *IEEE Commun. Surv. Tut.*, vol. 20, no. 2, pp. 870–913, 2018.

[17] T. L. Marzetta, "Noncooperative cellular wireless with unlimited numbers of base station antennas," *IEEE Trans. Wireless Commun.*, vol. 9, no. 11, pp. 3590–3600, Oct. 2010.

[18] H. Q. Ngo, E. G. Larsson, and T. L. Marzetta, "Energy and spectral efficiency of very large multiuser MIMO systems," *IEEE Trans. Commun.*, vol. 61, no. 4, pp. 1436–1449, Feb. 2013.

[19] F. Rusek, D. Persson, B. K. Lau, E. G. Larsson, T. L. Marzetta, O. Edfors, and F. Tufvesson, "Scaling up MIMO: Opportunities and challenges with very large arrays," *IEEE Signal Process. Mag.*, vol. 30, no. 1, pp. 40–60, Dec. 2013.

[20] A. K. Gupta, M. N. Kulkarni, E. Visotsky, F. W. Vook, A. Ghosh, J. G. Andrews, and R. W. Heath, "Rate analysis and feasibility of dynamic TDD in 5G cellular systems," in *Proc. 2016 IEEE Int. Conf. Commun. (ICC)*, Jul. 2016, pp. 1–6.

[21] 3rd Generation Partnership Project. 3GPP, TS 38.213 Ver. 15.3.0, "NR; Physical layer procedures for control," Oct. 2018.

[22] Ericsson, "Ericsson mobility report november 2022," Nov. 2022. [Online]. Available: https://www.ericsson.com/en/reports-and-papers/mobility-report/reports/november-2022

[23] ——, "Ericsson mobility visualizer - mobility report," 2022. [Online]. Available: https://www.ericsson.com/en/reports-and-papers/mobility-report/mobility-visualizer

[24] W. Saad, M. Bennis, and M. Chen, "A Vision of 6G Wireless Systems: Applications, Trends, Technologies, and Open Research Problems," *IEEE Netw.*, vol. 34, no. 3, pp. 134–142, Oct. 2020.

[25] M. Alsabah, M. A. Naser, B. M. Mahmmod, S. H. Abdulhussain, M. R. Eissa, A. Al-Baidhani, N. K. Noordin, S. M. Sait, K. A. Al-Utaibi, and F. Hashim, "6G wireless communications networks: A comprehensive survey," *IEEE Access*, vol. 9, pp. 148 191–148 243, Nov. 2021.

[26] C. D. Alwis, A. Kalla, Q.-V. Pham, P. Kumar, K. Dev, W.-J. Hwang, and M. Liyanage, "Survey on 6G frontiers: Trends, applications, requirements, technologies and future research," *IEEE Open J. Commun. Soc.*, vol. 2, pp. 836–886, Apr. 2021.

[27] M. S. Akbar, Z. Hussain, Q. Z. Sheng, and S. Mukhopadhyay, "6G Survey on Challenges, Requirements, Applications, Key Enabling Technologies, Use Cases, AI integration issues and Security aspects," Jun. 2022. [Online]. Available: https://arxiv.org/abs/2206.00868

[28] N. H. Mahmood, H. Alves, O. A. López, M. Shehab, D. P. M. Osorio, and M. Latva-Aho, "Six key features of machine type communication in 6G," in *Proc. 2nd 6G Wireless Summit*, Levi, Finland, Mar. 2020, pp. 1–5.

[29] I. F. Akyildiz and J. M. Jornet, "Realizing ultra-massive MIMO (1024×1024) communication in the (0.06–10) terahertz band," *Nano Commun. Net.*, vol. 8, pp. 46–54, Jun. 2016, electromagnetic Communication in Nano-scale. [Online]. Available: https://www.sciencedirect.com/science/article/pii/S1878778916000107

[30] N. Y. Yu, K. Lee, and J. Choi, "Pilot signal design for compressive sensing based random access in machine-type communications," in *Proc. IEEE Wireless Commun. and Netw. Conf.*, San Francisco, CA, USA, Mar. 2017, pp. 1–6.

[31] M. Polignano, P. Mogensen, P. Fotiadis, L. Chavarria, I. Viering, and P. Zanier, "The inter-cell interference dilemma in dense outdoor small cell deployment," in *Proc. 2014 IEEE 79th Veh. Technol. Conf. (VTC Spring)*, Jan. 2014, pp. 1–5.

[32] T. Bai and R. W. Heath, "Coverage and rate analysis for millimeter-wave cellular networks," *IEEE Trans. Wireless Commun.*, vol. 14, no. 2, pp. 1100–1114, Apr. 2015.

[33] M. Di Renzo, "Stochastic geometry modeling and analysis of multi-tier millimeter wave cellular networks," *IEEE Trans. Wireless Commun.*, vol. 14, no. 9, pp. 5038–5057, May 2015.

[34] J. G. Andrews, X. Zhang, G. D. Durgin, and A. K. Gupta, "Are we approaching the fundamental limits of wireless network densification?" *IEEE Commun. Mag.*, vol. 54, no. 10, pp. 184–190, Oct. 2016.

[35] H. Iimori, G. T. F. de Abreu, D. González G., and O. Gonsa, "Mitigating channel aging and phase noise in millimeter wave MIMO systems," *IEEE Trans. Veh. Technol.*, vol. 70, no. 7, pp. 7237–7242, Jul. 2021.

[36] Da-Shan Shiu, G. J. Faschini, M. J. Gans, and J. M. Kahn, "Fading correlation and its effect on the capacity of multi-element antenna systems," in *Proc. ICUPC '98. IEEE 1998 Int. Conf. Universal Pers Commun. Conf. Proc. (Cat. No.98TH8384)*, vol. 1, Mar. 1998, pp. 429–433 vol.1.

[37] M. Banafaa, I. Shayea, J. Din, M. Hadri Azmi, A. Alashbi, Y. Ibrahim Daradkeh, and A. Alhammadi, "6G mobile communication technology: Requirements, targets, applications, challenges, advantages, and opportunities," *Alexandria Eng J.*, Sep. 2022. [Online]. Available: https://www.sciencedirect.com/science/article/pii/S111001682200549X

[38] D. C. Nguyen, M. Ding, P. N. Pathirana, A. Seneviratne, J. Li, D. Niyato, O. Dobre, and H. V. Poor, "6G internet of things: A comprehensive survey," *IEEE Internet Things J.*, vol. 9, no. 1, pp. 359–383, Jun. 2022.

[39] M. Duarte, C. Dick, and A. Sabharwal, "Experiment-driven characterization of full-duplex wireless systems," *IEEE Trans. Wireless Commun.*, vol. 11, no. 12, pp. 4296–4307, Nov. 2012.

[40] L. J. Rodríguez, N. Tran, and T. Le-Ngoc, "Performance evaluation of full-duplex relaying with direct link under residual self-interference," in *Proc. 2014 IEEE Int. Conf. Commun. (ICC)*, Aug. 2014, pp. 5712–5716.

[41] A. Lozano, R. W. Heath, and J. G. Andrews, "Fundamental Limits of Cooperation," *IEEE Trans. Inf. Theory.*, vol. 59, no. 9, pp. 5213–5226, Mar. 2013.

[42] X. Tao, X. Xu, and Q. Cui, "An overview of cooperative communications," *IEEE Commun. Mag.*, vol. 50, no. 6, pp. 65–71, Jun. 2012.

[43] G. Interdonato, E. Björnson, H. Quoc Ngo, P. Frenger, and E. G. Larsson, "Ubiquitous cell-free Massive MIMO communications," *EURASIP J. Wireless Commun. Netw.*, vol. 2019, no. 1, p. 197, Aug. 2019. [Online]. Available: https://doi.org/10.1186/s13638-019-1507-0

[44] A. Saleh, A. Rustako, and R. Roman, "Distributed antennas for indoor radio communications," *IEEE Trans. Commun.*, vol. 35, no. 12, pp. 1245–1251, Dec. 1987.

[45] W. Choi and J. G. Andrews, "Downlink performance and capacity of distributed antenna systems in a multicell environment," *IEEE Trans. Wireless Commun*, vol. 6, no. 1, pp. 69–73, Jun. 2007.

[46] H. Q. Ngo, A. Ashikhmin, H. Yang, E. G. Larsson, and T. L. Marzetta, "Cell-free massive MIMO: Uniformly great service for everyone," in *Proc. 2015 IEEE 16th Int. Workshop Signal Process. Adv. Wireless Commun. (SPAWC)*, Jun. 2015, pp. 201–205.

[47] E. Nayebi, A. Ashikhmin, T. L. Marzetta, and H. Yang, "Cell-free massive MIMO systems," in *Proc. 2015 49th Asilomar Conf. Signals, Syst. Comput.*, 2015, pp. 695–699.

[48] H. A. Ammar, R. Adve, S. Shahbazpanahi, G. Boudreau, and K. V. Srinivas, "User-centric cell-free massive MIMO networks: A survey of opportunities, challenges and solutions," *IEEE Commun. Surv. Tut.*, vol. 24, no. 1, pp. 611–652, Dec. 2022.

[49] H. Q. Ngo, A. Ashikhmin, H. Yang, E. G. Larsson, and T. L. Marzetta, "Cell-free massive MIMO versus small cells," *IEEE Trans. Wireless Commun.*, vol. 16, no. 3, pp. 1834–1850, Mar. 2017.

[50] H. Iimori and G. Thadeu Freitas de Abreu, "Two-way full-duplex MIMO with hybrid TX-RX MSE minimization and interference cancellation," in *Proc. 2018 IEEE 19th Int. Workshop Signal Process. Adv. Wireless Commun. (SPAWC)*, Jun. 2018, pp. 1–5.

[51] S. Mosleh, H. Almosa, E. Perrins, and L. Liu, "Downlink resource allocation in cell-free massive MIMO systems," in *Proc. 2019 Int. Conf. Comput. Netw. Commun. (ICNC)*, Feb. 2019, pp. 883–887.

[52] Y. Zhang, H. Cao, M. Zhou, and L. Yang, "Cell-free massive MIMO: Zero forcing and conjugate beamforming receivers," *J. Commun. Netw.*, vol. 21, no. 6, pp. 529–538, Dec. 2019.

[53] C. M. Yetis, E. Björnson, and P. Giselsson, "Joint analog beam selection and digital beamforming in millimeter wave cell-free massive MIMO systems," *IEEE Open J. Commun. Soc.*, vol. 2, pp. 1647–1662, Jul. 2021.

[54] Y. He, M. Shen, F. Zeng, H. Zheng, R. Wang, M. Zhang, and X. Liu, "Energy efficient power allocation for cell-free mmWave massive MIMO with hybrid precoder," *IEEE Commun. Lett.*, vol. 26, no. 2, pp. 394–398, Feb. 2022.

[55] K. Ando, H. Iimori, G. T. F. de Abreu, and K. Ishibashi, "User-heterogeneous cell-free massive MIMO downlink and uplink beamforming via tensor decomposition," *IEEE Open J. Commun. Soc.*, vol. 3, pp. 740–758, Apr. 2022.

[56] H. T. Dao and S. Kim, "Power allocation and user-AP connection in distributed massive MIMO systems," *IEEE Commun. Lett.*, vol. 25, no. 2, pp. 565–569, Nov. 2021.

[57] G. Femenias, N. Lassoued, and F. Riera-Palou, "Access point switch ON/OFF strategies for green cell-free massive MIMO networking," *IEEE Access*, vol. 8, pp. 21 788–21 803, Jan. 2020.

[58] F. Guo, H. Lu, and Z. Gu, "Joint power and user grouping optimization in cell-free massive MIMO systems," *IEEE Trans. Wireless Commun.*, vol. 21, no. 2, pp. 991–1006, Feb. 2022.

[59] H. T. Dao and S. Kim, "Effective channel gain-based access point selection in cell-free massive MIMO systems," *IEEE Access*, vol. 8, pp. 108 127–108 132, Jun. 2020.

[60] M. Alonzo and S. Buzzi, "Cell-free and user-centric massive MIMO at millimeter wave frequencies," in *Proc. 2017 IEEE 28th Annu. Int. Symp. Pers. Indoor Mobile Radio Commun. (PIMRC)*, Oct. 2017, pp. 1–5.

[61] M. Alonzo, S. Buzzi, and A. Zappone, "Energy-efficient downlink power control in mmwave cell-free and user-centric massive MIMO," in *Proc. 2018 IEEE 5G World Forum (5GWF)*, Jul. 2018, pp. 493–496.

[62] G. Femenias and F. Riera-Palou, "Cell-free millimeter-wave massive MIMO systems with limited fronthaul capacity," *IEEE Access*, vol. 7, pp. 44 596–44 612, Mar. 2019.

[63] ——, "Reduced-complexity downlink cell-free mmwave massive MIMO systems with fronthaul constraints," in *Proc. 2019 27th Eur. Signal Process. Conf. (EUSIPCO)*, Sep. 2019, pp. 1–5.

[64] J. García-Morales, G. Femenias, and F. Riera-Palou, "Energy-efficient access-point sleep-mode techniques for cell-free mmWave massive MIMO networks with non-uniform spatial traffic density," *IEEE Access*, vol. 8, pp. 137 587–137 605, Jul. 2020.

[65] E. Björnson and L. Sanguinetti, "Scalable cell-free massive MIMO systems," *IEEE Trans. Commun.*, vol. 68, no. 7, pp. 4247–4261, Jul. 2020.

[66] G. Interdonato, P. Frenger, and E. G. Larsson, "Scalability aspects of cell-free massive MIMO," in *Proc. ICC 2019 - 2019 IEEE Int. Conf. Commun. (ICC)*, May 2019, pp. 1–6.

[67] C. D'Andrea and E. G. Larsson, "User association in scalable cell-free massive MIMO systems," in *Proc. 2020 54th Asilomar Conf Signals Syst. Comput.*, Nov. 2020, pp. 826–830.

[68] M. Guenach, A. A. Gorji, and A. Bourdoux, "Joint power control and access point scheduling in fronthaul-constrained uplink cell-free massive MIMO systems," *IEEE Trans.Commun.*, vol. 69, no. 4, pp. 2709–2722, Apr. 2021.

[69] R. Wang, M. Shen, Y. He, and X. Liu, "Performance of cell-free massive MIMO with joint user clustering and access point selection," *IEEE Access*, vol. 9, pp. 40 860–40 870, Feb. 2021.

[70] C. Yoon and D.-H. Cho, "Energy Efficient Beamforming and Power Allocation in Dynamic TDD Based C-RAN System," *IEEE Commun. Lett.*, vol. 19, no. 10, pp. 1806–1809, Oct. 2015.

[71] H. Thomsen, P. Popovski, E. d. Carvalho, N. K. Pratas, D. M. Kim, and F. Boccardi, "CoMPflex: CoMP for In-Band Wireless Full Duplex," *IEEE Wireless Commun. Lett.*, vol. 5, no. 2, pp. 144–147, Apr. 2016.

[72] H. Kim, H. Lee, T. Kim, and D. Hong, "Cell-Free mMIMO Systems with Dynamic TDD," in *Proc. 2022 IEEE 95th Veh. Technol. Conf.: (VTC2022-Spring)*, Jun. 2022, pp. 1–6.

[73] A. Chowdhury, R. Chopra, and C. R. Murthy, "Can dynamic TDD enabled half-duplex cell-free massive MIMO outperform full-duplex cellular massive MIMO?" *IEEE Trans. Commun.*, vol. 70, no. 7, pp. 4867–4883, May 2022.

[74] H. Kamboj, B. Anand, S. Gupta, A. Meshram, S. Balijepalli, and C. R. Murthy, "Hardware Implementation of Cell-Free MIMO and Dynamic TDD using the OAI 5G NR Codebase," in *Proc. WSA 2021; 25th Int. ITG Workshop Smart Antennas*, Nov. 2021, pp. 1–5.

[75] D. Wang, C. Zhang, Y. Du, J. Zhao, M. Jiang, and X. You, "Implementation of a Cloud-Based Cell-Free Distributed Massive MIMO System," *IEEE Commun. Mag.*, vol. 58, no. 8, pp. 61–67, Aug. 2020.

[76] Y. Xin, R. Zhang, D. Wang, J. Li, L. Yang, and X. You, "Antenna clustering for bidirectional dynamic network with large-scale distributed antenna systems," *IEEE Access*, vol. 5, pp. 4037–4047, Mar. 2017.

[77] M. Wang, Y. Feng, D. Wang, J. Wang, and X. You, "Spectral Efficiency Analysis of Network-Assisted Full Duplexing for Large-Scale Distributed Antenna Systems," in *Proc. 2019 IEEE 90th Veh. Technol. Conf. (VTC2019-Fall)*, Sep. 2019, pp. 1–7.

[78] X. Xia, P. Zhu, J. Li, D. Wang, Y. Xin, and X. You, "Transceiver Design for Large-scale DAS with Network Assisted Full Duplex," in *Proc. 2020 IEEE 91st Veh. Technol. Conf. (VTC2020-Spring)*, May 2020, pp. 1–7.

[79] ——, "Joint Sparse Beamforming and Power Control for a Large-Scale DAS With Network-Assisted Full Duplex," *IEEE Trans. Veh. Technol.*, vol. 69, no. 7, pp. 7569–7582, May 2020.

[80] X. Xia, P. Zhu, J. Li, H. Wu, D. Wang, Y. Xin, and X. You, "Joint User Selection and Transceiver Design for Cell-Free With Network-Assisted Full Duplexing," *IEEE Trans. Wireless Commun.*, vol. 20, no. 12, pp. 7856–7870, Jun. 2021.

[81] H. Yang, X. Xia, J. Li, P. Zhu, and X. You, "Joint Transceiver Design for Network-Assisted Full-Duplex Systems With SWIPT," *IEEE Syst. J.*, vol. 16, no. 1, pp. 1206–1216, Apr. 2022.

[82] X. Xia, Z. Fan, W. Luo, A. Lu, D. Wang, X. Zhao, and X. You, "Joint uplink power control, downlink beamforming, and mode selection for secrecy cell-free massive MIMO with network-assisted full duplexing," *IEEE Syst. J.*, vol. 17, no. 1, pp. 720–731, Mar. 2023.

[83] ——, "Transceiver Design and Mode Selection for Secrecy Cell-Free Massive MIMO with Network-Assisted Full Duplexing," in *Proc. 2022 IEEE 95th Veh. Technol. Conf. (VTC2022-Spring)*, Jun. 2022, pp. 1–7.

[84] Y. Zhu, J. Li, P. Zhu, D. Wang, and X. You, "Flexible Duplexing Mode Selection Optimization for Network-Assisted Full-Duplex Cell-Free Massive MIMO Systems," in *Proc. 2021 13th Int. Conf. Wireless Commun. Signal Process. (WCSP)*, Oct. 2021, pp. 1–5.

[85] Y. Zhu, J. Li, P. Zhu, H. Wu, D. Wang, and X. You, "Optimization of Duplex Mode Selection for Network-Assisted Full-Duplex Cell-Free Massive MIMO Systems," *IEEE Commun. Lett.*, vol. 25, no. 11, pp. 3649–3653, Aug. 2021.

[86] Y. Zhu, J. Li, P. Zhu, D. Wang, H. Ye, and X. You, "Load-Aware Dynamic Mode Selection for Network-Assisted Full-Duplex Cell-Free Large-Scale Distributed MIMO Systems," *IEEE Access*, vol. 10, pp. 22 301–22 310, Feb. 2022.

[87] D. Wang, M. Wang, P. Zhu, J. Li, J. Wang, and X. You, "Performance of Network-Assisted Full-Duplex for Cell-Free Massive MIMO," *IEEE Trans. Commun.*, vol. 68, no. 3, pp. 1464–1478, Dec. 2020.

[88] Y. Hu, H. Ge, H. Wang, and D. Wang, "Spectral Efficiency of Network-Assisted Full-Duplex for Cell-Free Massive MIMO System Under Pilot Contamination," *IEEE Access*, vol. 9, pp. 110 826–110 841, Aug. 2021.

[89] J. Li, Q. Lv, P. Zhu, D. Wang, J. Wang, and X. You, "Network-Assisted Full-Duplex Distributed Massive MIMO Systems With Beamforming Training Based CSI Estimation," *IEEE Trans. Wireless Commun.*, vol. 20, no. 4, pp. 2190–2204, Dec. 2021.

[90] Y. Zhu, J. Li, P. Zhu, D. Wang, and X. You, "Network-Assisted Full-Duplex Enabled Ultrareliable and Low-Latency Communications," *Wireless Commun. Mobile Comput.*, p. 2233503, Oct. 2022, publisher: Hindawi. [Online]. Available: https://doi.org/10.1155/2022/2233503

[91] T. C. Mai, H. Q. Ngo, and T. Q. Duong, "Downlink spectral efficiency of cell-free massive MIMO systems with multi-antenna users," *IEEE Trans. Commun.*, vol. 68, no. 8, pp. 4803–4815, Apr. 2020.

[92] H.-C. Huang and J. Lu, "Retrospect and prospect on integrations of millimeter-wave antennas and non-millimeter-wave antennas to mobile phones," *IEEE Access*, vol. 10, pp. 48 904–48 912, May 2022.

[93] N. Jaglan, S. D. Gupta, and M. S. Sharawi, "18 Element Massive MIMO/Diversity 5G Smartphones Antenna Design for Sub-6 GHz LTE Bands 42/43 Applications," *IEEE Open J. Antennas Propag*, vol. 2, pp. 533–545, Apr. 2021.

[94] K.-L. Wong, J.-Y. Lu, L.-Y. Chen, W.-Y. Li, and Y.-L. Ban, "8-antenna and 16-antenna arrays using the quad-antenna linear array as a building block for the 3.5-GHz LTE MIMO operation in the smartphone," *Microw. Opt. Technol. Lett.*, vol. 58, no. 1, pp. 174–181, Nov. 2016.

[95] A. A. Al-Hadi, J. Ilvonen, R. Valkonen, and V. Viikari, "Eight-element antenna array for diversity and mimo mobile terminal in LTE 3500 MHz band," *Microw. Opt. Technol. Lett.*, vol. 56, no. 6, pp. 1323–1327, Mar. 2014.

[96] Z. Liu and L. Dai, "A comparative study of downlink MIMO cellular networks with co-located and distributed base-station antennas," *IEEE Trans. Wireless Commun.*, vol. 13, no. 11, pp. 6259–6274, Nov. 2014.

[97] J. Wang and L. Dai, "Asymptotic rate analysis of downlink multi-user systems with co-located and distributed antennas," *IEEE Trans. Wireless Commun.*, vol. 14, no. 6, pp. 3046–3058, Jun. 2015.

[98] U. Waheed and D. Kishore, "Uplink spatial fading correlation of MIMO channel," in *Proc. 2003 IEEE 58th Veh. Technol. Conf. VTC 2003-Fall (IEEE Cat. No.03CH37484)*, vol. 1, 2003, pp. 94–98 Vol.1.

[99] S. Loyka, "Channel capacity of MIMO architecture using the exponential correlation matrix," *IEEE Commun. Lett.*, vol. 5, no. 9, pp. 369–371, 2001.

[100] D.-S. Shiu, G. Foschini, M. Gans, and J. Kahn, "Fading correlation and its effect on the capacity of multielement antenna systems," *IEEE Trans.Commun.*, vol. 48, no. 3, pp. 502–513, Mar. 2000.

[101] J. Qiu, K. Xu, X. Xia, Z. Shen, and W. Xie, "Downlink power optimization for cell-free massive MIMO over spatially correlated rayleigh fading channels," *IEEE Access*, vol. 8, pp. 56 214–56 227, Mar. 2020.

[102] A. Abdallah and M. M. Mansour, "Efficient angle-domain processing for FDD-based cell-free massive MIMO systems," *IEEE Trans. Commun.*, vol. 68, no. 4, pp. 2188–2203, Apr. 2020.

[103] J. Zheng, J. Zhang, E. Björnson, and B. Ai, "Impact of channel aging on cell-free massive MIMO over spatially correlated channels," *IEEE Trans. Wireless Commun.*, vol. 20, no. 10, pp. 6451–6466, Oct 2021.

[104] H. Bolcskei, M. Borgmann, and A. Paulraj, "Impact of the propagation environment on the performance of space-frequency coded MIMO-OFDM," *IEEE J. Sel. Areas Commun.*, vol. 21, no. 3, pp. 427–439, Apr. 2003.

[105] E. Björnson, J. Hoydis, and L. Sanguinetti, "Massive MIMO networks: Spectral, energy, and hardware efficiency," *Found. Trends® Signal Process.*, vol. 11, no. 3-4, pp. 154–655, 2017. [Online]. Available: http://dx.doi.org/10.1561/2000000093

[106] E. Björnson and L. Sanguinetti, "Making cell-free massive MIMO competitive with MMSE processing and centralized implementation," *IEEE Trans. Wireless Commun.*, vol. 19, no. 1, pp. 77–90, Sep. 2020.

[107] M. Zhou, Y. Zhang, X. Qiao, and L. Yang, "Spatially correlated rayleigh fading for cell-free massive MIMO systems," *IEEE Access*, vol. 8, pp. 42 154–42 168, Feb. 2020.

[108] M. R. Akdeniz, Y. Liu, M. K. Samimi, S. Sun, S. Rangan, T. S. Rappaport, and E. Erkip, "Millimeter wave channel modeling and cellular capacity evaluation," *IEEE J. Sel. Areas Commun.*, vol. 32, no. 6, pp. 1164–1179, Jun. 2014.

[109] M. Steinbauer, A. Molisch, and E. Bonek, "The double-directional radio channel," *IEEE Antennas Propag. Mag.*, vol. 43, no. 4, pp. 51–63, Aug. 2001.

[110] G. Kwon, A. Conti, H. Park, and M. Z. Win, "Joint communication and localization in millimeter wave networks," *IEEE J. Sel. Topics Signal Process.*, vol. 15, no. 6, pp. 1439–1454, Sep. 2021.

[111] M. Cui and L. Dai, "Channel estimation for extremely large-scale MIMO: Far-field or near-field?" *IEEE Trans. Commun.*, vol. 70, no. 4, pp. 2663–2677, Apr. 2022.

[112] F. C. Commission *et al.*, "Spectrum frontiers report and order and further notice of proposed rulemaking: Fcc16-89," *Washington, DC*, 2016.

[113] H. Hojatian, J. Nadal, J.-F. Frigon, and F. Leduc-Primeau, "Decentralized beamforming for cell-free massive MIMO with unsupervised learning," *IEEE Commun. Lett.*, vol. 26, no. 5, pp. 1042–1046, May 2022.

[114] M. Bashar, K. Cumanan, A. G. Burr, M. Debbah, and H. Q. Ngo, "On the uplink max–min SINR of cell-free massive MIMO systems," *IEEE Trans. Wireless Commun.*, vol. 18, no. 4, pp. 2021–2036, Apr. 2019.

[115] A. Zhou, J. Wu, E. G. Larsson, and P. Fan, "Max-min optimal beamforming for cell-free massive MIMO," *IEEE Commun. Lett.*, vol. 24, no. 10, pp. 2344–2348, Oct. 2020.

[116] T. C. Mai, H. Q. Ngo, and T. Q. Duong, "Uplink spectral efficiency of cell-free massive MIMO with multi-antenna users," in *Proc. 2019 3rd Int. Conf. Recent Adv. Signal Process. Telecommun. Comput (SigTelCom)*, Mar. 2019, pp. 126–129.

[117] A. Ghazanfari, H. V. Cheng, E. Björnson, and E. G. Larsson, "Enhanced fairness and scalability of power control schemes in multi-cell massive MIMO," *IEEE Trans. Commun.*, vol. 68, no. 5, pp. 2878–2890, May 2020.

[118] H. Yu, H. D. Tuan, E. Dutkiewicz, H. V. Poor, and L. Hanzo, "Maximizing the geometric mean of user-rates to improve rate-fairness: Proper vs. improper gaussian signaling," *IEEE Trans. Wireless Commun.*, vol. 21, no. 1, pp. 295–309, Jan. 2022.

[119] M. Farooq, H. Q. Ngo, E.-K. Hong, and L.-N. Tran, "Utility maximization for large-scale cell-free massive MIMO downlink," *IEEE Trans. Commun.*, vol. 69, no. 10, pp. 7050–7062, Oct. 2021.

[120] H. D. Tuan, A. A. Nasir, H. Q. Ngo, E. Dutkiewicz, and H. V. Poor, "Scalable user rate and energy-efficiency optimization in cell-free massive MIMO," *IEEE Trans. Commun.*, vol. 70, no. 9, pp. 6050–6065, Sep. 2022.

[121] S. Kim and B. Shim, "FDD-based cell-free massive MIMO systems," in *Proc. 2018 IEEE 19th Int. Workshop Signal Process. Adv. Wireless Commun. (SPAWC)*, Jun. 2018, pp. 1–5.

[122] A. Abdallah and M. M. Mansour, "Efficient angle-domain processing for FDD-based cell-free massive MIMO systems," *IEEE Trans. Commun.*, vol. 68, no. 4, pp. 2188–2203, Apr. 2020.

[123] T. Han and D. Zhao, "On the performance of FDD cell-free massive MIMO with compressed sensing channel estimation," in *Proc. 2021 IEEE 21st Int. Conf. Commun Technol. (ICCT)*, Oct. 2021, pp. 238–242.

[124] ——, "Downlink channel estimation in FDD cell-free massive MIMO," *Phys. Commun.*, vol. 52, no. C, Jun. 2022. [Online]. Available: https://doi.org/10.1016/j.phycom.2022.101614

[125] H. Kim, J. Kim, and D. Hong, "Dynamic TDD systems for 5G and beyond: A survey of cross-link interference mitigation," *IEEE Commun. Surv. Tut.*, vol. 22, no. 4, pp. 2315–2348, Jul. 2020.

[126] M. S. El Bamby, M. Bennis, and M. Latva-aho, "UL/DL decoupled user association in dynamic TDD small cell networks," in *Proc. 2015 Int. Symp. Wireless Commun. Syst. (ISWCS)*, Aug. 2015, pp. 456–460.

[127] B. Soret, P. Popovski, and K. Stern, "A queueing approach to the latency of decoupled UL/DL with flexible TDD and asymmetric services," *IEEE Wireless Commun. Lett.*, vol. 8, no. 6, pp. 1704–1708, Dec. 2019.

[128] P. Jayasinghe, A. Tölli, J. Kaleva, and M. Latva-aho, "Bi-directional signaling for dynamic TDD with decentralized beamforming," in *Proc. 2015 IEEE Int. Conf. Commun. Workshop (ICCW)*, Jun. 2015, pp. 185–190.

[129] L. Xue, Y. Cheng, Y. Zhou, and B. Qu, "Next generation TDD cellular communication," in *Proc. 2015 49th Asilomar Conf. Signals Syst. Comput.*, Nov. 2015, pp. 1036–1040.

[130] 3rd Generation Partnership Project. 3GPP, TR 36.213 Ver. 10.9.0, "Evolved Universal Terrestrial Radio Access (E-UTRA); Physical layer procedures," Mar. 2013.

[131] 3rd Generation Partnership Project. 3GPP, TR 25.996 Ver. 14.2.0, "Study on new radio (NR) access technology; Physical layer aspects," Sep. 2017.

[132] J. M. B. da Silva, G. Wikström, R. K. Mungara, and C. Fischione, "Full duplex and dynamic TDD: Pushing the limits of spectrum reuse in multi-cell communications," *IEEE Wireless Commun.*, vol. 28, no. 1, pp. 44–50, Feb. 2021.

[133] T. T. Vu, D. T. Ngo, H. Q. Ngo, and T. Le-Ngoc, "Full-duplex cell-free massive MIMO," in *Proc. ICC 2019 - 2019 IEEE Int. Conf. Commun. (ICC)*, May 2019, pp. 1–6.

[134] H. V. Nguyen, V.-D. Nguyen, O. A. Dobre, S. K. Sharma, S. Chatzinotas, B. Ottersten, and O.-S. Shin, "On the spectral and energy efficiencies of full-duplex cell-free massive MIMO," *IEEE J. Sel. Areas Commun.*, vol. 38, no. 8, pp. 1698–1718, Aug 2020.

[135] ——, "A novel heap-based pilot assignment for full duplex cell-free massive MIMO with zero-forcing," in *Proc. ICC 2020 - 2020 IEEE Intern. Conf. Commun. (ICC)*, Jun. 2020, pp. 1–6.

[136] S. Dey and R. Budhiraja, "FD cell-free massive MIMO systems with downlink pilots: Analysis and optimization," *IEEE Trans. Commun.*, vol. 70, no. 11, pp. 7591–7608, Nov. 2022.

[137] A. Sabharwal, P. Schniter, D. Guo, D. W. Bliss, S. Rangarajan, and R. Wichman, "In-band full-duplex wireless: Challenges and opportunities," *IEEE J. Sel. Areas Commun.*, vol. 32, no. 9, pp. 1637–1652, Sep. 2014.

[138] E. Everett, C. Shepard, L. Zhong, and A. Sabharwal, "SoftNull: Many-antenna full-duplex wireless via digital beamforming," *IEEE Trans. Wireless Commun.*, vol. 15, no. 12, pp. 8077–8092, Dec. 2016.

[139] R. Chowdhury and A. K. M. Sharoar Jahan Choyon, "Performance analysis of Tx-Rx isolated distributed antenna system implementing in-band full-duplex for up-link communication to mitigate self-interference in 5G," in *Proc. 2019 1st Int. Conf. Adv. Sci. Eng. Robot. Technol. (ICASERT)*, May 2019, pp. 1–5.

[140] A. Ghazanfari, H. V. Cheng, E. Björnson, and E. G. Larsson, "A fair and scalable power control scheme in multi-cell massive MIMO," in *ICASSP 2019 - 2019 IEEE Int. Conf. Acoust., Speech Signal Process. (ICASSP)*, May 2019, pp. 4499–4503.

[141] S. S. Christensen, R. Agarwal, E. De Carvalho, and J. M. Cioffi, "Weighted sum-rate maximization using weighted MMSE for MIMO-BC beamforming design," *IEEE Trans. Wireless Commun.*, vol. 7, no. 12, pp. 4792–4799, Dec. 2008.

[142] A. Bandi, B. S. Mysore R, S. Maleki, S. Chatzinotas, and B. Ottersten, "A novel approach to joint user selection and precoding for multiuser miso downlink channels," in *Proc. 2018 IEEE Global Conf. Signal Inform. Process. (GlobalSIP)*, 2018, pp. 206–210.

[143] H. Guo, Y.-C. Liang, J. Chen, and E. G. Larsson, "Weighted sum-rate maximization for reconfigurable intelligent surface aided wireless networks," *IEEE Trans. Wireless Commun.*, vol. 19, no. 5, pp. 3064–3076, May 2020.

[144] K. Shen and W. Yu, "Fractional programming for communication systems-part II: Uplink scheduling via matching," *IEEE Trans. Signal Process.*, vol. 66, no. 10, pp. 2631–2644, May 2018.

[145] W. Abid, M. Hajjaj, and R. Bouallegue, "Weighted sum rate maximization for MIMO interfering channels," in *Proc. 2018 Int. Conf. Internet Things, Embedded Systems and Commun. (IINTEC)*, Dec 2018, pp. 109–113.

[146] A. Z. Yalcin, M. K. Cetin, and M. Yuksel, "Max-min fair precoder design and power allocation for MU-MIMO NOMA," *IEEE Trans. Veh. Technol.*, vol. 70, no. 6, pp. 6217–6221, Jun. 2021.

[147] R. Jiao and L. Dai, "On the max-min fairness of beamspace MIMO-NOMA," *IEEE Trans. Signal Process.*, vol. 68, pp. 4919–4932, Aug. 2020.

[148] J. Estrada, "Geometric mean maximization: An overlooked portfolio approach?" *The J. Investing*, vol. 19, no. 4, pp. 134–147, 2010. [Online]. Available: https://joi.pm-research.com/content/19/4/134

[149] A. Zappone and E. Jorswieck, "Energy efficiency in wireless networks via fractional programming theory," *Found. Trends Commun. Inf. Theory*, vol. 11, no. 3, pp. 185–396, Jun. 2015.

[150] H. Iimori, G. T. F. de Abreu, and G. Alexandropoulos, "MIMO beamforming schemes for hybrid SIC FD radios with imperfect HW and CSI," *IEEE Trans. Wireless Commun.*, vol. 18, no. 10, pp. 4816–4830, Oct. 2019.

[151] K. Shen and W. Yu, "Fractional programming for communication systems-part I: Power control and beamforming," *IEEE Trans. Signal Process.*, vol. 66, no. 10, pp. 2616–2630, May 2018.

[152] A. L. Yuille and A. Rangarajan, "The concave-convex procedure," *Neural Comput.*, vol. 15, no. 4, pp. 915–936, 2003. [Online]. Available: https://doi.org/10.1162/08997660360581958

[153] M. Grant and S. Boyd, "CVX: Matlab software for disciplined convex programming, version 2.1," http://cvxr.com/cvx, Mar. 2014.

[154] O. Taghizadeh, S. Stanczak, H. Iimori, and G. T. F. De Abreu, "Full-duplex amplify-and-forward MIMO relaying: Design and performance analysis under erroneous CSI and hardware impairments," *IEEE Open J. Commun. Soc.*, vol. 2, pp. 1249–1266, May. 2021.

[155] A.Ben-Tal and A.Nemirovski, *Lectures on modern convex optimization: Analysis, algorithms, and engineering applications*. SIAM, 2001.

[156] Y. Zhang, B. Di, H. Zhang, J. Lin, Y. Li, and L. Song, "Reconfigurable intelligent surface aided cell-free MIMO communications," *IEEE Wireless Commun. Lett.*, vol. 10, no. 4, pp. 775–779, Apr. 2021.

[157] T. Zhou, K. Xu, X. Xia, W. Xie, and J. Xu, "Achievable rate optimization for aerial intelligent reflecting surface-aided cell-free massive MIMO system," *IEEE Access*, vol. 9, pp. 3828–3837, Dec. 2021.

[158] Y. Zhang, B. Di, H. Zhang, J. Lin, C. Xu, D. Zhang, Y. Li, and L. Song, "Beyond cell-free MIMO: Energy efficient reconfigurable intelligent surface aided cell-free MIMO communications," *IEEE Trans. Cogn. Commun.Netw.*, vol. 7, no. 2, pp. 412–426, Jun. 2021.

[159] A. A. Nasir, H. D. Tuan, H. Q. Ngo, T. Q. Duong, and H. V. Poor, "Cell-free massive MIMO in the short blocklength regime for URLLC," *IEEE Trans. Wireless Commun.*, vol. 20, no. 9, pp. 5861–5871, Sep. 2021.

[160] J. Zhang, Y. Wu, S. Zhou, and J. Wang, "Joint linear transmitter and receiver design for the downlink of multiuser MIMO systems," *IEEE Commun. Lett.*, vol. 9, no. 11, pp. 991–993, Nov. 2005.

[161] S. Serbetli and A. Yener, "Transceiver optimization for multiuser MIMO systems," *IEEE Trans. Signal Process.*, vol. 52, no. 1, pp. 214–226, Jan. 2004.

[162] H. Lee, I. Sohn, D. Kim, and K. B. Lee, "Generalized MMSE beamforming for downlink MIMO systems," in *Proc. 2011 IEEE Int. Conf. Commun. (ICC)*, Jun. 2011, pp. 1–6.

[163] D. M. Chiu and R. Jain, "Analysis of the increase and decrease algorithms for congestion avoidance in computer networks," *Comput. Netw. ISDN Syst.*, vol. 17, pp. 1–14, 6 1989.

[164] J. G. Andrews, T. Bai, M. N. Kulkarni, A. Alkhateeb, A. K. Gupta, and R. W. Heath, "Modeling and analyzing millimeter wave cellular systems," *IEEE Trans. Commun.*, vol. 65, no. 1, pp. 403–430, Oct. 2017.

[165] S. Khosravi, H. S. Ghadikolaei, J. Zander, and M. Petrova, "Location-aided beamforming in mobile millimeter-wave networks," in *Proc. 2022 IEEE 95th Veh. Technol. Conf.: (VTC2022-Spring)*, Jun. 2022, pp. 1–7.

[166] A. Zhou, X. Zhang, and H. Ma, "Beam-forecast: Facilitating mobile 60 ghz networks via model-driven beam steering," in *Proc. IEEE INFOCOM 2017 - IEEE Conf. Comput. Commun.*, May 2017, pp. 1–9.

[167] C. Studer, S. Medjkouh, E. Gonultaş, T. Goldstein, and O. Tirkkonen, "Channel charting: Locating users within the radio environment using channel state information," *IEEE Access*, vol. 6, pp. 47 682–47 698, Aug. 2018.

[168] G. Abreu and A. Ghods, "Turbo MRC-SMDS: Low-complexity cooperative localization from hybrid information," in *Proc. 2018 IEEE Global Conf. Signal Inf. Process. (GlobalSIP)*, Nov. 2018, pp. 76–80.

[169] D. Tse and P. Viswanath, *Fundamentals of Wireless Communication.* Cambridge, U.K: Cambridge Univ. Press, 2005.

[170] H. Xie, N. González-Prelcic, and T. Shimizu, "Blockage detection and channel tracking in wideband mmWave MIMO systems," in *Proc. ICC 2021 - IEEE Int. Conf. Commun.*, Jun. 2021, pp. 1–6.

[171] N. González-Prelcic, H. Xie, J. Palacios, and T. Shimizu, "Wideband channel tracking and hybrid precoding for mmWave MIMO systems," *IEEE Trans. Wireless Commun.*, vol. 20, no. 4, pp. 2161–2174, Apr. 2021.

[172] E. E. TR, "138 901-2018 5g study on channel model for frequencies from 0.5 to 100 ghz (3gpp tr 38.901 version 14.3. 0 release 14)."

[173] H. Kawabata, K. Ishibashi, S. Vuppala, and G. T. F. de Abreu, "Robust Relay Selection for Large-Scale Energy-Harvesting IoT Networks," *IEEE Internet Things J.*, vol. 4, no. 2, pp. 384–392, Jun. 2017.

[174] A. El Abbous and N. Samanta, "A modeling of GPS error distributions," in *Proc. 2017 Eur. Navigation Conf. (ENC)*, May 2017, pp. 119–127.

[175] F. Wu, N. Kubo, and A. Yasuda, "Performance evaluation of GPS augmentation using quasi-zenith satellite system," *IEEE Trans. Aerosp. Electron. Syst.*, vol. 40, no. 4, pp. 1249–1260, Oct. 2004.

[176] S. Elhoushy, M. Ibrahim, and W. Hamouda, "Cell-free massive MIMO: A survey," *IEEE Commun. Surv. Tut.*, vol. 24, no. 1, pp. 492–523, Oct. 2022.

[177] K. Ando, H. Iimori, T. Takahashi, K. Ishibashi, and G. T. F. de Abreu, "Uplink signal detection for scalable cell-free massive MIMO systems with robustness to rate-limited fronthaul," *IEEE Access*, vol. 9, pp. 102 770–102 782, Jul. 2021.

[178] F. Li, Q. Sun, X. Ji, and X. Chen, "Scalable cell-free massive MIMO with multiple CPUs," *Mathematics*, vol. 10, no. 11, 2022. [Online]. Available: https://www.mdpi.com/2227-7390/10/11/1900

[179] S. Chen, J. Zhang, E. Björnson, J. Zhang, and B. Ai, "Structured massive access for scalable cell-free massive MIMO systems," *IEEE J. Sel. Areas Commun.*, vol. 39, no. 4, pp. 1086–1100, 2021.

[180] Y.-N. R. Li, B. Gao, X. Zhang, and K. Huang, "Beam management in millimeter-wave communications for 5G and beyond," *IEEE Access*, vol. 8, pp. 13 282–13 293, Jan. 2020.

[181] I. Orikumhi, J. Kang, C. Park, J. Yang, and S. Kim, "Location-aware coordinated beam alignment in mmWave communication," in *Proc. 2018 56th Annu. Allerton Conf. Commun. Control and Comput. (Allerton)*, Oct. 2018, pp. 386–390.

[182] V. Va, T. Shimizu, G. Bansal, and R. W. Heath, "Online learning for position-aided millimeter wave beam training," *IEEE Access*, vol. 7, pp. 30 507–30 526, Mar. 2019.

[183] J. Brun, V. Palhares, G. Marti, and C. Studer, "Beam alignment for the cell-free mmwave massive MU-MIMO uplink," in *Proc. 2022 IEEE Workshop Signal Process. Syst. (SiPS)*, Nov. 2022, pp. 1–6.

[184] H. Q. Ngo, L.-N. Tran, T. Q. Duong, M. Matthaiou, and E. G. Larsson, "On the total energy efficiency of cell-free massive MIMO," *IEEE Trans. Green Commun. Netw.*, vol. 2, no. 1, pp. 25–39, Mar. 2018.

[185] T. Van Chien, E. Björnson, and E. G. Larsson, "Joint power allocation and load balancing optimization for energy-efficient cell-free massive MIMO networks," *IEEE Trans. Wireless Commun.*, vol. 19, no. 10, pp. 6798–6812, Oct. 2020.

[186] K. Kim, J. Song, J.-H. Lee, S.-H. Hyun, and S.-C. Kim, "Robust beam management in position and velocity aware V2V communications using distributed antenna subarrays," *IEEE Trans. Veh. Technol.*, vol. 71, no. 11, pp. 11 703–11 716, Nov. 2022.

[187] X. Chen, A. Liu, Y. Cai, V. K. N. Lau, and M.-J. Zhao, "Randomized two-timescale hybrid precoding for downlink multicell massive MIMO systems," *IEEE Trans. Signal Process.*, vol. 67, no. 16, pp. 4152–4167, Aug. 2019.

Publications

Related Journal Papers

1. **Shuto Fukue**, Hiroki Iimori, Giussepe Thadeu Freitas de Abreu and Koji Ishibashi, "Joint Access Configuration and Beamforming for Cell-Free Massive MIMO Systems With Dynamic TDD," in *IEEE Access*, vol. 10, pp. 40130-40149, Apr. 2022.

Related International Conference Papers

1. **Shuto Fukue**, Giussepe Thadeu Freitas de Abreu and Koji Ishibashi, "Network-Assisted Full-Duplex Millimeter-Wave Cell-Free Massive MIMO with Localization-Aided Inter-User Channel Estimation," in *Proc. Int. Conf. Inform. Netw (ICOIN 2023)*, Feb. 2023.

Domestic Conference Papers

1. **福榮 秀都**, アブレウ ジュゼッペ, 石橋 功至, "ネットワーク全二重通信を用いたミリ波セルフリー大規模MIMOにおける位置情報を用いた端末間干渉の影響抑制に関する一検討," 信学技報, vol. 122, no. 252, RCS2022-164, pp. 55-60, 2022年11月.

2. **福榮 秀都**, 飯盛 寛貴, アブレウ ジュゼッペ, 石橋 功至, "ダイナミックTDDセルフリー大規模MIMOのための幾何平均最大化による資源割当およびビームフォーミング設計に関する一検討," 信学技報, vol. 121, no. 210, RCS2021-121, pp. 19-24, 2021年10月.

3. 伊藤 雅秋, 菅野 一生, 山崎 浩輔, 安藤 研吾, **福榮 秀都**, 飯盛 寛貴, 石橋 功至, "バックホール伝送容量制約を考慮した複数中央処理局を用いたスケーラブ

ルセルフリー大規模MIMOシステムの性能評価," 信学技報, vol. 121, no. 210, RCS2021-119, pp. 7-12, 2021年10月.

4. **福榮 秀都**, 飯盛 寛貴, アブレウ ジュゼッペ, 石橋 功至, "ダイナミックTDDを用いたセルフリー大規模MIMOのためのユーザの公平性を 考慮したリソース割当及びビームフォーミング設計に関する一検討," 信学技報, vol. 121, no. 153, RCS2021-115, pp. 85-90, 2021年8月.

5. **福榮 秀都**, 飯盛 寛貴, アブレウ ジュゼッペ, 石橋 功至, " セルフリー大規模MIMOのためのユーザの公平性を考慮したダイナミックTDD割当方式に関する一検討," 電子情報通信学会総合大会, B-1-150, 2021年3月.

6. **福榮 秀都**, 飯盛 寛貴, アブレウ ジュゼッペ, 石橋 功至, "セルフリー大規模MIMOのための分数計画法を用いたダイナミックTDD割当方式に関する一検討," 信学技報, vol. 120, no. 298, RCS2020-151, pp. 91-96, 2020年12月.

7. **福榮 秀都**, 飯盛 寛貴, 石橋 功至, アブレウ ジュゼッペ, 高山 茂, " パイロット汚染下におけるマルチセルMassive MIMOのための協調型パイロット 系列設計," 情報理論とその応用シンポジウム2019, pp. 587-592, 霧島市, 2019年11月.